CATALYTIC DNA MOLECULES FOR PORPHYRIN METALLATION

by

Yingfu Li

B.Sc., Anhui University, China, 1983

M.Sc., Beijing Agriculture University, China, 1989

THESIS SUBMITTED IN PARTIAL FULFILLMENT OF THE REQUIREMENTS FOR THE DEGREE OF DOCTOR OF PHILOSOPHY

in the Department of Chemistry

SIMON FRASER UNIVERSITY

August 1997

National Library of Canada
Acquisitions and Bibliographic Services
395 Wellington Street
Ottawa ON K1A 0N4
Canada

Bibliothèque nationale du Canada
Acquisitions et services bibliographiques
395, rue Wellington
Ottawa ON K1A 0N4
Canada

Your file Votre référence

Our file Notre référence

0-612-24327-3

Canada

APPROVAL

Name	Yingfu Li
Degree	Doctor of Philosophy (Science)
Title of thesis	Catalytic DNA Molecules for Porphyrin Metallation
Examining committee	Chair: Dr. D. Sutton

Dr. Dipankar Sen
Assistant Professor of Chemistry
Senior supervisor

Dr. B. M. Pinto
Professor of Chemistry
Committee Member

Dr. F. J. Borgford
Associate Professor of Chemistry
Committee Member

Dr. J. K. Scott
Assistant Professor of Biological Sciences
Internal Examiner

Dr. G. F. Joyce
Professor of Chemistry and Biology
The Scripps Research Institute
External Examiner

Date Approved: Aug 14, 97

ABSTRACT

Catalytic DNA molecules for porphyrin metallation were derived by utilizing *in vitro* selection and transition state analog (TSA) technologies. DNA clones were isolated from a random sequence DNA library on the basis of their affinity binding to N-methylmesoporphyrin IX (NMM), the proven TSA for porphyrin metallation. Various chemical, enzymatic and physical methodologies were used to successfully identify the binding motifs within these DNA clones. These guanine-rich binding motifs, in isolation, also showed high-affinity binding to NMM.

Two selected DNA clones and their binding motifs were first chosen to test for possible metallation activity. The binding site from PS5 was found to be catalytic towards the insertion of Cu(II) and Zn(II) into different porphyrins. This DNA enzyme showed several novel features, such as inhibition by Mg^{2+} and enhancement by potassium. Catalysis was found to be inhibited by NMM, and followed Michaelis-Menten kinetics at fixed copper concentrations. Values of k_{cat} of 13.7 hr^{-1}, and K_M of 2.9 mM, and k_{cat}/k_{uncat} of 1400 for mesoporphyrin IX (MPIX) were initially measured.

A subsequent thorough investigation of the properties of this DNA enzyme revealed the following: Three related porphyrins were acceptable as the substrates, of which protoporphyrin IX (PPIX) was preferred over MPIX; a 24-nucleotide sequence (PS5.M) was both the optimal and the minimal catalytic unit; and no catalytically relevant binding site for copper appeared to exist in the folded structure of the DNAzyme; and, K^+ was the only ion needed to support catalysis. This DNAzyme, PS5.M, functioned most

optimally at pH 6.2, a K^+ concentration range of 10-50 mM, and a temperature of 15°C. Various levels of optimization cumulatively contributed to a dramatic improvement in the DNAzyme's catalytic performance in terms of k_{cat} and K_M values, and k_{cat}/K_M as well as k_{cat}/k_{uncat}, these parameters compare well with those of natural ferrochelatses, as well as the artificially derived catalytic antibody and catalytic RNA using the same TSA.

Detailed examinations on all selected clones revealed that 25% sequences were strongly catalytic, and another 45% sequences were weakly active. The catalytic sequences folded in potassium solution to form a unique guanine quadruplex, which could be modelled as being made up of three guanine quartets, four loops and one gap. The experimental results suggested that the enzyme active site was possibly located at gap region. We propose that a structurally stressed DNA quadruplex deforms the porphyrin substrate to accelerate the metallation rate.

Spectroscopic studies on MPIX-DNA complex revealed that the MPIX-DNAzyme complex had a UV-visible spectrum close in many respects to that of the TSA (NMM), but significantly different from the spectra of MPIX itself. This seemed to corroborate the idea that the DNAzyme likely accelerates the metallation reaction by distorting the ground-state porphyrin toward the transition state for metallation.

Dedication

To my wife Hongjun, and my daughter Lily

Acknowledgments

I would like to express my sincere gratitude to my Senior Supervisor Dr. Dipankar Sen for his guidance, inspiration, enthusiasm, and trust over the last five year. I thank members of my supervisory committee, Dr. B. M. Pinto, and Dr. T. J. Borgford for encouragement and their very helpful suggestions and advice.

I also thank the following:

C. R. Geyer, my best labmate over the last five years, for sharing earlier frustrations and later happiness with me, and for constant valuable arguments. My past and present labmates for enjoyable memories.

Dr. Charles Boone for his inspiration and encouragement, and for helping me with some molecular biology techniques.

Dr. A. J. Bennet for his expert advice on enzyme kinetics.

Greg Ehlers for his excellent photographic assistance.

Friends in I.M.B.B and Chemistry Department.

Simon Fraser University, the Department of Chemistry, and the Institute of Molecular Biology and Biochemistry for providing me financial supports through scholarships.

And, last but not least, my wife Hongjun for trusting me always and helping me through tough times over the last five years.

TABLE OF CONTENTS PAGES

CHAPTER 4: OPTIMIZATION OF THE CATALYTIC PROPERTIES OF PS5.ST1

LIST OF TABLES

LIST OF FIGURES

CHAPTER 1

CHAPTER 2

CHAPTER 3

CHAPTER 4

ABBREVIATIONS

ATP	Adenosine 5'-triphosphate
b.p	Base pair
cDNA	Complementary DNA sequence for an RNA sequence
CPIII	Coproporphyrin III
DMS	Dimethyl sulfate
DMSO	Dimethyl sulphoxide
dNTPs	2'-Deoxyribonucleoside triphosphates
DPIX	Deuteroporphyrin IX
dsDNA	Double-stranded DNA
EDTA	Ethylenediaminetetraacetic acid
HIV	Human immunodefficiency virus
HPIX	Hematoporphyrin IX
HPLC	High pressure liquid chromatography
$H_2TPPS_4^{4-}$	Tetrakis(p-sulfophenyl)porphyrin
MES	2-(N-morpholino)ethanesulfonic acid
MPIX	Mesoporphyrin IX
NMM	N-methylmesoporphyrin IX
NTPs	Ribonucleoside triphosphates
PCR	Polymerase chain reaction
pKm	pKa value for a monoprotonated porphyrin
PPIX	Protoporphyrin IX

SELEX	Systematic Evolution of Ligands by EXponential enrichment
SDS	Sodium dodecyl sulfate, sodium lauryl sulfate
Tris	Tris (hydroxymethyl)methylamine
TSA	Transition state analog
UPIII	Uroporphyrin III

Chapter 1. A General Introduction

1. *In vitro* selection of catalytic RNA molecules

1.1. Discovery of ribozymes and theory of "RNA world"

In the early 1980s, the research groups led by Nobel Laureates Thomas Cech and Sidney Altman discovered that certain RNA molecules could perform enzyme-like functions *in vivo* (Kruger et al., 1982; Guerrier-Takada et al., 1983). This finding unequivocally challenged the predominant conception that only proteins can fulfill the task of biological catalysis. It also brought to light the unique status that RNA seemed to hold in the solving of the "chicken and egg" paradox regarding the origin and evolution of life on earth. That is, which came first, informational polynucleotides or functional polypeptides? Among the three potential candidates in modern biology--DNA, RNA, and protein, only RNA molecules could fulfill the dual role as both genetic carriers and biological catalysts. This was certainly supportive of the notion that RNA molecules were the very ancestral 'life' molecules on earth, and had both phenotypic and genotypic functions in a stage of evolution now termed the "RNA World". According to this hypothesis, in this "RNA world" (prior to the origin of protein synthesis), life was based entirely on RNA. Although the notion of an "RNA World" was first originated in the 1960s (Quastler, 1964; Woese, 1967; Crick, 1968; Orgel, 1968); it was more widely accepted only after the finding of catalytic RNA (Sharp, 1985; Lewin, 1986; Gilbert, 1986; Joyce, 1989).

However, natural ribozymes have only been found to catalyze a very limited range of chemical transformations, using nucleotide compounds as substrates and executing chemical actions almost exclusively at phosphorus centers. This raised fundamental questions for the "RNA world" proponents: could ribozymes catalyze chemical reactions beyond the scope of the extant ribozymes and use non-nucleotide compounds as substrates? Clearly, finding evidence for an expanded catalytic repertoire for RNA would be critical for making a stronger case for the "RNA world".

RNA molecules are capable of folding to form complex three-dimensional structures. This has been demonstrated magnificently in crystal structures of a select number of RNAs, such as tRNA molecules (Kim et al., 1973; Robertus et al., 1974; Schevitz et al., 1979; Moras et al., 1980; Woo et al., 1980), the hammerhead ribozyme (Pley et al., 1994; Scott et al., 1995; 1996), and fragments of a group I ribozyme (Cate et al., 1996). RNA can form innumerable folded structures in the following ways: by changing the linear sequences of its four nucleotide components, by increasing sequence length, and under different folding conditions. Some of the possible folded structures could in theory be catalytically active for a particular chemical reaction. How then could one find these catalytically active RNA structures? "Rational" selection is, at present, a poor choice, for there is an insufficient database of structural information that would allow scientists to accurately predict the tertiary folding of any given RNA molecule. It is certainly an even more daunting task to design the precise positioning of catalytically appropriate functionalities of a ribozyme, and of its substrates, in a three-dimensional

setting. Clearly, rational design of novel ribozymes is beyond our immediate reach and will only be feasible when ample structural data are available.

Fortunately, in 1990, a new technology, now generally termed as "*in vitro* selection" or "SELEX", was advanced by researchers in several laboratories (Blackwell et al., 1990; Blackwell & Weintraub, 1990; Ellington & Szostak, 1990; Green et al., 1990; Kinzler & Vogelstein, 1990; Pollock & Treisman, 1990; Robertson & Joyce, 1990; Thiesen & Bach, 1990; Tuerk & Gold, 1990). Instead of using rational design, researchers in the field tried to isolate individual molecules, from an extremely large population of RNA or DNA sequences, that could perform a specific task with high efficiency. This methodology allows no prior conception of mechanisms by which the molecules selected would complete the desired task. As will be seen in next a few sections, this technology (reviewed recently by Szostak, 1993; Joyce, 1994; Gold et al., 1995; Lorsch & Szostak, 1996; Breaker, 1996, 1997) has been proven to be successful in deriving novel ribozymes.

1.2. *In vitro* selection using a random RNA/DNA library

Typically, there are three major stages involved in an *in vitro* selection experiment: 1) Creation of a random DNA or RNA library with sufficient numbers of variants; 2) Selection--enriching sequences with desired properties through a selection-amplification process; and 3) Post-selection--the cloning, sequencing, and characterization of the enriched sequences obtained (see Fig. 1-1).

1.2.1. Pre-selection

In a typical *in vitro* selection experiment, a random DNA library with 10^{14}-10^{16} sequence variants is constructed by chemical synthesis. The library sequences typically

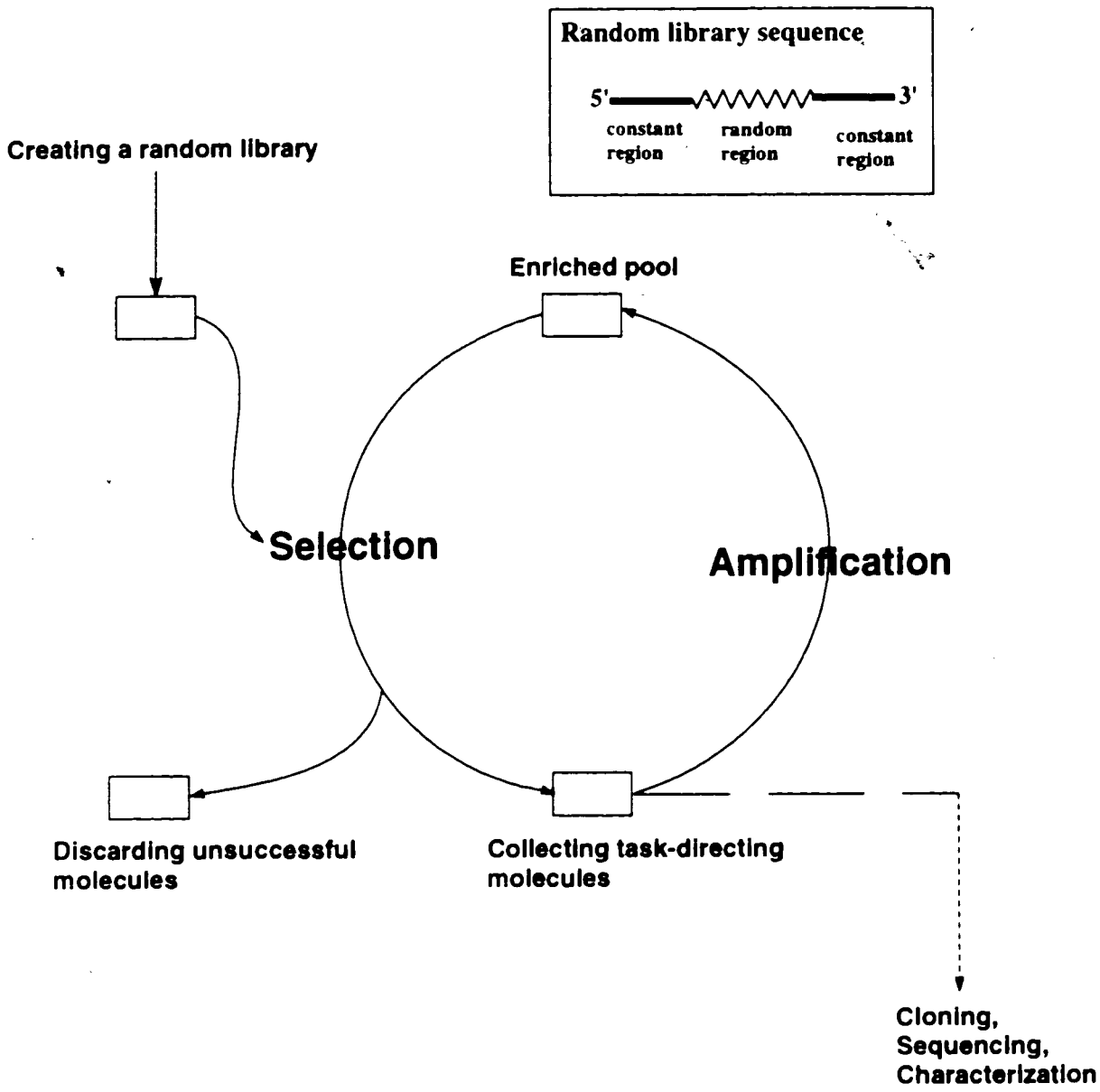

Fig. 1-1. A scheme for an *in vitro* selection experiment.

contain three regions (see Fig. 1-1, upper right corner): a central random region flanked by two defined regions at both 5' and 3' ends. The central random region brings complexity to a library, while the two constant-sequence regions serve as the primer binding sites for the polymerase chain reaction (PCR) or as RNA transcription promoter sites. A completely randomized DNA library can be made directly in an automated DNA synthesizer providing that the length of the library molecules is no larger than 100 nucleotides; libraries with longer sequences can be created using enzymes (restriction and ligation) to join together two or more synthesized short libraries (Bartel & Szostak, 1993), or by the so-called "overlap extension" method (Horton et al., 1989). There has been no consensus opinion regarding the optimal length of the random region, though longer sequences may be better for creating more complex folded tertiary structures, and hence in generating folded molecules better able to fulfill their directed tasks. The disadvantage of using long sequence libraries is that not every single sequence within the total "sequence-space" can be explored. For a random-region size of 25 nucleotides (with two 20-nucleotide constant regions), a complete sequence-space coverage requires that a total $4^{25} \approx 10^{15}$ molecules be synthesized. This size of library corresponds to 250 µg DNA, which is comparable to the amount of DNA typically produced by an automated DNA synthesizer in a 0.2 µmole scale synthesis. If the random region is 70 bases, however, the amount of DNA required to cover the entire sequence-space ($4^{70} \approx 1.4\times10^{42}$) is ~$10^{20}$ kilograms! Obviously, DNA synthesis at this level is not achievable. In other words, for a typical 0.2 µmole scale DNA synthesis (200 µg DNA produced) for a library with a 70-nucleotide random region and two 20-nucleotide constant regions, only 2.2×10^{-25} % of the

total sequence-space can be covered. Typically, for an *in vitro* selection experiment aimed at deriving sequences for the performance of completely novel functions, the random region length of a library is chosen to be between 50 to 100 nucleotides. In addition, mutagenic strategies for the introduction of low level random mutations are often incorporated into the amplification steps of the SELEX cycle to partially overcome the above-mentioned disadvantage associated with long sequence libraries (see discussion below).

1.2.2. Selection

Sequences of interest may be selected for interesting catalytic capabilities, for affinity to targeted ligands, or for any other task for which a distinction can be made between task-performing molecules and those that are incompetent. In a initial library of 10^{15} different molecules, there might only be very limited numbers of molecules capable of performing a specific task, this may range from no sequences at all to thousands of different sequences (Gold et al., 1995; Lorsch & Szostak, 1996). This initial low abundance, however, can be amplified thousands of times by PCR reactions following each screening step, and the resulting enriched pool can be further enriched by simple repetition of the selection and amplification procedures until an activity plateau is reached. The number of cycles required for reaching this plateau may vary from selection to selection, ranging from as few as five cycles (Breaker & Joyce, 1994) to as many as 27 cycles (Tsang & Joyce,1994). Typically, about 10 cycles are needed (Gold et al., 1995).

Random mutations can also be introduced during the amplification steps to create a better sequence (Beaudry & Joyce, 1992; Bartel & Szostak, 1993). This is especially useful when the library to be investigated has a random region size longer than 25 nucleotides, because the original library in these instances can only cover a limited portion of the sequence-space (see discussion in Section 1.2.1).

1.2.3. Post-selection

The final steps in an *in vitro* selection experiment consist of the cloning, sequencing and characterization of the individual sequences present in the final selection pool. At this stage, sequence comparison between individual DNA clones may be made to look for consensus motifs; and, to build a secondary structure model for the selected sequences. Sometimes, the final selection pool contains a single family of closely related sequences (Prudent et al., 1994); however, in most cases, the selected sequences fall into several family categories (Lorsch & Szostak, 1996; Gold et al., 1995). Occasionally, sequences from the final pool do not have obvious consensus motifs (see Chapter 2), but instead are able to fold to form a common tertiary structure, such as a guanine-quadruplex (see Chapter 5).

1.3. Selection of catalytic RNA sequences: two approaches

To obtain a catalytic RNA from a random library, one must choose an isolation strategy capable of successfully separating relatively small abundances of catalytic RNA molecules from a vast background of catalytically incompetent sequences. There are two

general approaches to achieve this goal: direct selection (self-modification) and indirect selection (affinity screening using transition state analogs).

1.3.1. Self-modification -- "direct selection" techniques

The first strategy of selecting catalytic RNA sequences out of a random pool is the "self-modification" approach, often referred to as "direct selection". The idea is as follows: in a random RNA pool, there might be individual molecules capable of catalyzing a chemical reaction, a catalysis that leads to modifications in their own sequences. As a consequence of such self-modifications, these active molecules gain some special physical and/or chemical properties which allow their separation from their inactive pool-companions.

The successful emergence of an active molecule using direct selection processes relies on the molecule possessing the following inherent property: not only should it have catalytic capability, but most importantly, it must integrate its catalytic domain and its substrate (such as in a cleavage reaction, see Section 2.1) or one of its substrates (such as in the case of a ligation reaction, see Section 1.3.1.2) within a single molecule. This requirement may work both as an advantage and as a disadvantage. On the one hand, the selection for catalysis is straightforward (as opposed to the transition state analog approaches, see discussions in Section 1.3.2): the catalytic domain of an RNA sequence catalyzes a chemical reaction for modifying its own substrate domain; the modification results in certain changes of chemical or physical properties of the sequence itself; these changed properties will then be explored for the separation of the modified molecule

from those unmodified sequences. On the other hand, the initially selected molecules are not true enzymes; they can only accelerate the target chemical reaction for a single reaction turnover. Nevertheless, in many reported instances, a self-catalyzing molecule can be converted into a true, multiple-turnover, ribozyme by separating the catalytic domain from its substrate domain or domains.

1.3.1.1. Engineering a group I ribozyme to use a DNA substrate

Robertson and Joyce (1990) reported a simple yet very powerful selection scheme for the selection of group I ribozyme mutants capable of using a DNA substrate. They constructed an RNA pool containing only six mutants of the *Tetrahymena* ribozyme that lacked one or more of the stem-loop regions of the wild-type ribozyme, and sought to select the best mutant in using a DNA substrate. The selection was designed such that the DNA substrate was annealed to the ribozyme's 5'-end through a six base-pair stretch. Upon substrate scission, part of the DNA substrate became covalently attached to the 3' end of the ribozyme. This "tagged" short DNA sequence then served as the primer binding site for the generation of cDNAs of ribozymes so that only those ribozymes that cleaved the DNA substrate could be converted into their cDNA and further amplified by PCR (see Fig. 1-2a). One mutant (ΔP9) was selected, which cleaved DNA more efficiently than the wild-type ribozyme cleaves RNA, under conditions of high temperature (50°C) and/or high $MgCl_2$ concentration (50 mM).

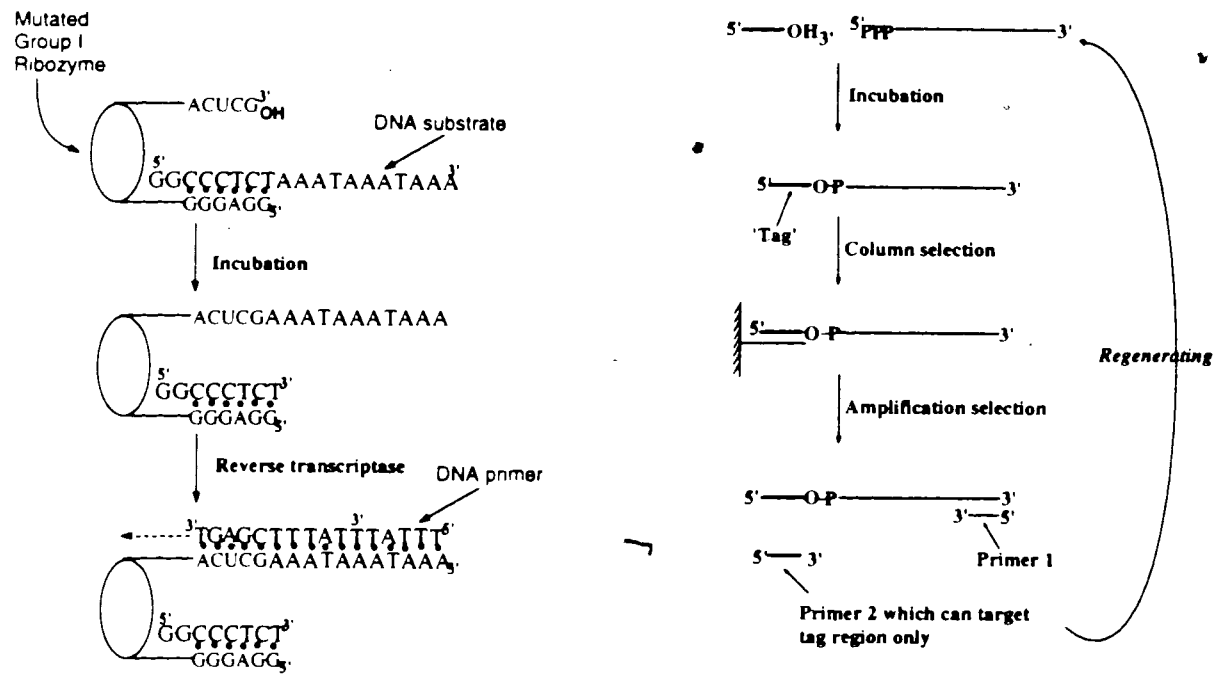

Fig. 1-2. Strategies used for the selection of DNA-cleaving ribozymes (left), and for the isolation of RNA ligases (right).

Joyce and his coworker (Beaudry & Joyce, 1993) next chose to screen a large library of 10^{13} *Tetrahymena* ribozyme mutants with a similar selection scheme to the above. Besides starting the selection with a partially randomized *Tetrahymena* ribozyme library, they also introduced low level random mutations during the selection-amplification process itself (0.1 % per base per generation) by performing PCR reactions under mutagenic conditions (Cadwell & Joyce, 1992). After 9 generations of selection, mutation and amplification, two selected ribozyme mutants cleaved a DNA substrate 100 times more efficiently than the wild-type enzyme under physiological conditions (Beaudry & Joyce, 1993). Later on, Joyce and coworkers further improved the DNA-cleaving capability of the selected ribozymes 1000 times more by going through another 18 stringent selection-amplification cycles (Tsang & Joyce, 1994). Recently, Joyce and

his coworkers have attempted to develop one of selected sequences into a potential therapeutic agent, and have shown that the selected ribozyme can be engineered to specifically target HIV-1 cDNA for cleavage *in vitro* (Raillard & Joyce, 1996).

1.3.1.2. Selection of novel RNA ligases

Bartel and Szostak (1993) set out to search for novel ribozymes for RNA ligation, from a large random library, that catalyze RNA ligation. They sought to select the ribozymes that catalyze the ligation of a short RNA substrate onto the selected ribozymes, with the incoming RNA substrate displacing the pyrophosphate group from the 5'-triphosphate on the random RNA sequences. The newly attached short RNA "tag" was then used as a tool for these researchers to perform a two-fold selection. The reaction mixture was first purified on an oligonucleotide affinity column complementary to the tag region, followed by a selective PCR of the cDNA with the use of a tag-specific primer (Fig. 1-2b). The selection strategy was so successful that they obtained a selected pool rich in catalytic sequences after only three rounds. In the next phase of selection, the system was pushed towards a mimicking of Darwinian evolution: Mutagenic PCR coupled with selective pressure applied by decreasing ligation times. After a total of ten rounds of selection and amplification, the enriched final pool catalyzed the self-ligation very efficiently, at a rate 7×10^7 times faster than that of the uncatalyzed template-directed reaction.

In the work that followed, Bartel and coworkers engineered a multiple turnover version of the RNA ligase, which has 10^3-fold improved activity over the initially

selected ribozymes (Ekland et al, 1995), with a k_{cat} at 1 min^{-1}, which corresponds to a rate acceleration of 10^9 times over the uncatalyzed template-directed reaction. This ribozyme's structure is very complex, with a catalytic domain of ~90 bases, demonstrating that complex ribozymes can indeed be isolated via *in vitro* selection experiments.

Recently, Ekland and Bartel (1996) have reported that their ligase ribozyme can also catalyze the template-directed polymerization of mononucleoside 5'-triphosphates (NTPs). The catalyzed condensation reaction proceeded not only with high efficiency, but also had high fidelity in accordance with Watson-Crick pairing rules. The ribozyme was found to be able to add up to six bases to the 3'-hydroxyl group of the directed template, with a k_{cat} of 0.3 min^{-1} for the addition of the first base. This k_{cat} corresponds to at least a 10^6-fold increase over the rate of the uncatalyzed ligation of two oligonucleotides (the real rate acceleration over uncatalyzed template-directing base addition was believed to be much higher, as the uncatalyzed rate was too slow to measure). This work has been regarded as a significant step toward the isolation of a true RNA enzyme with RNA replicase activity (Joyce, 1996), a type of ribozyme that has been suggested to have played a very important role in the "RNA World".

1.3.1.3. Other examples

Direct selections have proven very successful in the isolation of novel ribozymes. To date, more than a dozen of new ribozymes have been identified, and the number is continuing to increase. The catalyzed reactions are diverse in nature, such as the

polynucleotide kinase reaction (Lorsch & Szostak, 1994a), RNA alkylation (Wilson & Szostak, 1995), RNA acylation by an activated amino acid (Illangasekare et al., 1995), amide bond formation using aminoacyl RNA substrate (Lohse & Szostak, 1996), phosphoanhydride bond formation (Chapman & Szostak, 1995), Pb^{2+}-dependent tRNA cleavage (Pan & Uhlenbeck, 1992), and RNA self-cleavage (Williams et al.,1995).

1.3.2. TSA-binding aptamers – "indirect selection" techniques

A second major strategy for deriving novel RNA catalysts uses transition state analogs (TSAs). This strategy is sometimes termed "indirect selection", to contrast with "direct selection". The use of TSAs for the derivation of novel catalytic biomolecules is based on the transition state theory for chemical reactions (Pauling, 1946; Jencks, 1966; Lienhard, 1973; Wolfenden, 1972; recently reviewed by Kraut, 1988). The successful application of TSAs in the creation of catalytic antibodies (Tramontano et al., 1986; Pollack et al., 1986; and recently reviewed by Schultz & Lerner, 1995) has persuaded ribozyme-searching scientists that sequences with a high binding affinity for TSAs might also have catalytic activity (Szathmary, 1990; Abelson, 1990; Ellington & Szostak, 1992). In this strategy, random libraries are screened using transition state analogues as the binding targets. The isolated tight-binding RNA sequences ("aptamers", Ellington & Szostak, 1990) are then assayed for their ability to catalyze the corresponding chemical reactions. The advantage of the TSA approach is that the selected catalytic sequences will always exhibit multiple-turnover kinetics; the disadvantage is reflected in the fact

that even though a sequence might have a good binding affinity for a TSA, there is no absolute guarantee that it will be found to be catalytic.

- To date, this second approach has been much less successful than the "direct selection" approach. Only two novel ribozymes (Prudent et al., 1994; Conn et al., 1996) and one deoxyribozyme (one of the subjects of this thesis, and also published as Li & Sen, 1996) have been identified, although there have been several reported instances in which TSA-binding aptamers have failed to catalyze the targeted reactions (Lorsch & Szostak, 1996; Gold et al., 1995).

1.3.2.1. Successful examples

Schultz and coworkers reported the first successfully derived ribozyme using a TSA approach (Prudent et al., 1994). They screened a library of 10^{14} RNA molecules containing a random region of 128 nucleotides, and isolated only a single RNA sequence which bound specifically to a TSA for the isomerization of two diasteriomeric biphenyl compounds (as shown in Fig. 1-3). The ribozyme catalyzed the non-covalent interconversion of the bridged biphenyl substrate, with a k_{cat} of 2.8×10^{-5} min^{-1} and a K_M of ~0.5 mM. The rate acceleration was also very modest--only 88-fold over the uncatalyzed reaction. However, the successful derivation of this ribozyme certainly confirmed previous speculations that the TSA approach towards the isolation of novel ribozymes was achievable.

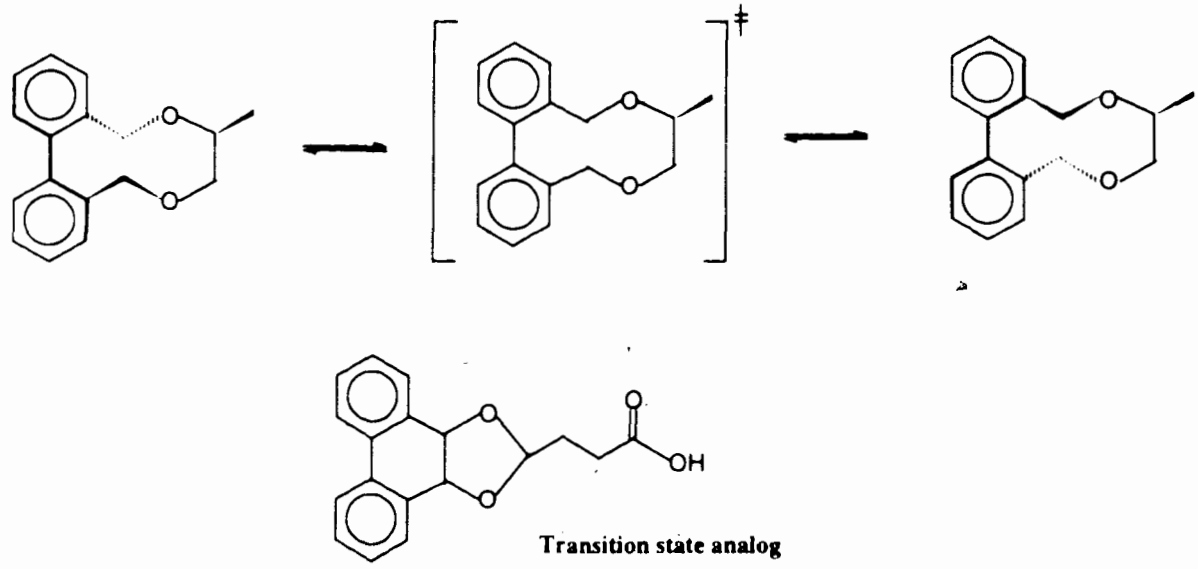

Fig. 1-3. Isomerization of RS and SS diasteromers of a bridged biphenyl compound and its TSA.

Schultz and coworkers (Conn et al., 1996) also applied a similar strategy to screen a RNA pool of ~10^{15} molecules having a random domain of 50 nucleotides, for RNA aptamers which could catalyze porphyrin metallation (see detailed discussions in Section 3 of this chapter). After 12 rounds of selection and amplification, several aptamers in the final pool exhibited the desired catalytic activity towards metallation of mesoporphyrin IX (MPIX). (The results of their experiments will be discussed in Chapter 4 in a comparison with our own results for catalytic DNA, and also with the data for natural ferrochelatases and catalytic antibodies).

1.3.2.2. Failed cases

There have been a number of reported failures in using the TSA approach to obtain catalytic RNAs. The reactions attempted include a Diels-Alder reaction (Morris et

al., 1994), ester and carbonate hydrolysis reactions (revealed by Lorsch & Szostak, 1996), a trityl cleavage reaction (revealed by Gold et al., 1995), an intermolecular pericyclic reaction (revealed by Lorsch & Szostak, 1996). No detailed description for those failed attempts has been provided except for one case in which RNA aptamers were selected for a TSA (Fig. 1-4a) of a Diels-Alder reaction (Morris et al., 1994). The RNA library used contained a random region of 80 bases. The selection was performed for 20 rounds, and the best aptamer in the final pool had only a weak affinity for the TSA (a K_d of 0.35 mM). Even so, the experimenters screened extensively the sequences in the final pool-- nearly 200 different molecules were assayed for the catalysis of the targeted Diels-Alder reaction, and none of them were active. The failure was attributed to the inability of obtaining oligonucleotide sequences that bound the TSA more tightly than to the substrates, and, also to the modest affinity of the aptamers for the TSA (Gold et al., 1995).

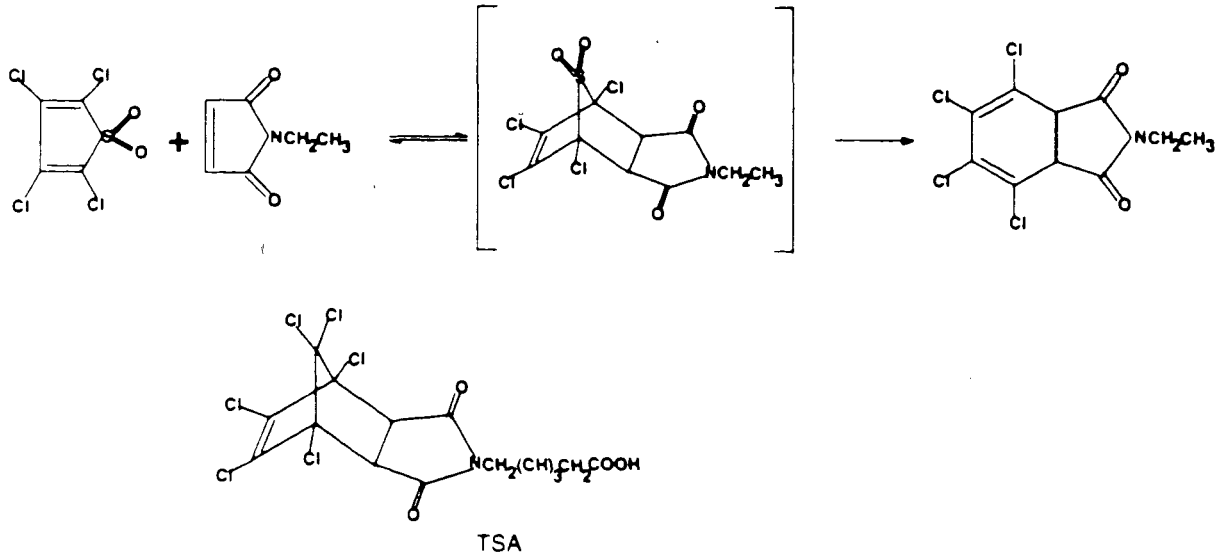

TSA

Fig. 1-4a. A Diels-Alder reaction and its TSA.

Subsequently, Morris and coworkers applied a similar strategy to identify RNA aptamers capable of binding to a TSA for the cleavage of a trityl ether (Fig. 1-4b). This time, the RNA sequences selected were claimed to have a much higher affinity for the TSA (a K_d of 7 μM), and these had been counter-selected for diminished affinity for the substrate. In spite of this, no catalysis was found with the isolated aptamers (revealed by Gold et al., 1995).

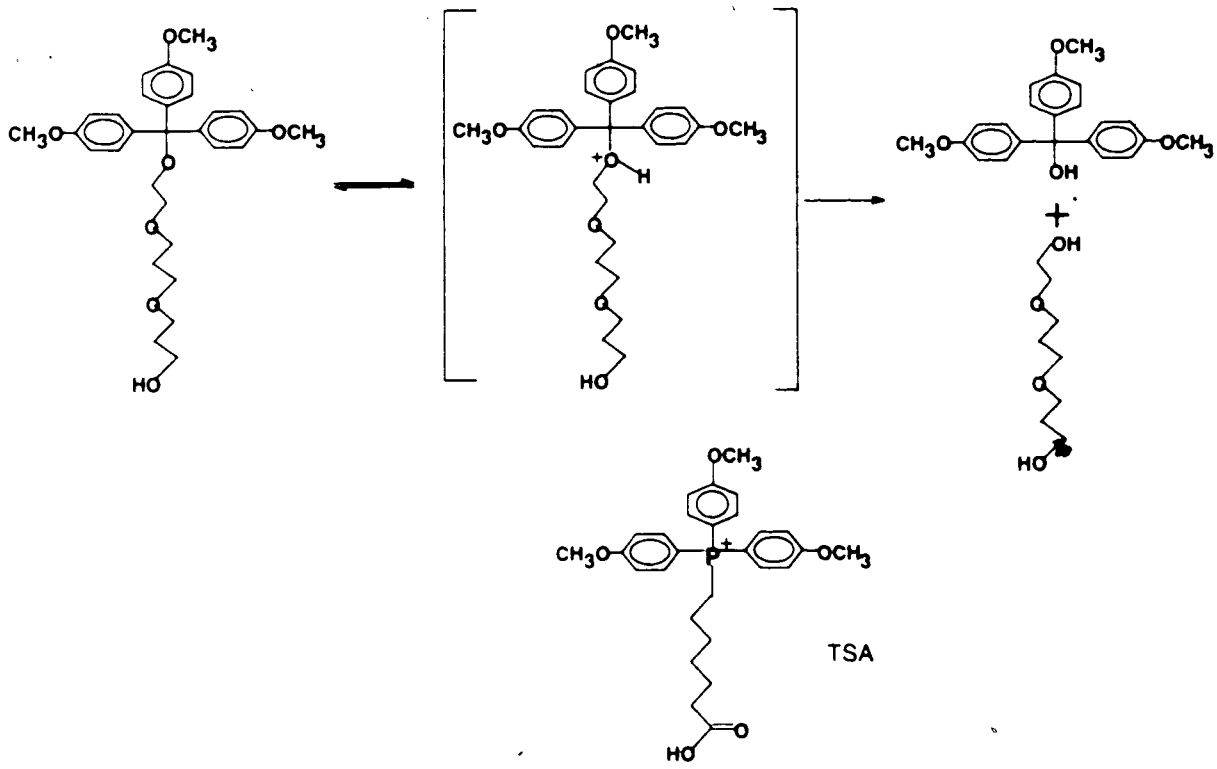

Fig. 1-4b. A trityl ether cleavage reaction and its TSA.

The limited success in deriving catalytic RNA molecules by TSA approaches raised questions about the effectiveness of the methodology in general. Even in the three successful examples, RNA or DNA molecules most likely played the role of only providing binding energy to bend or deform the structures of the substrates; no bond formation and bond breakage were likely involved in the transition states of the reactions. However, it was believed that difficulties encountered with this approach did not imply that RNA molecules lacked capabilities for catalyzing these chemical transformations (Gold et al., 1995). Instead, those failures were most likely caused by scientists' inability to use either ideal transition state analogs specifically for RNA aptamers to interact with, or in deriving RNA aptamers with very high binding affinity and specificity for a given TSA. Firstly, any transition state analog is only an approximation, but not a high-fidelity representation of the transition state of a reaction. It is believed that TSAs need to be specially designed in a way such that strong and specific interactions can be brought together between TSAs and RNA molecules (Lorsch & Szostak, 1996). Secondly, no RNA aptamers reported this far which could bind to TSAs in the nanomolar and picomolar range, and no selection procedures have employed mutational strategies to optimize the binding properties of RNA aptamers. Clearly, improved selection strategies need to be taken to derive tight-binding and highly specific RNA sequences for any TSA.

2. Catalytic DNA versus catalytic RNA

In nature, RNA molecules have very diversified functions. They not only perform their main duties as genetic messengers (messenger RNAs), amino acid activators and

carriers for protein synthesis (transfer RNAs), ribosome structure organizers (ribosomal RNAs), but also take the role of biological catalysts (catalytic RNAs or ribozymes) as their minor duties.

DNA molecules, on the other hand, work exclusively as the genetic material of free-living organisms, and lack the functional diversities exhibited by RNA molecules. This may be explained by considering the fact that DNA molecules exist almost exclusively as double-stranded in nature, which are much less structurally diverse than single-stranded RNA in terms of forming complex tertiary structures.

The chemical composition of DNA, however, is not very different from that of RNA--the only significant difference lies on their sugar moieties--DNA lacks the hydroxyl groups at the 2' position of every sugar moiety. Although double-stranded DNA molecules may lack tertiary structural diversity, single-stranded DNA molecules (ssDNAs) can form structures as complex as RNA molecules, and *in vitro* selection experiments have shown that single-stranded RNA and DNA can both provide good solutions for solving the same problem in terms of binding to organic and biological ligands (Ellington & Szostak, 1990, 1992; Huizenga & Szostak, 1995; Sassanfar & Szostak, 1993; Boch et al., 1992). Based on these results, it is reasonable to believe that single-stranded DNA molecules may function as non-natural biological catalysts.

In the last three years, several catalytic DNA molecules have been generated through *in vitro* selection experiments. Besides the catalytic DNA molecules for porphyrin metallation (which will be fully described in this thesis), the *in vitro* selected DNA enzymes described catalyze the following reactions: 1) the cleavage of an RNA-

linkage embedded in a DNA sequence, in the presence of lead (Breaker & Joyce, 1994), other divalent metal ions (Breaker & Joyce, 1995; Faulhammer & Famulok, 1996), trivalent ions (Geyer & Sen, 1997b), and in the absence of divalent and higher-valent ions (Geyer & Sen, 1997a); 2) DNA ligation (Cuenoud & Szostak, 1995); 3) DNA oxidative cleavage in the presence of Cu(II) (Carmi et al., 1996); and 4) RNA cleavage under physiological conditions (Santoro & Joyce, 1997).

2.1. DNA enzymes that cleave an internal RNA-linkage phosphate bond

The first DNAzyme was reported by Breaker and Joyce (1994). They started with a pool of 10^{14} ssDNA molecules in a search for catalytic DNAs which cut their internal RNA linkage at phosphodiester bonds. The library they used contained a random region of 50 bases. A special PCR primer was designed and used to finalize the library sequences with two important features: its 5'-end and 3'-end contained a biotin moiety and a ribo-nucleotide, respectively. After PCR with this primer, the sequences were immobilized on a streptavidin column in the double-stranded form. Denaturation with sodium hydroxide removed the "antisense" strands, and salt conditions were then provided to fold the ssDNA molecules immobilized on the column matrix. Those molecules catalyzing the cleavage of their internal RNA-linkage in the presence of lead ions released themselves from the column, were collected and amplified for the next round of selection (Fig. 1-5a).

After only five rounds of selection, Pb^{2+}-dependent RNA-cutting DNA sequences were recovered with a k_{obs} of ~1 min^{-1}, which corresponds to a ~10^5-fold rate acceleration

over the uncatalyzed reaction. A secondary structure model was proposed, and based on it, the self-cleavage catalytic DNA was engineered into a true enzyme capable of using external substrates with multiple turnovers.

Breaker and Joyce also applied the same methodology to search for RNA-cleaving DNA enzymes which could function in the presence of either Zn^{2+}, Mn^{2+}, or Mg^{2+} (Breaker & Joyce, 1995). This time, they chose to use random library sequences which biased the formation of the secondary structure shown in Fig. 1-5b: two base-pairing stems of six and four bases flanking two bulged regions, one of which was a 40-base random region and the other an eight-base region containing the targeted RNA linkage located right in the middle (Fig. 1-5b). Five rounds of selection were needed to isolate DNA catalysts using Mn^{2+} as cofactors, and six rounds were needed for Zn^{2+} and Mg^{2+}-

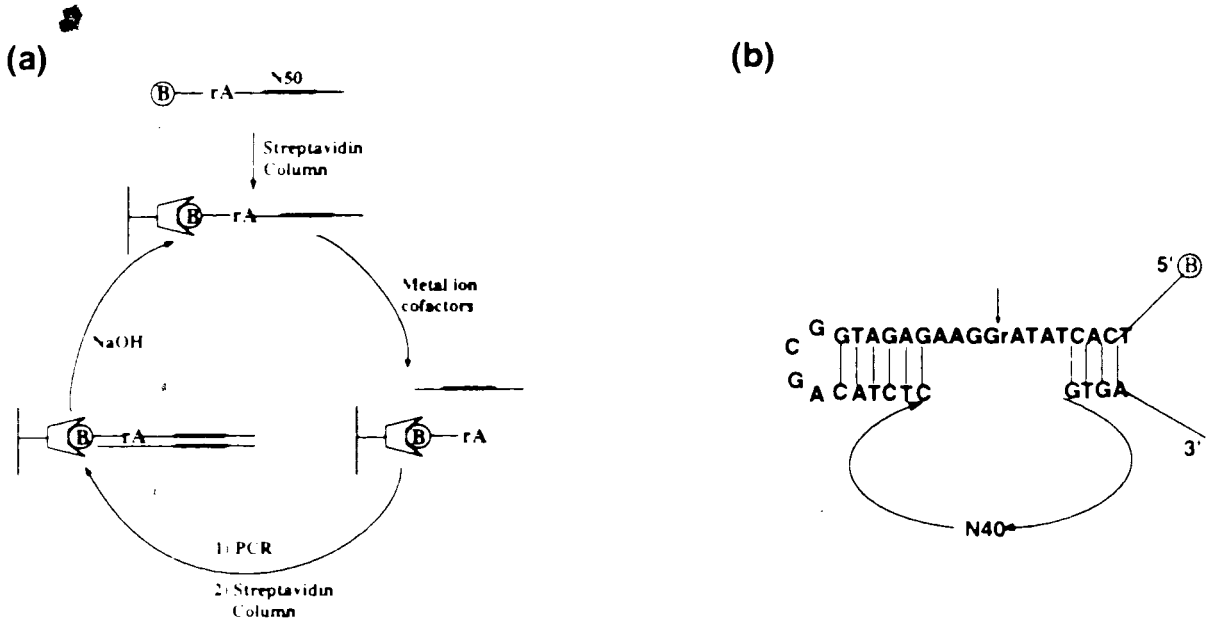

Fig. 1-5. Selection of RNA-cleaving DNA enzymes. (a) Scheme of the selection strategies. (b) The biased pool used for the selection of Mg(II), Mn(II), or Zn(II)-dependent RNA-cleaving DNA enzymes.

dependent DNAzymes. One of the Mg^{2+}-dependent enzymes displayed a k_{obs} of 0.002 min^{-1} and was further optimized by an additional seven rounds of selection on a partially randomized pool with 15% degeneracy over the originally randomized region of the selected catalyst. The newly generated catalysts had an improved activity (a k_{obs} of 0.01 min^{-1}), representing a 10^5 times rate acceleration over the uncatalyzed reaction. Once again, the self-cleaving catalysts were engineered into a true enzyme that used an external substrate, and could carry out cleavage reaction under physiological conditions (Breaker & Joyce, 1995).

Recently, Geyer and Sen have produced results showing that this RNA-linkage cleavage reaction can be catalyzed by various sets of DNA sequences using different metal ion cofactors (Geyer & Sen, 1997a; 1997b). Most surprisingly, one set of DNA sequences catalyzed the reaction without using any divalent and higher-valent metal ions as catalytic "helpers", a phenomenon that is unusual for ribozymes and deoxyribozymes, and goes against the traditional view that all ribozymes have to use divalent or higher valent metal ions as catalytic cofactors to perform tasks of catalysis (Yarus, 1993).

2.2. A general-purpose RNA-cleaving DNA enzyme

One goal of developing RNA-cleaving DNA enzymes is to make them to cleave a "true" RNA substrate and use them as therapeutic agents to inactivate viral RNA sequences. Clearly, the above-described DNA enzymes have little utility in this regard. Very recently, Joyce and coworker have taken a step further toward this goal (Santoro & Joyce, 1997). They built a random library of following sequence: 5'-biotin-

d(GGAAAAA)r(**$G_1U_2A_3A_4C_5U_6A_7G_8A_9G_{10}A_{11}U_{12}$**)d(GGAAGAGATGGCGAC)-$N_{50}$CGGTAAGCTTGCTTGGCAC-3'. The strategy used to select catalytic DNA sequences for cleaving the RNA motif was similar to that of Breaker and Joyce (1994). Two types of DNA sequences have been found to cleave the RNA motif at specific sites. One enzyme, termed **10-23**, was found to be highly generalizable with respect to substrate sequences and could cleave any RNA substrate at a purine-pyrimidine site (though A•U was most preferred). The enzyme was then used to target any mRNA start codon (AUG). For instance, the translation initiation region of HIV-1 *gag/pol* mRNA (5'-GGAGAG AGA•UGGGUGCG-3') can be specifically cleaved by the DNA enzyme **10-23** under simulated physiological conditions, with a k_{cat} of 0.15 min^{-1} and K_M of 0.47 nM. These parameters compare favorably to those of the known RNA-cleaving RNA enzymes. When compared to the protein enzyme ribonuclease A, however, the DNA enzyme has a much lower k_{cat} (10^4 times lower) and a much smaller K_M (10^5 times lower).

This type of RNA-cleaving DNA enzymes could certainly be used as an enzymatic tool to cut RNA sequences in the laboratory manipulation of RNA molecules, and possibly to inactivate cellular RNAs if *in vivo* expression system could be created.

2.3. DNA ligase

Cuenoud and Szostak (1995) used the *in vitro* selection to derive DNA enzymes catalyzing the ligation of two DNA oligomers. A library of 10^{14} ssDNAs were used, which contained a random region of 116 nucleotides; the substrate was a short DNA oligomer with a 5'-end biotin moiety and a 3'-terminal phosphorimidazole function.

Those DNA sequences having the ability of using their 5'-OH groups to replace the imidazole group were isolated through a biotin-straptavidin technology. The selection was carried out for nine rounds, and one catalyst thus isolated was recast into a system of two substrates and one enzyme. The 45-nucleotide Zn^{2+}/Cu^{2+}-dependent metallo-DNAzyme catalyzed the ligation of the two substrates with a k_{cat} of 0.07 min^{-1}, corresponding to a rate enhancement of ~3000 over the template-directed reaction and 1.7×10^{5} over the non-template-directed reaction.

2.4. A DNA-cleaving DNAzyme

Breaker and coworkers (Carmi et al., 1996) used a selection scheme similar to that shown in Fig. 1-5a to search for catalytic DNA molecules that cleaved themselves by a redox-dependent mechanism. Beginning with a DNA pool of $\sim2\times10^{13}$ sequences randomized over central 50 bases region, they performed an *in vitro* selection experiment in the presence of $CuCl_2$ and ascorbate for seven rounds. Sequence analysis revealed several classes of self-cleaving DNA enzymes. One class, termed CA3, was most efficient and performed self-cleavage at one specific site with a k_{obs} of 0.14 min^{-1} under conditions of 10 μM each of Cu(II) and ascorbate; the sequence could still execute the self-cleaving reaction in the presence of 10 μM Cu(II) only, but the reactivity was much lower, with a k_{obs} of 8×10^{-4} min^{-1}. A mutagenized CA3 pool was created with 15% degeneracy over the original random region, and subjected for an additional five rounds of selection using 10 μM Cu^{2+} as the sole cofactor. The re-selected pool displayed an improved activity of nearly 100 times using Cu(II) as the sole cofactor, with a k_{obs} of the

individual sequences between 0.03-0.05 min^{-1}, corresponding at least 10^6-fold rate enhancement over the uncatalyzed reaction.

3. My research project

When this project was conceived in 1992, the *in vitro* selection methodology was still in its debut phase. Encouraged by the experiments of Ellington & Szostak (1990, 1992), which successfully selected RNA and DNA sequences for the binding of small organic ligands, we decided to develop catalytic DNA sequences using TSA approaches. By screening a large random DNA library for binding to certain transition state analogs that had proven to be successful in eliciting catalytic antibodies, we considered that it might be feasible for us to isolate catalytic DNA molecules.

There have been many successful examples of the use of TSAs to develop catalytic antibodies. Theoretically, all of these TSAs could be used to search for catalytic DNA or RNA sequences. But at a time when there were many technical uncertainties and difficulties regarding this new technology, and no examples of DNA catalysis, we decided to challenge potential DNA aptamers to carry out the catalysis in a simple way--by stabilizing transition states through structural bending or deformation of substrates.

There is an excellent reaction that falls in this category—porphyrin metallation. This important metabolic reaction involves the insertion of a metal ion into a porphyrin ring. In living cells, protein enzymes, called ferrochelatases, provide catalysis for this reaction. Based on results from studies on the catalysis of ferrochelatases and their inhibition by a unique class of porphyrin compounds—N-alkylporphyrins, Cochran and

Schultz proposed N-methylmesoporphyrin IX (NMM) to be a transition state analog for the metallation of mesoporphyrin IX (MPIX). They then successfully derived catalytic antibodies for the reaction by the use of NMM. We chose to see whether the same TSA could be used to derive catalytic DNA sequences for the same reaction.

3.1. Porphyrins and their metallation

Porphyrins and metalloporphyrins are found widely in nature and are utilized by organisms as cofactors for a variety of enzymes and other specialized proteins. Metalloporphyrins are extraordinarily versatile, and participate in oxygen transport, electron transfer, photosynthesis, and a variety of redox chemistries, such as those associated with catalases, peroxidases, and monooxygenases.

Iron is added into porphyrin rings in the final step of the biosynthesis of hemes. Previous studies have shown that ferrochelatases (protoheme ferrolyase, EC 4.99.1.1), provide catalysis for the insertion of Fe(II) into protoporphyrin IX (PPIX) (Reviewed by Lavallee, 1988). The enzymes provide binding sites for both the porphyrin and metal ion substrates, bringing them into close proximity. Besides using PPIX and Fe(II) as substrates, ferrochelatases are able to utilize other porphyrin substrates such as MPIX, deuteroporphyrin IX (DPIX), hematoporphyrin (HPIX); and other metal ions, such as Co(II), and Zn(II). Table 1-1 shows the structure, names and side chains of various porphyrins; and Fig. 1-6 illustrates the porphyrin metallation reaction scheme, as well as the structure of NMM--the proposed TSA.

Table 1-1. Porphyrins tested as substrates[a]

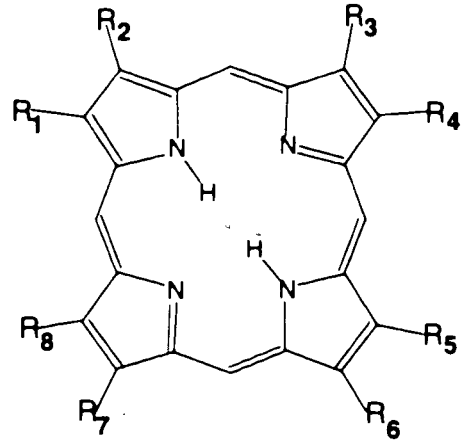

Porphyrin	R1	R2	R3	R4	R5	R6	R7	R8
Mesoporphyrin IX (MPIX)	Me	Et	Me	Et	Me	P^H	P^H	Me
Protoporphyrin IX (PPIX)	Me	V	Me	V	Me	P^H	P^H	Me
Deuteroporphyrin IX (DPIX)	Me	H	Me	H	Me	P^H	P^H	Me
Hematoporphyrin IX (HPIX)	Me	CH(OH)Me	Me	CH(OH)Me	Me	P^H	P^H	Me
Coproporphyrin III (CPIII)	Me	P^H	Me	P^H	Me	P^H	P^H	Me
Uroporphyrin III (UPIII)	A^H	P^H	A^H	P^H	A^H	P^H	P^H	A^H

[a] Names, abbreviations, and side-chain (R1-R8). Side-chain abbreviations: Me = Methyl; Et = Ethyl; V = Vinyl; P^H = CH_2CH_2COOH; A^H = CH_2COOH. Side chains for R6 and R7 =P^H for all porphyrins.

3.2. Reaction mechanism for porphyrin metallation.

Porphyrin metallation was believed to have a general reaction mechanism as shown in Fig. 1-7 (Hambright & Chock, 1974; Bain-Ackerman & Lavallee, 1979; Funahashi et al., 1984).

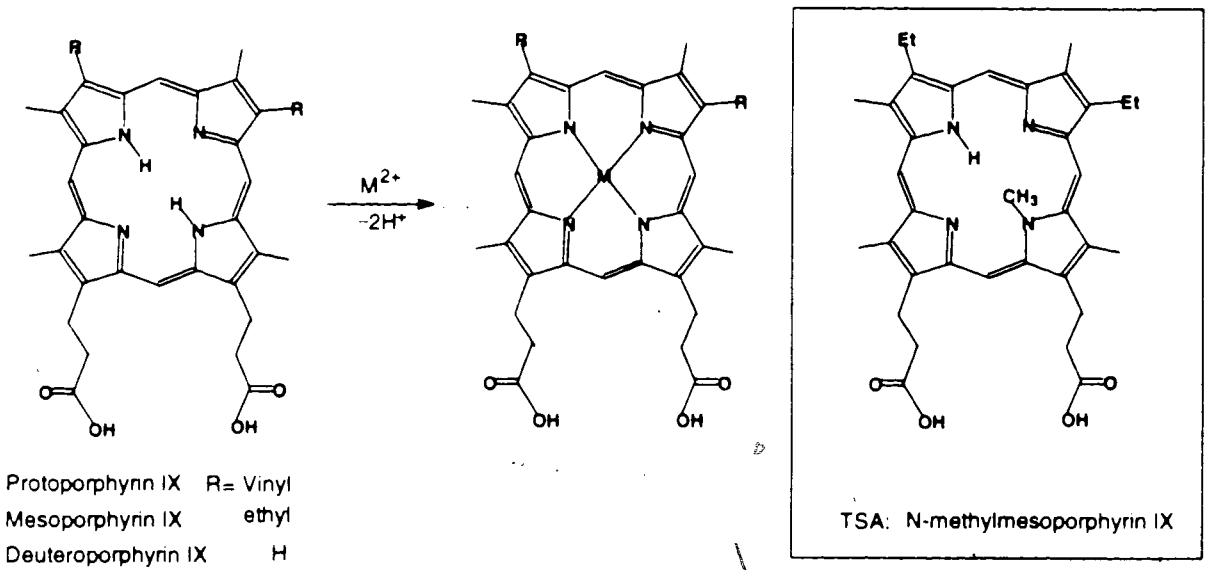

Fig. 1-6. Porphyrin metallation and its TSA. The central macrocycle is often called porphinato core (Smith, 1975). There are four nitrogen atoms in the porphinato core: two pyrrole-type (with the attached hydrogen) and two imine-type (with lone-pair electrons). The imine-type nitrogens could accept protons for protonation (see Chapter 6).

Porphyrin distortion was proposed as one of the most important steps of any porphyrin metallation. In the ground state, porphyrin compounds are expected to have a planar configuration with all four pyrrole rings in the same plane, but the planar porphyrin ring can be distorted. For instance, temperature-jump studies on tetrakis(N-methyl-4-pyridyl)porphyrin have shown that the free energy difference between planar and

distorted states is not too large, at about 8 KJ/mol (Pasternak et al., 1976). This ring distortion was also evident in some X-ray crystal structures (Fleischer, 1970).

The distortion of the porphyrin ring had a significant consequence for porphyrin metallation: it made the reaction proceed at a much faster rate (Lavallee, 1985, 1988). This conclusion came from the studies of N-alkylporphyrins. These porphyrins had a permanently distorted ring structure, as shown in X-ray crystal structure studies (Goldberg & Thomas, 1976; Lavallee, 1982; Mclaughlin, 1974), which exposed nitrogen lone-pair electrons to an incoming metal ion. Thus, N-alkylporphyrins bound metal ions 10^3-10^5 times more rapidly than their corresponding planar counterparts (Shah et al., 1971; Bain-Ackerman & Lavallee, 1979; Funahashi et al., 1984). These porphyrins were believed to be still aromatic, as reflected in their absorption maxima being very close to those of their planar analogs (with ~10 nm red shift), and their extinction coefficients being as high as or higher than that of their planar analogs. The bond lengths of both groups were also similar (Lavallee, 1987).

Outer-sphere complexation was proposed as the second step in metallation of porphyrin compounds. It was believed to be a rapid process (Lavallee, 1985), and parameters such as charge, size, and the polarity of the medium affected the magnitude of this equilibrium.

The third step of the above mechanism was the loss of two ligands from the outer-sphere complex and the formation of the two nitrogen-metal bonds. This process was thought to be concomitant to the porphyrin-metal bond formation, occurring at the same time when the metal-ligand bonds were being broken down (Lavallee, 1988).

1. Porphyrin deformation

$$H_2P \longrightarrow H_2P^*$$

2. Outer-sphere complexation

$$ML_6 + H_2P^* \longrightarrow [ML_6 \bullet H_2P^*]^{2+}$$

3. Ligand dissociation and first metal-nitrogen bond formation

$$[ML_6 \bullet H_2P^*]^{2+} \longrightarrow [ML_5 \cdots L \cdots H_2P^*]^{2+} \longrightarrow L_5M{-}H_2P^{2+} + L$$

4. Second metal-nitrogen bond formation

$$L_5M{-}H_2P^{2+} \longrightarrow L_nM{=}H_2P^{2+} + (5-n)L$$

5. Metalloporphyrin formation (proton release)

$$L_nM{=}H_2P^{2+} \longrightarrow MP + nL + 2H^+$$

Fig. 1-7. A general reaction mechanism for porphyrin metallation.

The final step was the loss of two protons from the porphyrin-metal complex. Lavallee and Onady (1981) provided the data showing that this step was not a rate-determining step because no rate difference was observed for a porphyrin with protons or deuterons bound to the pyrrole nitrogens ($H_2TPPS_4^{4-}$ and $D_2TPPS_4^{4-}$), respectively.

A non-enzymatic metallation process can be viewed as follows: a metal-ligand complex in which a ligand has begun to detach and a porphyrin molecule that is substantially deformed collide and form an outer-sphere complex. If the lone-pair electrons from a porphyrin nitrogen are at the appropriate geometry to occupy the vacant site by the leaving ligand, then the first metal-nitrogen bond is formed. Up to this point, the reaction proceeds in a reversible way; the formation of second metal-nitrogen bond

brings the reaction to completion; then two protons are released from the newly formed complex.

An enzyme mechanism was proposed as follows (Dailey & Fleming, 1983; Dailey, 1988): The enzyme first binds the divalent iron with the concomitant release of two protons from the enzyme, followed by the binding and distortion of PPIX. Iron insertion into the porphyrin macrocycle occurs with the exchange of the two pyrrolic protons to the enzyme. Then, the enzyme releases the metallation product from its active site, and initiates a new cycle. The ferrochelatases were believed to catalyze the reaction in two ways: providing binding sites for both substrates and bringing them to close proximity; and stabilizing the transition state of the porphyrin deformation step.

3.3. NMM as the TSA for porphyrin metallation

As stated above, the protein enzymes (ferrochelatases) were believed to catalyze porphyrin metallation by the stabilization of the transition state of porphyrin substrate distortion (Lavallee, 1988). The postulation of such a transition state for porphyrin metallation was drawn from the following lines: 1) N-methylprotoporphyrin was a very potent competitive inhibitor for ferrochelatase enzymes (De Matteis et al., 1980; Tephly et al., 1979; Ortiz de Montellano et al., 1981; Dailey & Fleming, 1983; Lavallee, 1988). 2) The unique feature of N-alkyl porphyrins, compared to non-alkyl substituted porphyrins, is that the pyrrole ring substitution forces one or two of the pyrrole rings to be bent out of the plane shared by the other pyrrole rings. This buckling of the pyrrole rings has been shown in a number of X-ray crystallographic studies (Goldberg & Thomas,

1976; Lavallee, 1982; Mclaughlin, 1974). 3) Owing to the easy access by metal ions to the lone-pair electrons of the nitrogen on the bent pyrrole ring, the metallation rate of a N-alkyl porphyrin is much higher than its non-alkylated counterpart (Bain-Ackerman & Lavallee, 1979; Matsushima & Sugata, 1979; Funahashi et al., 1984; Shah et al., 1971). Therefore, it was believed that in the transition state of the reaction, one pyrrole ring was distorted out of macro-porphyrin plane, exposing the lone-pair electrons of that pyrrole nitrogen to an incoming metal ion so that the metallation was accelerated (Cochran & Schultz, 1990).

This property was taken advantage of by Cochran and Schultz (1990) to generate catalytic antibodies (reviewed by Schultz & Lerner, 1995) that mimicked ferrochelatases. Cochran and Schultz obtained monoclonal antibodies by immunizing mice with NMM; two of these antibodies were then found to catalyze the insertion of Zn^{2+}, Co^{2+}, Mn^{2+}, and Cu^{2+} into MPIX.

Subsequently, Schultz and coworkers used the same TSA to derive a novel ribozyme to catalyze the same reaction (Conn et al., 1996), using an *in vitro* selection methodology. At the same time, we showed that a similar strategy could be applied to obtain catalytic DNA sequences as well for the same reaction.

3.4. Thesis overview

In this thesis, I will give a full description of the creation, optimization, and structural determination of several catalytic DNA molecules derived from an *in vitro*

selection experiment using NMM as the binding target (some of our results have also been published in the following papers: Li et al., 1996; Li & Sen, 1996, 1997).

In Chapter 2, I will first describe the *in vitro* selection experiment towards the isolation of NMM-specific DNA aptamers from a random DNA library, followed by a description of detailed studies carried out on the interaction of the selected aptamers with various porphyrins, including NMM (the TSA of the target reaction), MPIX (the reactant), and several metalloporphyrins (the products).

Chapter 3 will report the results of our findings that the short oligomer PS5.ST1, the binding domain from a parent aptamer, PS5, catalyzes the insertion of Cu(II) and zinc ions into MPIX, and other related porphyrins.

In Chapter 4, I will describe the thorough investigation on the optimization of the catalytic properties of PS5.ST1 and its even shortened version--PS5.M. I will also make a comparison of some key catalytic parameters of all types of enzymes.

A guanine quadruplex model is presented in Chapter 5. The model is based on our catalytic and DMS-footprinting data on PS5.ST1, its mutated sequences or structure variants. The model is supported by the other catalytic sequences from the final selection pool. I will also describe our efforts in modifying the thrombin aptamer into a catalytic structure for porphyrin metallation, and in converting some non-catalytic aptamers in the final selection pool into catalytic ones.

Chapter 6 summarizes some preliminary spectroscopic data on interaction of NMM, MPIX with PS5.ST1 and various other catalytic and non-catalytic sequences, with the emphasis on the finding that after binding to PS5.ST1 or other catalytic sequences,

MPIX gives a visible spectrum close in many aspects to that of NMM but not to that of monomeric MPIX itself. We further found that the DNAzyme increased the basicity of the imine-type nitrogen (for protonation) of MPIX by 2 to 3 pH units. This observation is interpreted as the consequence of the deformation of MPIX by the catalytic DNA sequences.

Chapter 2. Selection and Characterization of NMM-binding DNA Aptamers

1. Introduction

To realize our goal of finding DNA sequences catalytic for porphyrin metallation using a TSA approach, we wanted to isolate DNA sequences with high and specific affinity for NMM, the TSA for the targeted metallation of MPIX.

Although a variety of protein-porphyrin complexes and conjugates exist in nature, no functional role *in vivo* has yet been attributed to porphyrin-nucleic acids complexes. Indeed, naturally occurring anionic porphyrins such as NMM and MPIX have not been found to associate with double-helical DNA, either *in vivo* or under experimental conditions *in vitro*. However, that porphyrins have the potential to interact with nucleic acids has been demonstrated by the studies on a class of synthetic cationic porphyrins, including meso-tetra-(4-N-methylpyridyl)porphine, containing two or more positive charges, which have been found to bind double-helical DNA (reviewed by Fiel, 1989; Gibbs et al., 1988; Marzilli, 1990).

We tested first whether it was possible to isolate NMM-binding ssDNAs through *in vitro* selection experiments. Besides being successfully used to derive catalytic nucleic acid sequences (see text in Chapter 1), *in vitro* selection techniques have also been extensively used to isolate RNA and DNA sequences that bind a variety of target molecules (reviewed recently by Gold et al, 1995; Osborne & Ellington, 1997). The targets include small molecules such as dyes (Ellington & Szostak, 1990, 1992); amino

acids (Famulok & Szostak, 1992; Connell et al., 1993); cofactors such as cyanocobalamin (Lorsch & Szostak, 1994b), flavin and nicotinamide (Lauhon & Szostak, 1995); bases and nucleotides (Sassanfar & Szostak, 1993; Jenison et al., 1994; Huizenga & Szostak, 1995); as well as proteins (Tuerk & Gold, 1990; Tuerk et al., 1992; Bock et al., 1992, Jellinek et al., 1993, 1994). The specifically binding aptamers have been found in a number of instances to bind their targets with sub-micromolar and nanomolar affinities (Gold et al., 1995). The large, aromatic, ring structures of porphyrins should make them attractive targets for binding by specific DNA secondary/tertiary structures. The first published reports on DNA and RNA aptamers had, in fact, described the isolation of molecules that bound polycyclic dyes (Ellington & Szostak, 1990; 1992).

If indeed anionic porphyrin-binding DNA aptamers could be isolated, would these aptamers be able to distinguish between homologous porphyrins with subtle structural differences? This directly relates to the question of whether selected NMM-binding aptamers could successfully catalyze porphyrin metallation. According to the transition state theory, enzymes catalyze chemical reactions by providing much higher affinities for transition states than for ground state substrates. Applying this principle to the case of porphyrin metallation, we have to make sure that the selected DNA aptamers have high affinity for NMM (the TSA) and weak affinity for MPIX (the substrate). Fortunately, the *in vitro* selection technologies used to obtain nucleic acid aptamers are unique in the sense that DNA or RNA molecules can be selected in a positive sense for binding to a given target (such as NMM in this case), then subjected to negative selections for diminishing binding affinities for closely related molecules (such as MPIX in our case).

That aptamers can be highly discriminating for recognition of closely related structures has been notably demonstrated with RNA molecules that discriminate between caffeine and theophylline (Jenison et al., 1994). Since then, other examples have been reported.

Given this, it is possible to pose the question that if discriminating aptamers could be isolated, which bound with higher affinity to NMM than to MPIX, whether such aptamers would then show chelatase-like activity.

In this chapter, I will first describe the *in vitro* selection experiments carried out by us for the isolation of NMM aptamers from a random DNA library; then I will describe the data from various chemical, enzymatic, and physical studies on interactions of the selected NMM aptamers with NMM, MPIX, and various metalloporphyrins (potential products of porphyrin metallation).

2. Materials and methods

2.1. Materials

Porphyrins were purchased from Porphyrin Products (Logan, Utah) and used without further purification. Avidin-conjugated agarose beads and oxirane-acrylic beads were from Sigma. Deoxynucleotide triphosphates (dNTPs) and the T7 Sequencing Kit were from Pharmacia; [γ-^{32}P]ATP (3000Ci/mol) from Amersham; T4 polynucleotide kinase, T4 DNA ligase, *Bam*HI, *Hind*III, *Pvu*II, and DNaseI from BRL; *Ban*I and *Sty*I from New England Biolabs; *Taq* DNA polymerase from Perkin Elmer; Bluescript M13+ plasmid and MC1061 competent *E. coli* were gifts of Dr. C. Boone at Simon Fraser

University; the "random" DNA oligomers (R1, R2) and the biotinylated oligonucleotide primers were synthesized at the University Core DNA Services at the University of Calgary.

2.2. DNA library

The random-sequence DNA library used in this work was constructed according to the method of Bartel and Szostak (1993), with minor modifications. Two synthetic polynucleotides, R1: 5'-TTGATCCGGTCGGCACC-N_{76}-CCTTGGGTCATTAGGCGA; and, R2: 5'-CGGGACTCTGACCTTGG-N_{76}-GGCACCTGTCCACGCTC, were each rendered double-stranded by PCR. R1 was divided into two pools and restriction-digested-- one pool with *Ban*I (cutting at GGCACC) and the other with *Sty*I (cutting at CCTTGG); R2 was digested with both enzymes. A two-fold ligation was then carried out with T4 DNA ligase, to give duplexes of the form R1-R2-R1, containing a total of 228 random base-pairs. 540 µg of ligated product was obtained, corresponding to 1.8×10^{15} different molecules. This library was then amplified with a large-scale (500 ml) PCR, using the primers R1P1-biotin (5'-biotin-TCGCCTAATGACCCAAGG) and RLS (5'-GGATCTTTTTGATCCGGTCGGCACC).

Single-stranded DNA was purified from these amplified sequences by allowing the biotinylated duplexes to bind to avidin-agarose beads (avidin : biotin = 10:1). After washing with 15 volumes of avidin column buffer (50 mM Tris, pH 7.4, 200 mM NaCl, 0.1 mM EDTA) to remove non-biotinylated duplexes, the unbiotinlyated strand of bound duplexes was recovered with 3 column volumes of 0.2 M NaOH. The eluant was

neutralized immediately with 0.2 M HCl + 0.5 M Tris, and the DNA recovered by ethanol precipitation. A total of 7.14 mg of ssDNA was obtained, corresponding to ~26 library equivalents.

The final, 283-nucleotide, single-stranded DNA had the sequence:

5'-GGATCTTTTTGATCCGGTCGGCACC-N_{76}-CCTTGG-N_{76}-GGCACC-N_{76}-CCTTGGGTCATTAGGCGA.

2.3. Selection columns

NMM selection columns were prepared by the derivatization of oxirane acrylic beads with NMM. The beads were allowed to react with NMM in 0.1 M phosphate buffer (pH 4.0) for 48 hours in the dark at room temperature. The disappearance of NMM with time was monitored by HPLC. After 48 hours, the NMM was attached quantitatively to the beads (10 column volume washes with 0.2 M NaOH washed off less than 2% of NMM from the column). After the completion of the attachment reaction, the column was washed with 1 M Tris (pH 8.0) and incubated for a further 48 hours with 4% mercaptoethanol to inactivate unreacted epoxy groups. Finally, the column was equilibrated with SB buffer (100 mM Tris acetate, 200 mM sodium acetate, 25 mM potassium acetate, 10 mM magnesium acetate, 0.5% Triton X-100, and 5% dimethyl sulfoxide, final pH 7.1). Columns treated in this way were found to have very low non-specific binding of single-stranded DNA (<1%).

To obtain blocked column material for negative selections, the oxirane beads were allowed to react with excess mercaptoethanol at pH 8.0 for 48 hours, and then assayed for their level of non-specific ssDNA binding. This was also found to be low (<1%).

2.4. Selection protocols

The NMM columns were washed and pre-equilibrated in SB buffer. To further reduce the non-specific binding of single-stranded DNA molecules to the column matrix, an initial negative selection was carried out on a "negative column", which contained oxirane-acrylic beads inactivated with mercaptoethanol (as above). For a given round of selection, 5'-end labeled ssDNA was denatured in TE buffer at 90°C for 5 minutes, then allowed to cool slowly (over an hour) to room temperature. The solution was subsequently made up to SB buffer.

The folded DNA (^{32}P-labelled) samples in SB were treated to a 100 µl negative column (containing no attached NMM); the DNA was allowed to equilibrate with the column for 30 minutes, following which the unbound DNA was washed directly onto a 400 µl NMM column with three volumes of SB buffer, and incubated with the NMM column for 2-3 hours at room temperature. Unbound DNA was washed away with SB buffer until no more radioactivity could be detected in the washes.

In round 1, a total of 3.0 mg DNA was applied to a 4 ml NMM column; in rounds 2 and 3, ~100 µg of DNA was used; from the 4th to the 12th rounds, 20-50 µg of DNA was applied. While in the first three rounds, TE' buffer (10 mM Tris, pH 7.4, 10 mM EDTA) had been used to elute the specifically bound DNA molecules from the NMM

column, in rounds 4-6, high concentrations of free NMM (2.1 mM) were used to compete the DNA away from column-bound NMM (the column NMM concentration = 0.5 mM). In round 6, the DNA was applied to NMM columns twice in succession; in rounds 7-12, a "negative" elution with free MPIX (0.1 mM) was used on the bound DNA prior to "positive" elution with free NMM, as above. This was done to eliminate those NMM-binding DNA molecules that also bound with high affinity to MPIX.

2.5. PCR

PCR was carried out in the following buffer: 10 mM Tris, pH 8.3-9.3, 50 mM KCl, 2.5-10 mM $MgCl_2$, 0-5% glycerol, 0.2 mM of each dNTP, 1 unit of Taq polymerase, 1 μM of each primer (RLS and R1P1-biotin), and 0.01-0.05 μM 5'-^{32}P-labeled RLS, for each 100 μl of the PCR solution. Reactions were usually carried out in 100-300 μl volumes. In the later rounds of selection, PCR yields were consistently low, owing presumably to the formation of strong secondary structures in the DNA molecules being enriched; therefore the PCR conditions were re-optimized before each new round, generally by changing one of three parameters: buffer pH, $MgCl_2$ concentration, and glycerol concentration. The amplified DNA was phenol/chloroform extracted, ethanol precipitated, and bound to avidin columns for the generation of single-strands (see above). In most rounds, the single-stranded DNA obtained was further purified by preparative gel-electrophoresis before being subjected to a new round of selection.

2.6. Cloning and sequencing

Following the completion of 12 rounds of selection on NMM columns, the DNA pool was amplified for cloning by PCR amplification with the following two "cloning" primers: RLC: 5'-CTTGTCTGCAG**GGATCC**TTTTGATCCGGTCGGC-3'; and, R1P1C: 5'-GATATC**AAGCTT**CTCGAGTCGCCTAATGACCAAGG-3'. The highlighted sequences show *Bam*HI and *Hind*III sites, respectively. The PCR products were gel-purified, digested with the above enzymes, and gel-purified again prior to ligation to the *Bam*HI and *Hind*III-digested and gel-purified large piece of the Bluescript M13+ plasmid. MC1061 competent cells were transformed with the ligation mixtures. Sixty recombinant clones were picked for the long sequences (P series) and fifty that contained the shorter sequences (PS series; see Results). Twenty-four clones of the PS series and 24 of the P series were sequenced (the P clones in both directions) by the dideoxy method, using a T7 Sequencing Kit (Pharmacia).

2.7. Dissociation constant determinations

The binding affinities of different aptamers to NMM and, indirectly, to other porphyrins, were measured using the methodology of Connell et al.(1993). ^{32}P-labeled DNA was applied in SB buffer to a 0.1 ml NMM column, allowed to equilibrate for 30 minutes, then quickly washed with a few column volumes of SB buffer until the unbound DNA had been washed away. Specific elutions were then carried out with solutions of 100 μM NMM as well as solutions of other porphyrins, in SB. K_d was calculated according to the formalism: $K_d = L \{(V_{eL} - V_n)/ (V_e - V_{eL})\}$ (Connell et al., 1993), where

L was the concentration of the free ligand in solution, V_{eL} the elution volume in the presence of free ligand in solution, V_e the buffer elution volume in the absence of free ligand, and V_n the void volume of the column (taken to be 70% of the volume of the packed column).

2.8. Footprinting

Final DNA concentrations used in all footprinting experiments were between 1-3 ng/µl. Reactions were carried out in SB buffer at room temperature, unless otherwise specified. Single-stranded aptamer DNAs were 5'-end-labeled with polynucleotide kinase and [γ-^{32}P]ATP, and gel-purified. The DNA was denatured and then allowed to fold in SB buffer, as above. Porphyrins were prepared as stock solutions in SB buffer. Final DNA-porphyrin complexes were made up by combining appropriate aliquots of the DNA and porphyrin stocks, which were then made up with SB buffer to final volumes of 15 µl (for DMS methylation), and 10 µl (for hemin/KO_2 and DNase I cleavages).

2.8.1. Methylation protection

Aliquots (0.8 µl) of a freshly made 2% dimethyl sulfate (DMS) in double distilled water were added to 15 µl DNA/porphyrin solutions. Samples were incubated at room temperature for 30 minutes, then ethanol precipitated. The pellets were washed and treated with piperidine using standard Maxam-Gilbert protocols, and the cleaved DNA analyzed in 10-20% denaturing polyacrylamide gels.

2.8.2. Hemin/KO_2 footprinting

Aliquots (2.5 µl) of a freshly made solution of 150 mM KO_2 in SB were added to 10 µl DNA/porphyrin samples. These were incubated at 37°C for 30 minutes, and the reaction quenched by adding 6 µl of formamide gel-loading buffer and heating at 85°C for 3 minutes (Ward et al., 1986). One-fifth portions of the samples were analyzed in 10-15% denaturing polyacrylamide gels.

For the aptamer PS5, the hemin/KO_2 footprinting was carried out within gel fragments containing the aptamer. Separate samples of end-labeled PS5, with added hemin (0.5 mM) and without, were run in a non-denaturing gel. The gel bands containing the aptamer were cut out, crushed, and pre-incubated with 50 µl of 1 mM hemin in SB for 30 minutes at room temperature. 50 µl of 30 mM KO_2 in SB was then added, and incubated for 30 minutes at 37°C. Finally, the DNA was eluted from the gel slices and ethanol precipitated prior to running in a 15% denaturing gel.

2.8.3. DNase I footprinting

These were carried out under conditions similar to the hemin/KO_2 experiments, except that 1 µl of DNase I (from a 0.02 unit/µl stock) was added to each 10 µl DNA/NMM solution in SB buffer.

2.9. Gel mobility shift studies

Single-stranded aptamers were denatured and re-folded as above, then either incubated or not incubated with 100 µM NMM for 30 minutes before loading in a non-

denaturing polyacrylamide gel run at 4°C in 50 mM Tris-Borate + 10 mM KCl + 5 mM $MgCl_2$ buffer.

2.10. Spectroscopic studies

2.10.1. UV-visible spectroscopy

The concentration of DNA used for UV-visible spectrometry was 5 μM; and, measurements were carried out in a dual-beam Cary 3E UV-Visible Spectrophotometer. PS2 DNA was allowed to fold in SB buffer in the sample cuvette. This DNA solution (as well as DNA-free SB buffer in a separate cuvette) were then made progressively to 0, 1, 3, 5, 10, 15, 20, and 30 μM of NMM and scanned from 300 to 700 nm (spanning the Soret and visible absorption regions of the porphyrin) in comparison with a cuvette containing only buffer, following each addition.

2.10.2. Circular dichroism spectroscopy

Circular dichroism measurements were carried out in a J-700 CD-spectrometer. 3 μM folded aptamer (PS2, PS2.ST1) in SB buffer was first scanned in the absence of added NMM. Then, 1, 3, 5, 10, 15, 20, and 30 μM of NMM were introduced, and CD spectra taken for both the DNA absorption regions (200 to 300 nm) and the Soret and visible absorption regions of the NMM (300 to 550 nm).

3. Results

3.1. Selection

Selection was carried out for a total 12 rounds, and the percentage of NMM-binding DNAs from each selection pool versus selection round is presented in Fig. 2-1. There was very little DNA bound to NMM from the selection pools 1-3, but the binding percentage increased as the selection was in progression. By round 6, ~15% of the sequences in the pool could bind to NMM. In order to obtain the sequences with higher affinity for NMM than for MPIX, a "counter-selection" strategy was applied, in which the

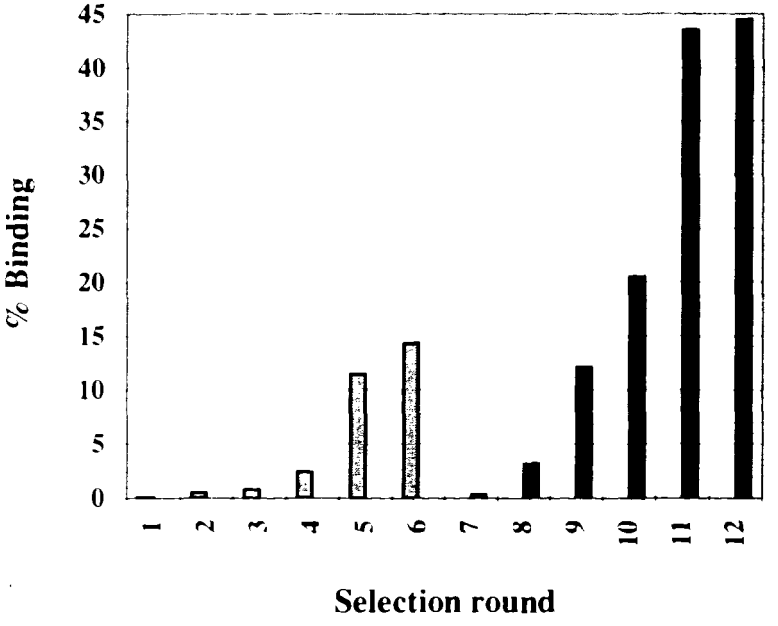

Fig. 2-1. Results of *in vitro* selection for NMM-binding DNA aptamers. Gray bars indicate selection rounds without counter-selection for MPIX while dark bars represent selection rounds with pre-elution of MPIX.

elution with the MPIX solution was carried out before the elution with the NMM solution. The data in Fig. 2-1 (p.46) shows that most of the NMM-binding DNA sequences in pool 6 could bind to MPIX as well. However, the counter-selection strategy showed its effectiveness in diminishing this MPIX-binding affinity of the further enriched pools. By round 11, the pool DNAs bound quite specifically to NMM but not strongly to MPIX. The binding percentage was leveled off at round 12, and DNA aptamers in this pool were cloned and sequenced.

3.2. Appearance of a "small" porphyrin-binding DNA library

During the selection procedure on the 283-nucleotide DNA library, particularly in the later rounds of selection, a significantly smaller-sized DNA began to appear in large amounts following PCR amplifications of recovered DNA. In general, two sizes of DNA PCR products were always to be seen with this particular random-sequence library: One the normal sized 283 nucleotides, and the other approximately 120 nucleotides long. By the third selection, the small-sized DNA was the dominant product after 20 rounds of PCR amplification, arising, presumably, from mispriming by the primers RLS and R1P1-biotin off the two six-nucleotide constant regions (CCTTGG and GGTGCC) separating the three random regions. To correct for this situation, a separate primer, RLT, was synthesized to replace RLS (RLT lacked the last five nucleotides of RLS at the 3' end). This improved the yield of the full-sized 283 nucleotides somewhat. However, in the later rounds of selection, it became increasingly difficult to amplify the 283-nucleotide product, even when gel-purification was used to eliminate the smaller product prior to

each new selection. Beyond round 10, the "small" and "large" aptamers were subjected to separate selection and PCR cycles and were cloned as distinct populations of aptamers. The "PS" family of clones described in this paper refers to the small aptamers and the "P" family to the full-sized ones.

3.3. Comparison of aptamer sequences

Twenty four clones were sequenced from each size class of aptamer, to determine whether a common sequence (and therefore folded structure) motif was responsible for the binding of NMM. Fig. 2-2 (p49) shows the random sequences from twenty four each of the smaller (PS) and normal size (P) classes of aptamers. The most notable feature of these sequences is the presence of at least one highly guanine-rich motif (underlined and italicized) in each sequence. The pool of the larger class of aptamers (the P class) had similar motifs, and in some cases (such as in P3, described later) more than one of these motifs in a given aptamer. A rigorous comparison of the sequences using the FASTA program revealed the highest degree of homology to be present, in fact, in the guanine-rich regions, which were typically 15-30 nucleotides long. From this collection of clones, two small aptamers, PS2 and PS5, and three large aptamers, P3, P7, and P9, were randomly selected for a more in-depth study of their properties. Most of our studies focused on PS2, which gave the most defined footprints. At a later stage (described below), a short oligomer, PS2.ST1, corresponding to the guanine-rich region of PS2, was also synthesized for study.

Fig. 2-2. NMM-binding sequences from generation 12. The random regions of twenty-four short (PS family) and the large (P family) aptamers. Each aptamer appeared to have a single, very guanine-rich motif (the motifs containing between 55% and 78% guanine, with the balance being overwhelmingly thymine). No unambiguous consensus could be found between these sequences in terms of the positioning and number of contiguous guanines. The large family sequences contained similar guanine-rich motifs, with at least one such motif per aptamer.

PS series

ps2 TTGCC TAACC GTGAA GGTAA AACGA TTTAG TCAAA C*GTGG GAGGG CGGTG GTGTT G*ACTG ATCGA TTTTA TTCCA (65% G)

ps3 AGGGT TGATC AACTA *G GGTA GTCGG GAGGT GGTGG GG*CTT GTTTG TGTCA GCCTG CAGTG GACAA CTCTT AATCT G (68% G)

ps4 AGGTG TTATC ATTCA TTTCA CTGAA *GGAGG CGGAG GTTGG TTCAG GTG*CT TTCAG GGAAA TTCCG CGGTG CTTA (56% G)

ps5 GTGTC GAAGA TCGTG GGTCA TT*GTG GGTGG GTGTG GCTGG* TCCGA TCCGC GATCT GCTGA CGCTG GTTAG GT (66% G)

ps6 ATCTG GCTAT GTTAG TCTTA TCACC ATGAC CGGAT GCCCC AAAA*G GTGGG TGGGT GGCGG* TAGAA TTTTG GTGTG T (75% G)

ps7 GAGCC TCTGA TCAAT TAAAC ATTGT GTTAC T*GGTG GGTTT ATGCA GGTGG GTGGG* AACCA GGAAC ACTAT GTCCA (56% G)

ps8 ATAGG TTTTG CTGGG GTAC*G GAGGT GGGCG GATGG TAGTG GTG*CC TGGCC CAGGA AAAAT TAGGG GCGAT GTCCA (62% G)

ps9 ATCTA TGCTT ATTGG CCAAG AGTCG AATAA GGTGA TTC*GGG TAGGG CGGGC GG*TTC AATTA TTCGA CCTCG CTTTT (73% G)

ps10 AATTG TGCAC AGCAG GACCG AATTT TTGAC TC*GGT GGGGC CATGG CGGGT GGGGC GGAG*A AATTT GGTCT AAGC (66% G)

ps11 GATAA AGTTG TC*GGA TGGAT GCGGG TTGGG CTG*AT ATGAG AACTT TCAAG GGACA GACCT CAGGA TTCTA AATCG (57% G)

ps12 CATCA TGAGT TT*GGG GAAGG GTCGG TGGGT G*CAAA AGTGG AATCC GCGAT TGATG GGGAC TCGTC ATCCC TAGGG A (68% G)

ps13 CTTGG TCATT AGGCG AAGTA CCGGG GAGCG AACTA C*GGGC GGTGG GTACG GG*AAA GATTG TTCTG TAGTG ATGGT C (68% G)

ps14 ATTTC GAGAG AGTAC *GGGTT GGGTT TGGGC AGG*AT AACAG TTTGG TGCTC TCTGG ATTAT GCCGA TGCCG GCC (61% G)

ps16 TGATT GAACA CAATT CTGCA GACTC TGAGC AAGGG TATGG GGTTT TTGAC *GGGTG TGGTC GGCGG* TAACC TACAT C (67% G)

ps17 TAGAT TTGTA CCC*GG GTTGG CGGGT GGTCT GTAAG GGG*TA CAAAA TCATG TGGGT AGTCT TTCTG CTTTG CCTGC AA (60% G)

ps18 ATTTC *GAGGG AGTAC GGGTT GGGTT TGGGC AGG*AT AATAG TTTGG TGCTC TCTTG AAGTA TGCCG ATGCC GGCT (57% G)

ps19 ATTAC AACAT AGTCA GGTTA TA*GGG CGGGA GGGTG G*TACA ACTGG CATTG TAAAT AGACG GATGC ATGTT GACTC (79% G)

ps20 TAATC CTATG GTTTT TGCGA CTCGG CAATT CGTAA *GTGGG AGGGT GGTGG AG*ATA CGTAT GCTAG GTCAC GGGTA (71% G)

ps21 ATTTC GAGAG AGTAC *GGGTA GGGTT TGGGC AGG*AT AATAG TTTGG GTCTC TCTGG AAGTA TGCCG ATGCC GCA (61% G)

ps22 GATTA GCGGG TTAGT GGCAT TCGCT GCT*GA GGGGT GGGAG GTTGG* ATAAA TTGCG AATCC CATTA AAAGA TCC (71% G)

ps24 AGGAT CGAGA ACAAT GACCA TGAAT GGAAA CATA*G AGGTG GGTGG TTTTT AGTGG G*TTGC ATTTA TGTTT ACATA C (54% G)

ps25 GGTCC ATTCG GCTAT CCAGA C*GGGA GGGTG GGTGG ATTGG* ACACT TATGA ATGGA CCCTG CCCCC TTTCA TGTGC (68% G)

(Continued from last page)

ps26 ATCAT TAGGT AACTC GAC*GG GGTTG GGTCC GGGCG GTAGG* TTGAG TTTCC ATAAA ATCCG GTGAC GATTA TTATG A (64% G) .

ps30 ATAGG TTTTG CT*GGG GTACG GAGGT GGTCG GATGG* TAGAG GTGCC TGGCC CAGGA AAAAT TAGGG GCGAT GTCCA (61% G)

P series

p1 ACCAT TAATA GATGT TAAAC TAGAG GCTTA *GGGTG GGATG GGAGG AGCCT TGGGG* TTACA TCATT ATGCG GTGTT CGTTA TATCC GTGGA CTTAT ACAAC AGCGT CTATC ATGGG TCGTG TCCTC GGGTG AGGGA GGAAA CCCAT TAGTA ACACC GTCCG TGATG AAGTT GTTAA CGGCA CCTCG TCCAC TAAGA ATGTC CGTTT ATTTA TCTAG GAGGA AGTGG TTCCG GCCTA TCGTA AGCCT TTTAT GTACC (64% G)

p2 GGCCC TGTGG AAGAG CGATA GTGCC TTTAA TAGTT GAGGG CGAAG TGACA GTCTT CCCTG AGCTT TCGTT CCTTG GTATA TTACC ATATA AGCCT CTTGG TTGTG TATAA TAATG ACCTA GAAGT CGATT GAACT CATAG GCACC TAACG CGCCA TAAAG GCAAT CTTGT GGACA C*GAGA CGGGG TGGGA GGGTT G*ACTG ATTGT GT (65% G)

p3 TCCAA TGCGG TTAGT TATC*G CGGAC GGGGC AGAGG G*ATGT ACAAG ACTT*G TTGGG TGGTC ATGTG GGTGG* TTATT CCTTG GATAT CACAG TTGTC TGGCA TTTGG TAACT TCCTT CTCAC CTCGT GAAAG TTTGC ATCAT AGCCA GATTC TGGGT GGGCA CCTTG CAAAC TTTCA CAAGG TTGAG GATTT GCTGA CCCGG ACTCG CACGT AACTT TCCTT TGCAA ACATT ACGCT AGA (65% G and 57% G)

p4 ATTCC GAGAG TATGT AC*GGG TTGGG TTTGG GCAGG* ATAAT AGTTT GGCGC TCTCT ATAAG TATGC CGATG CCGCG CCCTT GGTCA TTAGG CGAAC CTTGG TCATT AGGCG AATAC AAGCG TGGTT AATAA CCGGA TCTTT TGATC CGTCG GATAA TAGTT GGCGC TCTCT ATAAG TATCG ATGCC GGCCC CTTGG TCATT AGGCG AACCT TGGTC ATTAG GCGAA TAGAA GCGTG GTTAA TAACG GATCT TTTTG (61% G)

p5 GAGAC CCGAA CAAGA GTTGA ACAGA GAATG GTCAG CCGGA GTGTT ACGTC GAAGT GTTCT TAGCA ACCGA ATCCT TGGTG CAACT ACAGC GACCG GATTC TGTAG ACCTT ATGAT GGGTA TGTGA CAGCT CCACG ATCTA TGGCA CCAAG GAGAG TGCA*G TGGTC GAGGT GGGAG GG*TTT ATTTT ATGAT CCTTG GGTGA CAATG AATGT GGAGT TTGCA CCCTT GGTCA TTAGG CGAC (67% G)

p6 GTGGA TCTTT TTGAT CCGGT CGCAC CAATA GGATC GGGGC AGGCT CTCGC TTCCA CAGGT AAAAC GAT*GG AGGGC GTGGG AGG*TT TTGTA GAGCG TTGTT CCTTG GAAAG CGGGA TGCCG GGCCC AACCG TGTGG TGTAC ATTGT CACGT AACGC AAGGA GATAA ACTGT AATCT GGGCA CCTAG CCGGT TAGTG CATTG TCAAC GCGCT GTTGC ACTAT TAGAC AACCC TGCTA ACAAG GCAAA CCACT ATTGT (73% G)

p7 GCATC GGTCG ACCAA AGCGT CGTTG TTTGC TCTTA TGGTC AGGAC GGTGT GTCGT GGAAG TCATG AACCT TGGCG CAGGA TACGG GTTTG CATAT TGCGT GCATT AATAT *GGGAA GGTGC ATGGC GGGCG GTTGG GTGG*T TATGT AACGG CACCT GTCCG GTACT TAATA GTGCG CTAGG AGATG CCCGT CTATA GCCCT GAAGG AGCAA CGATC TTACT CGTCA TCTTA (62% G)

p8 ATATT ACCTT GGTCA TTAGG CGAAC GTGGA TCTTT TTGAT CCGGT CGGCA CCTTG GTCAT TAGGC GATGG ATAAT TCT*GT GGGTG GGCTG TGGTT GGAG*A AGTAT CCGGA GCTGT CCCCT TGGTC ATTAG GCGAA TATGC CTTGG TCATT AGGCG AATAT GCCTT GGTCA TTAGG CGGAT ATGCC TTGGT CATTA GGCGA ATTAG GCGAC CACGG ATCTT TTTGA TCCGG TCGGT A (62% G)

p9 GGGGA GACAG AATCT AGACT CCTAC TACGC TTGTG ATTGG TTGTT ATTAT TTGCG TGCAA AAAAT TTATT AATTC CTAGG AAGGT GGCTT GATC*G GCAGG GGATG TGGTG GGTAT GGGCC GACGG G*CACC TATCA GATGT GAGGC AACTA TGGAA ATCAT CTGGG ACCTA TAGCA ACTGA GTTTGC GTTTC TCGAT TGTAT AT (59% G)

(Continued from last page)

p10 CTTGG TCATT AGGCG ACCAG GGATC TTTTT GATCC GAACG GCATG GATCT TTTTG ATCCG GTCGG CACCT TGCTC ATTAG GTGAA TGGAT CTTTT TGATC CGGTC GGCAC CAATA TAGGA GTATG TGCAA CTTCT GGACA TATTG CGGTG GGAAG GGAAT AGCGG TGGCA CTCCC A (74% G)

p11 GAAAT AGATC TTTTA CTTTT GGATG CCAGA CACTT ATGTT CCCTC TAGCG AGGCT GCGGA TTTCT TTGAA GTAGA TCCTT GGCTT AGGGA GGGAG GGTGG AAGAA GGACT CTACT GACAA TCCGT ACATG AGTAA ACCGT ATCAT CGGGC ACCAT ACCTG TTTCC AGGAC TAAGT ATACA CAGTT AATGA CTGGC TTTGC AGTGT GATTG TTTCA CAGAT CAATC CTAC (67% G)

p13 AAGAA AATGC AGGGT TTCAA CGGGA TGTGT TGGGT GGGAA TCGGG TGGCA ATAGC GGTGA AGTAC TTTTC TTCTC TCCTT GGTTT CGAAG ATACT CCGTG GATAC TTGAA CATCT CTCTC TTGGA GGACG TTCGA AGGGA TAGCG TCAAT GTAAT CAGGC ACCAT CCGAC TGTAG TATGG ATGGT GCTCA AGTAA GCACG GGAAT GCATC GTGAA CTATG TGTCT CGTTG CTTAA TCAA (59% G)

p14 AGACC CGAAG TGCAC GGAGA CCCGG TTATT CTTAG GCCAG TATGG GAGGG ATGGG AGGCT GCCTT AGTAT AACCT TGGTC ATTAG GCAAG TGGAT CTTTT TGATT CCGGT CCGGC ACCAT TTCGA GAGAG TACGG GTTGG GTTTG GGCAG GATAA TAGTT TGGTG CTCTC TGGAA GTATC GGATG CCGGC CCCTT GTCAT TAGGC GAAGT GCA (73% G, and 61% G)

p15 GTATG GTCTA CAGCG AACCC TGCAT TAACT CGGGA GTTGT GGTGT GGTGG GCGGG ATTCT GTCGA ATGTG AATGA ACCTT GGCAA TGTGG TAATC AAGGT ACATT GTTCG CCCTC GCTTT TCGTT TGCCT GGGCA AGTGG TGTCA AGAAA TGTAG GCACC TGAAT AGCAC TCGAC GCCTC TGGAT ATGGA GGCTC ACTCT CTAAG TCATT GATTA ATTCA CAGCA GTTCT TGTCT C (67% G)

p16 TTGTC ATTAG GCGAA GTATT CCAGG GTGGA GGTGG TTTCA ATGTA CTCAA TACGC CCGTC CTTGG TCATT AGACG AGGCT GGATC TTTTT GATCC GGTCG TCACC CCTTG GTCAT TAGGC GAACA ACAAA TACCA CCCTT GGTCA TAGGC TAAGG TGGAT CTTTT TGATC CGGTC GCACC ATATA (75% G)

p17 GGACG GAAGT GAACC ATTGT ACAAT CATTG TCGGC TGGCA AAATT ATTAA GTTGT TCGTA AAAAT GAGGT TAGGC CTTGG GGTCG GAGGT GGGTT AATTT TAAGG AGGAT TTAGG ACTAT ACTCC ATCGA ATGTT GCTAG TCCGA CTTAT TATAT ATTTT GTCAC CATGG GTGCG CTAGA GGTTT GATGT GCCCA GTTTT TTATT CTTTA GATCT ACATG GTACG CCTTG TACAT ATTGT GTA (57% G)

p19 GGAGA AGAAG AGCCT TGGTC ATTAG GCGAG CATGG ATCTT TTTGA CCGGT CGTAC CTTGG TCATT AGGCG AACTA ATCCT TGGTC ATTAG GCGAG CTGGA TCTTT TTGAT CCGGT CGGCA CCCTT CAGGG ATAAA GGTTG GGGTG GGTAA GTGGG GAAAG GTTTA ATTTT GTTAC TCCCT GAAGG CCCTT GATCA T (67% G)

p20 GCGCC AATCG GCAAT TGATT CTTCC TCTTA CCGGA AAGCC GCATC CCATT GGCTC TGATT CGGTT ACCCC TTGGA AATAT GTCTT GTGGT AGGAG ACTAT AAGGG AATTA CTTTG ACGGT GGTTG GATGG TTGGA GGCGA AGTAC TTCCC GGCAC CTGAA TGATC TAAAG TCTTT TCGGT AGACT CACTT ACCAA GAGCG CGTTT TAGAT AATAT TATCT GTACT CGATT T (59% G)

p21 TGTCT CTACT CACCA ACTGA CATGG GCGTT TTTTA TATAT TCTTG GGCGG GTATG GGTTG TGGAT CTAAA AAACT GACCA TGGCA CATAT CCCGG ATACA TCACA CCCTG GAACT CAACG GTTTA TTGCG CCCTC TCTTC GCACC TCAGT GTATG ATACA CAATT TCTCT GGGTA ACGCT GTTAT CACTG AGGTT TCGTT ACATT GCCTC ACAAG TCTAA A (63% G)

p23 ATCGA GAACA ATGAC CATGA ATGGA AACAT AGAGG TGGGT GGTTT TTAGT GGGTG GCATA TATGT TTACA CACCT TGGTC ATTAG GCGAA GTATT CTAGG GTGGA GGTGG TGTCA ATGTA TCTGA ATACG CCGT(73% G; and 71% G)

(Continued from last page)

p24 GCATC GGTCG ACCAA AGCGT CGTTG TTTGC TCTTA TGGTC AGGAC GTTGT GTCTT GGAAG TCAGG AACCT TGGCG CAGGA TACGG GTGTT CATAT TGCGT GCATT AATAT *GGGAA GGTGC ATGGC GGGCG GTTGG GTGG*T TATGT AACGG CACCT GTCCG GTACT TAATA GTGCG CTAGG ACATG CCCGT CTATA GCCTT GAAGG AGCAA CGATC TTACT CGTCA TGTTA (62% G)

p27 CGTTG CGGAG TGCTC TCGAT ATCTA GAAGC CTAAT GCTTC TACTA GAGAT TGACT TTGTA TAGTG TCCAT CGAAG GTCCT TGTT*G GGTGG TGGGT GGTTT GATGT GAGAG GG*CAA TATTA TTGTA AGGCA CCCGC AATCC CTTGA GGATA AGGTC GTGCA TTGTA TGCTT CTCCG TCATC CAGAT CAAAG GATCA TTCAG CTGTT GTA (61% G)

p29 AGGGG ACCCG ATTGA ACCTG TTATT GGGAA ACACG TGCTT CGTAA GGACT TAAAA CCTAT CATAA GTCGG TCCAC TCCTT GGATC ACATG ACTTC CTGGG CTAGC CCATA TCATA TCTTT CT*GGA GGGTG GTGGG TGG*TT TTGTA GAGAT GCTTG CTACG GCACC TGGAA AGTAG CTGGG AAATA TTTAA TGGGC TTTGG TTCTA CGTTC ACTCG TTACT CTCGA GGTCG GTGCG TA (75% G)

p30 TTTGC TTGAG GAGAC C*GCGG GGCGC GGCGG TTGGG* AAAAG GTCTC CTAGC CTTTT TTAAT TGTGC CTTGT GGTCC AGATT TAATT TGTAA CAATC CCCTC AATCT AACTG CTTCG TAGTA TGGCA CCTAG AGATA GAACG GGGCC AAACG TTCAT TTTAA CATGA GGCCC ATGTA TATGG TAAAG CTAGG TTACC GCCGC CA (68% G)

3.4. Binding Affinities

In order to determine whether the selection scheme had succeeded in enriching for DNA aptamers that preferentially bound to NMM, the binding affinities of the different DNA clones for NMM and, indirectly, for other porphyrins, were measured, using the methodology of Connell et al.(1993). The equilibrium distribution of aptamer molecules between column-bound ligand and free ligand in solution were used to compute dissociation constants. Table 2-1 shows the dissociation constants measured for clones PS2 and P7, and the oligomer PS2.ST1, for binding to different porphyrins. Separate measurements were taken in a number of instances, to gauge the accuracy of the K_d measurements (found to be within 80-100% accuracy). All three aptamers bound to NMM with submicromolar affinity, whereas their binding affinities to MPIX were

Table 2-1. Dissociation constants[a]

	NMM	MPIX	Fe(III)MPIX	hemin	Ni(II)-MPIX	Zn(II)-MPIX
PS2	0.5	1.5	2.8	1.4	1.7	1.8
	0.5					
PS2.ST1	0.8	3.6	2.6	1.7	3.6	4.9
	0.7	3.0	2.1			
P7	0.4	3.1	2.1	ND[b]	ND	ND

[a] In micromolar; [b] ND = Not determined

reproducibly lower (by three to eight-fold), as were their affinities for a number of metalloporphyrins derived from MPIX (as well as hemin). These data indicate that the selection strategy used to enrich for these aptamers (with negative selection against MPIX followed by positive selection against NMM) was successful, to a point, in enriching for aptamers with differences in affinity for the two porphyrins. However, the discrimination between MPIX and NMM is not very large. To what upper limit these differences in affinity can be enhanced will be the subject of future investigations.

3.5. Footprinting of aptamer-porphyrin complexes

The precise binding sites of NMM and related porphyrins within the folded aptamers were investigated using footprinting experiments. Three approaches were attempted: methylation protection using dimethyl sulfate (DMS), which reveals the involvement of specific guanine N7 nitrogens in hydrogen-bonding or in metal binding. The other two techniques were partial digestion by DNase I and DNA strand cleavage by bound hemin or mesohemin moieties in the presence of superoxide (KO_2). The data shown in Table 2-1 confirmed that MPIX, a number of its metallo-derivatives, as well as hemin [Fe(III)-protoporphyrin IX] did bind to PS2 and to the other aptamers tested, albeit with a lower affinity than did NMM. Fe(III)-porphyrins, such as hemin or mesohemin, in the presence of strong oxidizing agents such as superoxide, are able to generate lesions in DNA, which lead to strand scission. We therefore reasoned that hemin (or mesohemin), bound to the aptamers, could be used to generate footprints *in situ*, and help define

Fig. 2-3. Footprinting results for PS2.

(A). Methylation protection of aptamer PS2, under different buffer conditions, and in the presence and absence of NMM. (Lane 1) in TE buffer with no added NMM; (lane 2) in SB buffer with no added NMM; (lane 3) in SB with 50 μM NMM; (lane 4) as in lane 2; (lane 5) in SB with 1mM NMM; (lane 6) in SB' buffer [50 mM potassium cacodylate (pH7.0), 10 mM $MgCl_2$, and 5% DMSO] with 100 μM NMM; (lane 7) in SB' buffer with 1mM NMM; (lane 8) in SB' + 100 mM NaCl with 100 μM NMM; (lane 9) in SB' + 100 mM NaCl with 1 mM NMM. The extreme left-hand lane shows a 10 b.p. ladder (with the 100 b.p. band darker than the others).

(B). DNaseI, hemin/KO_2, and mesohemin/KO_2 footprinting of PS2. (Lane G) Maxam-Gilbert guanine-ladder of PS2; (lane 0): PS2 without hemin treated with KO_2; (lanes 1-3) PS2 in the presence of hemin (30, 100, and 400 μM, respectively), treated with KO_2; (lane 4): PS2 in the presence of mesohemin (400 μM), treated with KO_2; (lane 5) PS2 without NMM treated with DNase I; and (lane 6) PS2 in the presence of NMM (100 μM), treated with DNase I.

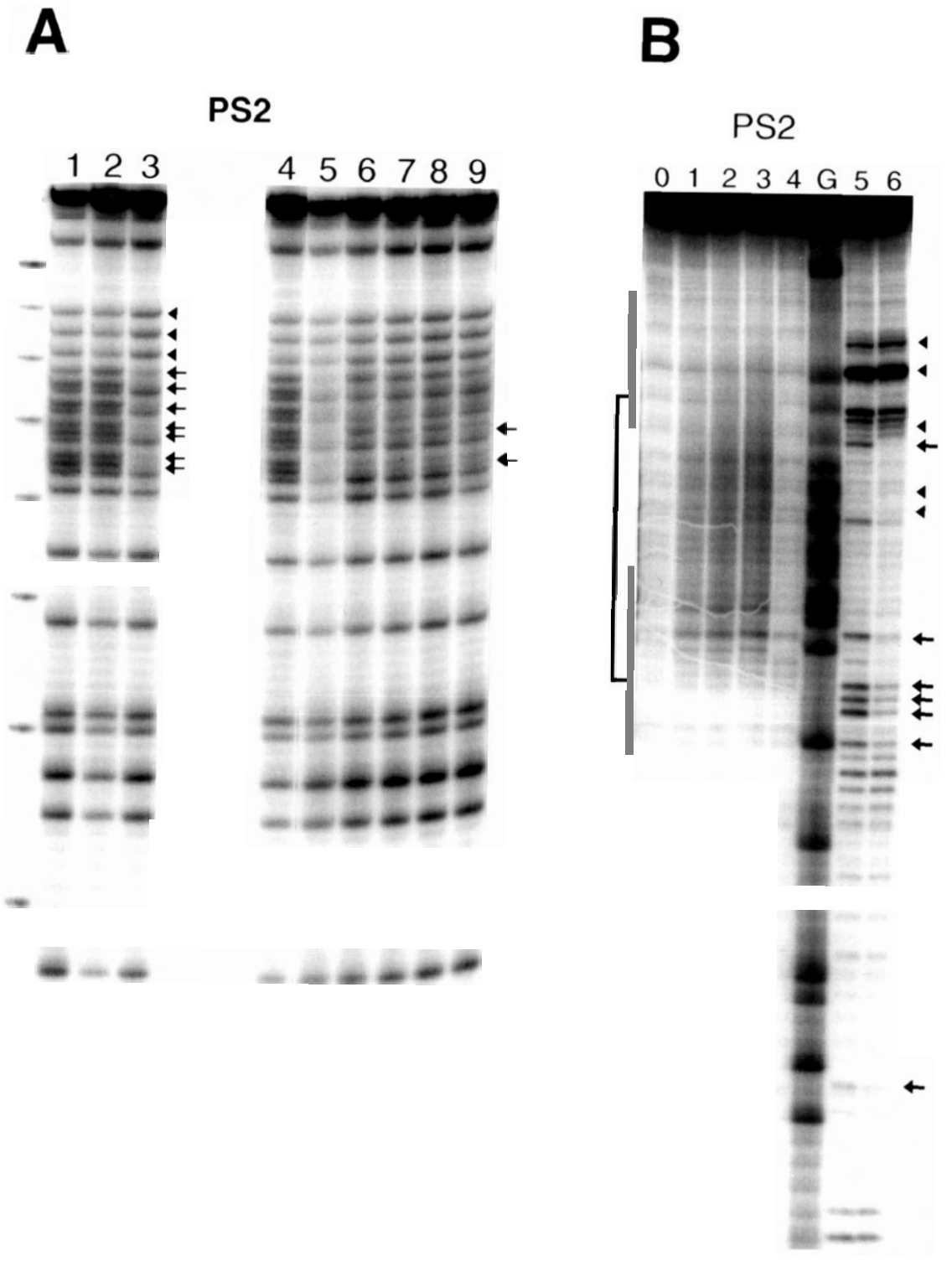
A
PS2
1 2 3
4 5 6 7 8 9
B
PS2
0 1 2 3 4 G 5 6

"binding domains" on the basis of the proximity of specific DNA regions to the bound hemin.

Fig.2-3A (p55) shows the methylation protection patterns of PS2 in different buffers, both in the presence and absence of NMM. When PS2 was methylated in either TE or SB buffers (lanes 1 & 2), all of its guanines were reactive. However, methylation in the presence of 50 μM NMM in SB buffer gave a clear footprint (lane 3), with certain guanines (indicated by arrows) fully protected, and others (indicated by arrowheads) enhanced. A very high concentration of NMM (1 mM, lane 5) appeared to protect all but the 3'-most and 5'-most guanines in the aptamer. Arguably, under these conditions, the DNA-porphyrin interaction was qualitatively different, and possibly, non-specific. Lanes 6-9 show footprints in the presence of 50 μM NMM but in buffers that lacked one or more components of SB [such as SB': 50 mM potassium cacodylate (pH7.0), 10 mM $MgCl_2$, and 5% DMSO; and SB'+100 mM NaCl]. In all of these cases, there was a partial footprint, with some of the guanines protected in lane 3 protected here, and others not. The arrows next to lane 9 indicate the two most protected guanines in that lane, although the overall pattern is similar to that shown in lane 3. The pattern in lane 9 makes the interesting point that PS2 is able to fold and form its NMM binding site in a magnesium-independent manner.

Fig. 2-3B (p.55), lanes 0-3, show PS2 footprints generated by hemin and KO_2 (lane 0 contained no hemin; lanes 1-3: 30, 100, and 400 μM hemin, respectively), and by mesohemin and KO_2 (lane 4 contained mesohemin at 400 μM). Whereas in the absence of bound hemin (lane 0) there is only a background DNA breakage pattern by KO_2; lanes

1-3 show the progressive appearance of a defined zone of cleavage, which superimposed well upon the methylation protected zone (Fig.2-3A). Interestingly, the mesohemin cleavage zone(lane 4) is consistent with that of hemin (lane 3), but the cutting is much less.

Fig. 2-3B, lanes 5 and 6, show partial DNase I digests of PS2, in the absence (lane 5) and the presence (lane 6) of bound NMM. Whereas there is broad agreement between the methylation protection and hemin/KO_2 cleavage zones, the DNase pattern differences between lanes 5 and 6 extend for tens of nucleotides beyond the borders of the putatively binding domain, indicating a significant tertiary structure change in the aptamer following the binding of NMM.

Fig. 2-4A (p.58) shows DMS as well as KO_2/hemin footprints for the aptamer PS5. PS5 is unlike PS2 (above) in that the aptamer itself, in SB buffer at room temperature, shows strong variation in the DMS-reactivity of individual guanines in its G-rich motif (lane 1; G-rich motif indicated by a bracket). This suggests that these partially protected guanines were involved in hydrogen-bonding with their N7 positions, and that the G-rich motif of PS5 (unlike PS2) was possibly folded into a modestly stable secondary/tertiary structure in SB buffer. The binding of NMM, in progressively higher added concentrations (lanes 2-4), however, did not simply enhance the pre-existing guanine protection pattern, but altered this pattern in several ways, including enhancing the reactivity of certain guanines and further protecting others. Thus, in the absence of NMM, the motif showed the following reactivity pattern: gtgGGtgGGtgtGgctGgt, where guanines shown in the upper case were less reactive. The presence of NMM, however, gave rise to a more comprehensive protection pattern, with effectively all guanines in the

Fig. 2-4. Footprinting results for PS5, P3, P7, P9 clones.

(A). Methylation protection and hemin/KO_2 footprints of aptamer PS5. (Lane 1): methylation pattern in SB buffer, in the absence porphyrin; (lane 2-4): methylation pattern in SB buffer, in the presence of NMM (10, 100, and 300 μM, respectively); (lane 5): as lane 1; (lanes 6,7) in SB buffer with hemin and KO_2, treated with the DNA trapped within gel fragments: in lane 6, showing DNA recovered with no bound hemin, and in lane 7, with bound hemin (see Materials and methods).

(B). Methylation protection patterns of aptamers P3, P7, and P9. (lane 0): in SB buffer, in the absence of NMM; (lane 1): in SB buffer, in the presence of NMM; and (lane 2): in SB buffer lacking magnesium chloride, and in the presence of NMM. The protected regions in lanes 1 and 2 are indicated with brackets.

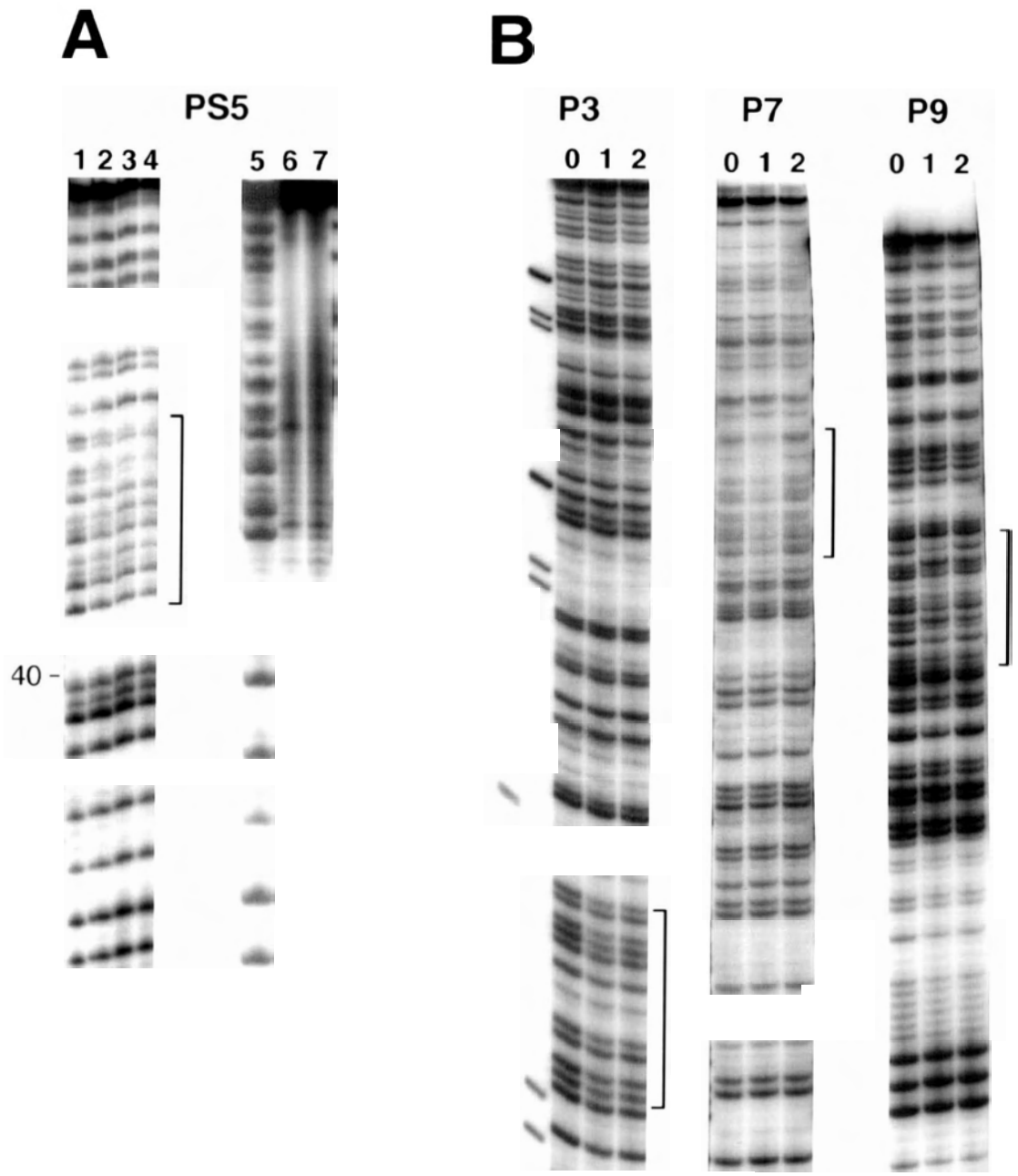
A
PS5
1 2 3 4
5 6 7
40 -
B
P3
P7
P9
0 1 2
0 1 2
0 1 2

motif underreacting; however, at a finer level, some guanine reactivities decreased, while others remained the same or were enhanced (one guanine within the motif, underlined above; another is located beyond the 3' edge of the motif).

Fig. 2-4B (p.58) shows the methylation protection patterns of the larger aptamers P3, P7, and P9, in the absence and presence of 50 μM NMM. Single areas of protection (shown by brackets) were seen for each aptamer (Fig. 2-4B). The most notable feature of these footprints is that none of the these larger aptamers had complete protection of their binding site guanines, although partial protection was observed in all cases (lanes 1). Addition of progressively higher concentrations of NMM, up to 800 μM, to P3, still did not give a total protection of any guanine (data not shown). An interesting difference among these three aptamers was that while P7 appeared to require magnesium in the binding buffer in order to footprint with bound NMM (lane 2, showing incubation in SB buffer without magnesium), aptamers P3 and P9 gave footprints with NMM regardless of the presence (lanes 1) or absence (lanes 2) of magnesium in their binding buffers (vide PS2 versus PS5, above). An additional feature of the pattern for P3 is the following: the aptamer has at least two highly guanine-rich regions of comparable size and guanine-content: from positions 35 to 55 (GcGGacGGGGcaGaGGGatG) and from 65 to 85 (GttGGGtGGtcatGtGGGtGG). However, the latter is the only motif that footprints (the 35-55 region, with no footprint, is not shown in Figs. 2-4B), suggesting that it is not a sufficient condition simply to have a guanine-rich motif in order to generate an NMM-binding site. Similar conclusions can also be drawn about P7 and P9.

Fig. 2-5 (p.61) shows the DNase I and hemin/KO_2 footprints for P3, P7, and P9. There were strong hemin/KO_2 footprints in all three cases (lanes 2), essentially coinciding with the zones identified by methylation protection. Treatment of all three aptamers with KO_2 only, in the absence of bound hemin, gave low, background cleavages (lanes 1). DNase footprinting of the aptamers in the presence and absence of NMM showed only modest differences, however, for all three aptamers; the few differences were located in the same general area as the other two classes of footprints. The modest DNase I cleavage differences for these large aptamers stand in marked contrast with the case of PS2 (Fig. 2-3B).

3.6. Interactions of PS2 with porphyrins, metalloporphyrins, and ATP

We investigated whether porphyrins such as MPIX, as well as a host of metalloporphyrins derived from MPIX, gave footprinting patterns comparable to or different from that of NMM. Fig. 2-6 (p.63) shows the DMS footprinting patterns of aptamer PS2 in the presence of a variety of porphyrins, metalloporphyrins, as well as ATP (which has been proposed recently to have a guanine quartet-containing binding motif formed by DNA, Huizenga & Szostak, 1995). Footprints in the presence of three different concentrations of NMM (50, 5, and 0.5 μM NMM, respectively, in lanes 2-4) indicate that the lower concentrations gave partial footprints; whereas their final form was reached only in the 50 μM incubation (the protected area is indicated with a bracket). Hemin, MPIX, and the Fe(III)-, Zn(II)-, Ni(II)-, and Cu(II)- derivatives of MPIX did not footprint at all at 50 μM incubations of the various porphyrins. Only Co(III)-MPIX

Fig. 2-5. Hemin/KO_2 and DNase I footprints of aptamers P3, P7, and P9. (Lanes G): Maxam-Gilbert guanine-ladders; (lanes 1): aptamers without hemin treated with KO_2; (lanes 2) aptamers in the presence of hemin (400 μM), treated with KO_2; (lanes 3): aptamers without NMM treated with DNase I; and (lanes 4) aptamers in the presence of NMM (100 μM), treated with DNase I.

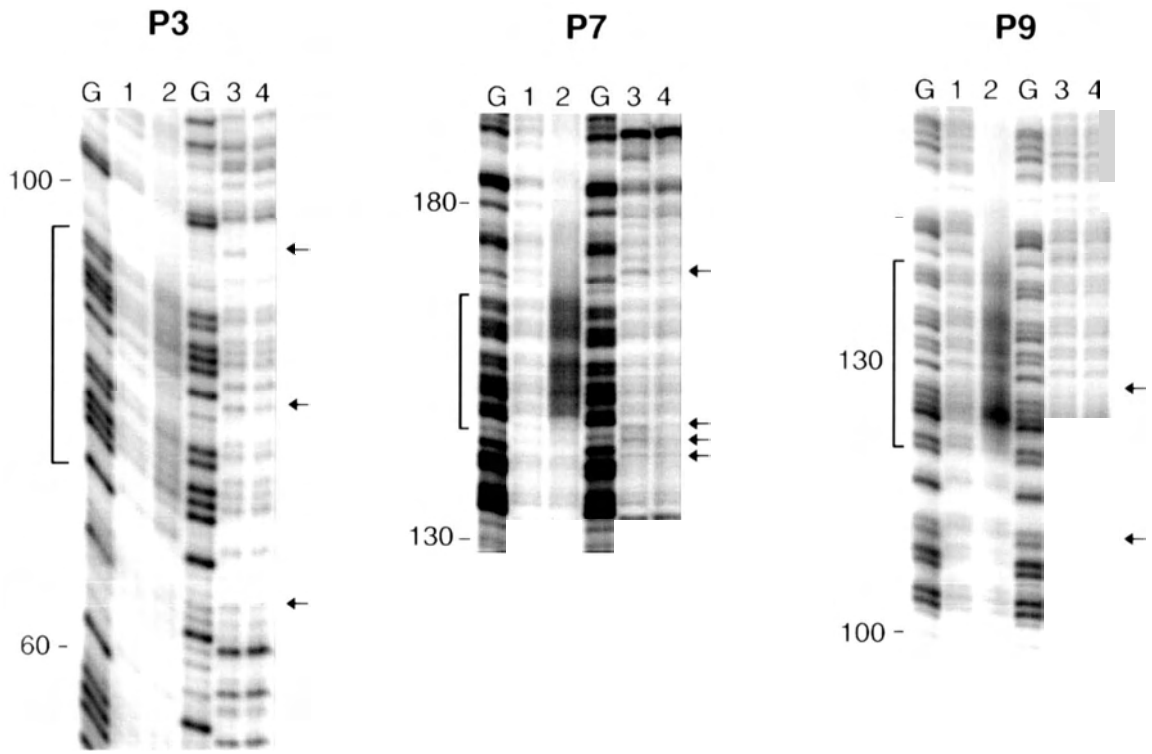
P3
G 1 2 G 3 4
100 -
60 -
P7
G 1 2 G 3 4
180 -
130 -
P9
G 1 2 G 3 4
130
100 -

showed a general and comprehensive protection of guanines in the binding motif (including those guanines that were not protected by 50 μM NMM; although resembling the pattern found with 1 mM NMM-- Fig. 2-3A). It is conceivable that Co(III)-MPIX, like NMM at high concentrations, shows a non-specific mode of binding, one which protects all of the guanines in the binding motif from methylation. As in Fig. 2-3A, NMM in SB' buffer gave a significant protection, and this was found even in the magnesium-free TE buffer. This is an interesting point of difference between PS2 and PS5, in that the former seems to fold to produce the NMM-binding site even in the absence of magnesium, whereas PS5 requires magnesium.

ATP, even at high concentrations (0.5 mM), did not give a footprint.

3.7. A small DNA aptamer

Both the methylation protection and hemin/KO_2 footprinting data on the five clones examined indicate that short, well-defined G-rich domains (a single, contiguous sequence of nucleotides in each aptamer) are responsible for binding porphyrins. The DNase I digestion data, however, at least in the case of PS2, indicates that changes in conformation and accessibility to the enzyme can extend well beyond the domains defined by the other two footprinting techniques. It is therefore interesting to test whether an isolated G-rich domain (as defined by the 5' and 3' limits established by the hemin/KO_2 and methylation protection cleavages on PS2), shorn of its neighbouring sequences, could still bind NMM.

A short, 25-nucleotide oligomer, PS2.ST1, encompassing the G-rich domain of PS2, with the sequence 5'AACGT GGGAG GGCGG TGGTG TTGAA3', was

Fig. 2-6. Methylation-protection patterns induced in PS2 by porphyrins and metalloporphyrins. From left: PS2 in SB buffer in the absence of porphyrins; in SB buffer in the presence of 50, 5, and 0.5 μM NMM, respectively; in SB with 50 μM each of MPIX; hemin; Fe(III)-MPIX; Co(III)-MPIX; Zn(II)-MPIX; Ni(II)-MPIX; and Cu(II)-MPIX; in TE buffer with 50 μM NMM; in SB' buffer with 50 μM NMM; in SB with 50 and 500 μM ATP, respectively; and, in SB without porphyrins. The extreme right-hand lane shows a 10 b.p. ladder.

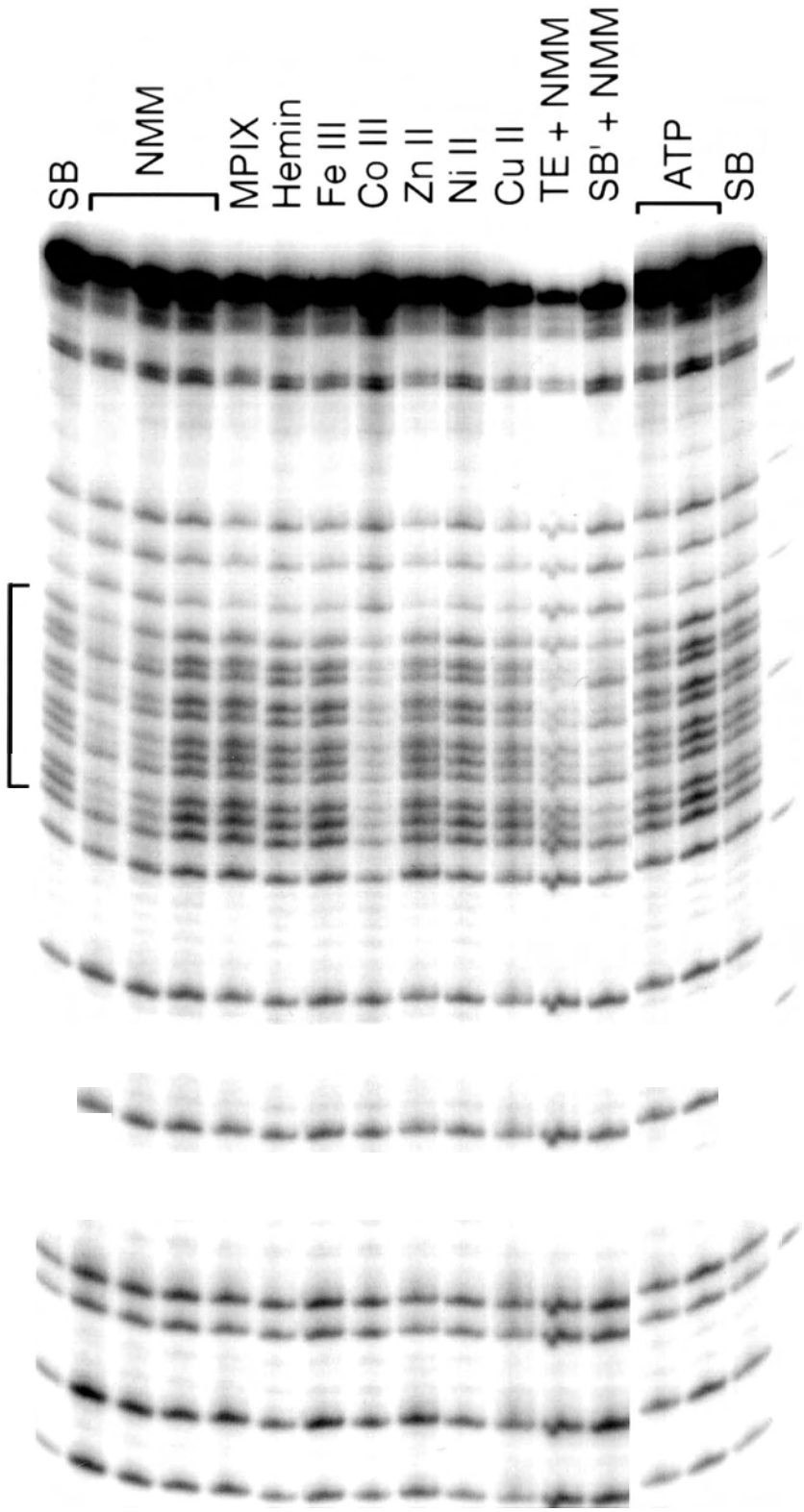
SB
NMM
MPIX
Hemin
Fe III
Co III
Zn II
Ni II
Cu II
TE + NMM
SB' + NMM
ATP
SB

PS2

synthesized. Dissociation constants of different porphyrins with PS2.ST1 were measured, and methylation protection and KO_2 cleavages carried out in the presence and absence of porphyrins. The results indicated that PS2.ST1 was competent to bind porphyrins almost as strongly as the parent aptamer PS2 (Table 2-1), but not in an identical manner. Fig. 2-7A (p65) shows the methylation protection patterns of PS2.ST1 with different porphyrins; the arrows on the left indicate those guanines that were protected in the presence of 50 μM NMM (whereas arrowheads indicate guanines that were enhanced). Comparison of Fig. 2-7A with Fig. 2-3A indicates that the PS2.ST1 pattern had fewer protected guanines (and each guanine protected to a lesser extent) than the PS2 pattern. However, like PS2, PS2.ST1 was not footprinted by incubations with 50 μM MPIX, mesohemin [Fe(III)-MPIX], or hemin. In addition, CoIII-MPIX induces a wholesale protection of all but the outermost guanines of PS2.ST1, as it did in PS2.

Treatment of PS2.ST1 with hemin/KO_2 showed cleavage of the entire oligomer (data not shown), as expected.

Like PS2 (but unlike PS5), PS2.ST1, in the absence of porphyrin, did not show much variation in the DMS-reactivity of its individual guanines (lane SB, Fig. 2-7A) in SB buffer at room temperature. However, guanine-rich telomeric oligomers similar in sequence to PS2.ST1 have been shown to form intramolecularly-folded G-G base pair- and guanine-quartet-containing structures under conditions of high salt and/or low temperature (Henderson et al., 1987; reviewed recently by Williamson, 1993, 1994). We therefore tested whether PS2.ST1 at 0°C (comparably to PS5 at room temperature), gave a modulated G-reactivity pattern with dimethyl sulfate , and whether the binding of NMM

Fig. 2-7A. Footprinting results for PS2.ST1. (Left) Methylation protection pattern of the short aptamer PS2.ST1with different porphyrins, and (Right) comparison of guanine reactivity in the absence of NMM at 0°C, relative to its presence, also at 0°C. Left panel: PS2.ST1 (1) in SB in the absence of porphyrins: (2) with added NMM; (3) hemin; (4) mesohemin [Fe(III)- MPIX); (5) Co(III)- MPIX; and (6) MPIX itself. The complete arrows indicate protection of guanines in lane 2 as compared to lane 1; arrowheads indicate enhancements of guanines. Right panel: (7) as in lane 1; (8) as in lane 1, but probed at 0°C; and (9) as in lane 2, but probed at 0°C.

Fig. 2-7B. Gel mobility test for PS2 and PS5. The non-denaturing gel was run at 4°C in TBbuffer + 10 mM KCl + 5 mM $MgCl_2$. Lane 1: PS2 in TE buffer; 2: PS2 folded in SB buffer; 3: PS2 folded in SB and treated with 100 μM NMM; 4: PS5 folded in SB; 5: PS5 folded in SB and treated with 100 μM NMM. The extreme left lane shows a double-stranded DNA marker (48 b.p.).

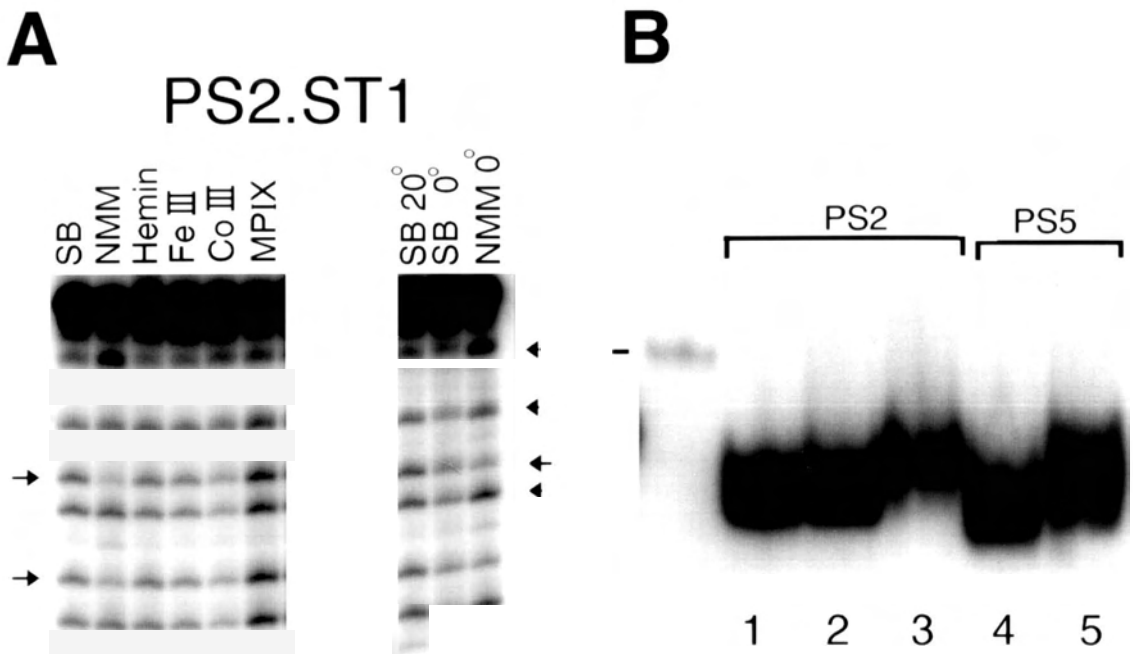
A
PS2.ST1
SB
NMM
Hemin
Fe III
Co III
MPIX
SB 20°
SB 0°
NMM 0°
B
PS2
PS5
1
2
3
4
5

simply intensified this pattern or gave rise to a different methylation protection pattern (as in the case of PS5). Comparison of the SB20° and SB0° lanes in Fig. 2-7A shows that at 0°C some guanines were indeed under-reactive compared to the situation at 20°C; however, methylation in the presence of NMM at 0°C gave a pattern different from both of the others (arrows indicate protections induced by NMM, and arrowheads, enhancements).

These mutually consistent data from PS2 and PS2.ST1 indicate, therefore, that it is probably not the case that NMM binds to a preexisting higher-order structure formed by the G-rich motif of PS2; rather, the presence of NMM appears to induce distinctive folding patterns for PS2. For clone PS5, it appears that a pre-folded structure does exist, and the binding of NMM causes certain changes to the structure.

3.8. Gel-mobilities of aptamer-NMM complexes

The footprinting/protection experiments above indicated that NMM-binding influenced the overall folded structure of a number of aptamers. This was indicated not only by changes in the methylation patterns of guanines within the binding motifs, but changes in the DNase I cutting patterns, which often (as in the case of PS2) extended significantly beyond the binding motif in both the 5' and 3' directions. We ran the aptamers PS2 and PS5, with added and no added NMM, in a non-denaturing, magnesium-containing gel, to see if there would be any gross differences in gel mobility of the aptamers in the presence versus the absence of NMM. Fig. 2-7B (p65) shows that both aptamers showed a discernibly slower mobility in the presence of added NMM (NMM

added to the relevant samples before loading, but not present in the gel buffer). The larger aptamers also showed this shift, although to a lesser extent. NMM itself would be expected to contribute 1-2 negative charges from its carboxylic acid side-chains to the aptamer-NMM complexes; however, the mobility differences observed were conceivably too large to be explained simply in terms of an increase in the overall negative charge of the complexes, from 120 to 121 or 122. It therefore appeared that NMM-binding gave rise to a moderate change in the overall tertiary structure of the binding aptamers, which was reflected in altered gel mobilities.

Interestingly, PS2.ST1 showed a relative gel shift in the presence of NMM that was not much larger than that of the parent aptamer PS2 (data not shown). PS2.ST1 is unusual in that it has no extraneous nucleotides other than the porphyrin binding site, so any structural changes induced by porphyrin binding are inherently 'local' rather than potentially 'global', as in the case of PS2.

3.9. A sequence consensus for the structure of the binding site

Fig. 2-8 summarizes the methylation and DNase I footprinting data for the five aptamers we have examined in detail. Guanines shown in upper case are those that are found to be less reactive to dimethyl sulfate in the presence of NMM than in its absence (although, as stated earlier, in the case of PS5, some guanines shown to be 'unaffected' by the presence of NMM in Fig. 2-8 (p68) were already underreactive in the absence of NMM, Fig. 2-4A). Fig. 2-8 shows that a reasonable alignment of four separate stretches of 1-3 guanines each can be made. However, this possibly does not represent a

structurally meaningful "consensus". It is conceivable that there are a number of closely related tertiary structures formed by the guanine-rich sequences, any of which can constitute a reasonable binding site for NMM. More detailed structural work revealed that for a sequence to have good catalytic activity for porphyrin metallation, 12 guanines are needed and they have to be arranged in the following way: G-N_x-GGG-N_y-GGG-N-GGG-N_z-GG, in which, N is any nucleotide but in favour of T, x, y, z are between 1-7. I will describe such results in Chapter 5.

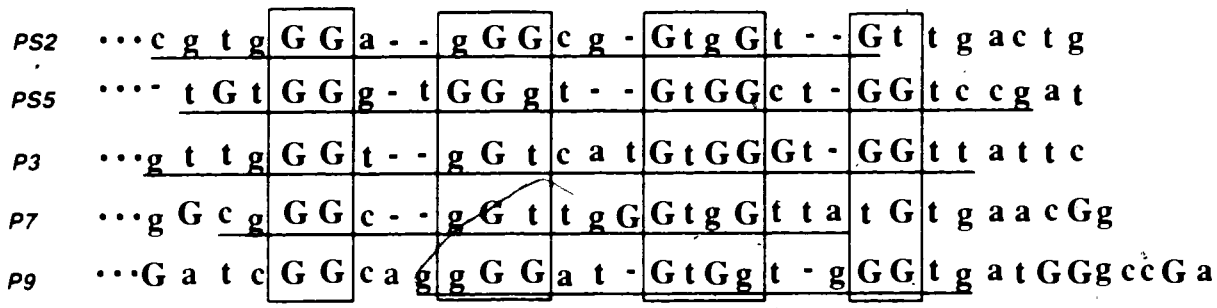

Fig. 2-8. Comparison of the methylation protection patterns of PS2, PS5, P3, P7, and P9. The guanines that show a greater level of protection in the presence of NMM are shown in upper case, whereas those that are not, shown in lower case. The underlined regions indicate zones defined by footprinting with hemin and KO_2.

3.10. Spectroscopic studies of aptamer-NMM complexes

We investigated the mode of binding of NMM to the folded aptamers using ultraviolet-visible absorption and circular dichroism spectroscopy.

3.10.1. UV absorption spectroscopy

Fig. 2-9 shows the ultraviolet-visible absorption spectra (from 325 to 625 nm and showing the Soret and visible absorption regions of NMM) of 1 μM NMM in the presence (gray line) and absence (dark line) of 5 μM PS2. The presence of the excess aptamer induced a ~10% hypochromicity in the Soret absorption but an almost negligible shift (~1 nm towards the red) of the absorption maximum. The visible bands appeared not to be significantly affected, in terms of both hypochromicity and position(s) of the absorption maxima. This overall pattern is significantly different from those seen in any of the proposed three modes of binding of cationic porphyrins to double-stranded DNA (Carvlin et al., 1983).

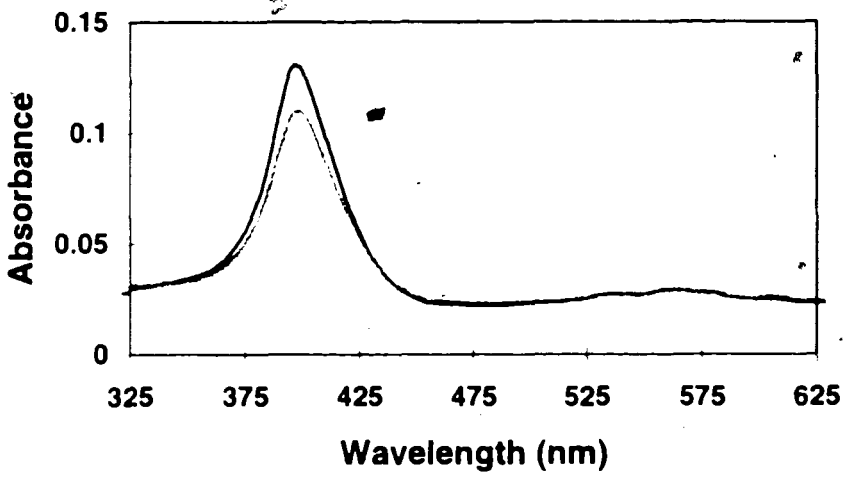

Fig. 2-9. Ultraviolet-visible absorption spectra of 1 μM NMM, in the presence (gray line) and in the absence (dark line) of PS2 (5 μM).

3.10.2. Circular dichroism spectroscopy

The CD spectra in the presence and absence of NMM were examined for the small aptamer PS2.ST1 and for PS2. In the DNA absorption region, PS2.ST1 did not give a significant CD signal, even at 0°C, suggesting that it is essentially non-helical in terms of its secondary and tertiary folding. The presence of added NMM, however, did not induce a spectrum in the DNA absorption region. Undoubtedly, PS2.ST1 bound to NMM is more structured than it is in the absence of NMM; however, the overall helical content for this small DNA molecule may not be very great, even in the presence of NMM. PS2 gave a standard B-DNA CD spectrum on its own, and this did not substantially change in the presence of NMM. Undoubtedly, folded PS2 has elements of double-helix within it, although these regions may not be relevant to NMM-binding. In both the Soret and visible absorption regions for the porphyrin, neither PS2 nor PS2.ST1 gave rise to induced CD spectra.

4. Discussion

4.1. DNA sequences that bind NMM

It was not yet clear, at this stage of our research, whether the "sequence consensus" derived from the sequence comparisons and from methylation protection studies, shown in Fig. 2-8, has more than a very general relevance to the folded structure actually responsible for binding NMM. This possibility was raised by the inspection of the methylation-protected guanines of the individual aptamers. While the derived

consensus sequence did incorporate a high proportion of these protected guanines, in each case there existed a number of others that sit outside of the consensus region. The existence of this array of very diverse but all guanine-rich sequences in the final selection pool may be explained in two ways. The first explanation is that there do exist quite many forms of G-quartet mediated structures capable of NMM binding; and the other is that all the selected sequences could form very similar tertiary structures or NMM-binding pockets. This sequence diversity may further point to the extreme possibility that any guanine-quartet containing complex would bind NMM and the other porphyrins. However, more detailed work at later stages indicated that guanine-quadruplex structures formed by sequences unrelated to this selection experiment did not significantly bind to NMM and perform catalysis for porphyrin metallation. Most interestingly, there may have been many different G-rich sequences capable of NMM-binding, but, all *catalytic* sequences are unique in the sense that they seemed to be able to fold into a very special guanine quadruplex structure to carry out the catalysis. Those results will be presented in detail in Chapter 5.

4.2. Mode of NMM-binding

How might NMM bind to folded DNA structures that possibly contain one or more guanine quartets? Both porphyrins and guanine-quartets are large and substantially planar aromatic systems; it might be expected that the two might interact via the intercalation of porphyrins between successive guanine quartets.

A number of changes in physical and spectroscopic properties associated with the binding of ligands by double-stranded DNA have been recognized as defining for an intercalative mode of binding (reviewed in Pasternack et al., 1983; Chaires, 1990). These include: DNA helix stabilization against thermal denaturation, helix unwinding, and increase in solution viscosity as a consequence of the DNA lengthening. These, unfortunately, are not properties that can be tested with single-stranded aptamers. Other expected features of porphyrin intercalation are: substantial hypochromicity and red-shifts of DNA ultraviolet absorption bands as well as that of the Soret absorption of the porphyrin; and, induced optical activity in the visible region for the porphyrin, as well as changes in the ellipticity of DNA in the near ultraviolet. Thus, Carvlin & Fiel (1983) reported for the intercalation of meso-tetra(3-N-methylpyridyl)porphine into calf thymus DNA a substantial red-shift of the porphyrin visible band, from ~416 nm to ~433 nm, and a large hypochromicity of ~47%.

As discussed earlier, it is likely that the porphyrin binding site (at least when NMM is bound) contained one or more guanine quartets. The interaction of DNA-binding drugs with guanine-quartets has been studied in one single instance, the binding of ethidium bromide to the parallel tetraplex formed by the self-association of dT4G4 (Guo et al., 1992). In that study, ethidium was found to intercalate in a classical manner between G-quartets (giving rise to a red-shift of ~35 nm and hypochromicity of ~20% for the ethidium visible absorption band). An intercalative mode of binding between adjacent G-quartets is therefore theoretically possible for porphyrins.

We measured UV-visible absorption and circular dichroism spectra for NMM in the absence and presence of excess aptamer PS2, and found a ~10% hypochromicity in the porphyrin Soret absorption, and a very small red shift (<1 nm). The visible absorption of the porphyrin appeared largely unchanged. In addition, no significant change in the circular dichroism spectrum of the DNA, and no induced CD spectrum around the Soret and visible absorption regions of the porphyrin were found. These observations seemed to suggest that the interaction of NMM with the aptamer PS2 was not by a classic intercalation mechanism suggested for the association of water-soluble cationic porphyrins with double-helical DNA. However, our latest results indicated that detergents, which has to be used in the assay buffer, have dramatic impact on both visible absorption of the hydrophobic porphyrin compounds tested in this work and their binding to the selected aptamers (see Chapter 6). It did not seem appropriate to simply use UV-visible absorption data to rule out the intercalation as the binding mode of the selected aptamers with those porphyrins. As I will discuss later in chapter 5, our catalytic sequence data seemed to be better explained if an intercalating mode is actually responsible for the porphyrin-DNAzyme interaction.

4.3. Relevance to the RNA-world

The definition of a binding site within folded single-stranded DNA for a naturally occurring anionic porphyrin has important theoretical connotations. Ribozymes that have been found to date in nature are relatively narrow in the range of their catalytic activities, and extant ribozymes probably represent a vestige of a previously much larger group of

enzymes, which catalyzed a broad range of chemical reactions connected with metabolism, in the so-called "RNA world". The lack of a diversity of functional groups within RNA (and DNA) as compared to proteins has been noted (White, 1976; Gilbert, 1986; Benner et al., 1989). It is therefore of interest that DNA is able to form high-affinity and specific binding sites for naturally occurring anionic porphyrins and their metallo-derivatives, for the latter currently constitute a large and versatile class of cofactors and prosthetic groups. It is conceivable that in such an "RNA world", RNAs catalyzing metabolically important redox reactions might have recruited porphyrins or porphyrin-like molecules as cofactors. It is therefore of interest that DNA is able to form high-affinity and specific binding sites for such porphyrin compounds.

5. Summary and next stage of experimentation

In this chapter, I have described the selection and charaterization of NMM aptamers from a large random DNA library. These aptamers bound to NMM with sub-micromolar affinity but bound to MPIX as well as various metallo-derivatives of MPIX with lower affinity. Footprinting experiments with DMS, DNase I, and bound hemin molecules activated by superoxide identified a series of short guanine rich motifs to be the binding sites for porphyrins. One clone, PS2, examined in depth, gave a methylation footprint with bound NMM but not with bound MPIX nor with a number of metalloporphyrins. The binding domain of PS2, synthesized as a short oligonucleotide, itself showed high-affinity binding to NMM. The binding sequences from different

clones were loosely homologous, and the footprinting data were consistent with their folding to form one or more guanine quartets in the presence of NMM.

The isolation of DNA aptamers that bind to NMM with a high affinity and to other, related porphyrins with lesser affinity, will permit us to examine whether such aptamers can carry out a similar catalytic function as the antibodies described by Cochran & Schultz (1990), that of inserting metal ions into the porphyrin MPIX. Detailed studies indicated chelatase activity for a number of our clones, and I will describe the results in next Chapter.

Chapter 3. Catalysis of Porphyrin Metallation by NMM Aptamers

1. Introduction

In Chapter 2, I described the successful isolation of NMM aptamers by the *in vitro* selection methodology; we also carried out detailed studies on the interaction of some of the selected aptamers with NMM (the TSA of the target metallation, see Chapter 1), MPIX (the substrate of the reaction), and various metalloporphyrins (the reaction products) by various chemical, enzymatic, and physical methods. The high affinity of the selected aptamers for NMM and lower affinity for MPIX as well as various metalloporphyrins bodes well for the catalysis of metallation by those NMM aptamers. To test this, single stranded DNA from aptamers PS2 and PS5 as well as oligomers corresponding to their NMM-binding sites PS2.ST2 and PS5.ST1(Fig. 3-1), were chosen at random to test for their ability to catalyze the insertion of Zn^{2+} and Cu^{2+} into MPIX. The short oligomer PS5.ST1 was found to have a significant catalytic activity, with a measured k_{cat} of 13.7 per hour, and a K_M of 2.9 mM for the insertion of Cu(II) into MPIX (with the copper concentration fixed at 1 mM) at conditions initially chosen for the selection experiment. At a later stage, we have examined extensively the catalytic behaviors of the binding motifs from PS family sequences (see Chapter 2), and found, among them, 25% of aptamer fragments have strong activity, 45% have weak activity, and 30% have no activity. In this chapter, we will describe such findings.

2. Materials and methods

2.1. DNA oligomers

The single-stranded aptamers PS2 and PS5 were obtained by PCR and avidin column as described in Chapter 2; their approximate binding sites PS2.ST2 and PS5.ST1 as well as other oligomers were obtained through automated DNA synthesizer, purified by denaturing polyacrylamide gels and recovered by ethanol precipitation. Sequence REP2 (independent of the selection) and a quartet-forming sequence OXY4 (Williamson et al., 1989) were used as control oligomers. Fig. 3-1 gives the sequences of all DNA oligomers tested in this study.

PS2 (117): GGATC TTTTT GATCC GGTCG GCACC TTGCC TAACC GTGAA GGTAA AACGA TTTAG TCAAA CGTGG GAGGG CGGTG GTGTT GACTG ATCGA TTTTA TTCCA CCTTG GTCAT TAGGC GA

PS2.ST2 (42): GATTT AGTCA AACGT GGGAG GGCGG TGGTG TTGAC TGATC GA

PS5 (112): GGATC TTTTT GATCC GGTCG GCAGT GTCGA AGATC GTGGG TCATT GTGGG TGGGT GTGGC TGGTC CGATC CGCGA TCTGC TGACG CTGGT TAGGT CCTTG GTCAT TAGGC GA

PS5.ST1 (33): TCGTG GGTCA TTGTG GGTGG GTGTG GCTGG TCC

REP2 (40): AATAC GACTC ACTAT AGGAA GAGAT GGTTT TTCCA TCTCT

OXY4 (32): TTTTG GGGTT TTGGG GTTTT GGGGT TTTGG GG

Fig. 3-1. Sequences of the DNA molecules tested for the catalysis (with sizes given in parentheses). The underlined sections in PS2 and in PS5 indicate the sequences of PS2.ST2 and PS5.ST1, respectively. REP2 is a control oligomer, not derived from the aptamer selections; OXY4 is a guanine-rich telomeric sequence.

2.2. Reaction conditions

Reactions were carried out in SB buffer (100 mM Tris acetate, 200 mM sodium acetate, 25 mM potassium acetate, 10 mM magnesium acetate, 0.5% Triton X-100; 5% dimethyl sulfoxide; final pH7.1), at 25°C, if not otherwise specified. The reaction mixtures contained 1 mM copper acetate, 33 μM MPIX, and 5 μM of relevant DNA oligomer. The reactions were monitored by HPLC (a Waters 600E Multisolvent Delivery System with a Waters 991 Photodiode Array Detector). The column used was a μBondapak C18 10 μm, and the mobile phase was 85% methanol and 15% 1M ammonium acetate (pH 5.2). Ni(II)-MPIX was used as an internal standard. One volume of each reaction mixture was mixed with one volume of Ni(II)-MPIX in the same buffer, and the mixture injected directly into the C18 column. The Zn(II)-MPIX peak was monitored at 400 nm, and the Cu(II)-MPIX peak at 390 nm; and they were both verified by co-injecting with the pure compounds. Individual points in Fig. 3-2 showed <10% variation when duplicated.

2.3. Lineweaver-Burk plot

Rates of metallation in the presence of both the catalytic PS5.ST1 and non-catalytic REP2 were assayed at 30, 70, 100, 186, 250, 369, 450, and 500 μM concentrations of MPIX, respectively, all at a fixed Cu^{2+} concentration of 1 mM and DNA concentration of 5 μM. Assay methods were identical to those described in the last section. For initial rate measurements, good linear relationships between the product formation and time were found in each case at <15% reaction completion.

2.4. Salt-dependence and inhibition experiments

For the magnesium-dependence measurements (shown in Fig. 3-5a), the catalyzed initial rates were measured in SB buffer at 25°C, but containing varying concentrations of Mg^{2+}. All reactions contained 5 μM PS5.ST1, 33 μM MPIX, and 1 mM $Cu(OAc)_2$. For the general cation-dependence experiments (shown in Fig. 3-5b and 3-5c), the experiments were carried out in SB' buffer [100 mM Tris, pH7.1(final), 5% DMSO, 0.5% Triton X-100, and 1 mM $Cu(OAc)_2$], to which other salts were added, as shown in Fig. 3-5b and 3-5c. For the inhibition studies with NMM and with various metalloporphyrins (Table 3-1), experiments were carried out at 5 μM PS5.ST1 and 100 μM MPIX concentrations in SB buffer. Inhibitors were present at concentrations indicated in the Table 3-1.

3. Results and discussion

3.1. Catalysis of metallation of MPIX by PS5.ST1

Fig. 3-2a and 3-2b show time-courses for Cu^{2+} and Zn^{2+} insertion into MPIX in the absence of DNA, with 5 μM of oligomers REP2 or OXY4 (non-aptamer controls), and 5 μM each of various aptamers. REP2 and the guanine-rich telomeric oligomer, OXY4, showed no rate enhancement over the background, whereas low-level rate enhancements were seen with PS5 and PS2.ST2. A relatively high metallation rate, particularly with Cu^{2+}, was seen with PS5.ST1.

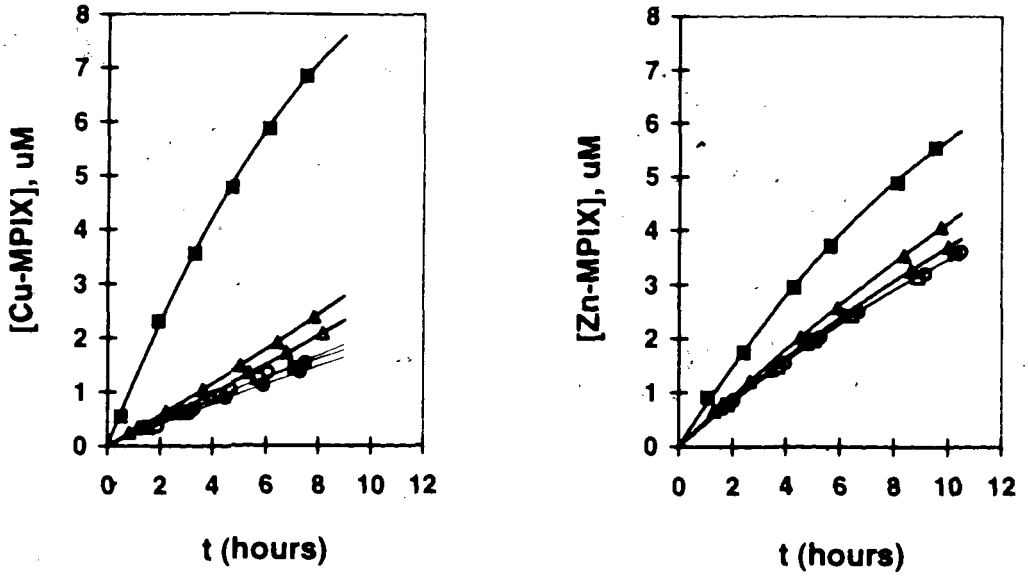

Fig. 3-2. Cu(II) and Zn(II) insertion into MPIX in the presence of various DNA oligomers. Time-dependence plots for the formation of Cu (II)-MPIX (left panel) and Zn(II)-MPIX (right panel) in the absence of DNA (open circle), in the presence of the non-aptamer control REP2 (open square), and, respectively, the aptamers PS5 (open triangle), PS2.ST2 (filled triangle), and PS5.ST1 (filled square); and, the telomeric oligomer OXY4 (filled circle).

To test whether metallation with PS5.ST1 showed the saturation kinetics typified by many enzymes, the initial velocities of Cu^{2+} insertion (at a constant Cu^{2+} concentration of 1 mM) as a function of MPIX concentration were measured. Fig. 3-3a shows that at our experimental DNA concentrations (5 μM), the uncatalyzed reaction rate (in the presence of 5 μM REP2) was a significant fraction of the total rate. The data indicated mixed-order kinetics, which could be modelled, in the presence of the catalytic oligomer PS5.ST1, as $v_{total} = k_i$ [MPIX] + k_u [MPIX]^2 + k_{cat} [E-MPIX]. That is, the kinetics can be modelled as containing three components: an enzyme-catalyzed reaction (k_{cat} [E-MPIX]),

a porphyrin-catalyzed reaction (k_{ii} [MPIX]^2), and an uncatalyzed reaction (k_i [MPIX], where $k_i = k_{uncat}$). The rate law in the absence of PS5.ST1 (but in the presence of REP2) could likewise be modelled as $v_{background} = k_i$ [MPIX] + k_{ii} [MPIX]^2.

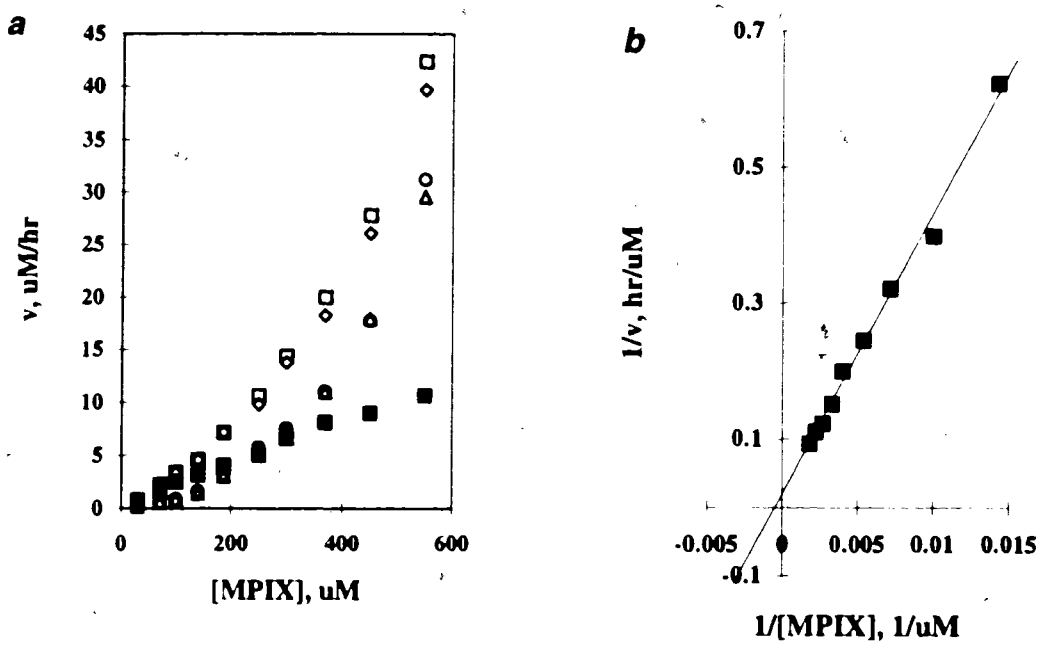

Fig. 3-3. Cu(II) insertion into MPIX catalyzed by PS5.ST1.

(a). Initial rates (v) of Cu (II)-MPIX formation plotted against MPIX concentration. Measurements from two separate experiments are shown for the observed total rates, v_{total}, (open square and diamond), and for the uncatalyzed rates, v_{uncat} (in the presence of REP2) (open circle and triangle). Data points in filled square show the catalyzed rate, v_{cat}, obtained by subtracting the mean v_{uncat} value for each substrate point from the corresponding mean v_{total} value.

(b). Lineweaver-Burk plot of $1/v_{cat}$ versus 1/[MPIX]. Each data point represents the mean of at least two sets of independent measurements.

The net enzyme rate, v_{cat}, shown in Fig. 3-3a, equalled $v_{total} - v_{background} = k_{cat}$ [E-MPIX]. The Michaelis-Menten equation was then used to calculate k_{cat} and K_M. Fig. 3-3b shows a Lineweaver-Burk plot of these data. A straight line was obtained. Analysis

of the data with the GraFit 3.0 program gave k_{cat} and K_M values of 13.7 + 3.5 hour^{-1} and 2.9 + 0.9 mM, respectively. The uncatalyzed rate (Fig. 3-3a) was not purely first order with respect to MPIX concentration, but appeared to contain a second order component as well. At low MPIX concentrations, however, the uncatalyzed rate was approximately first-order, and a k_{uncat} of 0.0096 hour^{-1} was calculated (at 1 mM Cu^{2+} concentration). The rate enhancement (k_{cat}/k_{uncat}) was therefore ~1400. The corresponding k_{cat} and catalytic efficiency reported for the catalytic antibody for this reaction were 8.7 hour^{-1} and 1700 (Cochran & Schultz, 1990), respectively (k_{uncat} in the two studies were both measured at 1 mM Cu^{2+}, but under somewhat different buffer conditions). The efficiency of substrate usage by the two catalysts, though, were strikingly different (the antibody K_M was 50 μM, Cochran & Schultz, 1990).

3.2. Assays for catalytically relevant Cu(II)-binding site on PS5.ST1

Porphyrin metallation is a two-substrate reaction, involving both a porphyrin and a relevant metal ion. Protein enzyme ferrochelatases have binding sites for both porphyrin and metal ion substrates, and bring them into close proximity (Lavallee, 1988). However, the *in vitro* selection scheme used by us focused primarily on the porphyrin as it might appear in the transition state (Chapter 2), no driving force has been provided in the selection scheme to generate a catalytically relevant metal ion binding site. On the other hand, there are many metal ions bound either to negative charged DNA backbone or to bases, it was not inconceivable if the catalytic sequence PS5.ST1 provides such a binding site for copper; and if so, the observed catalysis with PS5.ST1 would be in part or

wholly due to the presence of a copper binding site close to the porphyrin binding site, which could serve to increase the effective copper (II) concentration in the vicinity of the porphyrin substrate. Enzyme activity was therefore measured as a function of copper concentrations between 0.05 and 2.5 mM (with MPIX concentration fixed at 33 μM, and enzyme at 5 μM); however, no saturation of the catalyzed rate with increasing copper concentration was found (Fig. 3-4). These data were consistent with the absence of a catalytically relevant strong copper-binding site (K_M at < 2.5 mM). However, the existence of a weak copper-binding site could not be ruled out, for saturation kinetics might be observable at higher copper concentrations (which, however, may have perturbed the folded structure of the enzyme). We will investigate these possibilities in the next chapter.

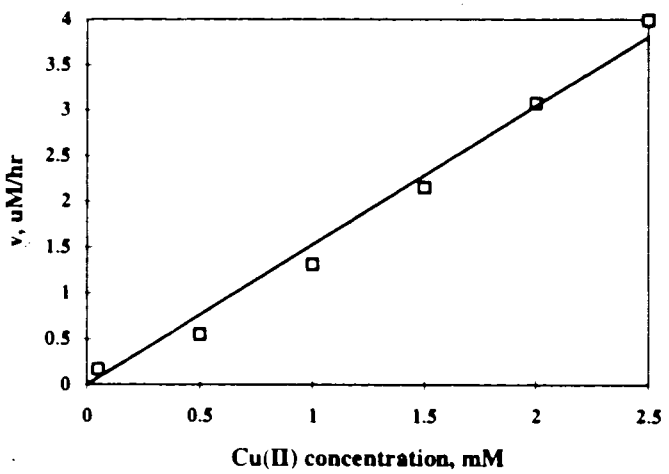

Fig. 3-4. Enzyme rate versus copper concentration. The DNA concentration was at 5 μM, MPIX at 33 μM. The reaction was performed at 25°C in SB buffer.

3.3. Inhibition studies using NMM and metalloporphyrins

TSAs are effective competitive inhibitors of the catalyzed reaction. Table 3-1 shows the effect of added NMM, as well as of various metalloporphyrins [including the products, Cu(II)-MPIX and Zn(II)-MPIX, of the experiments described above] on the catalyzed rates. NMM was indeed an efficient inhibitor; at 1:1 and 1:3 ratios of the enzyme to NMM, the catalytic activity was reduced by 26% and 48% respectively [the catalytic antibody (Cochran & Schultz, 1990) was inhibited by 40% and 100% respectively].

Table 3-1. Results of inhibition studies using NMM and various metalloporphyrins*

Porphyrin concentration	% I (1:1)	% I (3:1)	% I (6:1)
NMM	26	48	81
Zn(II)-MPIX		5	3
Cu(II)-MPIX		8	5
Fe(II)-MPIX		19	30
Hemin		20	43

***Inhibition experiments were carried out at 5 μM PS5.ST1 and 100 μM MPIX concentrations in SB buffer. All other conditions were as in Fig. 3-2. The concentrations of the inhibitors used were: 5 μM ("1:1"), 15 μM ("3:1") and 30 μM ("6:1"). Individual data points varied <10% on duplication. Catalytic initial rates were calculated by subtracting the uncatalyzed rates from the corresponding total rates, both determined in the presence of inhibitors. Percentage inhibition (*I*%) was calculated as follows: $I\% = (v_0 - v_I)/v_0$, where v_0 was the catalytic initial rate without inhibitor, and v_I the catalytic initial rate with inhibitor.**

Cu(II)-MPIX and Zn(II)-MPIX, up to 30 μM concentrations, did not significantly inhibit catalysis. However, Fe(III)-MPIX and its protoporphyrin analog (hemin) were good inhibitors. N-alkylporphyrins have much bigger basicity than non-alkylated porphyrins (see Chapter 1), so at the pH condition used in the studies, NMM was protonated and has a positively charged center. Metalloporphyrins with more positive charge density at the metal center, such hemin, may mimic more closely to NMM (Cochran & Schultz, 1990), and will have inhibitory effects. Our inhibition results agree well with those described for the catalytic antibody (Cochran & Schultz, 1990).

3.4. Metal ion requirements

Ribozymes, in general, require divalent or higher-valent cations in order to fold to their active tertiary structures (Yarus, 1993). Fig. 3-5a shows the influence of magnesium concentration on catalysis by PS5.ST1. Although the selection process for NMM-binding had been carried out in the presence of 10 mM magnesium, the catalysis by PS5.ST1 was found to be inversely corrected with magnesium concentration (with other buffer components being held constant). A complete absence of magnesium gave the maximal catalysis (at 180% of the rate measured in the selection buffer). Thus, it appears that PS5.ST1, unlike other ribozymes, can be catalytic in the absence of divalent or higher-valent cations.

We therefore examined for possible requirements for either sodium or potassium or both in the reaction buffer. Fig. 3-5b shows that PS5.ST1 was fully functional in 225 mM potassium acetate but was not at all catalytic in 225 mM sodium acetate. This

Fig. 3-5. Metal ion requirements for the formation of Cu(II)-MPIX catalyzed by PS5.ST1.

(a) Histogram of the PS5.ST1-catalyzed rates of Cu (II)-MPIX formation in SB buffer, but containing varying magnesium concentrations. The white bar (10 mM Mg^{2+}) represents the rate in standard SB buffer, and was taken to be the standard against which the other rates were measured. The reaction conditions and sampling procedures were as in Fig. 3-2. Individual data points varied <10% on duplication.

(b) Histogram of the PS5.ST1-catalyzed rates of Cu (II)-MPIX formation (with respect to the catalyzed rate in SB buffer) under different salt conditions. SB' buffer consisted of 100 mM Tris (pH 7.4), 5% dimethylsulfoxide, 0.5% Triton X-100, and 1 mM of $Cu(OAc)_2$. The conditions for the experiment were as in Fig. 3-2. Individual data points varied <10% on duplication.

(c) Histogram of the PS5.ST1-catalyzed rates of Cu (II)-MPIX formation (with respect to the catalyzed rate in SB buffer) in the absence of sodium and magnesium and in the presence of different concentrations of potassium. Reactions were carried out in SB' buffer (as above), supplemented with the potassium acetate concentrations indicated. The two data points for each potassium concentration show independent experiments. The conditions for the experiments were as in Fig. 3-2.

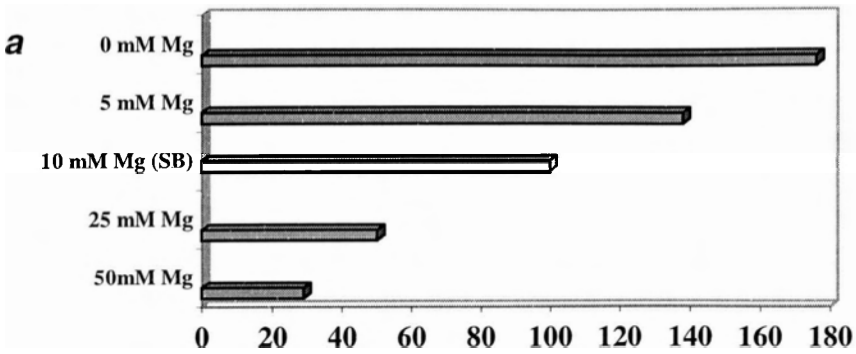
a
0 mM Mg
5 mM Mg
10 mM Mg (SB)
25 mM Mg
50mM Mg
0 20 40 60 80 100 120 140 160 180
Relative Activity (%)

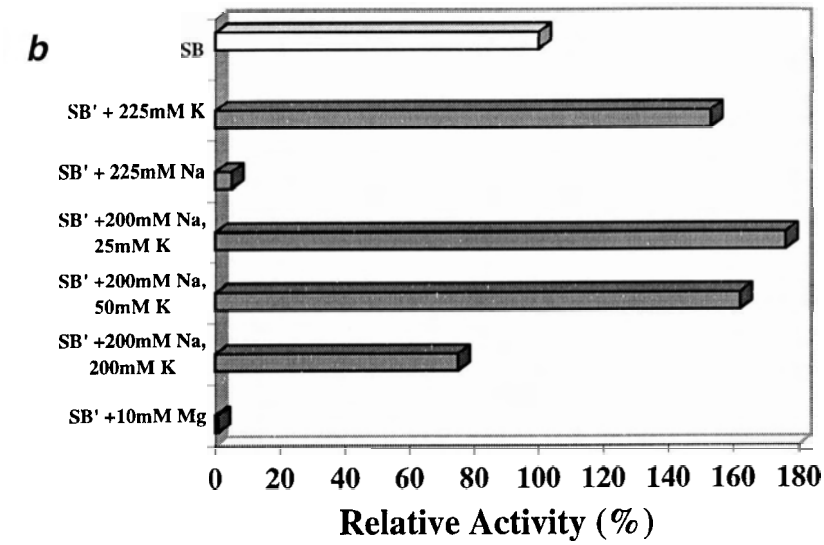
b
SB
SB' + 225mM K
SB' + 225mM Na
SB' +200mM Na, 25mM K
SB' +200mM Na, 50mM K
SB' +200mM Na, 200mM K
SB' +10mM Mg
0 20 40 60 80 100 120 140 160 180
Relative Activity (%)

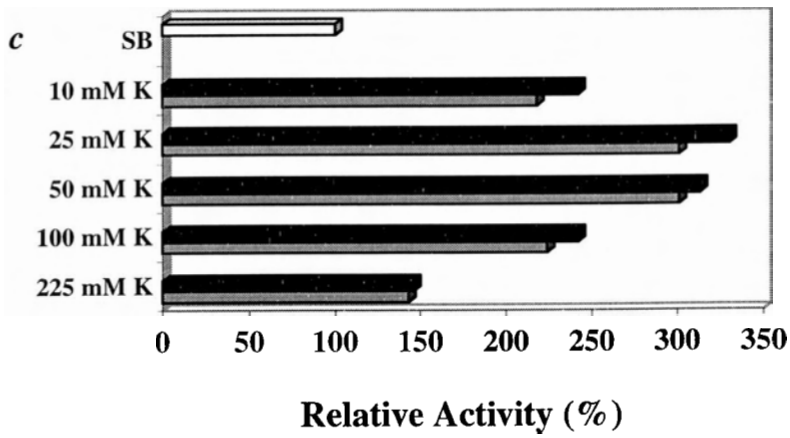
c
SB
10 mM K
25 mM K
50 mM K
100 mM K
225 mM K
0 50 100 150 200 250 300 350
Relative Activity (%)

potassium-sodium switch, and the strongly guanine-rich sequence of PS5.ST1, were powerfully suggestive of the presence of guanine-quartets (which are strongly stabilized by potassium but not by sodium; Williamson et al., 1989; Sundquist & Klug, 1989; Sen & Gilbert, 1990) in the enzyme's folded structure. Fig. 3-5c shows that in the absence of both sodium and magnesium, 25-50 mM potassium gave the optimal catalysis.

3.5. Substrate discrimination

The catalytic antibody reported for porphyrin metallation (Cochran & Schultz, 1990) was highly discriminating in terms of substrate; thus, PPIX was not a substrate for the catalytic antibody. PPIX, however, was an excellent substrate for PS5.ST1; the observed catalytic ratio ($v_{cat + uncat} / v_{uncat}$) at 100 μM PPIX concentration was 9.5 (compared to 4.5 at 100 μM MPIX concentration). PPIX therefore appeared to be a better substrate for metallation by PS5.ST1 than MPIX, the substrate for which it was selected. (More detailed work in Chapter 4 confirmed this preliminary finding).

3.6. Other catalytic aptamers from the final selection pool

As we reported before, after 12 rounds of the *in vitro* selection using random DNA library, we have cloned, isolated and sequenced 24 PS-series aptamers (Chapter 2). Among them, PS2 and PS5 were randomly selected initially to test for their catalytic abilities towards the metallation of MPIX. Questions remained as regard to how many catalytic clones existed in the final selection pool and how efficient the selection scheme was. Therefore, it is important for us to examine extensively the catalytic behavior of the

binding sites from all clones. Twenty new short oligomers corresponding to the G-rich binding site of every sequence (PS14, 18, 21 are almost identical clones) were synthesized and their chelating activity was assayed. We found that, among them, 30% sequences were not catalytic (catalytic rates < 0.1 μM/min, assayed in 40KB buffer which is the optimized buffer condition for the catalysis, see Chapter 4), 45% were weakly active (catalytic rates at 0.1 μM/min to 0.3 μM/min, data not shown), and 25% were strongly active. Table 3-2 shows the sequences of those catalytic oligomers and their catalytic rates.

Table 3-2. Catalytic G-rich sequences derived from small aptamers

Oligomer name	Sequence	Sequence length	Activity μM/min
PS5.ST1	**5'TCGTGGGTCATTGTGGGTGGGTGTGGCTGGTCC3'**	33mer	2.06
PS9.ST1	**5'GGTGATTCGGGTAGGGCGGGCGGT3'**	24mer	0.52
PS12.ST1	**5'GAGGTTTGGGGAAGGGTCGGTGGG3'**	24mer	0.62
PS19.ST1	**5'AGGTTATAGGGCGGGAGGGTGGT3'**	23mer	1.83
PS22.ST1	**5'GAGGGGTGGGAGGGTTGG3'**	18mer	0.85
BLD			0.05

Clearly, the data in Table 3-2 indicate that catalysis by PS5.ST1 was not a one time oddity. Interestingly, the initially randomly picked sequence PS5.ST1 was actually the best sequence from the selection pool. Once again, the inspection of the above active sequences did not reveal any apparent consensus alignment except that they are all very G-rich and have good potentials to form guanine-quadruplex structures. So do the

weakly active and non-active sequences. Detailed work in later stage, however, did indicate that the above five sequences could all form a class of quadruplex structures, which have very unique features different from quadruplex structures formed by those non-NMM-binding but G-rich sequences. I will describe the results in Chapter 5.

4. Summary and next stage of experimentation

In summary, we found that DNA is competent to catalyze porphyrin metallation, with a maximal efficiency comparable to that of a catalytic antibody for the same reaction. The derivation of this catalytic DNA broadens our conception of the chemistries that nucleic acid catalysts could have catalyzed in a prebiotic world. This DNAzyme (the fourth catalytic DNA reported) is small (33 nucleotides), and is maximally active in the presence of potassium. Its successful derivation based on the preferential binding of its parent aptamer, PS5, to NMM, confirms NMM to be a TSA for porphyrin metallation. Most importantly, it showed once again that the strategy of selecting novel catalytic nucleic acids via TSA-affinity binding is achievable.

Two aspects of detailed studies will be pursued after the initial findings of catalysis by NMM aptamers for porphyrin metallation. Based on the fact that the catalysis can be inhibited by magnesium and has no requirement for sodium which are both present in the selection buffer, it is necessary for us to systematically examine the effects on the DNAzyme's catalytic capability by each and every buffer components, as well as by reaction parameters such as temperature and pH. We also wanted to investigate usage range of porphyrin substrates by PS5.ST1, to derive the minimal and

optimal catalytic sequence from clone PS5; to check whether there is a weak catalytically relevant copper binding site on the catalytic DNA sequence, and to determine possible effects on the DNAzyme's stability by copper ion (a known denaturant for double helical DNA). The results will be described in next chapter (Chapter 4).

Several lines of evidence supported our speculation that the catalytic DNAzyme PS5.ST1 folds to form a G-quadruplex-related structure. We wanted to produce more results to confirm this speculation. If indeed the DNAzyme folds into a quadruplex structure, we would like to know whether the quadruplex core is actually the enzyme's active site or it only functions as a supporting structural foundation to hold the catalytic active site. I will describe those results in Chapter 5.

Chapter 4. Optimization of the Catalytic Properties of PS5.ST1

1. Introduction

In Chapter 3, I described a small DNA oligomer, PS5.ST1 (33 nucleotides), which catalyzed the insertion of Cu(II) and Zn(II) into MPIX. This DNA enzyme exhibited a k_{cat} of 13.7 per hour, a K_M of 2.9 mM, and a catalytic ratio (k_{cat}/k_{uncat}) of ~1400 for the formation of Cu(II)-MPIX at a fixed copper concentration of 1 mM. The k_{cat}/k_{uncat} value was comparable to that of a catalytic antibody derived using the same transition state analog (Cochran & Schultz ,1990). The DNAzyme, however, was much less efficient at binding and processing MPIX compared to the catalytic antibody as well as a number of naturally occurring ferrochelatases (Lavallee, 1988). On the other hand, we have shown that the DNAzyme could use porphyrin substrates other than MPIX, for which the DNA enzyme was derived. This was contrary to the antibody which only recognized MPIX as the substrate (Cochran & Schultz, 1990), but similar to the ferrochelatases which could use several porphyrins as their substrates, including PPIX (the natural substrate), MPIX, DPIX and HPIX (Lavallee, 1988). In this chapter, we firstly investigated the scope of substrates recognizable by our DNA enzyme (for the structures of the above porphyrins, see Table 1-1 of Chapter 1).

The sequence of PS5.ST1 was chosen on the basis of footprinting studies carried out on its parent sequence, PS5 (see Chapter 2). PS5.ST1 might not be the precise representation of the best catalytic sequence from within clone PS5. Therefore, we were

interested in finding out both the optimal and the minimal sequences responsible for the catalysis.

For our selection experiment, we had used a buffer that contained the same components for the studies carried out on the catalytic antibody (Cochran & Schultz, 1990), with the addition of 10 mM $MgCl_2$ (Mg^{2+} is frequently used to fold DNA or RNA sequences). Our initial findings that Mg^{2+} was inhibitory towards the enzyme activity and that Na^+ was not required for the catalysis, made us think it necessary to investigate how the catalytic ability of the DNA enzyme was affected by the other buffer components, as well as by such experimental parameters as pH and temperature. In other words, we were interested in establishing an optimal condition for the catalytic DNA to perform its best catalysis, by a thorough examination of the effects imposed on the catalysis by the buffer components and other reaction parameters.

The roles of Mg^{2+} and K^+ were quite well understood in our previous study (Chapter 3), but that of sodium was not well defined except the understanding that it was not required for catalysis. The fact that potassium enhanced the enzyme activity, along with the G-rich nature of PS5.ST1 and the results of our DMS probing experiment on PS5 (Chapter 2), suggested that the folded form of PS5.ST1 probably contained guanine quartets. Sodium is known to have the ability to promote and stabilize the formation of G-quartets, although it is much less efficient than potassium (Sen & Gilbert, 1990). Therefore it was interesting to know whether high concentrations of sodium would support the catalysis by PS5.ST1.

In addition to the above, we carried out experiments to investigate the existence of a catalytically relevant copper-binding site within the DNAzyme as well as possible denaturation effects of copper(II) ions on the DNAzyme.

Finally, we made appropriate comparisons of the catalytic properties of various protein, DNA and RNA catalysts that now exist for porphyrin metallation.

2. Materials and methods

2.1. Materials

Porphyrins were purchased from Porphyrin Products (Logan, UT) and used without further purification, except that in the sodium dependent catalysis experiments (section 3.9) MPIX was washed extensively with double-distilled water to remove any possible metal ion contaminants. High concentration stock solutions of the various porphyrins were made by directly dissolving the porphyrins in the appropriate buffer solution in which the enzyme activity was going to be assayed. These stocks were stored in the dark at 5°C. All porphyrin concentrations were quantitated by standard spectroscopic methods (Smith, 1975; Gunter et al., 1989). Under these conditions, the MPIX stock solution was found to be stable for weeks without decomposition or precipitation; stocks of PPIX, however, needed to be made up fresh daily, for the solutions showed a significant decomposition with prolonged storage (assayed by HPLC, data not shown) (Dinello & Chang, 1978).

2.2. Purification and treatment of DNA oligomers

DNA oligomers were synthesized at the University Core DNA Services at the University of Calgary. Synthesized DNA sequences for DNAzyme assays were purified as follows: the oligomers were size-purified in preparative polyacrylamide gels; the gel slices containing the DNA were eluted with TE buffer (10 mM Tris, pH 7.4, 0.1 mM EDTA) overnight. The eluants were then passed through Spice C18 (Rainin) columns, and the retained DNA washed with water and eluted with 30% acetonitrile. DNAs purified in this way were lyophilized and dissolved in 10 mM Tris acetate, pH 7.4, and stored at -20°C. It was important to avoid all salt solutions during the C18 purification procedure because metal ions (Mg^{2+}, Na^{+}, K^{+}, and possibly, others) had significant effects on the catalytic rates (see Results and discussion section). For the metallation assays, the DNAzyme oligomer was denatured in 10 mM Tris acetate buffer at 90° for 5 minutes and allowed to cool slowly (over 1h) to room temperature.

2.3. General assay protocols

For the HPLC analysis of all metallation reactions, Ni(II)-MPIX was used as an internal standard.

For accuracy in the making up of the final reaction mixtures, each of MPIX, copper, and Triton, were assembled from 2× to 20× stock solutions made up in the appropriate buffer solutions. The order of addition of the different reaction components was particularly important. DNA was preincubated with MPIX at the assigned reaction temperature, for 10-20 minutes, then combined with appropriate volumes of the same

solution containing the copper acetate (all stock buffers were brought to the reaction temperature first). For the HPLC analysis, aliquots of the reaction mixture were withdrawn at a given time, quenched with 200 mM Tris, pH 9.0 and 15 mM EDTA, mixed with a fixed volume of buffer containing the internal standard, and injected into the HPLC column. Initial rates were calculated from the linear portions (at less that 10% product formation, at least five time points taken for this portion and no end-point correction made) of product concentration versus time plots. The initial rate measurements were duplicated (with <15% variation), and average values were taken.

Once quenched, as above, the reaction mixtures were very stable [with the ratio of Cu(II)-MPIX:MPIX remaining virtually unchanged for at least one week after quenching, at 25°C storage]. The reactions were analyzed by HPLC (a Waters 600E Multisolvent System with a Waters 991 photodiode Array Detector), at 25°C. The column used was a μBondapak C18 10 μm, and the mobile phase was 85% methanol and 15% 1 M ammonium acetate, pH 5.2.

2.4. Protocols for individual experiments

2.4.1. Substrate usage

The metallation reactions were carried out in SB buffer [100 mM Tris, pH 7.1 (note: all pH values in this chapter were for the final solution, and measured at 20°C), 200 mM NaOAc, 25 mM KOAc, 10 mM $Mg(OAc)_2$, 5% DMSO, 0.5% Triton X-100]. PS5.ST1 was at 5 μM, and the Cu^{2+} and porphyrin ([S]) concentrations were as indicated

in Table 4-1. The reactions were allowed to proceed at 25°C. HPLC conditions used to separate and analyze the different porphyrins and their product metalloporphyrins are summarized in Table 4-2.

2.4.2. Sequence optimization

The reaction was carried out at 25°C in 225KB buffer (100 mM Tris, pH 7.1, 225 mM KOAc, 5% DMSO, and 0.5% Triton X-100), with 33 μM of MPIX and 5 μM DNA. All the DNA oligomers had been gel-purified and recovered by ethanol precipitation.

2.4.3. pH dependence

The reactions were carried out under conditions similar to those described for the sequence optimization experiments, except that the buffers were as follows: For the buffers at pH ≥ 7.0, 100 mM Tris was used; for pH 5.5-7.0, 100 mM MES was used; for pH 4.0-5.6, 50 mM potassium acetate buffer was used (the MES and acetate buffers also contained 100 mM Tris acetate). Each buffer also contained 50 mM potassium acetate, 5% DMSO, and 0.5% Triton X-100. Individual buffers were made up as 2× stocks, and their pH was adjusted by titrating with 10% acetic acid. The MES buffers (containing Tris acetate) appeared to buffer their specified pH stably.

2.4.4. Temperature dependence

The reactions were performed in a thermal cycler (utilized as a constant temperature bath). The buffer used was the MES-Tris buffer 50KB (100 mM MES, pH

6.2. 50 mM KOAc, 100 mM Tris acetate, 5% DMSO, and 0.5% Triton X-100), with DNA at 5 μM, MPIX at 33 μM, and $Cu(OAc)_2$ at 1 mM. Metallation initial rates were measured at 0, 5, 15, 20, 25, 35, 40, 45, 55, and 65°C.

2.4.5. DNA concentration dependence and $Cu(OAc)_2$ concentration dependence

These were both carried out at 15°C, under the same conditions as described for the temperature dependence experiments, except for that the DNA concentrations and Cu(II) concentrations were varied, respectively. For the copper ion concentration assays, the DNA was incubated first with MPIX, for 10-20 minutes, followed by the addition of the copper acetate to start the reaction. The reactions in which the copper was added first gave unpredictable and irregular results.

The DNA preincubation experiments in the presence of copper were carried out as follows: The DNAzyme samples, in 50KB buffer, had copper acetate added to them to final concentrations of 2, 10, and 20 mM, respectively. After an appointed period of pre-incubation, aliquots were withdrawn and mixed with an equal volume of 66 μM MPIX (2× MPIX) in the same buffer, and the metallation reactions allowed to proceed for 20, 3, and 1 minutes, respectively. The analysis of product and substrate was carried out by HPLC, as usual.

To monitor for the precipitation of the DNA following the copper pre-incubations, ^{32}P-labeled PS5.M was used, and the samples spun in a microfuge at 13,000 rpm. The counts remaining in solution were monitored by scintillation counting.

2.4.6. DMSO and Triton X-100 concentration dependence

The xperimental conditions were as described for the temperature dependence experiments, at 15°C, except that the DMSO and, separately, Triton X-100 concentrations of the buffer were varied. DMSO concentrations (v/v%) of 0, 0.8, 2.5, 5, 10, 20 %, were assayed; as were Triton X-100 concentrations of 0.08, 0.25, 0.5, 1.0, and 2.5% (w/v).

2.4.7. Buffer effects

These were tested with 2.5 μM DNA, 33 μM MPIX, 50 mM KOAc, 0.25% Triton X-100, and 1% DMSO held constant. The buffers used were made up as described in the pH dependence section.

2.4.8. Sodium and potassium dependence

They were carried out at 25°C, in 50 mM Tris, pH 7.3, 1% DMSO, and 0.25% Triton, with variations in the concentrations of either sodium (at 0, 5, 10, 25, 50, 100, 225, 500 mM) or potassium (at 0.1, 1, 10, 25, 50, 100, 200 mM).

2.4.9. k_{cat} and K_M measurements for MPIX and PPIX

These were carried out at 15°C, in 40KB buffer, with DNA at 1.5 μM and $Cu(OAc)_2$ at 1.0 mM. The initial rates were determined for both enzymatic and background reactions at 10, 15, 20, 30, 45, 70, and 100 μM of MPIX and, separately, at 3.5, 5.0, 7.0, 10.0, 14.0, and 20.0 μM of PPIX, respectively. The k_{cat} and K_M values were calculated using the GraFit 3.0 program.

3. Results and discussions

3.1. Substrate range of PS5.ST1

Although PS5.ST1 had been derived to have MPIX as its expected substrate (on the basis of the fact that PS5 had been selected for binding to methylated MPIX, i.e., NMM), our previous study (Chapter 3) had indicated that the porphyrin PPIX was possibly an even better substrate for PS5.ST1 than MPIX. We therefore examined six different porphyrins to see if they were acceptable as substrates by PS5.ST1, for copper insertions. Table 1-1 of Chapter 1 (p27) summarizes their names and structures. Experiments were carried out in SB buffer, at 25°C, in the presence of either 5 μM of PS5.ST1, or 5 μM of a non-catalytic oligomer, REP2 (see Fig. 3-1 of Chapter 3, p77).

Table 4-1 (p100) shows the results for both the enzymatic and nonenzymatic reactions. The acceptable substrates for PS5.ST1 are MPIX, PPIX, and DPIX, whereas the other porphyrins are not. The three substrate porphyrins are closely related to one another in structure; however HPIX (which differs from MPIX in the replacement of one secondary hydrogen atom from each of the two ethyl groups, at positions 2 and 4, by a hydroxyl group) is not a substrate. Thus, the acceptable functionalities at positions 2 and 4 of the porphyrin ring may be vinyl or ethyl or hydrogen; however, the presence of the hydroxyl groups in HPIX abolished the catalysis. The experiments above do not reveal whether HPIX simply does not bind to PS5.ST1, or whether, having bound, it is not amenable to the structural distortion necessary for catalysis. Conceivably, the hydroxyl groups could interfere with binding into the active site by being sterically larger than the

hydrogen atoms they replace, or by introducing polar entities into what might be a hydrophobic region of the active site. Future experiments with other porphyrins, and mutagenesis of PS5.ST1, should clarify these findings.

Table 4-1 Rate parameters for DNAzyme-catalyzed and background (noncatalyzed) metallations of different porphyrins

Porphyrin	[S], μM	[Cu(II)], mM	V_{total}, μM/hr	V_{uncat}, μM/hr	V_{total}/V_{uncat}
MPIX	100	1	3.71	0.82	4.5
PPIX	100	1	10.55	1.06	9.9
DPIX	100	1	20.25	5.51	3.7
HPIX	100	1	~95	~95	1
CPIII	50	0.2	~600	~600	1
UPIII	50	0.2	~1200	~1200	1

The finding that CPIII and UPIII were not the substrates for PS5.ST1 could be rationalized in terms of their divergent structures, and the high degree of steric clash their extra carboxylic groups might encounter in the active site, and electrostatic repulsion between the highly negatively charged DNA and the carboxylates.

In terms of substrate usage, PS5.ST1 shows both similarities and differences with natural ferrochelatases (from various sources), in that both appear to act on MPIX, PPIX and DPIX (Taketani & Tokunaga, 1981, 1982; Dailey & Smith, 1984; Lavallee, 1988), but not on CPIII (Taketani & Tokunaga, 1981, 1982). However, the ferrochelatases also use hematoporphyrin as a substrate, at the same level as protoporphyrin (Taketani & Tokunaga, 1982; Dailey & Smith, 1984; Lavallee, 1988). And, by contrast to both the

Table 4-2. HPLC conditions for the analysis of metallation by different porphyrins

Porphyrin	Flow rate (ml/min)	Retention time for substrate (min)	Retention time for product (min)	Wavelength for monitoring (nm)
MPIX	2.0	6.2	15.6	390
PPIX	2.0	7.1	16.5	400
DPIX	1.5	4.7	10.0	390
HPIX	1.0	4.1	5.8	390
CPIII	1.0	3.6	4.7	390
UPIII	1.5	3.1	5.2	400

DNAzyme and the ferrochelatases, the catalytic antibody for porphyrin metallation (Cochran & Schultz, 1990) accepts only MPIX as substrate. No data on substrate usage have been reported for a recently described catalytic RNA for porphyrin metallation (Conn et al., 1996). Although the high substrate-specificity of the catalytic antibody was consistent with the properties of many protein active-sites and binding-sites in general, recent papers have also reported highly specific bindings of small organic ligands by RNA aptamers (Famulok & Szostak, 1992; Jenison et al., 1994; Geiger et al., 1996). The nature of interactions between active sites and substrates in the different DNA, RNA, and protein catalysts for metallation remains, therefore, an important area for investigation in the future.

3.2. Optimally catalytic fragment of aptamer PS5

The 5' and 3' boundaries of the PS5.ST1 fragment of the 112-nucleotide, and NMM-binding, aptamer PS5 (Chapters 2 and 3), had been chosen initially on the basis of footprinting studies carried out on PS5 (in the presence of bound NMM and hemin, see Chapter 2). Those data had indicated that the first G-motif (underlined, below) within PS5.ST1 (5'-<u>TCGTG GG</u>**TCA TTGTG GGTGG GTGTG G***CTGG TCC*-3'), was not footprinted (whereas the guanines in the sequence not underlined did footprint). However, the 5' motif, being directly adjacent to the footprinted region within PS5, had been included in the design of PS5.ST1. To determine whether the motif was required after all, and to pinpoint the most optimal catalytic sequence within PS5, a number of oligomers centered around the footprinted region were synthesized (Fig. 4-1, p103), and tested for their ability to catalyze metallation. The results are summarized in Fig. 4-1. Even the deletion of TCG from the 5' end (as in PS5.A) resulted in a 56% loss in activity, whereas the deletion of the entire 5'-most motif (as in PS5.B) essentially abolished catalytic activity. By contrast, the 3'-most G-motif (italicized above), which footprinted in the presence of NMM in PS5 (Chapter 2), appeared not to be important for catalysis. The optimal (and minimal) catalytic sequence therefore corresponded to the 24-nucleotide, very guanine-rich (14 guanines out of 24 bases) oligomer PS5.M (shown in bold type above), and this was the sequence chosen for the further studies described below.

Two points of interest are raised by the above results: (a) that the NMM-footprinted region within PS5, and the catalytic sequence, overlap but do not coincide;

and (b) that the relatively low catalytic activity of the parent sequence, PS5, compared to those of the fragment PS5.ST1 (and PS5.M), may be connected with somehow different folding patterns for the two. Regarding point (a), it is conceivable that the guanines identified by methylation protection in PS5 participated purely in the DNA folding (i.e., that the footprint reflects intra-DNA interactions, rather than DNA-NMM interactions). If so, some residues that did not footprint could yet be involved in NMM binding, and therefore required for catalysis. As for point (b) it may be that the PS5 and PS5.M sequences fold similarly but not identically, leading to differences in catalytic activity; or else, that the non-catalytic elements of PS5 interfere with the diffusion of substrate

	DNA sequence	Relative activity
PS5.ST1	5'-TCGTG GGTCA TTGTG GGTGG GTGTG GCTGG TCC-3'	100
PS5.A	5'-TG GGTCA TTGTG GGTGG GTGTG GCTGG TCC-3'	44
PS5.B	5'-TCA TTGTG GGTGG GTGTG GCTGG TCC-3'	4
PS5.D	5'- TTGTG GGTGG GTGTG GCTGG-3'	15
PS5.E	5'- TG GGTGG GTGTG GCTGG T-3'	4
PS5.F	5'-TCGTG GGTCA TTGTG GGTGG GTGTG GCTGG T-3'	78
PS5.G	5'-TCGTG GGTCA TTGTG GGTGG GTGTG GCT-3'	117
PS5.H	5'-TCGTG GGTCA TTGTG GGTGG GTGT-3'	4
PS5.J	5'-TGG GTGTG GCT-3'	0
PS5.K	5'-GAAGA TCGTG GGTCA TTGTG GGTGG GTGTG GCT-3'	106
PS5.L	5'-GTGTC GAAGATCGTG GGTCA TTGTG GGTGG GTGTG GCT-3'	111
PS5.M	5'-GTG GGTCA TTGTG GGTGG GTGTG G-3'	137
OTA	5'-TTTTG GGGTT TTGGG GTTTT GGGGT TTTGG GG-3'	0
REP2	5'-AATAC GACTC ACTAT AGGAA GAGAT GGTTT TTCCA TCTCT	0
BLD	5'-AATAC GACTC ACTAT AGGAA GAGAT GG-3'	0

Fig. 4-1. Sequences of DNA molecules used to determine the optimal catalytic sequence within the aptamer PS5. REP2 and BLD were control oligomers; OXY4 was a guanine-rich telomeric sequence. The relative activity was defined as follows: Relative Activity = 100 $(v-v_{bld})/(v_{PS5.ST1}-v_{bld})$, in which $v_{PS5.ST1}$, v_{bld}, and v are the initial rates for PS5.ST1, BLD (reference DNA) and other oligomers, respectively.

molecules into the active site. Detailed studies to resolve these possibilities have confirmed our speculations and the results will be discussed in Chapter 5.

3.3. Optimal pH for catalysis

The effectiveness of catalysis by PS5.M in the pH range of 4-8 was examined. Fig. 4-2 shows the velocities for the PS5.M-catalyzed and the uncatalyzed (in the presence of the control oligomer BLD, see Fig. 4-1) reactions. For our original experiments carried out around neutral pH (in SB buffer), Tris had been the buffer used. However, preliminary measurements carried out at non-neutral pHs, using other buffering agents (such as MES), showed sharp, and buffer-specific, changes in the background reaction rates. We found that the inclusion of a certain concentration of Tris (as Tris acetate) in the MES-buffered acidic solutions appeared to counter this effect (discussed in detail in a later section on buffer-specific effects, see Section 3.8). Therefore, for pH values > 7.0, 100 mM Tris was used for buffering; whereas below pH 7.0, 100 mM MES (between pH 5.5 and 7.0) or potassium acetate (between pH 4.0 and 5.5) were used (in each case, containing 100 mM Tris acetate, in addition to the other metallation reaction components such as potassium acetate, DMSO, and Triton X-100).

Fig. 4-2 (p105) shows that both the PS5.M-catalyzed and the background rates peaked at around pH 6.2. The DNA-mediated catalysis mechanism appeared to retain the pH-dependence of the uncatalyzed reaction. The bell-shaped profiles for both the catalyzed and background rates could reflect a number of events, including the following: The increase in rates from pH 7.6 to 6.2 correlated with progressively lower

concentrations of the unprotonated Tris base [Tris base is reported to chelate weakly with Cu^{2+} ions (Hall et al., 1971; Bai & Martell, 1969)]. In addition, at the basic end of the spectrum, the copper complexes become resistant to loosing water (necessary for

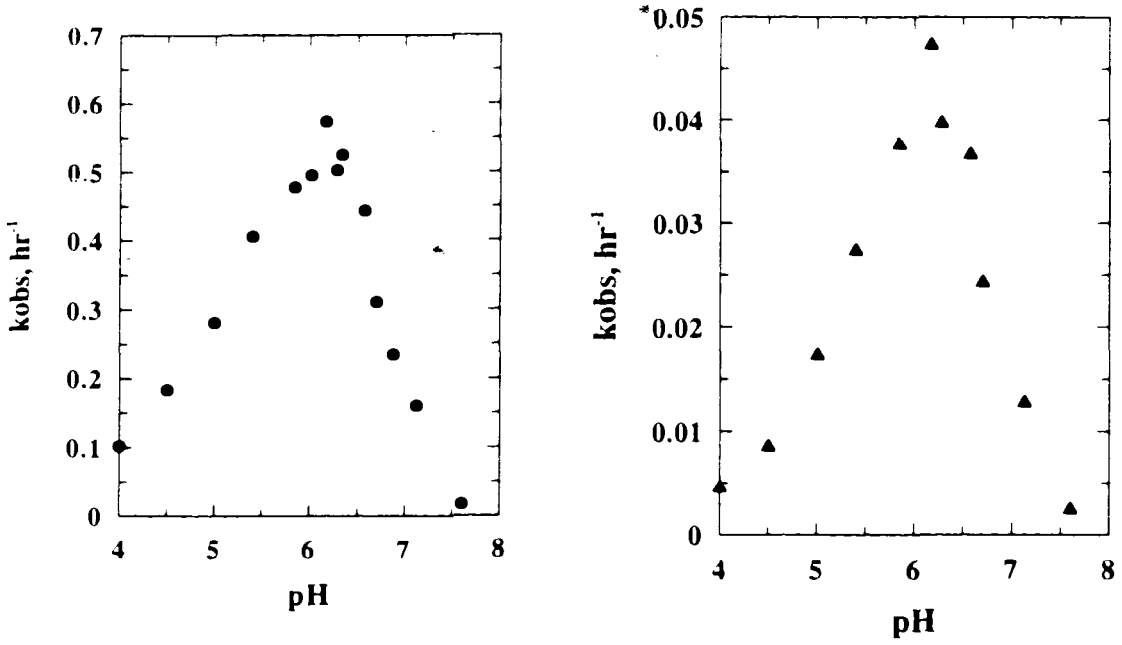

Fig. 4-2: pH profiles of the DNAzyme-catalyzed and background (noncatalyzed) metallations. (left panel) v_{cat} plotted against pH for the PS5.M-catalyzed reaction (filled circle), and (right panel) v_{uncat} plotted against pH for the uncatalyzed reaction, in the presence of the control oligomer BLD (filled triangle). The experimental protocols are described in Materials and methods.

metallation) by virtue of becoming hydroxyl complexes [the first pKa of Cu^{2+}-bound water is at ~ 6-7 (Burgess, 1978)]; and this, too, might be reflected in the overall metallation rate. On the other side of the curve, the drop in rate from pH 6.2 to 4.2 may reflect the protonation of a pyrollic nitrogen atom of the porphyrin (Smith, 1975). The

slope of log(V) vs. pH is only ~0.3, far smaller than 1, and this suggests that no proton transfer was taken place in the transition state.

Interestingly, a pH of approximately 8.0 was found to be optimal for catalysis by the ferrochelatases [utilizing as substrates MPIX and Zn^{2+} (Li et al., 1987), MPIX and Co^{2+} (Roberts, 1987), as well as MPIX and/or PPIX with Fe^{2+} (Taketani & Tokunaga, 1981; Labbe & Hubbard, 1960; Goldin & Little, 1969; Porra & Jones, 1963; Krueger et al., 1956)]. However, none of these studies reported the pH profiles for the background, uncatalyzed reactions, leaving it uncertain whether the pH had a direct influence on the structure and activity of these enzymes. Separate studies on the nonenzymatic formation of mesoheme [Fe(II)-MPIX] reported pH optima of 9.5 (Kassner & Walchak, 1973), and 8.8 (Taketani & Tokunaga, 1984), respectively, under similar experimental conditions as used for the ferrochelatase studies. Thus, it was conceivable that the reported pH optima of 8.0 for the ferrochelatases did reflect attributes of the enzymes themselves.

On the base of our own finding of a pH optimum of 6.2 for metallation (under our experimental conditions), this pH was used for all subsequent optimization experiments.

3.4. Catalyzed rate vs temperature

We investigated the rates of metallation of MPIX by copper at different temperatures, in the presence of PS5.M, or of the control oligomer BLD. Fig. 4-3a (p107) plots rate as a function of temperature for both the total (background plus catalyzed) reaction, and for the background reaction itself. Fig. 4-3b shows the net catalyzed rate, v_{cat} [obtained by subtracting the background rate, v_{uncat}, measured in the presence of BLD,

from the total rate, v_{total} (equal to v_{cat} + v_{uncat}), measured in the presence of PS5.M]. The background rate increases exponentially with temperature (Fig. 4-3a), whereas the net catalyzed rate (Fig. 4-3b) shows an approximately bell-shaped profile, with a maximum at

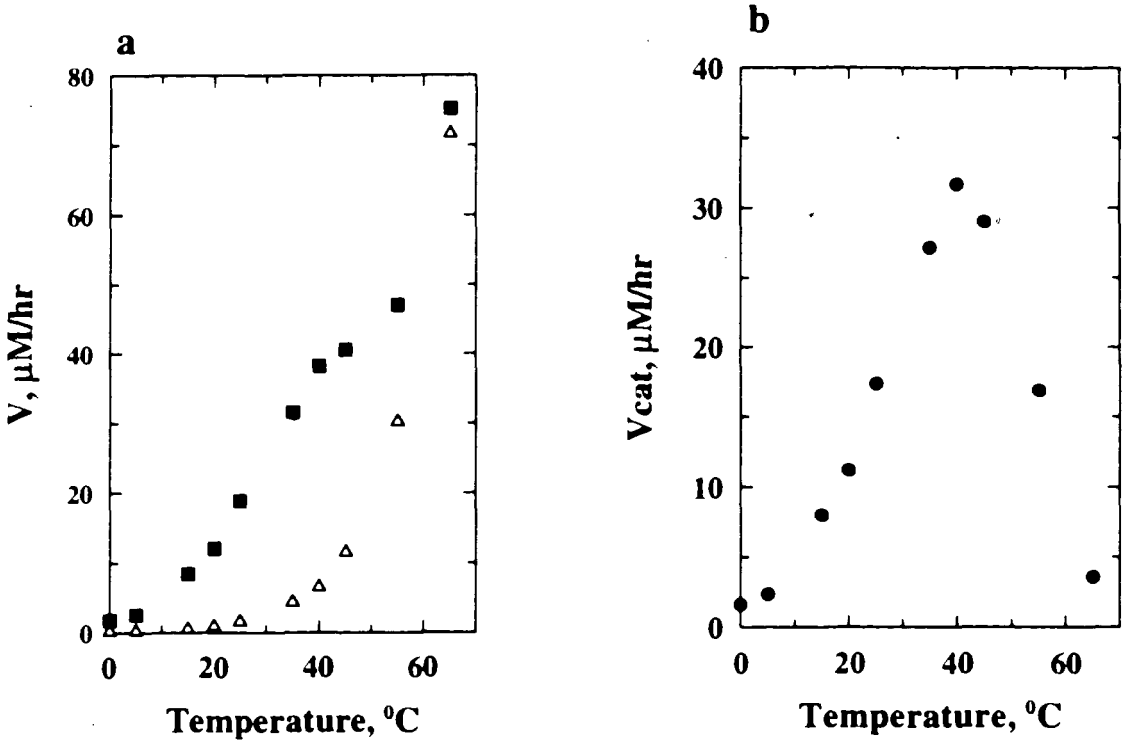

Fig. 4-3. Temperature profiles of the DNAzyme-catalyzed and background (noncatalyzed) metallations. (a) v_{total} (filled square, in the presence of 5 μM PS5.M) and v_{uncat} (open triangle, in the presence of 5 μM BLD) versus temperatures. (b) v_{cat} (filled circle; $v_{cat} = v_{total} - v_{uncat}$) vs temperature. The experimental conditions are outlined in Materials and Methods.

40°C. The bell-shaped catalyzed rate profile may be modelled as,a balance of two opposed tendencies: the natural temperature dependent increase of the catalyzed rate, combined with a progressive instability, and tendency to denaturation, of the folded

PS5.M. In addition, G-quadruplex structures are highly polymorphic class of structures, which are able to interconvert with changes in conditions (Williamson, 1994). A preliminary melting curve of PS5.M (data not shown) appears to be consistent with this notion. Interestingly, the ratio v_{cat}/v_{uncat} reaches a maximum at 15°C. For our remaining experiments, we picked 15°C as the reaction temperature (at which temperature it was also possible to measure accurately a number of very fast catalyzed reactions, described in later sections).

3.5. Catalyzed rate as a function of enzyme concentration

An important test for the catalytic behavior of any putative enzyme is that at constant substrate concentrations (and with all other parameters remaining unchanged), the rate of the catalyzed reaction is directly proportional to the concentration of the enzyme. Fig. 4-4 shows the catalyzed (total minus background) initial rates for different concentrations of PS5.M, measured at two different, and fixed, MPIX concentrations: 33 and 100 μM. Linear relationships between rates and DNAzyme concentrations were obtained in both cases, demonstrating unequivocally the catalytic aspect of PS5.M.

In carrying out these experiments, we observed anomalous results if the DNA had been purified in a certain way. Thus, at the higher DNA concentrations in particular, residual Mg^{2+} ions from ethanol precipitations were found to have an inhibitory effect on the catalysis. Elimination of the ethanol precipitation steps entirely (and the purification of the synthetic DNA oligomers on a desalting G-50 column, followed by water elution and vacuum lyophilization) led to the data reported above.

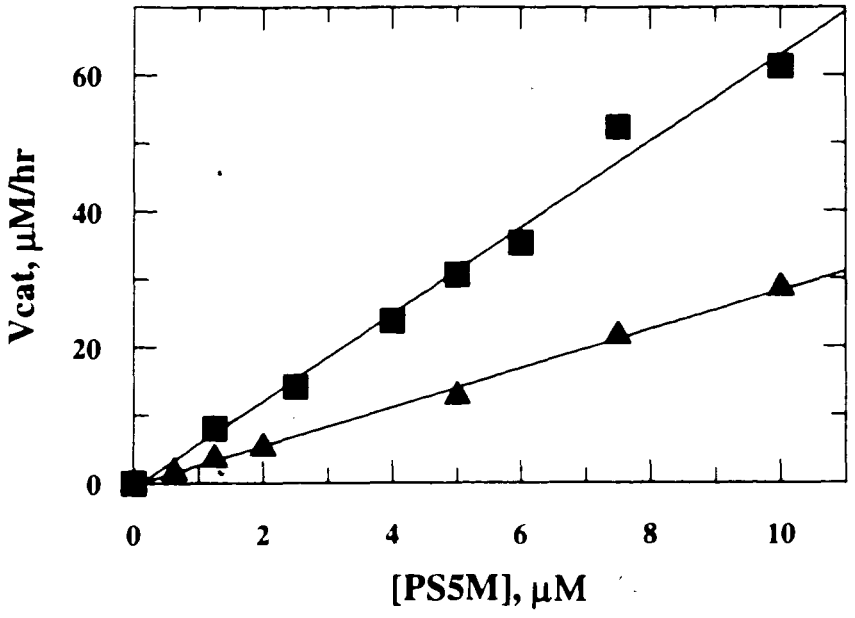

Fig. 4-4: v_{cat} (catalyzed initial rates) as a function of PS5.M concentration. The v_{cat} values were obtained at fixed MPIX concentrations of 33 μM (filled triangle); and, 100 μM (filled square). The reaction conditions are detailed in the Materials and Methods section.

3.6. Is there a binding site for copper at the active site of PS5.M?

An important question that had remained unresolved in the previous chapter concerned the existence or not of a catalytically relevant binding site for copper ion at the DNAzyme's active site. The dependence of the rate of the reaction, at a constant MPIX concentration, on copper concentration up to 2.5 mM had given a straight line plot, with no evident sign of saturation. This appeared to indicate that there was no strong, catalytically relevant copper binding site in the DNAzyme (as with the catalytic antibody,

but unlike the ferrochelatases). However, the possibility that a copper binding site, with a K_M value larger than 2.5 mM, could not rigorously rule out.

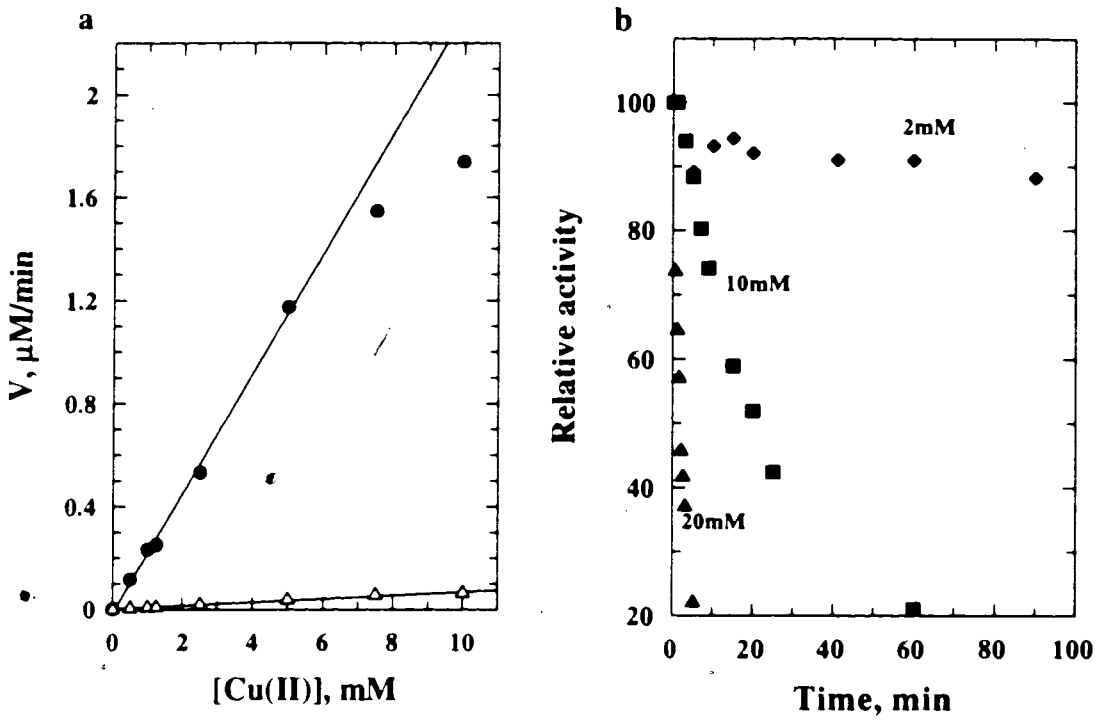

Fig. 4-5. Cu(II) effect on the catalysis and stability of PS5.M. (a): Metallation rates as functions of $Cu(OAc)_2$ concentrations. The metallations were carried out with a fixed MPIX concentration of 33 μM, and 5 μM of either PS5.M (filled circle) or BLD (open triangle). Other conditions are detailed in the Materials and Methods. (b): The enzymatic activity of PS5.M after pre-incubation with copper ions. The preincubations were carried out with $Cu(OAc)_2$ at 2 mM (filled diamond), 10 mM (filled square), and 20 mM (filled triangle), respectively, for the times indicated. Metallation reactions were carried out with PS5.M at 5 μM, and MPIX at 33 μM. The detailed protocols are given in the Materials and Methods section.

We therefore carried out metallation experiments in 50KB buffer (100 mM MES, pH 6.2, 100 mM Tris acetate, 50 mM potassium acetate, 5% DMSO, and 0.5% Triton X-100), and varied the copper ion concentration from zero up to 20 mM. Initial rates for the

metallation of MPIX (itself at a fixed concentration of 33 μM) were then measured. During the initial rate measurements it was found that for copper concentrations up to 10 mM, the formation of Cu-MPIX was reliably linear with time usually below 10% conversion levels of substrate (for both the enzymatic and the non-enzymatic reactions). With copper above 10 mM, linear initial rates could not measured at all, for the formation curves levelled off even before 5% of the substrate had been converted to product.

Fig. 4-5a (p110) shows the plots of the initial rates for both the PS5.M-catalyzed and the background (in the presence of the oligomer BLD) reactions; the rate of the catalyzed reaction was linear with copper concentration up to 5 mM copper, beyond which there appeared signs of a gradual saturation of rate, indicating that there might be a catalytically relevant but weak copper binding site in PS5.M. However, copper ions have been shown, in the absence of other salts, to be potent denaturants of double-stranded DNA (Eichhorn & Shin, 1968), and the "saturation kinetics" seen in Fig. 4-5a would also be consistent with the destruction of the active enzyme at high copper concentrations.

To distinguish between the two possibilities, we carried out experiments in which we preincubated the folded DNAzyme in buffer containing copper ions at 2, 10, and 20 mM, respectively, with each of these preincubations being carried out for a number of different time points. Following each pre-incubation, one volume of the copper- and PS5.M-containing solutions (in reaction buffer) were mixed with one volume of reaction buffer containing 66 μM MPIX (to give final MPIX concentrations of 33 μM). The measured initial rates of the various preincubated samples, as a function of the time of preincubation, are shown in Fig. 4-5b (p110). Enzyme samples preincubated in 2 mM

copper gave approximately the same initial rate, regardless of the length of the pre-incubation; however, in the 10 mM preincubations, the enzyme activity (as indicated by initial rates of the catalyzed reaction) dropped to 50% after as little as 20 minutes of preincubation. With the 20 mM copper samples, the initial rates dropped to 50% after only 2 minutes of pre-incubation.

These data demonstrated that the higher concentrations of copper clearly had a destructive effect on the active form of the DNAzyme. It was therefore likely that the "saturation" of rate seen in Fig. 4-5a did not reflect a real saturation of a binding site for copper in the DNAzyme, but was, rather, the consequence of a time dependent inactivation of DNAzyme in the high concentration copper samples. Clearly, saturation kinetics could not be used in this case to test for the copper binding site. Other experiments need to be designed to detect whether such a binding site does in fact exist.

To test whether the DNA was in fact precipitated in these samples, the samples (containing ^{32}P-labeled PS5.M) were centrifuged in a microfuge for extended periods. However, no radioactive pellet was detected. Therefore, the suspected DNA-copper aggregates, if indeed formed, were not sufficiently insoluble to precipitate. Another possibility is that, instead of forming DNA-copper aggregates, copper may destroy the catalytically active DNA folding by competing for essential hydrogen bonding site on the DNA.

As an interesting note, it was observed that the prior addition of the substrate MPIX to the DNAzyme (before the addition of copper) substantially preserved the DNAzyme from denaturation (data not shown). It was therefore a good practice for the

study of the metallation reactions (particularly at high copper concentrations) to incubate the DNAzyme first with MPIX, for 10 to 20 minutes to allow the formation of DNA-porphyrin complexes, prior to initiating the reaction by introducing copper.

Experiment was also carried out to determine whether the inactivation by copper was reversible--whether catalytic activity could be recovered by decreasing the copper ion concentration. Our result (data not shown) indicated that the inactivation was irreversible. Future experiments will focus on establishing the mode of copper-mediated inactivation of the DNAzyme, i.e., whether it is the result of DNA denatuation, or of a copper-mediated free radical destruction of the DNA, or both.

3.7. Effects of dimethyl sulfoxide and of detergent on catalysis

All the buffers described this far for the assaying of catalysis, contained 5% DMSO and 0.5% of the non-ionic detergent, Triton X-100. The reason for their inclusion was the presumption that they would help increase the overall solubility of the sparingly soluble substrate, MPIX. In addition, Triton X-100 and other non-ionic detergents have been widely used in kinetic studies of metallation reactions (Cochran and Schultz, 1990; Taketani & Tokunaga, 1981, 1984; Li et al., 1987; Roberts, 1987; Labbe & Hubbard, 1960; Goldin & Little, 1969; Porra & Jones, 1963; Krueger et al., 1956; Kassner & Walchak, 1973), mainly because they were found to reduce the background metallation rate, and helped prevent the aggregation of the dissolved hydrophobic porphyrins (Li et al., 1987). In the course of these studies, we observed that the presence of the 5% DMSO

could be dispensed with as long as the porphyrin stocks were made directly in a Tris-acetate buffer.

We therefore investigated the effect of the 5% DMSO, and the presence of DMSO in general, upon catalysis by PS5.M. Fig. 4-6 shows the k_{obs} values for metallation at various DMSO concentrations, for both the DNA-catalyzed and the background reactions carried out in 50KB buffer, pH 6.2. Even though DMSO had little effect on the

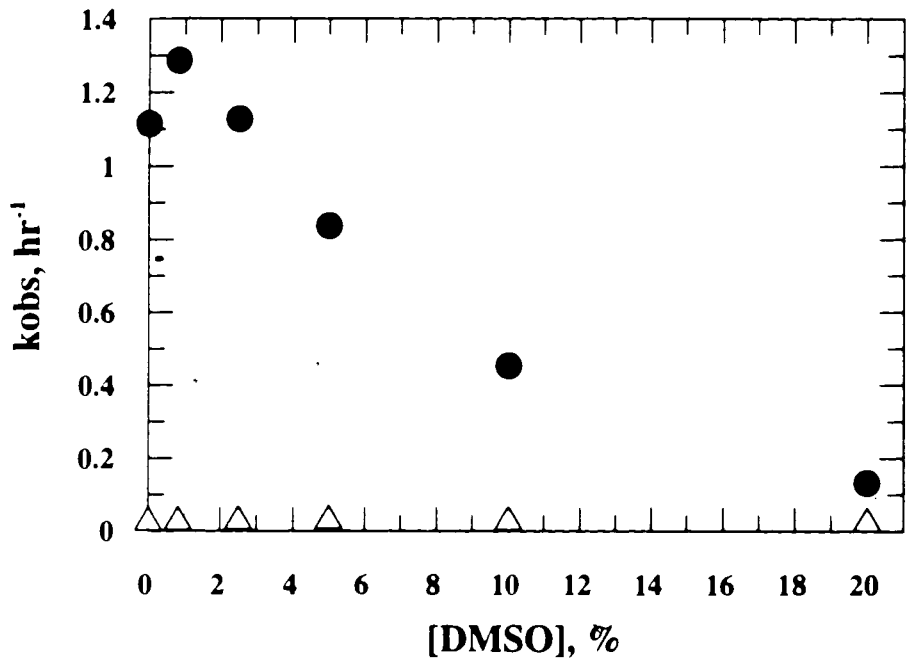

Fig. 4-6. The observed rate constant for metallation, k_{obs}, plotted as a function of DMSO concentration. k_{obs} for metallation reactions was obtained at various DMSO concentrations, in the presence of 2.5 μM of PS5.M (filled circle), and of BLD (open triangle). The detailed reaction conditions are outlined in the Materials and Methods section.

background reaction, its impact on the catalytic activity of PS5.M appeared profound. At 20% DMSO, the catalysis was only ~10% as effective as found at 1% DMSO, which,

rather surprisingly, gave the highest level of catalysis. The progressive denaturation of folded nucleic acid structure in the presence of increasing concentrations of ethanol and other organic solvents has been exhaustively documented. The decrease of the DNAzyme's activity at higher DMSO concentrations might be due to this, or due to changes in solvation of the DNA, the porphyrin, and the copper ions. It is interesting to note here, however, that even at 20% DMSO, the catalysis by PS5.M is not totally abolished; it is therefore conceivable, that with a greater stabilization of the DNAzyme's folded structure (by changes in sequence, or by other means), catalysis of metallation may be observable at quite high concentrations of DMSO and other organic solvents.

We also tested the effect of increasing concentrations of Triton X-100 on catalysis (data not shown). Increasing detergent concentrations (above 0.25%) appeared to reduce both the catalyzed and background rates exponentially. Below 0.25% Triton, however, the background reaction appeared to be unaffected; therefore, k_{obs}(catalyzed) / k_{obs}(uncatalyzed) was at a theoretical maximum with the detergent completely removed. However, the complete removal of detergent was not practical, owing to its requirement for substrate solubilization. Therefore, 0.25% Triton, as well as 1% DMSO, were retained in buffers for our further investigations.

3.8. Buffer effects on catalysis

In the section on the pH optimization of catalysis (above) we discussed the importance of Tris to porphyrin metallation, as carried out under our experimental conditions. Tris, which buffers effectively between pH 7 and 9, has also been used

widely for the study of ferrochelatase enzymes. In our own rate versus pH measurements (above), we found that the presence of > 50 mM Tris acetate in otherwise MES-buffered acidic solutions preserved the 'regular', or monotonic, behavior of the measured initial rates for both catalyzed and background metallations of MPIX with copper. Fig. 4-7 (p117, 119) illustrates the behavior of initial rates in a solution buffered by 100 mM MES, pH 6.2, as compared to one buffered by 100 mM MES, pH 6.2, but containing in addition, 50 mM Tris acetate (the effective buffering capacity of MES lies between pH 5.5 and 6.8). Fig. 4-7a (p117) shows the catalyzed rates in both buffers (which both also contained potassium acetate and the other buffer components) as functions of time; and Fig. 4-7b (p117) shows the background rates. These figures show that in the MES-only buffer, the background rate was much slower and curved off earlier than that in the MES buffer containing Tris acetate; whereas, the catalyzed reaction in the MES-only buffer experienced an early burst up to 10% conversion of the substrate to product, and then slowed dramatically, to the point where the metallation reaction had virtually stopped. In MES buffers containing Tris acetate at any level above 50 mM, by contrast, both the enzymatic and nonenzymatic reactions proceeded smoothly with time, and appeared to go on to completion.

Tris base has the ability to chelate Cu^{2+} in aqueous solution with modest equilibrium constants (with log$K$ values of ~3-4) (Hall et al., 1971; Bai & Martell, 1969). It is therefore likely that in the presence of Tris, the Cu^{2+} ion exists substantially as Cu^{2+}-Tris complexes. Because of the relatively modest complexing constant, such complexes would still dissociate relatively easily to give hydrated copper ions, which in turn could

be chelated by the porphyrins [the formation constants for the porphyrin metallation reactions are, by contrast, very high; for example, $\log K_f > 25$ for HPIX with $Zn(OAc)_2$, at 25°C (Smith, 1975)]. It has been reported that MES, too, forms coordination complexes with copper (II) ions, but with a smaller formation constant ($\log K = 1.39$) (Balikugeri, 1989). Therefore, in MES-only buffers, the hydrated copper ions may begin to chelate

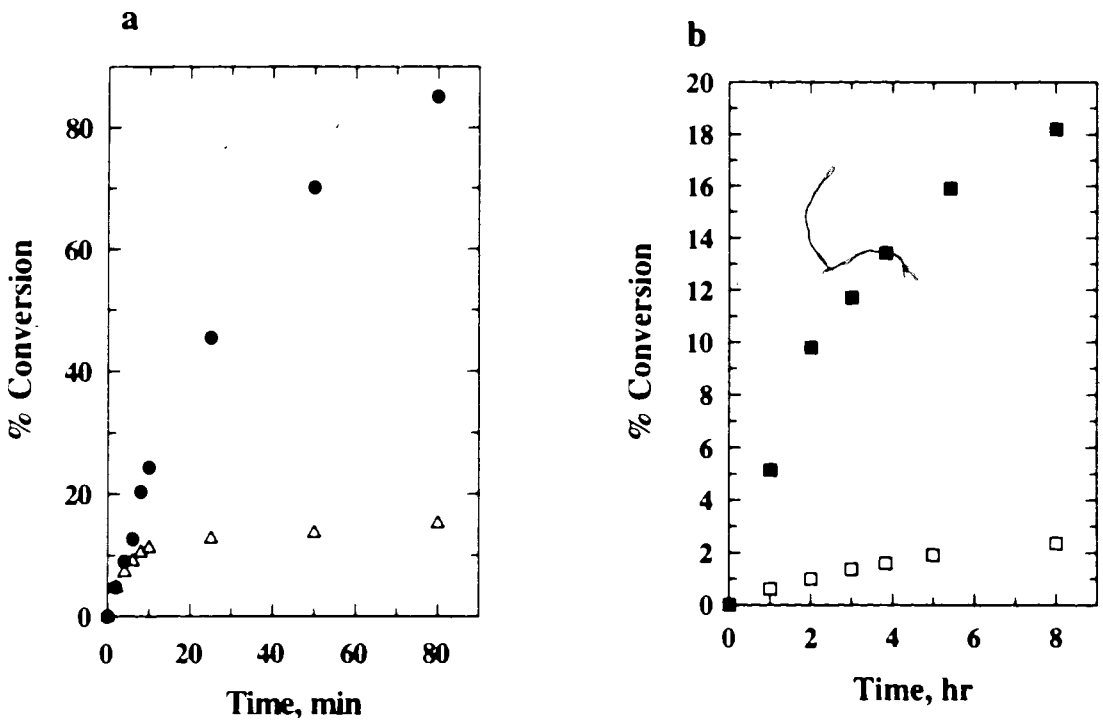

Fig. 4-7: Buffer effects. Percentage conversions of substrate to product, measured in different buffer solutions, and plotted as functions of time. (a) Time dependence plots for PS5.M-catalyzed metallations in 100 mM MES, pH6.2, + 50 mM Tris acetate (filled circle); and in 100 mM MES, pH 6.2 (open triangle). (b) Analogous time dependence plots for the background (noncatalyzed) metallations in the MES-Tris buffer (filled square); and, in the MES-only buffer (open square). Detailed reaction conditions are given in the Materials and Methods section.

instead with the carboxylate groups of the porphyrin, to form aggregated complexes (we observed a discernible colour change of the dissolved porphyrin in these situations). Assuming that the kinetics of the formation of such porphyrin-copper aggregates was not instantaneous, we would still observe experimentally the initial burst of the catalyzed reaction, seen in Fig. 4-7a, during the first few minutes of the reaction. The presence of relatively high concentrations of Tris in the buffer, on the other hand, and the formation of Tris base-Cu^{2+} complexes, might preclude the formation of such porphyrin-copper aggregates.

Of course, the chelation of copper ions by Tris base might be expected to slow down the overall metallation reaction. We examined the effect on metallation rate of raising Tris concentrations in purely Tris buffers (pH 7.3) containing the usual potassium acetate and DMSO and Triton X-100. Figs. 4-7c and 4-7d (p119) show data for the catalyzed and background reactions, respectively; both rates decrease exponentially with increases in Tris concentration. Interestingly, replotting the rates as reverse functions of the anticipated concentration of free Tris base in these buffers (v vs 1/[Tris base]) shows straight-line (data not shown), suggesting that the chelation of copper by Tris base was in fact a factor in the kinetics of the metallation.

By contrast, increasing MES concentrations in MES-buffered solutions at pH 6.2 (all solutions also containing Tris acetate, at 50 mM) did not significantly change the metallation rates.

In summary, our data suggested that Tris played two roles in the porphyrin metallation reactions (in both the catalyzed and background versions). First, it chelated copper ions and reduced the formation of presumptive "unproductive" copper-and-porphyrin aggregates; and, second, it reduced the overall metallation rates.

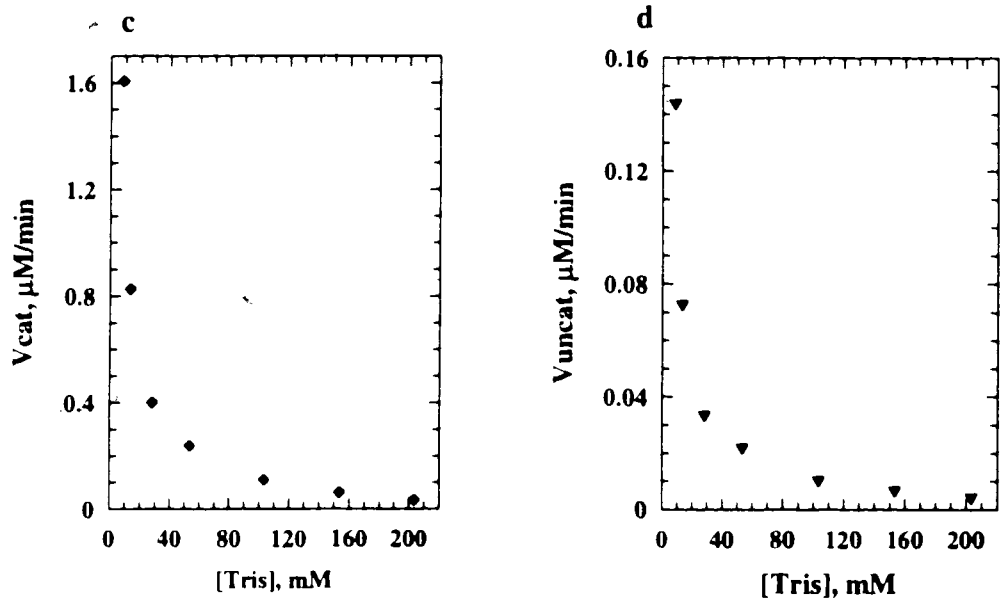

Fig. 4-7. Buffer effects (continued). Tris effects on metallation rates. (c): v_{cat} (filled diamond); and (d): v_{uncat} (filled reverse triangle) of metallations carried out in Tris-only buffers (pH 7.3), as functions of Tris concentration. Detailed reaction conditions are given in the Materials and Methods section.

3.9. Contrasting effects of sodium and potassium ions on catalysis

In Chapter 3, I had reported data that sodium and potassium ions had contrasting roles in the catalysis by PS5.ST1: K^+ was absolutely necessary for catalysis whereas Na^+, even up to 225 mM concentrations, was ineffective in supporting catalysis. We also

found that in the absence of sodium and magnesium, 25-50 mM K^+ was optimal for catalysis. This striking difference in the requirements for potassium and sodium, the heavily guanine-rich sequence of the DNAzyme, as well as methylation protection evidence from the parent aptamer, PS5 (Chapter 2), had cumulatively suggested that the folded and active form of the DNAzyme might contain guanine-quartets [which are significantly better stabilized by potassium ions than by sodium ions (Sen & Gilbert, 1990; Williamson et al., 1989; Sundquist & Klug, 1989].

Na^+ ions, however, do support the formation and stabilization of G-quartets, except that significantly higher concentrations are needed than K^+ ions required for a comparable task (Sen & Gilbert, 1990). The free energy difference for quadruplex formation by $d(G_3T_4G_3)_2$ in 100 mM NaCl and 100 mM KCl has been reported -4.2 kcal/mol at 25°C (Scaria et al., 1992), corresponding to an equilibrium constant in excess of 10^3. Besides, there is considerable evidence for the formation of different G-quadruplex structures by the same oligomer in potassium solutions versus sodium solutions (Sen & Gilbert, 1990; Venczel & Sen, 1993). In measuring catalytic rates of PS5.M across a large sodium concentration range (0, 5, 10, 25, 50, 100, 225, 500 mM), we found catalysis at no higher than 10-15% above the background rate (data not shown). This appeared to confirm our original conjecture (in Chapter 2 and 3) that the folded structure of the DNAzyme contained probably two or fewer complete G-quartets, which could be stabilized only in the presence of potassium ions. The other possibility is, of course, that in sodium-only solutions, PS5.M may form a folded structure different from the catalytically active one.

We wished to test whether the optimal K^+ concentration required for catalysis had changed after the various steps taken above for the optimization of catalysis. In addition, we would like to establish how little potassium was needed to support a significant catalysis. Reactions were therefore carried out in 50 mM Tris-acetate, pH 7.3, 1% DMSO, 0.25% Triton, and varying concentrations of potassium acetate. Fig. 4-8 shows the PS5.M-catalyzed and background rates as functions of potassium concentrations up to 200 mM. The DNAzyme appeared to function well even at very low (~10 mM)

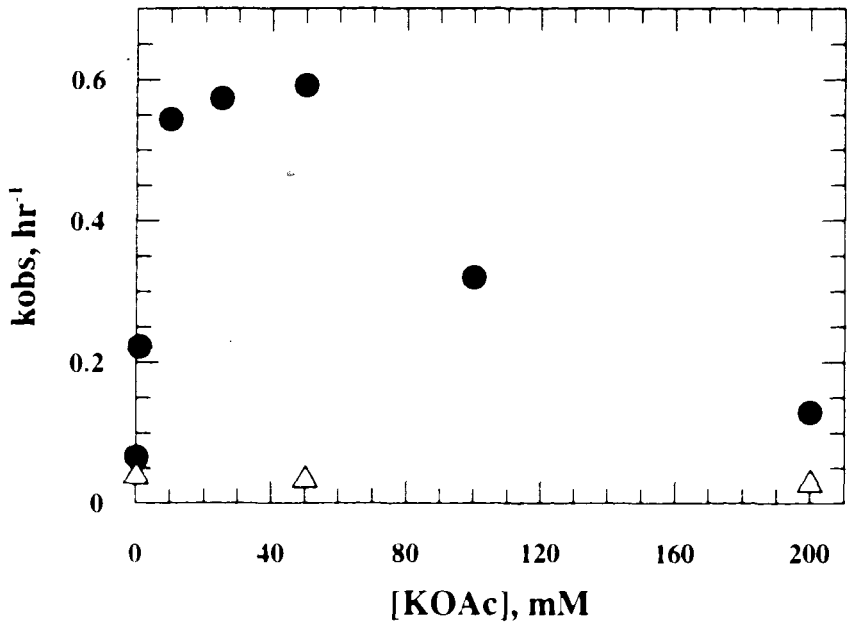

Fig. 4-8: Metallation rates plotted against potassium ion concentrations. k_{obs} for the catalyzed (in the presence of 2.5 μM PS5.M, filled circle); and, background (in the presence of 2.5 μM BLD, open triangle) reactions.

potassium concentrations, and the optimal activity extended at least to 50 mM K^+. At the lower end, in as little as 0.1 mM K^+, the enzyme activity was 70% above the background;

at 1 mM K^+, it had increased to 480%, and at 10 mM K^+, up to 1400%. At higher than 50 mM K^+, the catalytic activity began to decrease, but more slowly than the pace of its rise at lower potassium concentrations.

3.10. Optimized enzymatic parameters for the utilization of MPIX and PPIX as substrates

The above process of optimization of the various parameters connected with the catalytic reaction dramatically changed the observed $v_{cat+uncat} / v_{uncat}$ ratio from 4.5 in SB buffer (100 mM Tris, pH 7.1, 200 mM sodium acetate, 25 mM potassium acetate, 10 mM magnesium acetate, 0.5% Triton X-100, 5% DMSO, at 25°C, see Chapter 3) to a ratio of ~100 in 40KB buffer (100 mM MES, pH 6.2, 40 mM potassium acetate, 50 mM Tris acetate, 0.25% Triton X-100, 1% DMSO, at 15°C). It could therefore be expected that the kinetic parameters, k_{cat} and K_M, for the DNAzyme would also have changed. Experiments were therefore carried out to determine k_{cat} and K_M for the utilization of both MPIX and PPIX by PS5.M, in 40KB buffer, at 15°C (with 1.5 μM PS5.M and 1 mM copper acetate).

Figs. 4-9a and 4-9b (p123) show the catalyzed velocities of copper insertion into MPIX and PPIX, respectively, as functions of the concentrations of those porphyrins. These data were analyzed with the program GraFit 3.0, and the kinetic parameters obtained are shown in Table 4-3 (p124).

With MPIX as the substrate, the optimized conditions gave rise to a moderate, ~6-fold increase in k_{cat}, but a dramatic, 70-fold decrease in the K_M compared to those derived

in SB buffer (Chapter 3). Overall, these parameters combined to give a large, 400-fold increase in the DNAzyme's catalytic efficiency, k_{cat}/K_M. The major change in K_M implied

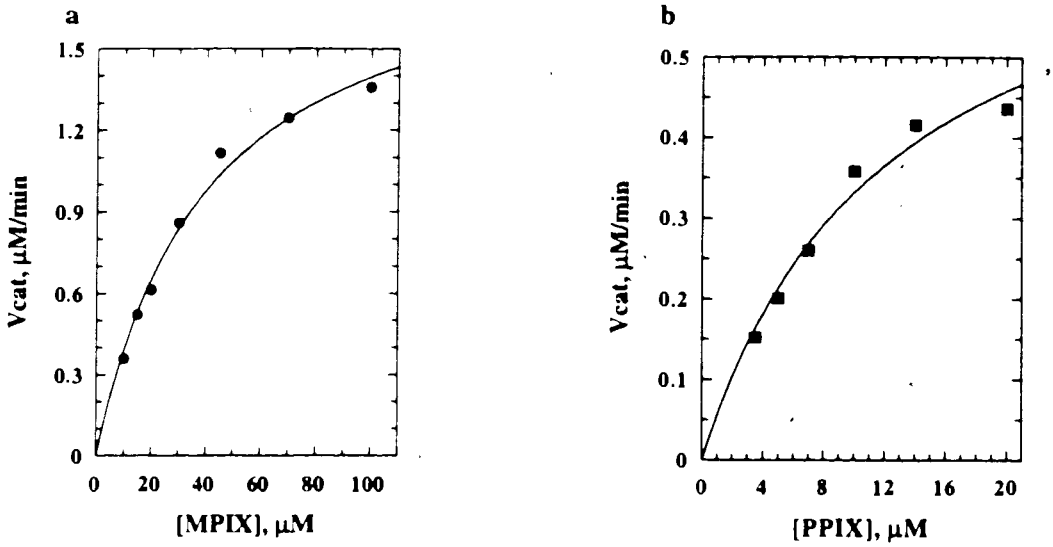

Fig. 4-9: Initial rates of metallation plotted against substrate porphyrin (MPIX, and PPIX) concentrations. (a) PS5.M-catalyzed rates (v_{cat}, equal to v_{total} - v_{uncat}) for Cu-MPIX formation, plotted against [MPIX], in the presence of 1.5 μM PS5.M (filled circles). (b) Analogous plot for the formation of Cu-PPIX (filled squares).

that the optimization process had worked significantly to improve the DNAzyme's affinity for its substrate, MPIX, presumably by eliminating or reducing detrimental conditions found in our initial selection buffer (SB buffer). On the other hand, the k_{cat} increase was probably not due to an increase in the robustness of the DNAzyme itself, for the background rate constant, k_{uncat}, also improved under the optimized conditions to almost the same extent (up ~7-fold, from 0.0096hr^{-1} to 0.065hr^{-1}). Thus, the catalytic "gain", k_{cat}/k_{uncat}, remained essentially unchanged through the optimization process.

Table 4-3 shows further that the K_M value for PPIX as substrate was superior to that for MPIX, the "intended" substrate for PS5.M. The k_{cat}/k_{uncat} for PPIX, too, was three-fold larger than that for MPIX, confirming our preliminary results (Chapter 3) that PPIX was in fact a superior substrate for this DNAzyme.

Table 4-3. Kinetic parameters for metallation of MPIX and PPIX prior to optimization (in SB buffer) and following optimization (in 40KB buffer).

Substrate	k_{cat}, min^{-1}	K_M, μM	k_{cat}/K_M, M^{-1} min^{-1}	k_{cat}/k_{uncat}
MPIX in 40KB	1.30 ± 0.07	39.7 ± 4.9	3.25×10^4	1200
PPIX in 40KB	0.49 ± 0.06	12.3 ± 2.9	3.97×10^4	3700
MPIX in SB	0.23 ± 0.06	2900 ± 900	79	1400

3.11. Ferrochelatases and the "artificial" biocatalysts for porphyrin metallation

Ferrochelatases are the protein enzymes that catalyze the insertion of Fe^{2+} ions into PPIX in the final step of heme biosynthesis (Lavallee, 1988). A number of studies have established that the N-methylporphyrins were a class of potent and reversible inhibitors of the enzymes (De Matteis et al., 1980; Tephly et al., 1979; Ortiz de Montellano et al., 1981; Dailey & Fleming, 1983), probably because these methylated porphyrins were close structural representations of the transition state for porphyrin metallation (Cochran & Schultz, 1990). This notion was successfully made use of by Cochran and Schultz , who immunized mice with NMM, and successfully derived antibodies catalytic for porphyrin metallation (Cochran & Schultz, 1990). A similiar

technology for isolating DNA and RNA sequences that bound specifically to NMM led eventually to the discovery of catalytic and RNA (Conn et al., 1996) and DNA molecules for this reaction.

On the basis of the fact that the catalytic antibody, DNA, and RNA, are all derived using the same transition state analog (NMM) for the same chemical reaction, it may be reasonable to make an initial assumption that they catalyzed the porphyrin metallation with similar mechanisms (which might in turn mirror those of ferrochelatases).

Table 4-4 (p126) summarizes the key kinetic parameters for all of these enzymes. As such, a detailed comparison of the individual properties of these catalysts is of limited utility, for the experimental conditions [such as particulars of pH, temperature, substrate metal ion (Cu^{2+}, Zn^{2+}, or Fe^{2+}) concentrations, as well as the concentrations of individual buffer components] were different in each case. Nevertheless, a perusal of the data summarized in Table 4-4 indicates that, qualitatively, all of the artificial enzymes are comparable in terms of their catalytic functions, having similar affinities for their porphyrin substrates, and similar catalytic efficiencies in terms of their respective k_{cat}/K_M and k_{cat}/k_{uncat} values. The k_{cat} of the ferrochelatase enzymes appears to be higher than that of the artificial enzymes, but under their particular assay conditions (50 μM Zn^{2+} or 100 μM Fe^{2+}), the ferrochelatases were already at saturation (*vide* K_M values, below) in terms of their binding capacity for the substrate metal ions, whereas the artificial enzymes (at least the antibody, and the DNAzyme) do not appear to have strong substrate metal ion binding sites (for the DNAzyme the K_M value would have to be higher than 10 mM copper ion concentration tested for data above).

Table 4-4. Comparison of key kinetic parameters of ferrochelatases, and catalytic antibody, DNA, and RNA.

Enzyme type	k_{cat}, min^{-1}	K_M(μM) for porphyrins,	K_M for metal ions, μM	k_{cat}/K_M, M^{-1} min^{-1}	k_{cat}/k_{uncat}
Ferrochelatase [a]	0.96 (Fe^{2+}) [e]	12.5 (MPIX and	11.8 (Zn^{2+})	76800 [e]	N/A
	7.2 (Zn^{2+}) [e]	PPIX)	6.7 (Fe^{2+})	576000 [e]	
Antibody [b]	0.14 (Cu^{2+}) [e]	50 (MPIX)	No binding	2900 [e]	1700
	1.3 (Zn^{2+}) [e]		site	26800 [e]	2600
DNA [c]	1.3 (Cu^{2+}, MPIX)	40 (MPIX)	No or weak	32500	1200
	0.49 (Cu^{2+}, PPIX)	12.3 (PPIX)	binding site	39700	3700
RNA [d]	2.0 (Cu^{2+})	16 (MPIX)	N/A	125000 [e]	460

Experiment conditions:
a, 100 mM Tris-HCl, pH 8.0, 0.1% Tween 20, 25 μM zinc acetate or 100 μM iron citrate, 37°C(Okuda et al., 1994).
b, 90 mM Tris acetate, pH 8.0, 0.5% (w/v) Triton X-100, 5% (v/v) DMSO, 1 mM copper acetate or zinc acetate, 26°C (Cochran & Schultz, 1990).
c, 50 mM Tris acetate, 100 mM MES, pH 6.2, 0.25% (w/v) Triton X-100, 1%(v/v) DMSO, 40 mM potassium acetate, 1 mM copper acetate, 15°C.
d, 20 mM Tris acetate, pH 8.0, 100 mM sodium chloride, 200 mM potassium chloride, 0.5% Triton X-100, 10% DMSO, 3 mM copper acetate, 25°C (Conn et al., 1996).
e, the values shown were calculated using the data in the cited references.

Unlike the artificial enzymes, ferrochelatases have very high affinities for their metal ion substrates (11.8 μM for Zn^{2+}; 6.7 μM for Fe^{2+}) (Okuda et al., 1994), and this is the most striking difference between the ferrochelatases, on the one hand, and the catalytic antibody and DNA, on the other. The lack of such binding sites in the artificial catalysts probably stems from the fact that no specific driving force (comparable to the use of the transition state analog, NMM, for creating a binding site for the substrate porphyrin) was built into the selection procedures to induce metal-ion binding sites in the catalytic antibody and DNA and RNA.

The two recently reported nucleic acid (DNA and RNA) catalysts for porphyrin metallation share a number of common features: they were both selected out of their respective random libraries for binding to the same transition state analogue, NMM; both were cloned after 12 cycles of binding, elution, and amplification; now, as we report in this paper, their catalytic capabilities appear to be very similar. Most interesting, however, is the almost identical size of their optimally functioning units (24 nucleotides for the DNAzyme PS5.M; 25 nucleotides in the conserved RNA loop) and the significant homology that appears to exist between the two G- and T (or U)-rich sequences. The G-richness of the catalytic RNA, and the fact that it was selected, as well as assayed, in a buffer containing a high concentration of potassium (Conn et al., 1996), suggest that as in the case of PS5.M, there may be guanine-quartets in its folded structure. The overall similarity of the two enzymes raises the interesting question: would a RNA version of our DNA sequence, or vice versa, also have catalytic properties? These, and other questions, will be the subjects for future investigation in our laboratory.

4. Summary

In this chapter, I reported a thorough investigation of the properties of the porphyrin-metallating DNAzyme. We have established that a 24-nucleotide sequence (PS5.M), from within PS5.ST1, is both the minimal and most optimal catalytic unit. We have found that three related porphyrins are acceptable as substrates by this DNAzyme, of which PPIX is preferred as a substrate over the expected substrate, MPIX. We have determined that it is unlikely that a strong, catalytically relevant binding site for copper

ions exists in the DNAzyme, and that high concentrations of copper destroy the active DNAzyme. This enzyme, whose folded structure likely contains guanine-quartets, requires potassium ions for activity; we have shown that as little as 1 mM potassium is sufficient for its catalytic robustness, whereas as much as 0.5 M sodium still will not support catalysis. As a consequence of various steps of optimization, we now have a vastly improved DNAzyme, one whose enzymatic parameters compare well both with those of natural ferrochelatases, as well as with those of artificially derived chelatases, composed of protein (a catalytic antibody), and RNA. The existence of this array of biocatalysts for porphyrin metallations allows one-to-one comparisons of the ways in which different biopolymers solve a given catalytic problem.

Chapter 5. A Guanine-Quadruplex Model for the Structure of A Porphyrin-Metallating DNAzyme

1. Introduction

I have described a DNA sequence, PS5.ST1, that has catalytic activity towards porphyrin metallation (Chapter 3 and 4). PS5.ST1 is the binding site of PS5 (Chapter 2), a sequence selected from a random DNA library, which has high affinity for NMM--a transition state analog for porphyrin metallation (Cochran & Schultz, 1990). This short oligomer is 33-nucleotide long and has the sequence $\mathbf{T_{-2}C_{-1}G_1T_2G_3G_4G_5T_6C_7A_8T_9T_{10}}$ $\mathbf{G_{11}T_{12}G_{13}G_{14}G_{15}T_{16}\,G_{17}G_{18}G_{19}\,T_{20}G_{21}T_{22}G_{23}G_{24}C_{25}T_{26}G_{27}\,G_{28}\,T_{29}C_{30}C_{31}}$. Previous experimental results suggested that PS5.ST1 most likely folds to form a guanine quadruplex as its active structure, based on the following observations: 1) The sequence of PS5.ST1 is very guanine-rich, containing 16 guanines out of 33 nucleotides. This type of guanine-rich sequence has a great tendency to form guanine quadruplex structures [Reviewed by Williamson (1994)]. 2) This DNA enzyme can only function effectively in the presence of potassium ions (Chapter 2 and 3). This agrees with the previous findings that potassium was much more effective in stabilizing guanine-quartets (Sen & Gilbert, 1990). 3) Methylation protection with DMS on its parent sequence PS5 clearly indicated that most guanines in this binding site region were fairly under-reactive (Chapter 2, p58), a phenomenon associated with the formation of guanine-quartets.

Guanine quadruplex structures have often been found to be the folded structures for a number of aptamers obtained from selections using DNA libraries. For example,

guanine quadruplexes have been selected to bind to thrombin (Boch et al., 1992) and ATP (Huizenga & Szostak, 1995). Also, many guanine-rich short oligomers, either DNA or RNA, are able to form various classes of guanine-quadruplex structures (Williamson, 1994). Nevertheless, as we reported earlier, other G-rich DNA sequences such as OXY4, which has been shown to form quadruplex structures, did not catalyze porphyrin metallation (Chapter 3 and 4). Therefore, the questions left for us are: Does PS5.ST1 indeed fold to form a guanine quadruplex as its active structure? If so, what kind of guanine quadruplex does this oligomer form and how does the folded active structure achieve its catalysis? What unique features does this quadruplex have, to differentiate it from other guanine quadruplexes for the catalysis of porphyrin metallation? Could we convert those other, noncatalytic, guanine quartet sequences, such as the thrombin binding aptamer, into catalytic sequences? In addition, there are some unsolved questions in our previous studies: 1) Why PS5.ST1, the binding site of PS5, was strongly catalytic for porphyrin metallation, while its parent sequence, PS5, only had a weak activity (Chapter 3)? 2) Why the binding site from PS2, another aptamer from the same selection, could bind to NMM (Chapter 2), but had only very weak activity for porphyrin metallation (Chapter 3)? Would it be possible to make this sequence highly catalytic?

In this chapter, I will address these questions.

2. Material and methods

All DNA oligomers were obtained by automated DNA synthesis and were purified in polyacrylamide gels as described in Chapter 4. Their sequences are given in

PS5.ST1	TCGTGGGTCATTGT**G**GGTGGGTGTGGCTGGTCC
PS5.A	TGGGTCATTGT**G**GGTGGGTGTGGCTGGTCC
PS5.B	TCATTGT**G**GGTGGGTGTGGCTGGTCC
PS5.D	TTGTGGGT**G**GGTGTGGCTGGT
PS5.G	TCGTGGGTCATTGT**G**GGTGGGTGTGGCT
PS5.H	TCGTGGGTCATTGT**G**GGTGGGTGT
PS5.M	GTGGGTCATTGT**G**GGTGGGTGTGG
PS5.MT1	GTGGGTCATTGT**G**GTTGGGTGTGG
PS5.MT2	GTGGGTCATTGTGGGTTGGTGTGG
PS5.MT3	GTGTGTCATTGT**G**GGTGGGTGTGG
PS5.MT4	GTGGGTCATTGTGGGTGTGTGTGG
PS5.MT5	GTGGGTCATTGT**G**GGTGGTTGTGG
PS5.MT6	ATGGGTCATTGTGGGTGGGTGTGG
PS5.MR	GGTGTGGGT**G**GGTGTTACTGGGTG
PS5.M2	GTGGGTGTTACTGGGTGGGTGTGG
PS5.M2R	GGTGTGGGTGGGTCATTGTGGGTG
PS5.M3	GTGGGTGTGGGTGGGTCATTGTGG
PS5.M3R	GGTGTTACTGGGTGGGTGTGGGTG
PS5.M4	GTGGGTGT**G**GGTGGGTGTTACTGG
PS5.M4R	GGTCATTGT**G**GGTGGGTGTGGGTG
PS5M.Short	GTGGGTTTGGGTGGGTGTGG
PS5M.BK.1	TGGGTCATTGT**G**GGTGGGTGTGGG
Three-T.loop	GTGGGTCATTGTGGGTTTGGGTGTGG
PS5.PI	GTGG**G**TCAAGCA
PS5.PII	TGCTTGT**G**GGTGGGTGTGG
PS5.MIN	GTGGGTGGGTGGGTGG
PS9.ST1	GGTGATTCGGGTA**G**GGCGGGCGGT
PS12.ST1	GAGGTTTGGGGAAGGGTCGGTGGG
PS19.ST1	AGGTTATAGGGC**G**GGAGGGTGGT
PS22.ST1	GAGGGGTGGGAGGGTTGG
PS2.ST1	AACGTGGGA**G**GGCGGTGGTGTTGAG
PS2.M	GTGGGTA**G**GGCGGGTTGG
TM	GGTTGGTGTGGTTGG
TM2	GGGTTGGGTGTGGGTTGGG
TM.M1	GTGGGTTGGGTGTGGGTTGG
TM.M2	GTGGGTT**G**GGTGGGTTGG

Fig. 5-1. Sequences of DNA oligomers tested in this Chapter. The guanine underlined in each sequence corresponds to the guanine in the footprinting gel labelled with an arrowhead.

Fig. 5-1 (p131). Enzyme activity assays were performed in 40KB buffer (50 mM Tris acetate, 100 mM MES, 40 mM potassium acetate, 1% DMSO, 0.25% Triton X-100, final pH 6.2), with DNA at 5 μM and MPIX at 33 μM, and other procedures were as described in Chapter 4. The DMS footprinting assays were performed in 40KB buffer with 0KB buffer as the control (0KB buffer contained all buffer components of 40KB but lacked potassium). The procedures were the same as those described in Chapter 2.

3. Results and discussions

3.1. DMS footprinting and enzyme activity assays on PS5.ST1 and its related oligomers

Fig. 5-3, panel I (p134) shows methylation protection patterns of PS5.ST1 in 0KB buffer (lane A) and in 40KB buffer (lane B). The guanine residues at positions 3, 4, 5, 13, 14, 15, 17, 18, 19, 21, 23, and 24 were protected from the methylation by DMS. The protection pattern could be most simply explained if PS5.ST1 folded to form an intramolecular guanine quadruplex structure as shown in Fig. 5-2 (p133). In this structure, guanines at 1, 3, 15, 17 form the first guanine quartet (Quartet A), guanines at 4, 14, 18, 24 form the second quartet (Quartet B), and guanines at 5, 13, 19, 23 form the third quartet (Quartet C). There are four loops as the connecting units in the structure: Loop 1 and Loop 2 are both one-T loops (T2 and T16, respectively); Loop 3 is made up of three bases (T20, G21, T22); and Loop 4 is a 7-base loop (T6, C7, A8, T9, T10, G11, and T12). There is a gap separating the top G-quartet (Quartet A) from the other two G-

quartets (Quartet B and C). I term this gap as "Gap1-24" because it separates Quartet A and B at G1 and G24. The unique feature of this proposed structure is that a G-quartet "cap" sits on a foundation made of the other two G-quartets.

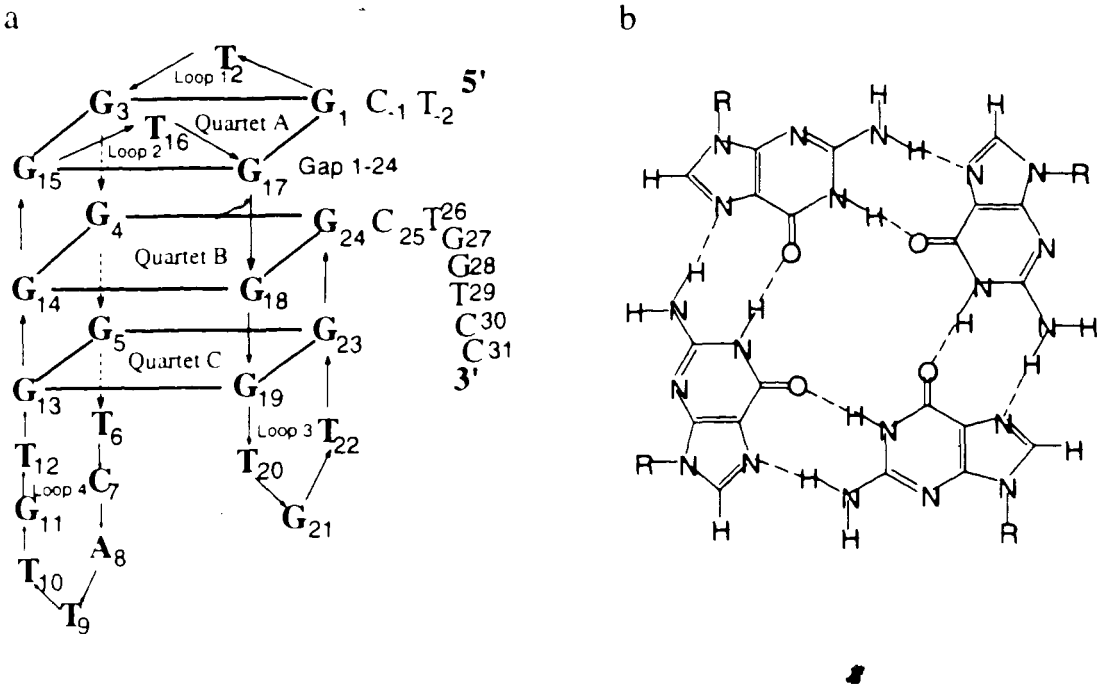

Fig. 5-2. A guanine quadruplex model for PS5.ST1. (a) The model is made up of three guanine quartets, four connecting loops, one gap between G1-G24. The sequence shown in bold is the essential sequence (PS5.M). The arrows indicate the sequence orientation. (B) Hydrogen bond arrays in a guanine quartet.

The protections of all guanine bases except G1 in the quadruplex core in the methylation reaction by DMS can be seen in the denaturing gels. Although it could not be determined whether G1 was protected (because it runs too close to the 5' end of the oligomer in sequencing gels), it is most likely that G1 was indeed involved in the quartet formation. The deletion of this guanine from the sequence (as in PS5.A) resulted in a 64% activity decrease and significant loss of

Figure 5-3. DMS methylation results on PS5.ST1 and its deletion sequences. Panel I lanes A and B: PS5.ST1 in 0KB buffer and 40KB buffer, respectively. Panels II, III, IV, V, and VI are for PS5.A, PS5.G, PS5.B, PS5.H, and PS5.M, respectively. The guanine labeled with an arrowhead in each panel corresponds to the guanine underlined in the sequence given in Fig. 5-1 (p131).

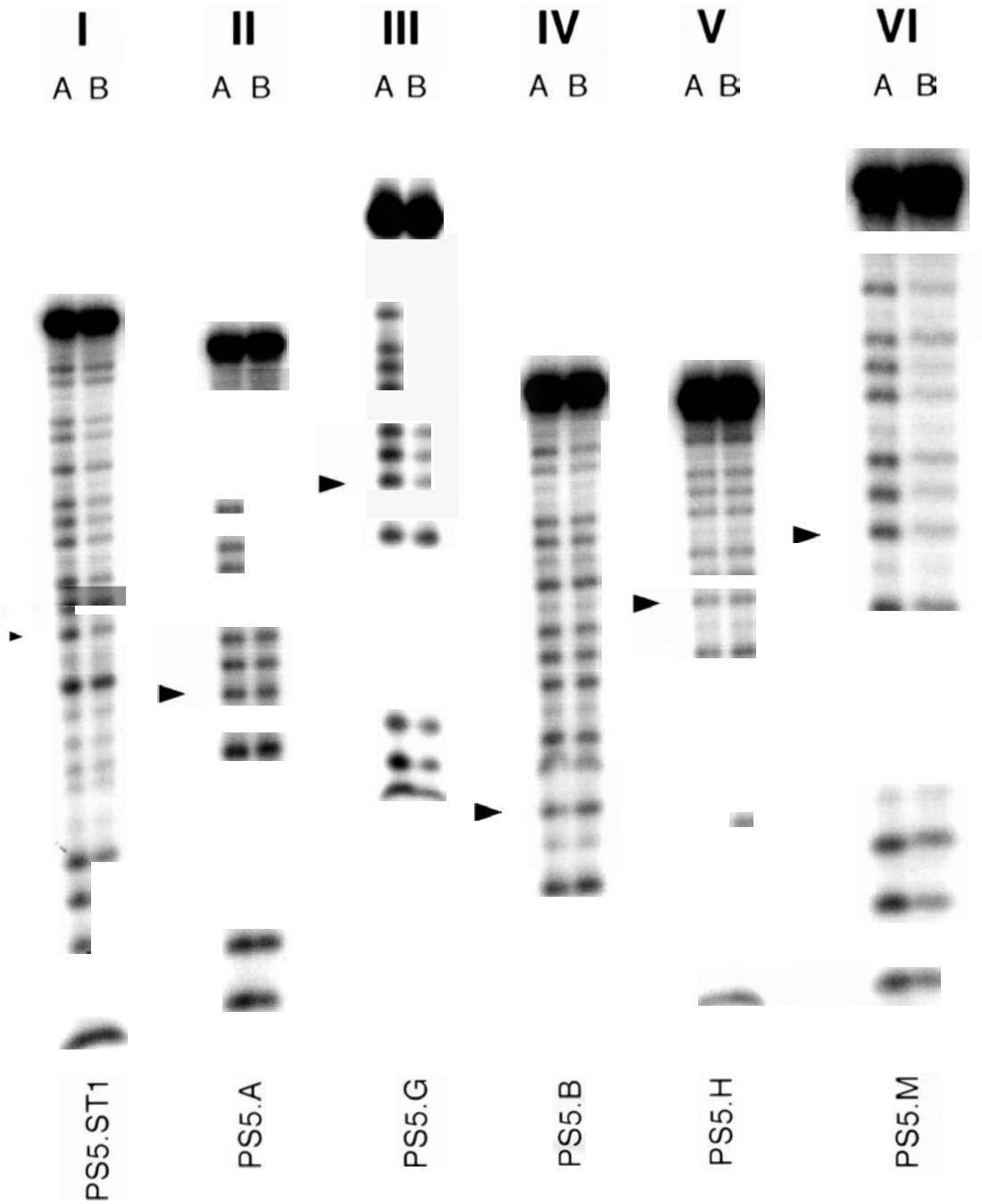
I
A B
II
A B
III
A B
IV
A B
V
A B
VI
A B
PS5.ST1
PS5.A
PS5.G
PS5.B
PS5.H
PS5.M

protection on all other guanine bases (Fig. 5-3, panel II, p134). On the other hand, that sequence A still maintained 36% activity of PS5.ST1 suggested that guanine interactions (hydrogen bonds) in Quartet A were possibly weak; and that Quartet A was possibly loosely constituted, compared to the other two quartets.

The above structural model was supported by other experiments carried out on deletion sequences of PS5.ST1. (The names, sequences and enzymatic activity of the deleted mutants are given in Fig. 4-1 of Chapter 4, p103). The deletion of motif $\mathbf{G_{27}\,G_{28}\,T_{29}C_{30}C_{31}}$ (as in the sequence PS5.G) had no effect either on the catalytic activity or the methylation protection pattern (Fig. 5-3, panel III, p134), but deletion of the motif $\mathbf{T_{-2}C_{-1}G_1T_2G_3G_4G_5}$ (as in the sequence PS5.B) or motif $\mathbf{G_{23}G_{24}C_{25}T_{26}G_{27}\,G_{28}\,T_{29}C_{30}C_{31}}$ (as in the sequence PS5.H) resulted in a complete loss of both enzymatic activity and protection from DMS methylation, as expected (Fig. 5-3, panel IV and V, p134).

As described in Chapter 4, results on various sequences that had deleted bases from both ends of PS5.ST1 had led to the finding that G1 and G24 are the boundaries of the optimal catalytic DNA sequence within PS5.ST1. The resulting sequence, $\mathbf{G_1T_2G_3G_4\,G_5T_6C_7A_8\,T_9T_{10}G_{11}T_{12}G_{13}G_{14}G_{15}T_{16}\,G_{17}G_{18}G_{19}\,T_{20}G_{21}T_{22}G_{23}G_{24}}$, named PS5.M, contained 24 nucleotides, and had superior catalytic activity (~20% activity increase over PS5.ST1) as well as a stronger protection for the guanines in the quadruplex core (Fig. 5-3, panel VI, p134), indicating that the bases to the 5'of G1 and 3' of G24 were not necessary for the proper folding and enzymatic functioning of this DNAzyme.

G21 was also seen to be protected from DMS methylation on the sequencing gels for the three catalytic sequences PS5.ST1, PS5.G, and PS5.M (Fig. 5-3, panels I, III, and VI, p134). However, we think that this guanine base was probably not involved in the quadruplex core formation since sequences lacking this base(such as PS5.MIN, and PS2.M, discussed in later sections) could still function catalytically.

3.2. Evidence from the sequences mutated around the G-quadruplex core

If the above structure model was correct, we reasoned that when a G → T mutation was introduced at various positions in the guanine quadruplex core, one or all guanine quartets could be destroyed; and, as a consequence of this, the catalytic activity of the mutated sequence would be severely reduced or abolished.

Using PS5.M as the reference sequence, sequences were designed that introduced a single mutation from G → T at different locations around the quadruplex core. The various mutations made were (see the structure in Table 5-1, p137): Mutations on Quartet A: G15 → T15 (PS5M.MT1), and G17 → T17 (PS5M.MT2); mutations on Quartet B: G4 → T4 (PS5M.MT3), and G18 → T18 (PS5M.MT4); mutations on Quartet C: G19 → T19 (PS5M.MT5). Both catalytic activity assays and methylation experiments with DMS were then carried out on these mutated sequences. The results are shown in Fig. 5-4 (p138) and in Table 5-1 (p137).

As shown in Table 5-1, all five mutants were completely devoid of catalytic activity or had very weak activity. In the methylation protection experiment, the mutated sequences had either no protection for guanines [in the case of PS5M.MT2 (data not

shown), PS5M.MT3 (Fig. 5-4, panel II, p138), PS5M.MT4 (data not shown)], or much weakened protection (in PS5.MT5, there was no protection on the 3'-most four Gs, see Fig. 5-4, panel III, p138). Only in the PS5.MT1 mutant did all guanines seem to be strongly protected (Fig. 5-4, panel I).

Table 5-1. Catalytic activity of G to T (A) mutants around quadruplex core.

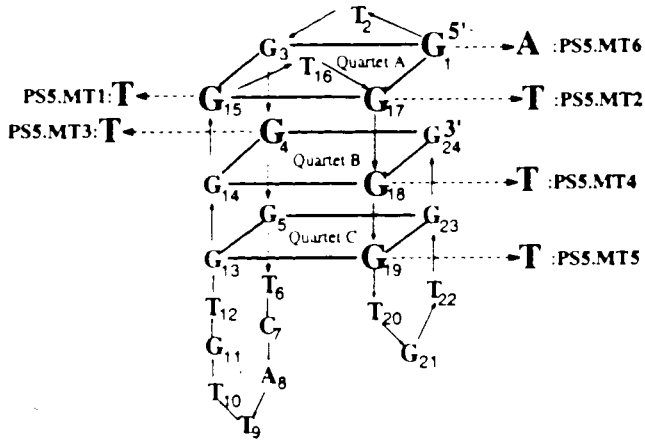

Quartet mutated	Mutation position[1]	Sequence name	Rate (μM/min)[2]	Relative activity
None	None	PS5.M	2.50	100
A	G15 to T15	PS5M.MT1	0.07	0
A	G17 to T17	PS5M.MT2	0.05	0
B	G4 to T4	PS5M.MT3	0.10	2
B	G18 to T18	PS5M.MT4	0.11	2
C	G19 to T19	PS5M.MT5	0.18	5
A	G1 to A1	PS5M.MT6	0.93	35
Ref. DNA		BLD	0.05	0

1) see the reference structure at the top; 2) assayed in 40KB buffer at 15°C, with MPIX at 33 μM and DNA at 5 μM.

Figure 5-4. DMS methylation on modified sequences of PS5.M. Panels I, II, III are for mutants PS5M.MT1, PS5M.MT3, and PS5M.MT5, respectively; Panels IV, V, and VI for PS5.M4, PS5.MR, PS5.M4R, respectively. Lane A in each panel was carried out in 0KB buffer, while lane B in 40KB buffer.

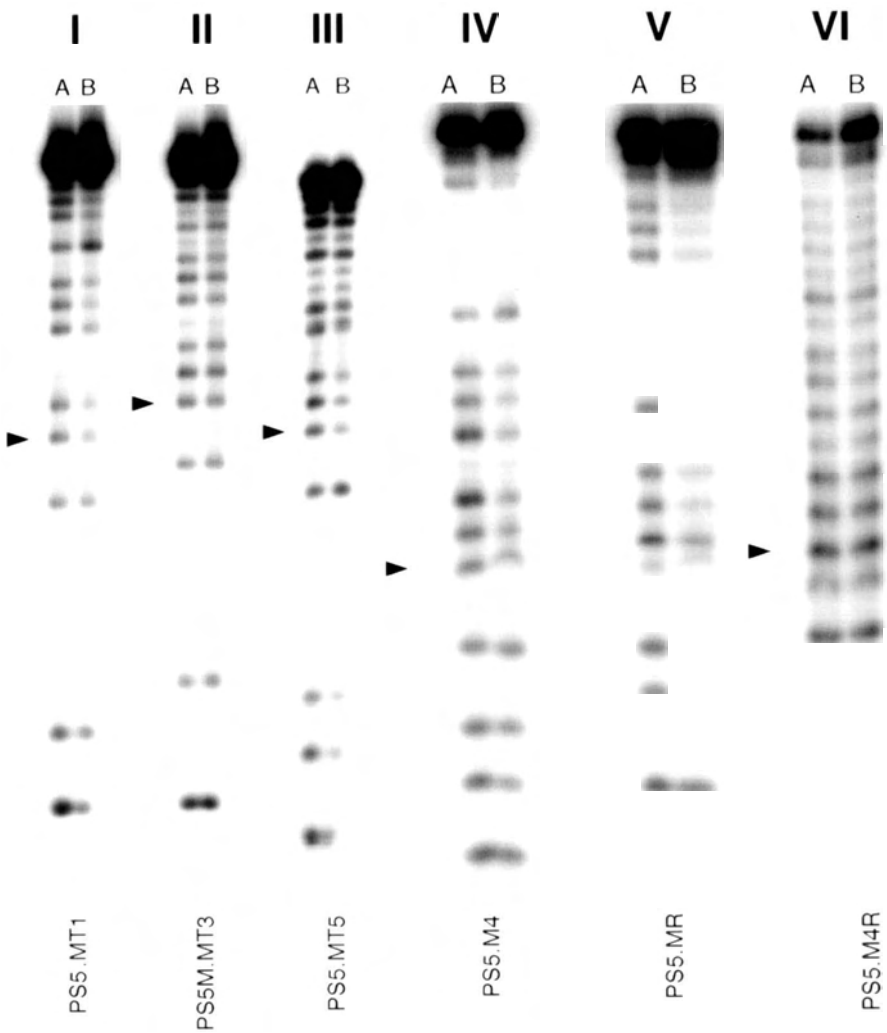
I
II
III
IV
V
VI
A B
A B
A B
A B
A B
A B
PS5.MT1
PS5M.MT3
PS5.MT5
PS5.M4
PS5.MR
PS5.M4R

It has been reported recently that adenine is able to form "mixed" quartets with guanines (Harada & Frankel, 1995). Therefore we designed an oligomer in which G1 was mutated to A1 (PS5M.MT6). We found that an adenine at this position could not adequately replace the guanine. The activity level of PS5.MT6 (~36% activity of PS5.M, Table 5-1, p137) was almost the same as that of PS5.A (~30% of PS5.M), in which G1 was completely eliminated. PS5.MT6 also had a similar methylation protection pattern as PS5.A (data not shown).

3.3. Evidence from structural manipulations within the quadruplex core

The main feature of the proposed model is that it has two standard G-quartets at the bottom part of the structure and a G-quartet "cap" which separates G1 and G24. In addition, the proposed structure is highly symmetrical at the region of the guanine quadruplex core. We reasoned that if this structure was correct, the above features would permit us to test certain structural manipulations. The first would be to generate a reversed sequence of PS5.M, that should also be able to form a similar quadruplex structure and might be catalytic as well. Here, the wording "forward" and "reverse", as used, have the following meaning: For PS5.M, the "forward" sequence means that the sequence reads 5'-GTGGG TCATT GTGGG TGGGT GTGG-3'; while the "reverse" sequence means that the original 5' end and the 3' end of the "forward" sequence have been switched. The reversed sequence, termed PS5.MR, reads 5'-GGTGT GGGTG GGTGT TCATG GGTG-3' (also see Fig. 5-5, on next page).

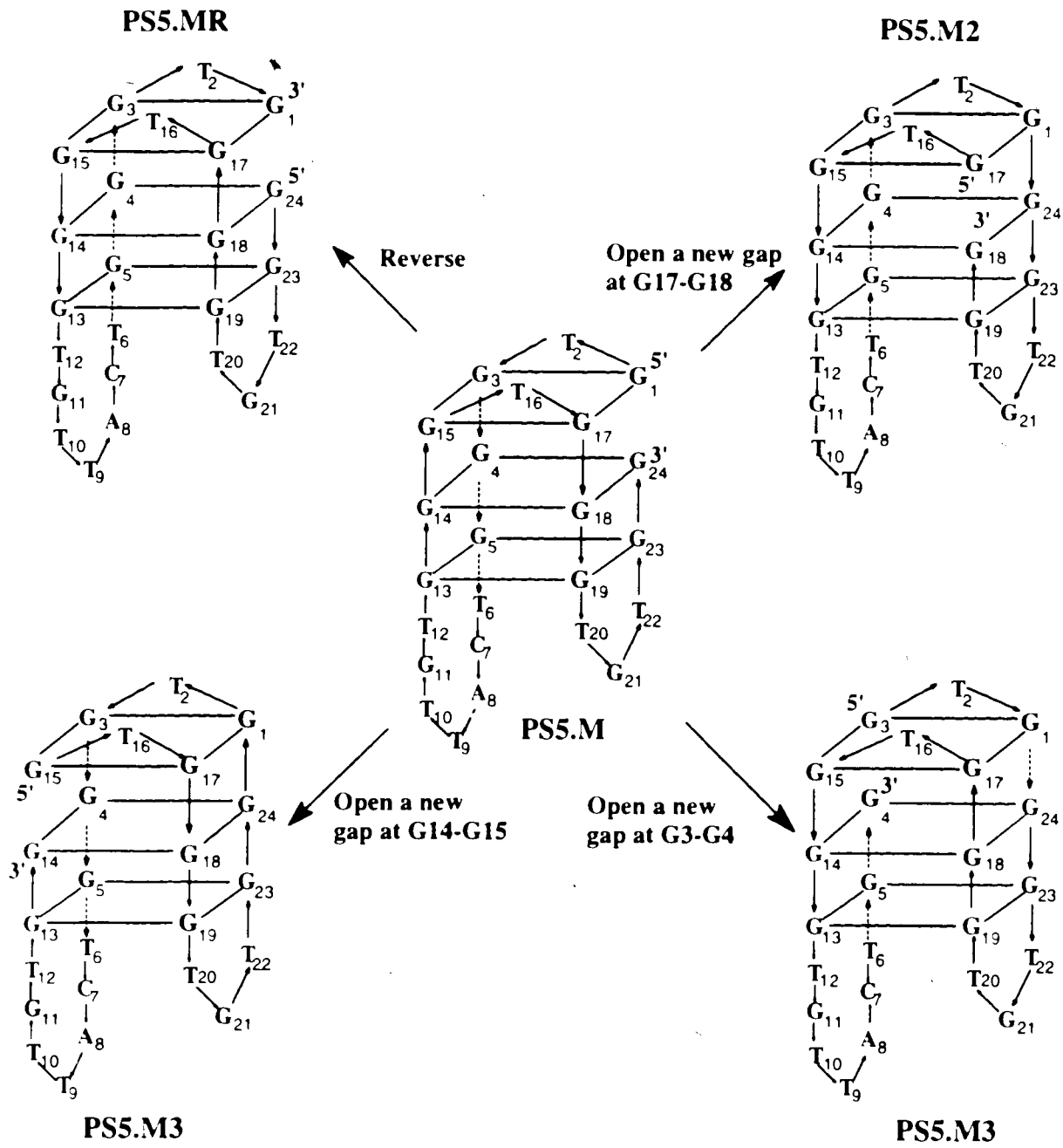

Fig. 5-5. Illustration of some structural manipulations for PS5.M (the middle structure). Reversing the 5' end and the 3' end of PS5.M gives the sequence PS5.MR. Closing the gap at G1-G24 and opening a new gap at G17-G18, at G14-G15, or at G3-G4 gives PS5.M2, PS5.M3, and PS5.M4 (and their reversing sequences, structures not shown), respectively. All base numbering is in reference to the numbering of PS5.M.

A second kind of structural manipulation was carried out by sequence permutation, in which the "gap" in the folded structure of PS5.M was moved around the quadruplex. For example, the gap between G1 and G24 could be closed, and a new gap opened between G17 and G18; between G15 and G14; or between G3 and G4 (see Fig. 5-5 for demonstration, p140). Of course, every time a new gap is opened, the resulting permuted sequences can be synthesized in either the "forward" or the "reverse" orientations. For consistency, the "forward" orientation of a given sequence was always the one starting with 5'GTGGG---- and ending with ----TGG3'. Therefore, the above sequence manipulations gave rise also to seven other structural isomers of the wild-type PS5.M. All these molecules should in principle be able to form structures similar, though not identical, to that of the wild type PS5.M. If indeed similar quadruplex structures could form, they might be catalytic as well, and would help to reinforce our original folded model for PS5.M.

We synthesized all eight oligomers and carried out enzymatic activity assays and DMS methylation experiments on them. The results are given in Table 5-2 (p142) and Fig. 5-4 (p138). As expected from the proposed model, the forward sequences, generated by opening the gap at different G connections, all had good metallation activity, though the structures with gaps between G1 and G24 (PS5.M), and between G17 and G18 (PS5.M2), were more efficient than the ones with the gap between G14 and G15 (PS5.M3), or between G3 and G4 (PS5.M4). The relative activities of these oligomers had the following order: PS5.M > PS5.M2 > PS5.M3 > PS5.M4 (Table 5-2, p142).

In the footprinting experiments with DMS on the above four sequences, all guanines in the putative quadruplex cores showed protections against methylation, as illustrated in PS5.M (Fig. 5-3, panel VI, p134) and PS5.M4 (Fig. 5-4, panel IV, p138). The data indicated that they all indeed formed G-quadruplex structures, as expected. Once again, these data supported the folded structural model we proposed in Fig. 5-2 (p133).

Table 5-2. Catalytic activity of sequences derived by structure manipulation within quadruplex (see Fig. 5-5)

Gap position*	Sequence orientation	Sequence name	Rate (μM/min)	Relative activity
G1-G24	forward	PS5.M	2.50	100
G1-G24	reverse	PS5.MR	0.78	29
G17-G18	forward	PS5.M2	2.20	86
G17-G18	reverse	PS5.M2R	0.53	19
G15-G14	forward	PS5.M3	0.85	32
G15-G14	reverse	PS5.M3R	0.11	2
G3-G4	forward	PS5.M4	0.68	25
G3-G4	reverse	PS5.M4R	0.05	0
Reference DNA		BLD	0.05	0

***These positions are in reference to the numbering of PS5.M**

Among the reverse sequences, PS5.MR and PS5.M2R had reasonably good enzymatic activity (Table 5-2), and had strong guanine protection against methylation around the guanine quadruplex core (Fig. 5-4, panel V for PS5.MR, p138). However,

PS5.M3R and PS5.M4R were both inactive (Table 5-2). The lack of catalytic activity of these two sequences was possibly due to their inability to form stable quadruplex structures. For instance, no significant protection from methylation had been observed for any guanine base of PS5.M4R (Fig. 5-4, panel VI, p138). We do not know at this point why these sequences were not be able to form the expected G-quadruplex structures.

3.4. Structural modifications at the gap and loop regions

3.4.1. The "Gap 1-24"

The most notable feature of the proposed structural model for PS5.M (see the structure of PS5.M shown below) is the existence of Gap 1-24. To assay the importance of this gap, an oligomer PS5M.BK.1 was synthesized in which the original G1 in PS5.M was separated from T2 but connected with G24 (see Fig. 5-6). Therefore, the new sequence PS5M.BK.1 was expected to form a quadruplex structure without the original gap.

With the gap closing, the catalytic activity of PS5M.BK.1 was significantly decreased, it had only 25% of the activity of PS5.M. Methylation protection data indicated that PS5M.BK.1 formed the expected quadruplex structure, as all the guanines in the quadruplex core were protected from methylation (Fig. 5-10, p148). The data were not only supportive of our proposed structural model, but also showed the importance of the existence of the "Gap 1-24".

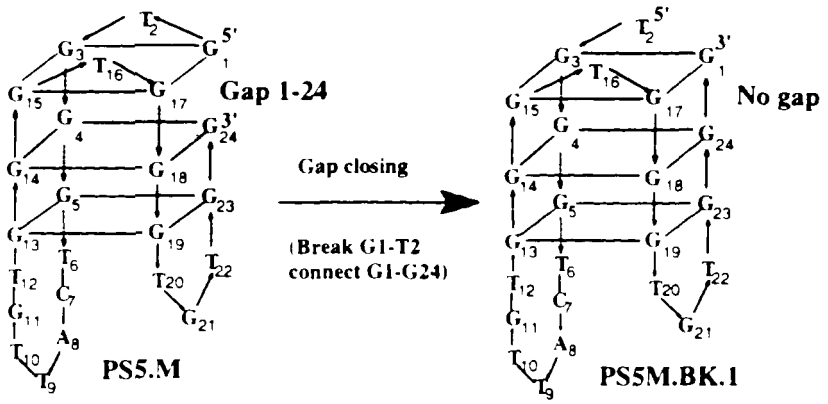

Relative activity: PS5.M: 100
PS5M.BK.1: 26

Fig. 5-6. The structure manipulation of PS5.M: The closing of "Gap 1-24".

3.4.2. The loops

In the proposed model of PS5.M, there are four loops: Loop 1 and Loop 2 are both one-T loops; Loop 3 have three bases (TGT); and Loop 4 is the biggest, which contains 7 bases. How important are these loops? Might the sizes of these loops be changed without loss of metallation activity? To address these questions, we synthesized and tested a series of short DNA oligomers. The following summarizes our findings:

(1) The optimized size of loop 4 is not necessarily 7 bases. With the deletion of four bases (C7, A8, T10, G11, as in PS5M.Short: structure shown in Fig. 5-7, p145), the catalytic activity increased by 20%.

(2) Both loop 3 and loop 4 could be shortened even further, into one-T loops. The resulting 16-nucleotide sequence PS5.MIN could still function as an effective catalyst for porphyrin metallation, having an activity level comparable to that of PS5.M (~40% of PS5.M). This finding completely ruled out the possibility that the enzyme's active site might be located at these two big loop regions.

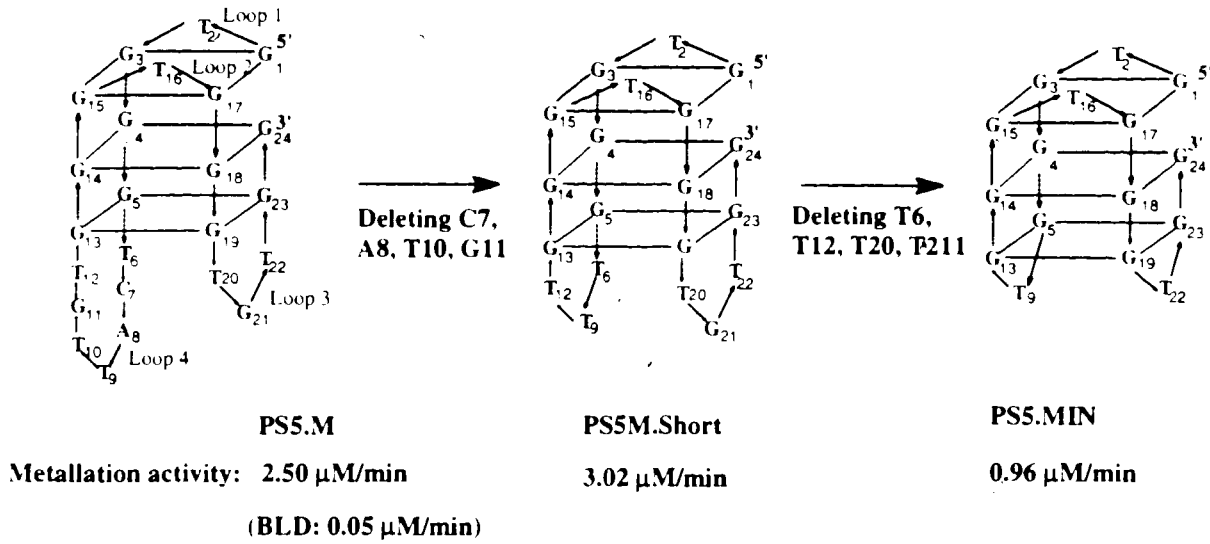

Fig. 5-7. Structural modifications at loop 3 and loop 4 of the proposed model for PS5.M.

(3) The one base Loop 2 in the proposed model of PS5.M appears to be very critical for the enzyme activity. It can not, for example, be changed into a loop of larger size. For instance, if this loop was changed to a TTT loop, the activity of the resulting sequence (Three-T.loop, as shown in Fig. 5-8) dropped very sharply.

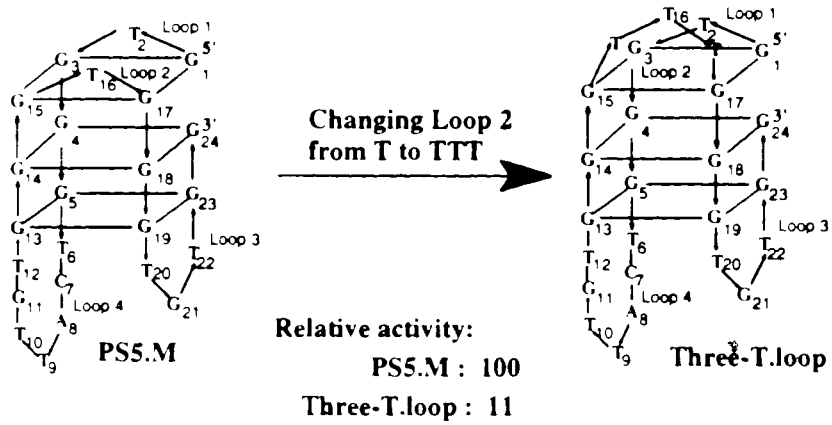

Fig. 5-8. Modification of Loop 2 of the proposed PS5.M structural model.

3.5. A quadruplex structure made up of two G-rich molecules

All DNA molecules we have tested this far were the sequences designed to form unimolecular quadruplex structures. We were interested in determining whether PS5.M could be broken into two molecules that together formed an intermolecular quadruplex structure. To do so, we designed two oligomers by breaking Loop 3 of PS5.M at A8 and T9 and by adding four more bases (AGCA) after A8 and three more bases (TGC) before T9, so that a stem of 6 base-pairs could form in theory to bring the two molecules together in a structure as shown in Fig. 5-9.

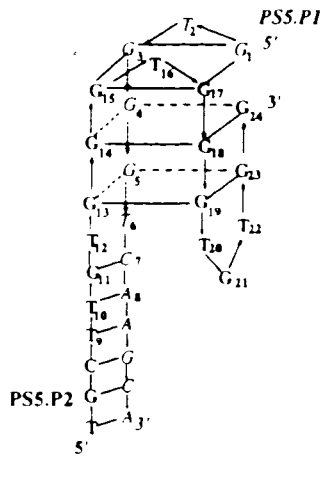

Fig. 5-9. Putative quadruplex structure formed by PS5.P1 (shown in italic) and PS5.P2 (shown in bold). The numbering is in reference to the numbering of PS5.M.

The data in Table 5-3 (next page) and Fig. 5-10 (panel IV and V, p148) clearly showed that the two broken parts did form the putative structure as shown in Fig. 5-9, and that this bimolecular quadruplex did maintain some catalytic activity--though this was fairly weak. The catalysis and strong guanine protection could only be realized when the two subunits of the structure were combined. Due to the fact that the formation of the

enzyme structure was a bimolecular association process, both incubation time and oligomer concentration had direct effects on the enzyme activity: The activity increased with increases in both the pre-incubation time and of the DNA concentrations (Table 5-3). The catalytic activity, however, levelled off at ~0.25 μM/min, which is much smaller than that of the unimolecular structure of PS5.M (2.5 μM/min).

Table 5-3. Catalytic study on the intermolecular quadruplex structure formed by PS5.P1 and PS5.P2.

Concentration of PS5.P1(μM)	Concentration of PS5.P2 (μM)	Incubation time (hours)	V (μM/min)
5	0	0.5	0.054
5	0	5	0.056
0	5	0.5	0.048
0	5	5	0.052
5	5	0.5	0.110
5	5	2	0.185
5	5	5	0.245
5	5	10	0.254
10	5	0.5	0.185
10	5	2	0.236
10	5	5	0.247

The data shown in Table 5-3 are consistent with the DMS protection results shown in Fig. 5-10, panel IV and V (p148). PS5.P1 and PS5.P2 by themselves did not show strong guanine protections, but the mixture of the two molecules gave full protection for the guanines in the putative quadruplex core.

Figure 5-10. DMS footprinting on PS5M.BK.1, PS9.ST1, PS19.ST1, PS5.P1, and PS5.P2. Panels I, II, and III are for PS5M.BK.I, PS9.ST1, and PS19.ST1, respectively. For each panel, lane A is the DMS methylation performed in 0KB buffer, lane B in 40KB buffer. Panel IV for PS5.P1, lane A PS5.P1 in 0KB, lane B PS5.P1 plus PS5.P2 in 0KB, lane C PS5.P1 plus PS5.P2 in 40 KB (PS5.P1 was ^{32}P-labeled but PS5.P2 was not). Panel V for PS5.P2, lane A PS5.P2 in 0KB, lane B PS5.P2 plus PS5.P1 in 0KB, lane C PS5.P2 plus PS5.P1 in 40KB (PS5.P2 was ^{32}P-labeled but PS5.P1 was not). The guanine labeled with an arrowhead in each panel corresponds to the guanine underlined in the sequence given in Fig. 5-1 (p131).

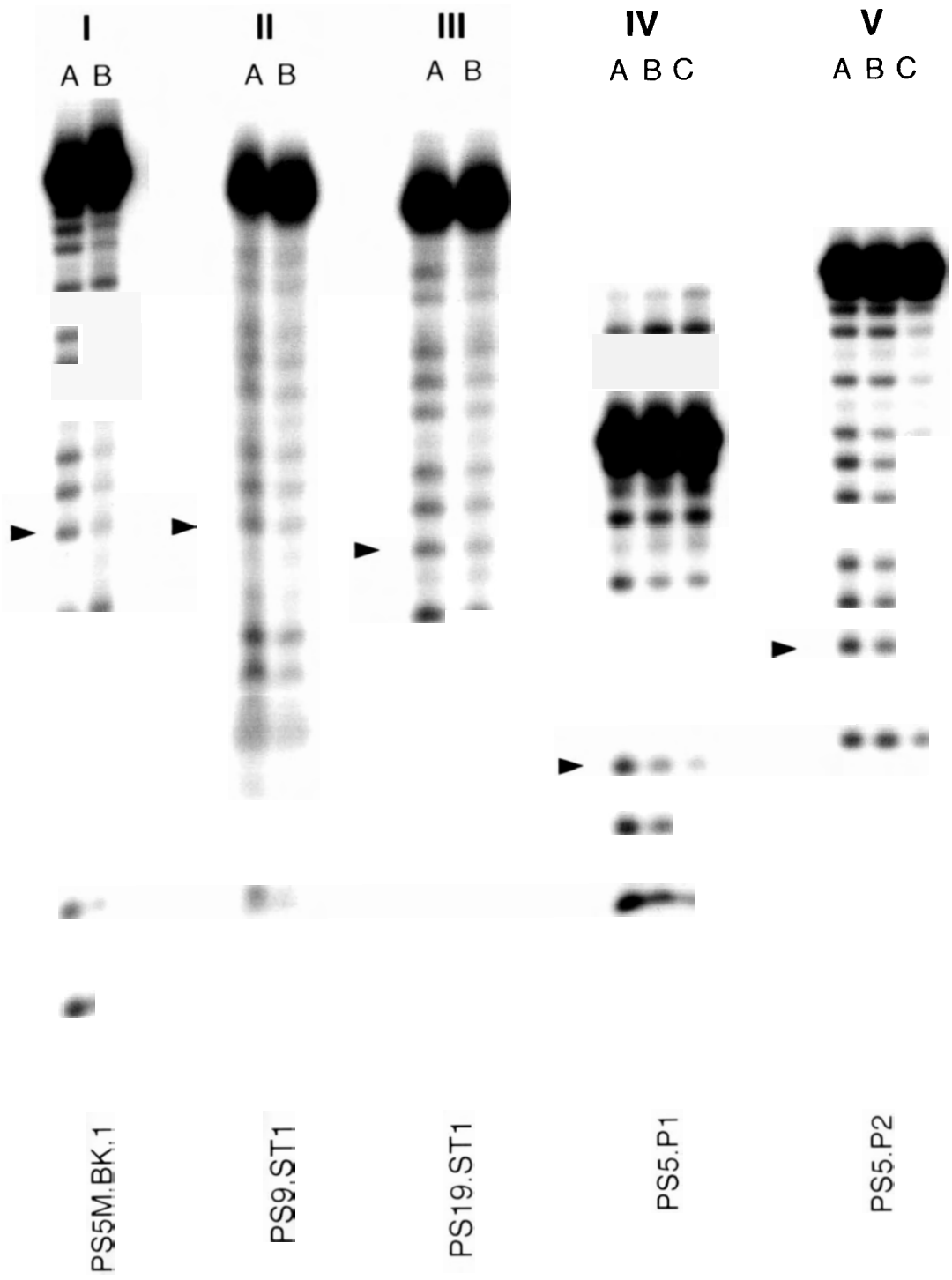
I
A B
II
A B
III
A B
IV
A B C
V
A B C
PS5M.BK.1
PS9.ST1
PS19.ST1
PS5.P1
PS5.P2

3.6. Other catalytic aptamers from the final selection pool

We have described earlier that among the binding site sequences from the PS family of clones, 30% of the sequences were not catalytic (catalytic rates at <0.1 μM/min); 45% were weakly active (from 0.1 μM/min to 0.3 μM/min, data not shown); and only 25% were strongly active. Table 3-3 of Chapter 3 (p88) gives the sequences of those catalytic oligomers and their catalytic rates.

Interestingly, footprinting data suggested that all these active sequences could fold into guanine quadruplex structures similar to that of PS5.M. Fig. 5-11 shows the putative guanine quadruplex structures for PS9.ST1 (left structure) and PS19.ST1 (right structure); their DMS protection patterns are given in Fig. 10 (panels II and III, p148). However, these structures do show some variations in the region of Loops 1, 3 and 4, which regions have already been shown to be less important than Loop 2, which has to be a one-base loop. These data again supported the model proposed in Fig. 5-3 (p133).

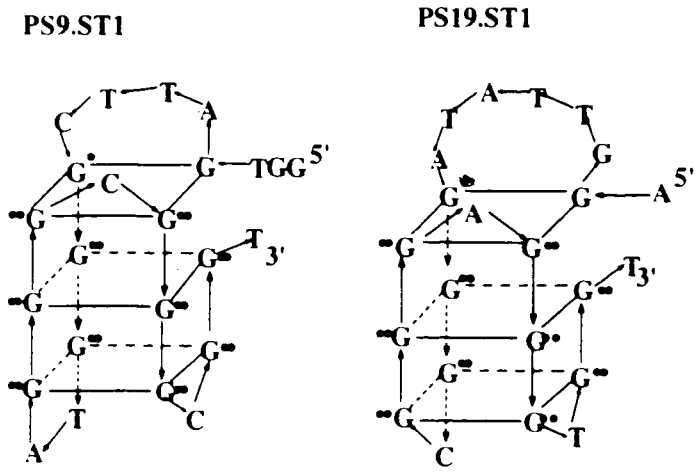

Fig. 5-11. The structure models for PS9.ST1 and PS19.ST1. The DMS methylation results are given along the structures. One filled circle: medium protection towards DMS methylation; two filled circles: strong protection.

The fact that the binding sites of all the selected catalytic clones are very G-rich and fold to form guanine quadruplexes as their active structures raises the question of whether the catalytic DNA sequences for porphyrin metallation need exclusively to be G-quadruplexes, or whether other, non-quadruplex, catalytic sequences may exist but may not get selected under conditions in which G-quadruplex structures are favored during selection (especially in the presence of potassium ions). This would be an interesting subject for future investigation.

3.7. Converting non-catalytic aptamers and the thrombin aptamer into catalytic DNA sequences

PS2.ST1 and PS5.ST1, derived as the porphyrin-binding sites of clones PS2 and PS5, respectively, showed a sharp contrast among one another: PS2.ST1 was very weakly active whereas PS5.ST1 was strongly catalytic (see Chapter 3). Nevertheless, PS2.ST1 has been shown to bind NMM with submicromolar affinity (Chapter 2, p53). Why could PS2.ST1 bind NMM but not be able to catalyze porphyrin metallation? This same question could also be raised for other non-catalytic aptamers.

When we tried to fit the PS2.ST1 sequence to the model shown in Fig. 5-3 (p133), we realized that it only can at best form Quartets A and B, but not Quartet C (as shown in Fig. 5-12, p151, left structure), because it lacked one guanine base necessary for the formation of the bottom quartet. We reasoned that if this G was now included, the resulting new sequence should be catalytic. A new oligomer, named PS2.M, was synthesized, in which this crucial G was introduced, along with the introduction of one T

each for Loops 3 and 4 (to make these two loops more stable), such that the resulting sequence might form a quadruplex structure as shown in Fig. 5-12 (right structure). The catalysis data are given underneath each structure and the DMS protection on guanines are also indicated by dots alongside each structure (the actual footprinting data are also shown in Fig. 5-14, panel I and II, p155).

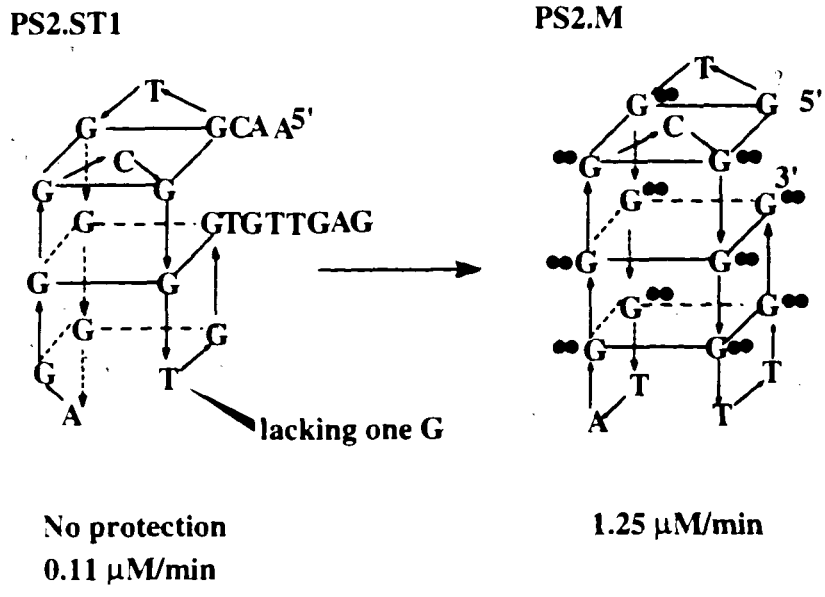

Fig. 5-12. Converting the noncatalytic sequence PS2.ST1 into the catalytic sequence PS2.M. The rates given underneath each structure were obtained in 40KB buffer. One filled circle: partial protection towards DMS methylation; two filled circles: strong protection.

With these modifications, the catalytic activity changed dramatically; it went up from almost no activity for PS2.ST1 (0.11 μM/min, 0.05 μM/min for background) to a high level of catalysis by PS2.M (1.25 μM/min), a reactivity jump of 20 times.

As for the DMS protection experiments, we had reported earlier that in both PS2.ST1 and its parent sequence PS2, some guanine bases only got protected in the presence of NMM (see Chapter 2); whereas without NMM, there was no sign of protection on any guanine of PS2.ST1 (Fig. 5-14, panel I, p155). But in the case of PS2.M (Fig. 5-14, panel II) as well as all of the other catalytic oligomers described in this work, the quadruplex structures were always *pre-folded*, without any help of NMM (the only promoter for structure formation being the potassium ion). Therefore, I would like to propose here that the pre-folding of the quadruplex structure is requisite for the eventual catalytic activity of an oligomer (although not all pre-folded quadruplexes are catalytic, such as OXY4 and other telomeric sequences). I propose that only a catalytic sequence like PS5.M, with a pre-folded active quadruplex structure and with its active site ready for action, readily takes a porphyrin substrate into the binding site, deforms it, and turns it into a product after an effective collision with a copper ion.

As for sequences like PS2.ST1, they can not form stable quadruplex structures by themselves. Instead, NMM has to be present to initiate DNA folding. In other words, the presence of NMM induces the folded structure formation by those sequences (as seen in Chapter 2). However, a planar porphyrin like MPIX, sufficiently different structurally from NMM, can not work as a structure "inducer" for those sequences. Significantly, there is also not much stable quadruplex structure formation (as defined by DMS protection) for these sequences in the presence of MPIX (see Chapter 2). Therefore these sequences could not function as a catalyst for porphyrin metallation.

We also focused our attention on the "thrombin aptamer". This 15-nucleotide G-rich sequence (named TM in this thesis), was obtained by Boch et al.(1992), through an *in vitro* selection experiment from a random DNA library. TM bound protein thrombin with nanomolar affinity . X-ray and NMR studies have shown that TM forms an intramolecular quadruplex structure (shown as the first structure in Fig. 5-13). However,

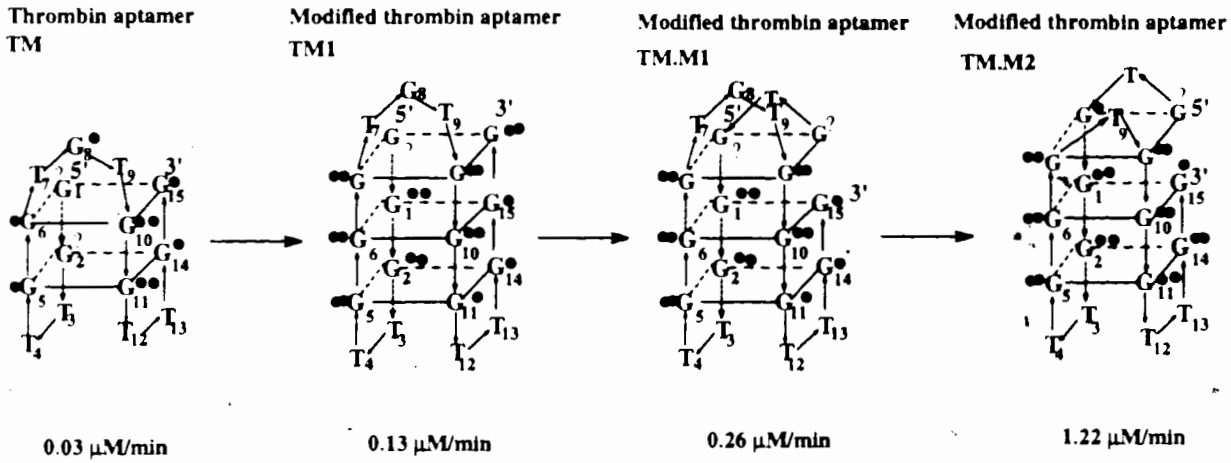

Fig. 5-13. Converting the noncatalytic thrombin aptamer TM into the catalytic sequence TM.M2. The rates given underneath each structure were obtained in 40KB buffer. One filled circle: partial protection towards DMS methylation; two filled circles: strong protection.

when tested for the catalysis of porphyrin metallation, this sequence did not show any catalytic activity. We reasoned that TM's lacking the catalytic activity for porphyrin metallation was due to the following: 1) It has only two layers of guanine quartets but not three layers; 2) it does not have two crucial features on the top portion of the structure (compared to the structure of PS5.M): the gap, and the one-T loop (Loop 2). Schultze et al (1994) have made a modified sequence of the thrombin aptamer, in which four more

guanines were incorporated so that the resulting sequence could form a structural analog of the original thrombin aptamer but with three layers of guanine quartets. The formation of the expected structure (shown as the second structure in Fig. 5-13) has been confirmed by the NMR data (Schultze et al., 1994). This modified thrombin sequence (named TM2 by this author) only showed very weak catalytic activity for prophyrin metallation (Fig. 5-13). In our first modification, we synthesized a sequence, named TM.M1, that had a gap between the top quartet and the bottom two quartets (shown as the third structure in Fig. 5-13). With this small modification, the catalytic activity indeed increased, but not dramatically (TM.M1 was twice as active as TM2, and 9 times as TM). In our second modification, we changed the top TGT loop (corresponding to Loop 2 of PS5.M) to a one-T loop. The resulting sequence, named TM.M2, showed a strong catalytic activity for porphyrin metallation, with a rate jump of 40 times over the original thrombin aptamer. Our DMS methylation data, too, clearly indicated that TM.M2 formed the expected quadruplex structure (shown as the fourth structure in Fig. 5-13, p153; and its methylation patterns shown in Fig. 5-14, panel III on page 155).

The successful derivation of an effective catalytic sequence (e.g. TM.M2) from the thrombin aptamer not only supported our structural model proposed for PS5.M (shown in Fig. 5-2, p133), but most importantly, the structural information obtained on the thrombin aptamer by X-ray and NMR studies (Schultze et al., 1994; Macaya et al., 1993; Padmanabhan et al., 1993; Wang et al., 1993) helped us to elucidate the catalytically active quadruplex structure in a more detailed way (see Section 3.10).

Fig. 5-14. DMS methylation data for PS2.ST1, PS2.M, TM.M2, PS5.ST1, and PS5.D. Panel I, II, III, and V are for PS2.ST1, PS2.M, TM.MII, and PS5.D, respectively. Lane A is in 0KB buffer, lane B in 40KB. Panel IV is for PS5.ST1, lane A is in 0KB buffer, lane B in 40KB buffer, lanes C and D also in 40KB buffer but containing 50 μM NMM and 50 μM MPIX, respectively.

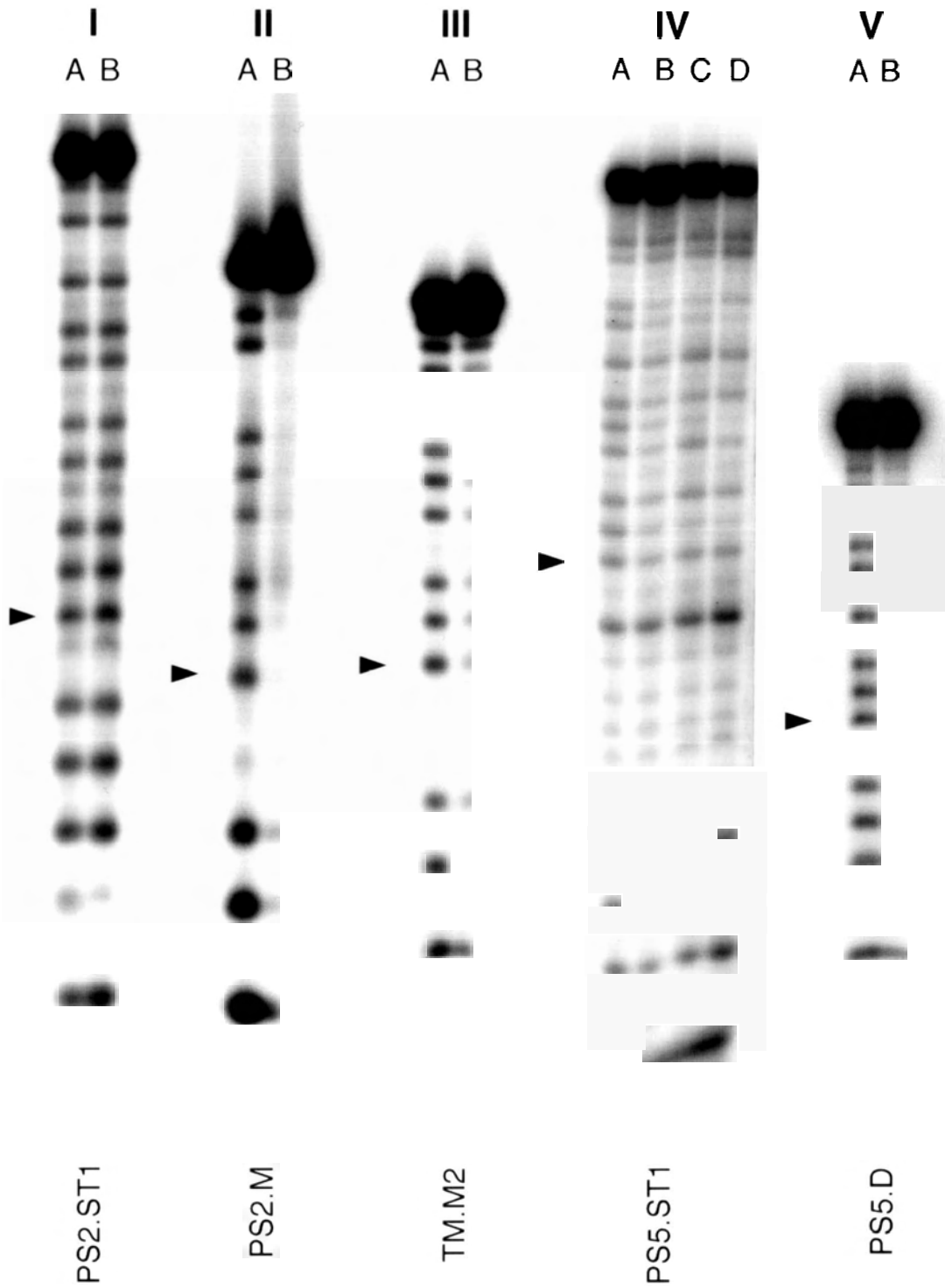
I
A B
II
A B
III
A B
IV
A B C D
V
A B
PS2.ST1
PS2.M
TM.M2
PS5.ST1
PS5.D

3.8. DMS Footprinting of PS5.M with and without the presence of NMM and MPIX

As pointed out above (p152), quadruplex formation by PS5.M and other *catalytic* sequences is mediated by potassium ions and without any help by NMM or MPIX. It is useful, however, to examine how NMM and MPIX affect the formation and stability of the folded structure. Therefore, DMS methylation experiments were carried out to detect guanine protection patterns of PS5.ST1, with and without the added NMM and MPIX. The result is shown in Fig. 5-14, panel IV (p155).

The methylation pattern of PS5.ST1 did not change significantly with the input of either NMM and MPIX. However, there were some noticeable changes in the methylation patterns of PS5.ST1 by the added NMM or MPIX. A few guanines (such as G4, G14, G16) gained extra protection from methylation, whereas protections on guanines at 3, 5, 13, 15, 17 were reduced (compared to the footprints obtained in the absence of the added porphyrins). We will discuss these results later in Section 3.10.

3.9. The activity of PS5.ST1 versus that of its parent sequence PS5--a structural explanation

We have reported that though PS5.ST1 had strong catalytic activity for porphyrin metallation, its parent sequence PS5 had only weak activity (<10 % of PS5.ST1, see Chapter 2). We have suggested in Chapter 4 (p102) that the differences in catalytic capability by PS5.ST1 and PS5 may be due to the following two reasons: 1) PS5.ST1 and PS5 may fold differently to give guanine quadruplex structures that are not identical to each other; or 2) the sequences outside of the PS5.ST1 domain within PS5 may prevent

this catalytic domain from functioning catalytically. By carefully examining the sequence of PS5, we hypothesized that PS5 could have two folding patterns, as shown in Fig. 5-15. For the parent sequence PS5, type II folding has to be dominant, because this type of folding will result in a structure not only containing a guanine quadruplex domain, but also having a long continuous stem region (12 b.p.); whereas in the type I folding this stem region is reduced to 5 base-pairs. Therefore, type II folding would give a more stable structure for the whole molecule of PS5. Our methylation data on PS5 were

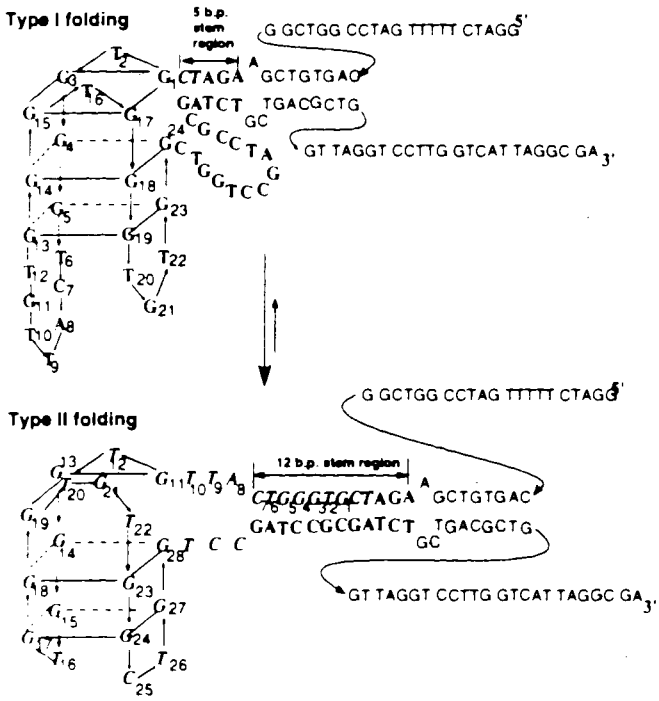

Fig. 5-15. Two folding patterns of G-rich region of PS5. Both patterns can give rise to a quadruplex structure which bind to NMM, but only Type I folding results in a structure highly catalytic for porphyrin metallation.

with the type II folding since G3, G4, G5 were not protected while G27 and G28 were protected (along with other guanines in the quadruplex core, see Fig. 2-4, p58). On the other hand, PS5.ST1 adopted type I folding, as suggested by its DMS methylation data (Fig. 5-3, panel I, p134), which showed that G27 and G28 were not protected. The fact that PS5.ST1 adopted the type I folding suggested that the guanine quadruplex portion in type I folding was more stable than that in type II folding.

The proposed type I-type II folding patterns for PS5 were also consistent with the catalytic data on the other deletion mutants of PS5, such as PS5.M, PS5.K, PS5.L, PS5.Cut, and PS5.D. PS5.M, PS5.K and PS5.L could only adopt type I folding (due to the deletion of G27 and G28, Fig. 5-16), and their activities were at the same level of PS5.ST1. On the other hand, PS5.D could only adopt type II folding (Fig. 5-16), which showed only low level of catalytic activity. As expected, sequence PS5.Cut behaved very much like its parent sequence PS5, and had only very weak activity (Fig. 5-16), and the guanines in the putative stem region were not protected from methylation.

To confirm that the guanine quadruplex portion of the type II folding are indeed capable of porphyrin binding, PS5.D (a 21mer, which corresponds to the quadruplex region of PS5 in the type II folding, see Fig. 5-16) was tested for its affinity for MPIX and NMM. Although catalytically, PS5.D was much poorer (see above), its porphyrin-binding ability was as effective as PS5.M (suggested by our UV-visible absorption data, which will be discussed in Chapter 6). Also, our data from DMS methylation experiments were clearly supportive of the idea that PS5.D formed a stable guanine quadruplex structure (Fig. 5-14, panel V, p155).

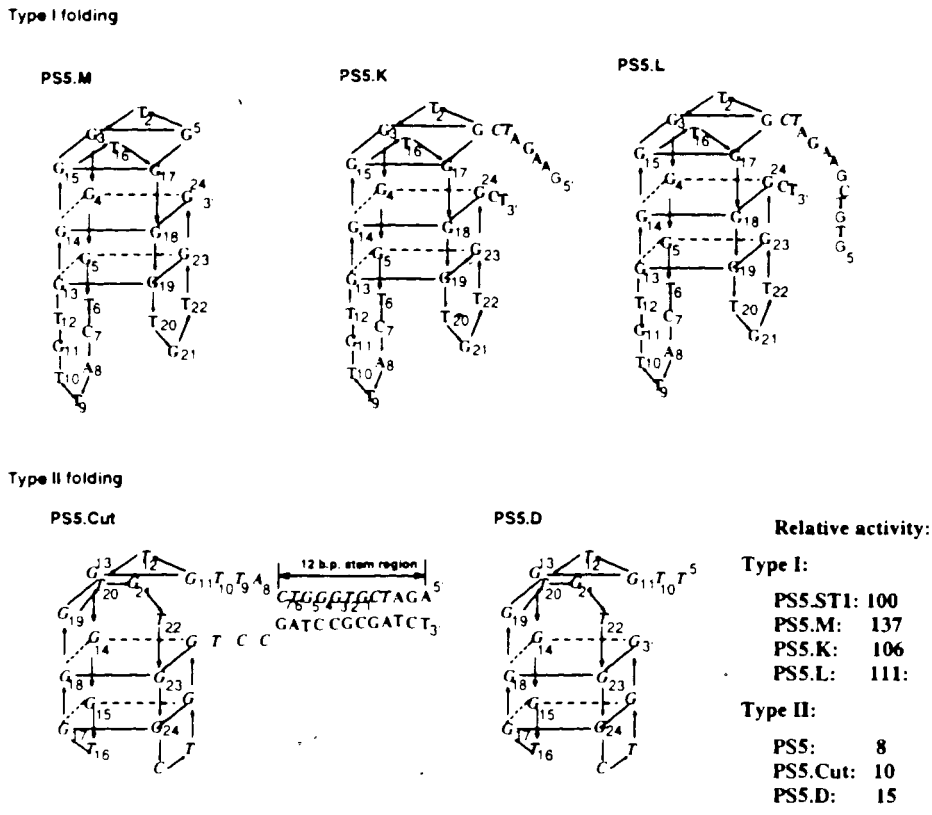

Fig. 5-16. Structures of PS5.M, PS5.K, PS5.L, PS5.Cut, and PS5.D.

3.10. A discussion on stabilization of the transition state of porphyrin metallation by the guanine-quadruplex structure of PS5.M

Four guanines can form a G-quartet (as shown in Fig. 5-2b, p133; Sen & Gilbert, 1988, 1990; Williamson et al., 1989; Sundquist & Klug, 1989), in which guanines associate with each other by hydrogen-bonding in a circular manner. Both porphyrins and guanine-quartets are large and aromatic systems. A G-quartet has an estimated planar area of ~104 $Å^2$ (estimated by the data of Kang et al, 1990) and a central cavity area of 16$Å^2$ (central non-aromatic area); the porphinato core of porphyrins has an estimated area of ~50$Å^2$ and an area of ~8$Å^2$ between the four central nitrogens (estimated by the data of Smith, 1978). Clearly, the porphinato core of a porphyrin structure has good potential to

interact with guanine-quartets via aromatic stacking (π orbital interaction). This sort of intercalation has in fact been reported between cationic porphyrins and double helical DNA [Reviewed in Pasternack et al. (1983) and Chaires (1990)], and between ethidium bromide and a guanine quadruplex (Gao et al., 1992). Therefore, it would not be surprising if porphyrins and guanine-quartets interacted via intercalation of a porphyrin between two successive guanine-quartets--that is, one porphyrin molecule sitting between two layers of guanine-quartets, forming a sandwich-like arrangement. The formation of this structure could be driven by π-orbital interaction between quartet and porphyrin ring.

Nevertheless, the porphyrin configuration in the transition state of its metallation is not planar, but instead is deformed, with one of the pyrrole rings bent out of the plane shared by the other three pyrrole rings (see Chapter 1 for discussion).

In order for a quadruplex structure to stabilize this "bent" transition state, simple intercalation is obviously not enough; instead, I would argue that the quadruplex structure has to arrange its guanines in a special "deformed" manner, similar to that of the bent porphyrin. In other words, two quartet layers sandwiching the porphyrin molecule would have to adopt a conformation such that three guanines share one plane but the fourth one buckles out of that plane. In this way, six guanines on two parallel quartet planes (three on each layer) interact with three pyrrole rings in the porphinato plane, and the two buckling guanines interact with the bent pyrrole ring. The question is: Do guanine-rich sequences have the ability to form a quadruplex structure with this sort of buckling guanines?

In fact in G-quadruplexes, it is a general phenomenon for one or more guanines to buckle out of the planes shared by other guanines (Kang et al., 1992; Wang, et al., 1993 a & b; Macaya et al., 1993; Padmanabhan et al., 1993; Schultze et al., 1994). For instance, X-ray crystallography study on the quadruplex structure formed by d(GGGGTTTTGGGG) showed that one guanine is buckled roughly 25 degree from the plane of the three other guanine residues (Kang et al., 1992). For the thrombin aptamer, X-ray study shows that for the G2-G5-G11-G14 quartet (see Fig. 5-13, p153), G11 and G14 are buckled about 15 degree out of the plane of other two guanines (Padmanabhan et al., 1993). In an NMR study of the same aptamer, a similar buckling phenomenon was found for a few guanines on both layers of quartets (Macaya et al., 1993; Schultze et al., 1994). Therefore, it is reasonable to assume the PS5.M forms guanine quartet structure with one or more buckling guanines in it.

By assaying the catalytic activity of various short DNA sequences, correlated with the DMS methylation data obtained on them, we have concluded that PS5.M folds to form a guanine quadruplex structure as shown in Fig. 5-2 (p133). We would like to use the data further to make the following speculations about the structure of the DNAzyme:

1) The binding site is located between Quartets A and B, and that a porphyrin substrate molecule diffuses into this active site by taking the advantage of this "nick" (which may also help product molecule to diffuse out of the active site easily). Closing this gap will result in the activity loss (as observed in PS5M.BK.1).

2) G17 and G18 (or G14 and G15) are buckled from the planes of Quartets A and B, respectively, but still parallel to each other. The tilting of these two guanines is mainly

caused by Loop 2. One-base Loop 2 is absolutely conserved in all the sequences having strong catalytic activity, such as PS5.ST1 (and its shortened sequences), TM.MII, PS2.M, PS9, PS19. The release of the stress at this portion will lead to the severe loss of the enzymatic activity, as we have observed in such sequences as Three-T.loop, TM.M1, PS5, PS5.D, and some of our weakly active clones (such as PS18, data not shown). This one-base loop is not necessarily T-based, as A (as in PS19.ST1) and C (as in PS2.M and PS9.ST1) have also been observed at this position.

3) Loops 1, 3 and 4 play the roles of structural and catalytic "helpers", and therefore are less crucial. The sizes of these loops can be varied, and they have been seen containing only one base to containing up to seven bases. The extreme case is that all four loops are one-T loops (as in PS5.MIN). However, PS5.M seems to have the best combination of these loops as it is the best catalytic sequence for porphyrin metallation, derived from the final selection pool.

4) The binding mode between the DNAzyme and the porphyrin substrate is intercalation. It is most likely driven by π-π interactions (base-stacking) between guanine bases (in Quartets A and B) and four pyrrole rings (in the porphinato core). This may explain the differences of the DMS methylation patterns of PS5.ST1 in the presence and absence of NMM and MPIX. As discussed earlier, with the presence of NMM or MPIX, certain guanines have gained the extra protection while others have lost some protection. This indicates that after the porphyrin binding, the strength of the hydrogen bonds in the original quadruplex core has been affected. From the studies of the DNA intercalating drugs such as daunomycin and ethidium with double-helical DNA, it has been found that

the intercalation of those drugs unwinds the DNA helices and causes the separation of base-pairs and the lengthening of double helices. For instance, by intercalating daunomycin into the oligomer d(CGTACG), the C:G intercalation site is opened by 3.4Å and base-pairs at adjacent sites are unwound by 8 degree, shown by X-ray crystallography (Wang et al., 1987). The changes of those helical parameters are not significant by groove-binding drugs. Although there was no report of similar structural studies on the intercalating drugs and G-quadruplex, it is not unreasonable to assume that similar phenomena also exist for guanine quartet structures, that is, the intercalation of big aromatic compounds into a quadruplex structure will most likely result in the following structure changes: space opening of the intercalation site, backbone distortions, as well as partial unwinding of quadruplex helices. These changes will most likely affect the strength of some hydrogen bonds between guanines in the quadruplex core. For instance, for a hypothetical guanine quartet made of G1-G2-G3-G4 (G4 also H-bonds to G1), if the intercalation of a porphyrin molecule makes G2 and G3 move a little closer to each other while makes G1 and G4 move away somewhat from each other, the hydrogen bonds between G2 and G3 could be stronger due to a shorter distance between G2-G3, whereas those hydrogen bonds between G1 and G4 may be weakened due to the distance increase between G1-G4. (The free energy loss caused by this, If there is any, can be compensated by the energy gain from the base stacking.). Reflecting in DMS methylation experiment, G2 (or G3, dependent on which guanine uses N7 in the hydrogen bond formation for this G2-G3 pair) could gain extra protection while G1 (or G4) would lose some protection.

This, I would like to suggest, is the reason for DMS protection pattern changes of PS5.ST1 when it binds to MPIX or NMM.

With the above speculations, we propose a three-dimensional model for the guanine quadruplex core of PS5.M, as shown very schematically in Fig. 5-17 (p165). This highly stressed quadruplex structure, with G17 and G18 significantly buckled out of Quartets A and B, may provide the means for the DNAzyme to bend the porphyrin substrate to the transition state of the metallation reaction, and accelerate the metallation rate.

Fig. 5-17. A schematic drawing of the three dimensional model proposed for the guanine quadruplex core of PS5.M. All guanines in the core are shown as a block, and the porphyrin substrate, shown as a square structure between the top two layers of G-quartets, is in its transition state for the porphyrin metallation.

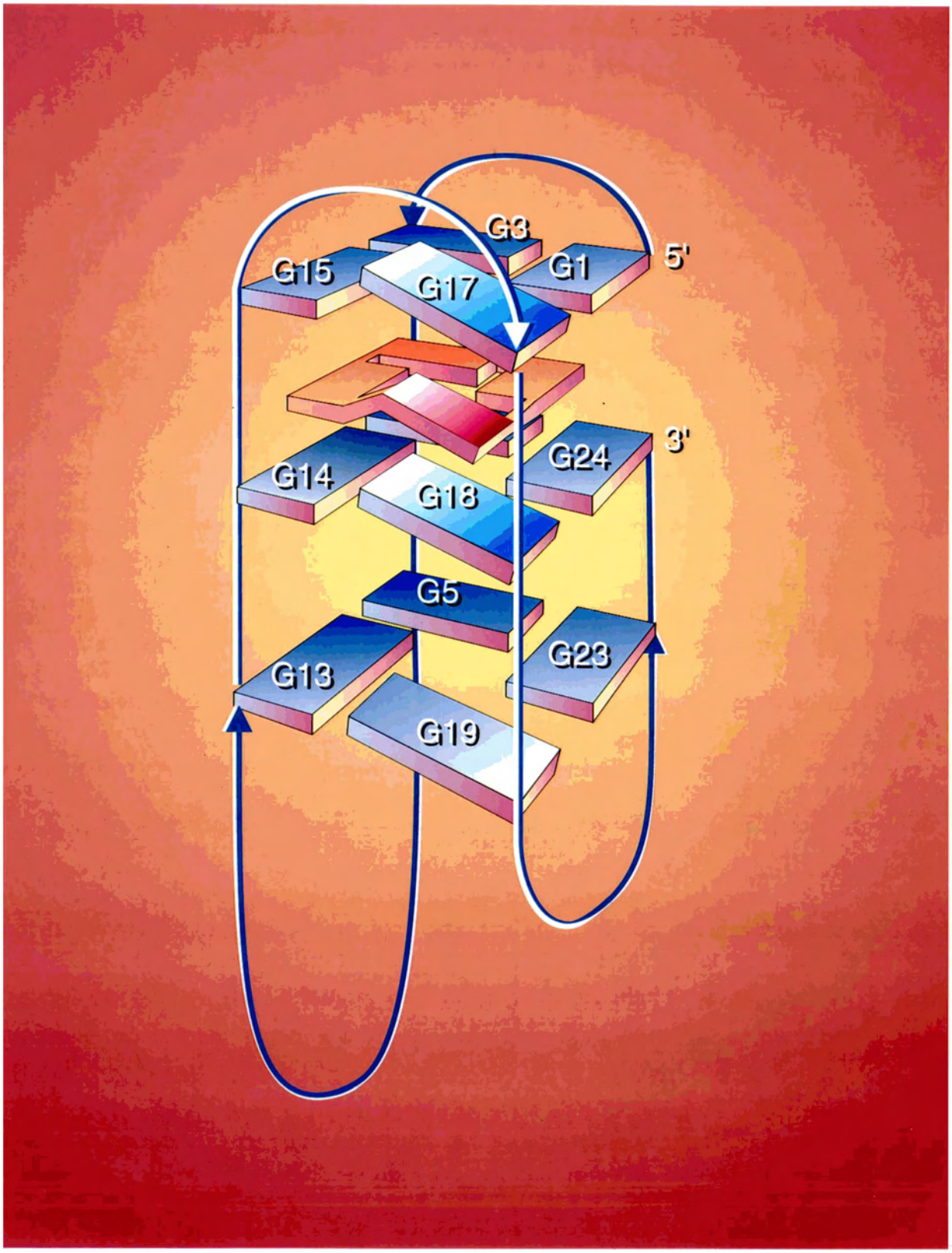
G3
G15
G1
5'
G17
3'
G24
G14
G18
G5
G23
G13
G19

Chapter 6. Spectroscopic Studies on DNA-NMM or DNA-MPIX Complexes

1. Introduction

In Chapter 5, I proposed a structural model for the porphyrin-metallating DNAzyme, on the basis of the kinetic and chemical probing data of PS5.ST1 and its related sequences. We suggested in Chapter 5 that the porphyrin substrate MPIX, when bound to the enzyme's active site, was bent by the DNAzyme and forced into a conformation resembling the deformed transition state for porphyrin metallation. In other words, in the DNAzyme-MPIX complex, MPIX might have a deformed porphinato ring structure with different properties from that of the normal planar structure of MPIX (but similar to the permanently bent structure of NMM). Investigation of physical properties of the DNAzyme-MPIX and DNAzyme-NMM complexes, therefore, seems necessary, for it might provide useful information regarding the possible mechanism of the catalysis by the DNA enzyme.

We sought to study and compare the spectroscopic properties of these complexes. Advantageously, porphyrin compounds have very strong ultraviolet (UV)-visible absorption as well as fluorescence emission properties. These simple yet very sensitive spectroscopic methods have been used widely by porphyrin researchers.

In this chapter, I will present some preliminary results on the spectroscopic studies of DNA-MPIX, and DNA-NMM complexes. The most interesting finding from these studies is that the DNAzyme-MPIX complex has a UV-visible spectrum close to that of

the DNAzyme-NMM complex, but significantly different from that of uncomplexed MPIX itself. Further, we found that this similarity is the result of an increased basicity of MPIX, when bound to the DNAzyme. These new findings are consistent with our previous hypothesis that the DNAzyme works to deform the planar porphyrin substrates for the rate acceleration of their metallation.

2. Material and methods

All ultraviolet-visible absorption measurements for both MPIX and NMM were carried out in a dual-beam Cary 3E UV-Visible Spectrophotometer, at 20°C. Fluorescence measurements were carried out in a SLM 4800C Spectrofluorometer, at room temperature.

2.1. Titration of MPIX and NMM absorptions with nonionic detergents

2 μM MPIX solutions [diluted from 100 μM stock solution in 40KB buffer (100 mM MES, 50 mM Tris, 40 mM potassium acetate, 0.25% Triton X-100, 1% DMSO, final pH 6.2)] were individually made in 40KBn buffer (which contained all the components of 40KB buffer except the Triton and the DMSO) containing different concentrations of either Triton X-100, Tween 20, or Nonidet P-40. These solutions were scanned over the wavelength range of 300 to 700 nm. Various concentrations for each detergent were tested to determine the detergent concentration at which MPIX started to give their saturated absorption profiles.

2.2. Porphyrin absorption in the presence of various DNA oligomers

Experiments for the comparison of the effects of various DNA oligomers on the absorption spectra of MPIX were carried out using solutions containing 1 μM MPIX and 10 μM DNA.

For the titration of MPIX absorption by increasing concentrations of PS5.M, the MPIX concentration was fixed at 1 μM while the PS5.M concentrations were at 0, 1, 3, 5, 7, 9, 12, 15, 20, 30, 50, 75, 100, 150, 200, 250, 300, and 366 μM. The solutions were prepared as follows: DNA was first incubated in 40KBn buffer for 20 minutes, then MPIX was introduced (from 100 μM stocks in 40KB). The mixtures were incubated for 10 minutes before the measurements were taken. MPIX was added last to minimize its dimerization in water.

For the titration of NMM absorption by PS5.M, DNA concentrations were tested up to 20 μM while NMM was fixed at 1 μM.

2.3. pH titration

Buffer solutions with different pH values were made as follows (using the standard methods): pH 1.0-2.0 were buffered by HCl-NaCl; pH 2.0-3.6 by glycine-HCl; pH 3.7-5.6 by sodium (or potassium) acetate-acetic acid; pH 5.8-8.0 by Na_2HPO_4-NaH_2PO_4 (or their potassium salts); pH 7.0-9.0 by Tris-HCl; pH 8.6-10.6 by glycine-NaOH (or KOH); pH 11.0-12.0 by Na_2HPO_4-NaOH; and pH 12.0-13.0 by NaOH-NaCl. All the buffer solutions contained either 100 mM K^+ or 100 mM Na^+. Potassium ions had to be used for PS5.M (for the structural folding of PS5.M), while sodium ions had to be

used for SDS solutions (SDS precipitates in the presence of low potassium concentrations). While the porphyrin-Triton or the porphyrin-SDS solutions were tested for the entire pH range from 1.0 to 13.0, porphyrin-PS5.M solutions were only tested at the range from pH 4.0 to pH 10.0. NMM concentration was at 3 μM, MPIX concentration at 1 μM, PS5.M concentration at 20 μM (80% binding saturation for 1 μM MPIX), Triton X-100 at 0.1%, and SDS at 1%.

3. Results and discussions

3.1. Detergent effects on the solubility and UV-visible absorption properties of MPIX and NMM

3.1.1. MPIX

MPIX is a very hydrophobic molecule, and has very low solubility in water or in buffered solutions around neutral pH. In addition to the low solubility, MPIX and other hydrophobic porphyrins and their metallo-derivatives tend to aggregate by forming dimers or polymers in aqueous solutions (Brown & Shillcock, 1976; Brown & Hatzikonstantinou,1978; Brown et al., 1980; Karns et al., 1979; Margalit & Rotenberg, 1984; Mazumdar & Mitra, 1990). For instance, MPIX starts to form dimers at concentrations as low as 0.05 μM (Margalit & Rotenberg, 1984). However, these problems have been overcome by the inclusion of detergents in assay buffers (Falk, 1964; Smith, 1975). The detergents can be anionic (such as sodium dodecyl sulphate--SDS),

cationic (e.g. cetyltrimethyl ammonium salts), and nonionic (e.g. the Tween and Triton series). As discussed in Chapter 4, nonionic detergents such as Triton X-100 and Tween 20 have been widely used in ferrochelatase assays to solubilize and monomerize hydrophobic porphyrin substrates (Pora and Jones, 1963; Falk, 1964; Smith, 1978; Li et al., 1987).

We investigated the effects of the nonionic detergent Triton X-100 on the absorption of MPIX. The solubility of MPIX in 40KBn buffer (see Material and methods section) was extremely low. For 2 μM MPIX in 40KBn buffer, no absorption could be detected even at the Soret region after the solution had been centrifuged at 13,000 rpm for 30 minutes. The solubility of MPIX increased with increasing Triton concentrations (reflected, among other things, by the fact that higher and higher absorption intensities could be measured for the supernatants following 30-minute spin of MPIX-Triton mixtures). Fig. 6-1 (p171) shows that the absorption intensity of MPIX-Triton solutions increased with the Triton concentration in both the Soret region (~400 nm) and the visible region (peaks I-II-III-IV between 500-700 nm; these peaks were named according to Smith, 1975). The absorption intensities reached saturation at a Triton concentration of 0.085%; and at this concentration; also no MPIX precipitation (detected by centrifugation) was observed (data not shown).

We also tested the solubility and the absorption of MPIX with other nonionic detergents: Tween 20 and Nonidet P-40. Both had the similar effect as seen with Triton X-100 (data not shown).

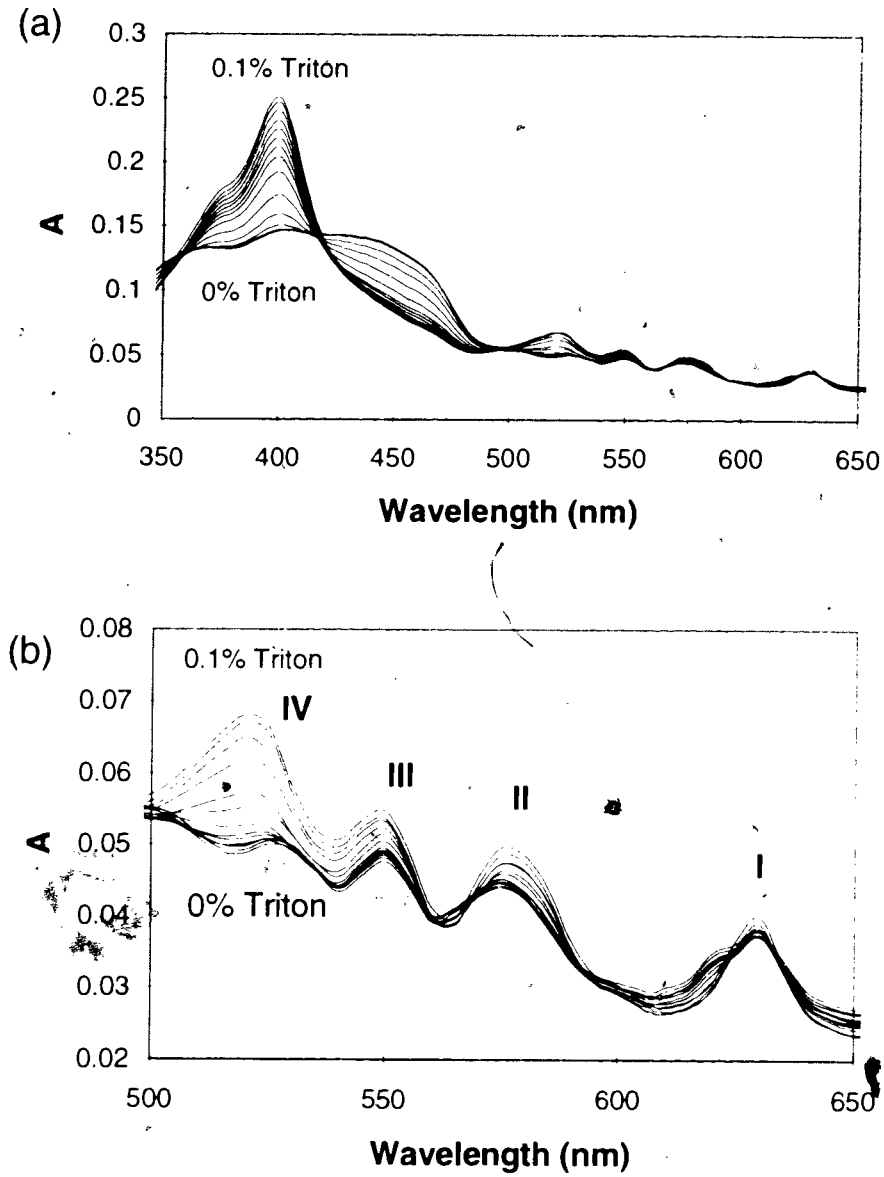

Fig. 6-1. Absorption spectra of MPIX with increasing detergent concentrations. (a) Absorption spectra from 350 to 650 nm; (b) the region from 500 to 650 nm. MPIX (1 μM) was titrated in 40KBn buffer with the following Triton concentrations: 0, 0.005, 0.0075, 0.01, 0.0125, 0.015, 0.0175, 0.02, 0.025, 0.03, 0.035, 0.06, 0.085, 0.1%.

3.1.2. NMM

Unlike MPIX, NMM is both more soluble and less aggregated in water and in buffered neutral solutions. For instance, no precipitation was detected in the 40 KBn solution containing 1-5 μM NMM. Nonionic detergents such as Triton X-100 and Tween 20, tested up to 0.1% (w/v), showed no significant effect on either the solubility or the absorption of NMM within this concentration range (data not shown). The higher solubility of NMM in the neutral aqueous solutions is most likely due to the increased basicity of NMM compared to that of MPIX (see Chapter 1 and also discussion below). At neutral pH, NMM exists mainly in a monoprotonated form and has a positively charged center. The protonated NMM interacts more strongly with water, and this results in an increased solubility of NMM over MPIX.

3.2. Effects of PS5.ST1 and other DNA oligomers on the solubility and absorption of MPIX and NMM

3.2.1. MPIX with PS5.ST1 and control DNA oligomers

Fig. 6-2 (p173) shows the absorption spectra of MPIX alone and in the presence of 10 μM of PS5.ST1 (the catalytic DNA); BLD (a noncatalytic control DNA); and OXY4 (a noncatalytic but G-quadruplex-forming DNA sequence, see Chapter 3) in 40KBn Buffer (which contained no detergent). While BLD and OXY4 had no effect on the absorption of MPIX, PS5.ST1 significantly enhanced the intensity of the Soret band of MPIX, suggesting that PS5.ST1 has a strong and specific interaction with MPIX. To

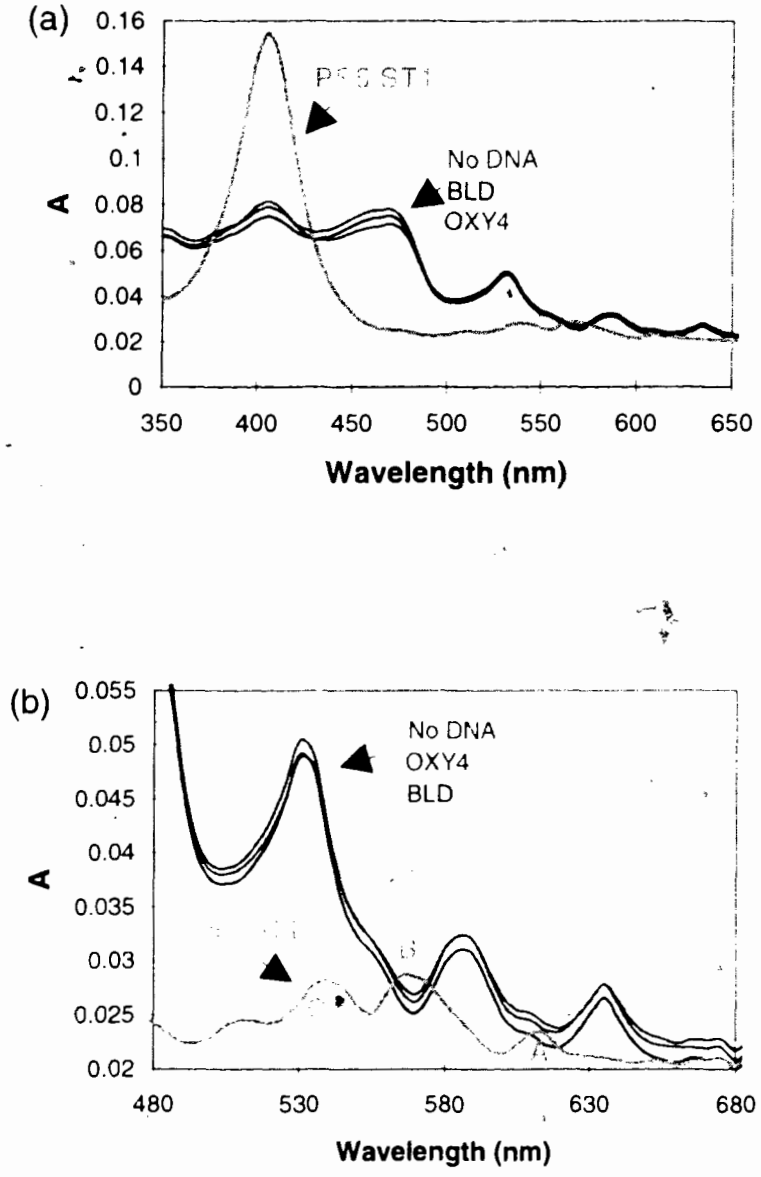

Fig. 6-2. Absorption spectra of MPIX as affected by the presence of different DNA oligomers. (a) The absorption spectra (in 40KBn) from 350 to 650 nm in the absence of DNA oligomers, in the presence of the control oligomers BLD and OXY4, and in the presence of the catalytic sequence PS5.ST1 (for the sequences of those oligomers, please refer to Fig. 4-1 of Chapter 4, p103). (b) The region from 480 to 680 nm. MPIX was at 1 μM, DNA concentration was at 10 μM.

demonstrate that MPIX bound to PS5.ST1, we rechecked the absorption spectra of all the samples following a 30-minute centrifugation at 13,000 rpm. Solutions containing either no DNA or the control DNA (BLD and OXY4) had no absorption after the spin. For contrast, ~ 70% absorption intensity (compared to that before the centrifugation) remained in the solution containing PS5.ST1. We also observed similar enhancement for the solubility and the absorption intensity of MPIX by the other catalytic sequences, such as PS19.ST1, PS2.M, TM.M2 (data not shown, for their sequences, see Chapter 5).

In addition to the intensity change in the Soret region, we also observed spectral shape changes, in both the Soret and the visible regions of MPIX-PS5.ST1, compared to the spectrum of MPIX itself. In the Soret region, the MPIX suspension (in the absence of detergent, whether alone or in the presence of the control DNA oligomers BLD and OXY4), had a broad peak between 370 to 500 nm (possibly due to the dimerization or aggregation), while the PS5.ST1-MPIX complex had a distinct absorption maximum at 399 nm. In the visible region, the MPIX absorption spectra in the presence of either no DNA or the control DNA sequences had no differences, whereas the MPIX-PS5.ST1 complex gave a completely different absorption pattern (an A-B-C pattern, named by this author). These data helped to support two conclusions we had made in previous chapters of this thesis, that the catalytic DNA sequences (such as PS5.ST1) have highly specific interactions with porphyrin substrates; and that not every guanine quadruplex structure is capable of catalyzing porphyrin metallation.

Interestingly, the MPIX-PS5.ST1spectrum also differed significantly from that of MPIX-Triton solution. In the Soret region, MPIX-Triton had a maximum absorption at

399 nm and a smaller shoulder peak at 375 nm, while PS5.ST1-MPIX solution had only one single peak at 399 nm, with no shoulders. In the visible absorption region, MPIX-Triton had peaks at ~510 nm (Peak IV), ~540 nm (Peak III), ~570 nm (Peak II), and ~630 nm (Peak I). The intensity of these peaks decreased in the following order: IV > III > II > I (see Fig. 6-1, p171). All of these peaks were significantly changed for PS5.ST1-MPIX, which a distinct A-B-C peak pattern was observed (Fig. 6-2, p173). These new peaks appeared either at new wavelength positions or with different intensities (for a direct comparison of the two patterns, see Fig. 6-6 in Section 3.3, p181).

Fig. 6-3 (p176) shows the absorption spectra of 1 μM MPIX titrated with various concentrations of PS5.M. It shows very convincingly that PS5.M had a profound influence on the absorption of MPIX in both the Soret and the visible regions. In the Soret region (Fig. 6-3a), the broad peak of MPIX formed a distinct peak at 399 nm, whose intensity increased with PS5.M concentration. This Soret band reached a complete saturation of intensity at a PS5.M concentration of 100 μM (also see Fig. 6-9b). In the visible (480 to 650 nm) region (Fig. 6-3b), the pattern of absorption peaks completely changed.

Interestingly, the changed absorption pattern of MPIX after binding to PS5.ST1 (or to PS5.M) was very similar to that of the NMM-PS5.ST1 complex (or of NMM alone). This similarity will be discussed in Section 3.3.

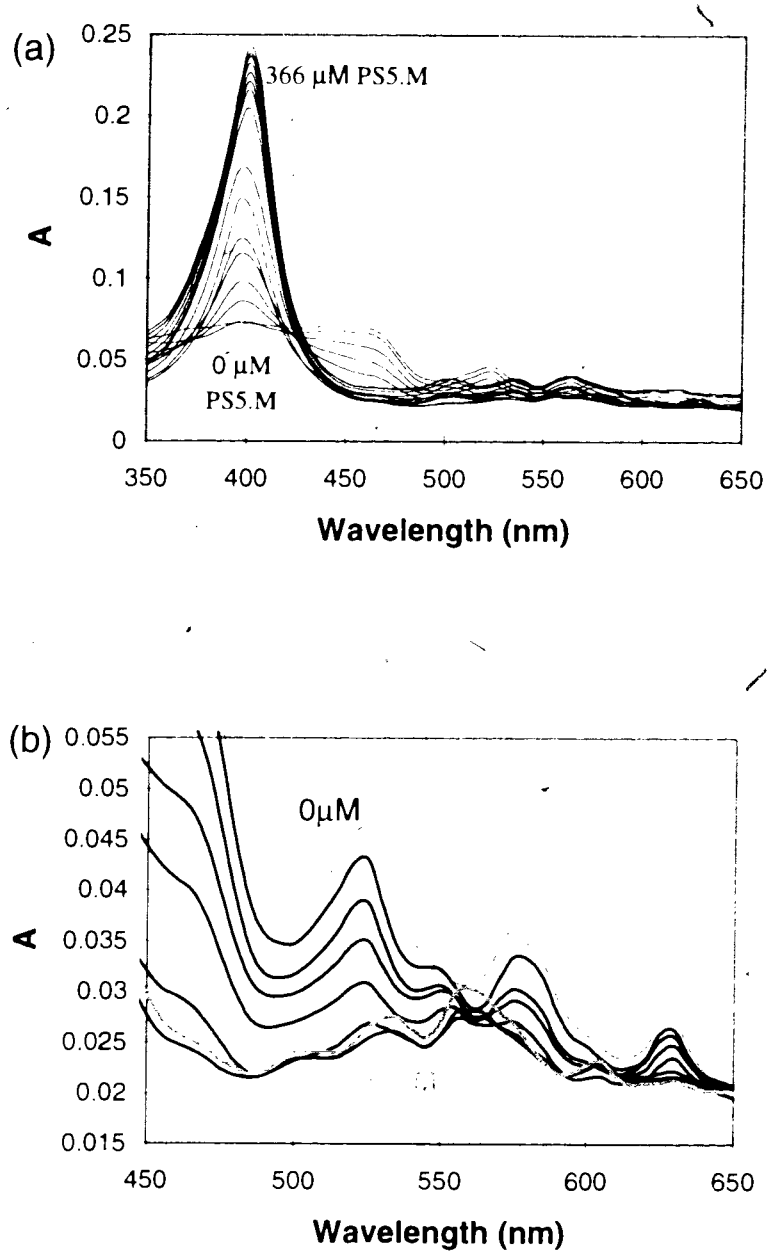

Fig. 6-3. MPIX absorption spectra titrated with increasing PS5.M concentrations. (a) The absorption spectra (350 to 650 nm) of MPIX (1 μM) in 40KBn buffer at PS5.M concentrations of 0, 1, 3, 5, 7, 9, 12, 15, 20, 30, 50, 75, 100, 150, 200, 250, 300, and 366 μM. (b) The 450 to 650 nm region. For simplicity, only the spectra at PS5.M concentrations of 0, 1, 3, 5, 7, 12, 20, and 50 μM are shown.

3.2.2. MPIX with PS5.ST1 plus Triton

Experiments were performed to assay the effect of Triton X-100 on the absorption spectra of PS5.ST1-MPIX complex, in which the absorption of MPIX-PS5.ST1 complex was titrated at various concentrations of Triton X-100 (Fig. 6-4, p178). With the introduction of Triton into PS5.ST1/MPIX solution, the absorption spectra changed to the pattern characteristic of Triton-MPIX spectra: A smaller shoulder peak appeared at the left hand side of the Soret maximum, and a I-II-III-IV peak pattern was seen in the visible region (see Section 3.1). These results indicated that Triton X-100 molecules compete with PS5.ST1 for MPIX binding, and was consistent with our earlier kinetic data that Triton had the negative effect on the catalytic rate of metallation (see Chapter 5). The high hydrophobicity of MPIX is probably responsible for the transfer of MPIX from the DNAzyme's active site (less hydrophobic) to the Triton micelles (more hydrophobic).

3.2.3. NMM-PS5.ST1 complex

Fig. 6-5 (p179) shows the spectra of NMM and the NMM-PS5.ST1 complex. PS5.ST1 had also affected the absorption of NMM. In the Soret region, the peak maximum shifted about 5 nm to the red, with the small intensity change. However, there was a noticeable change at the left hand side of the Soret band. A shoulder peak from the NMM spectrum disappeared in the PS5.ST1-NMM complex. In the visible region, we observed that PS5.ST1 enhanced the intensity of the maximal absorbance at 570 nm and 615 nm, but did not change the peak patterns from those of NMM alone. This stands in a marked contrast to the pattern change of MPIX absorption by PS5.ST1.

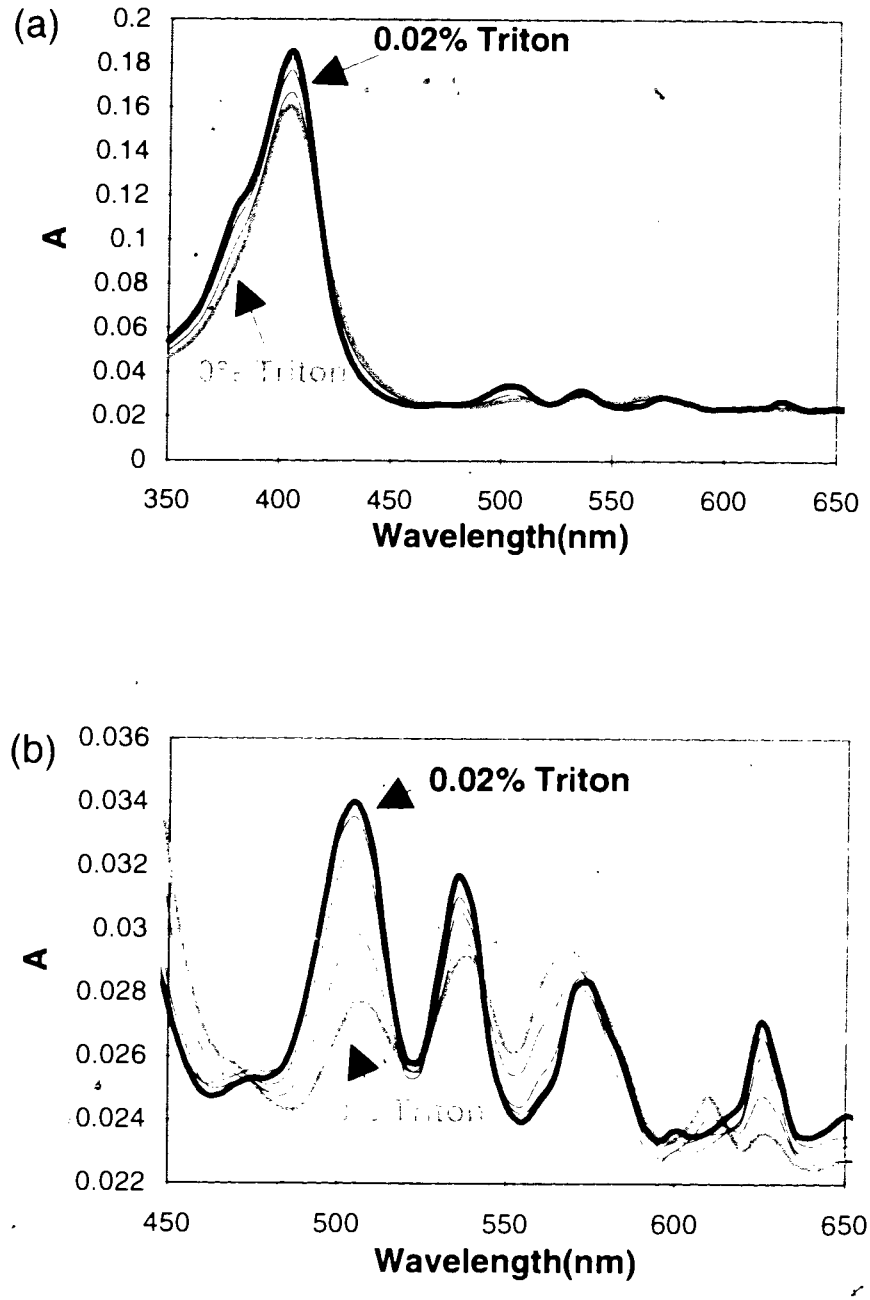

Fig. 6-4. Triton effects on the absorption spectra of MPIX-PS5.ST1 complex. (a) The absorption spectra of PS5.ST1-MPIX, from 350 to 650 nm, titrated at different Triton concentrations. PS5.ST1 is at 10 μM, MPIX at 1 μM, and Triton at 0, 0.005, 0.01, 0.015, and 0.020%. (b) The region from 450 to 650 nm.

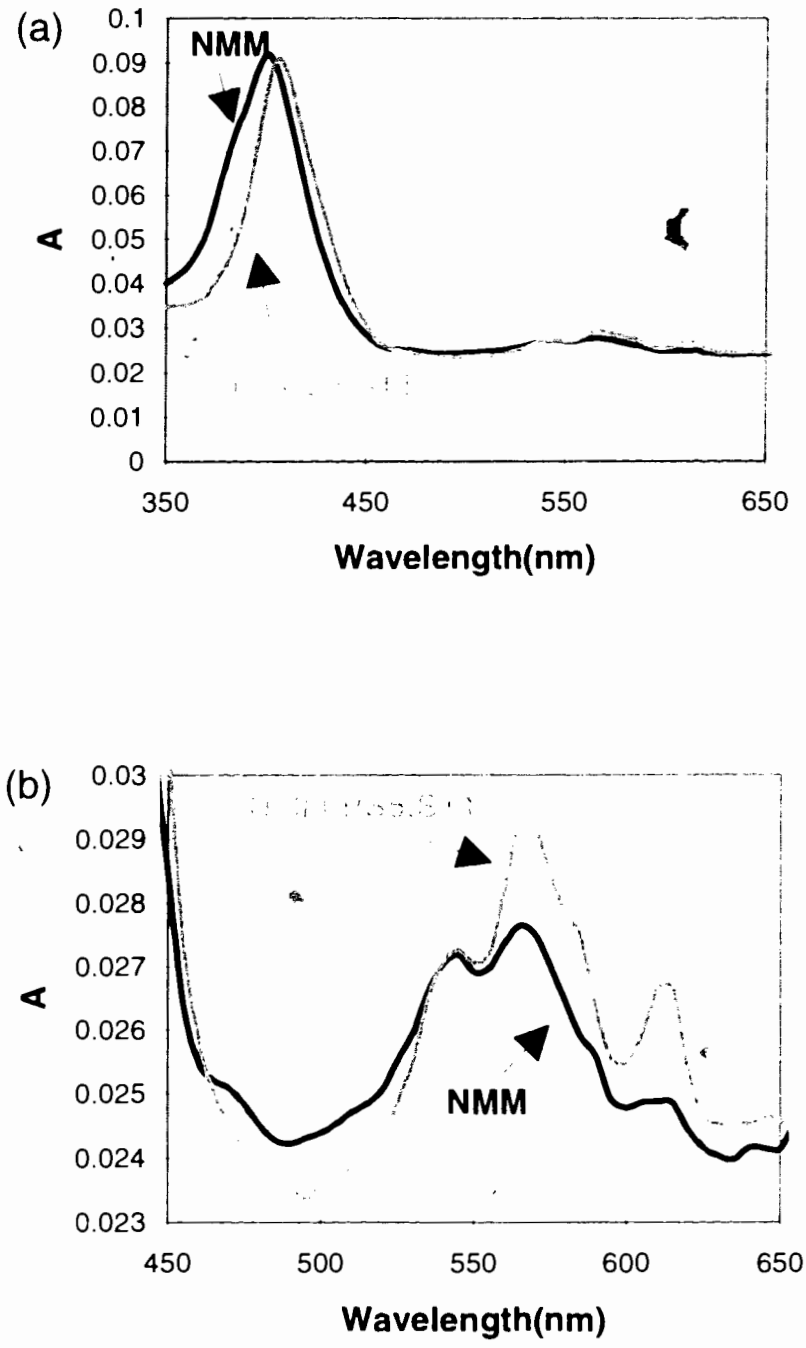

Fig. 6-5. Absorption spectra of NMM with and without PS5.ST1. (a) The spectra from 350 to 650 nm. (b) The 450 to 650 nm region. The scans were carried out in 40KBn buffer with 10 μM PS5.ST1 and 1 μM NMM.

Also unlike in the case of the MPIX-PS5.ST1 complex, Triton did not show any significant effect on the spectrum of the NMM-PS5.ST1 complex (tested up to 0.1% Triton X-100, data not shown), possibly due to the fact that PS5.ST1 interacts more strongly with NMM than with MPIX; and that NMM is less hydrophobic than MPIX because of its increased basicity and the protonation on one of its two imine-type nitrogens in neutral solutions.

3.3. MPIX-DNAzyme complex has an absorption spectrum closely resembling that of NMM-DNAzyme complex (or NMM alone)

Fig. 6-6 (p181) shows the spectra of the monomeric MPIX (in Triton solution); of the MPIX-PS5.ST1 complex; and of the NMM-PS5.ST1 complex. The spectrum of the MPIX-PS5.ST1 complex, while very different from that of either MPIX alone and the MPIX-Triton solution, closely resembles the spectrum of the NMM-PS5.ST1 complex in both the Soret and the visible regions. In the Soret region, the sepectra of both complexes were the same, with no shoulder peak observable. In the visible region, the two spectra were almost identical.

Why do the spectra of MPIX-PS5.ST1 and NMM-PS5.ST1 resemble each other? What are the molecular or structural bases for this spectral similarity? The answer we would like to give is that the DNAzyme has indeed done the job being demanded of: Bending the ground-state planar porphyrin structure and forcing the porphyrin substrate into its transition state. It is because the forced transition state of MPIX is structurally

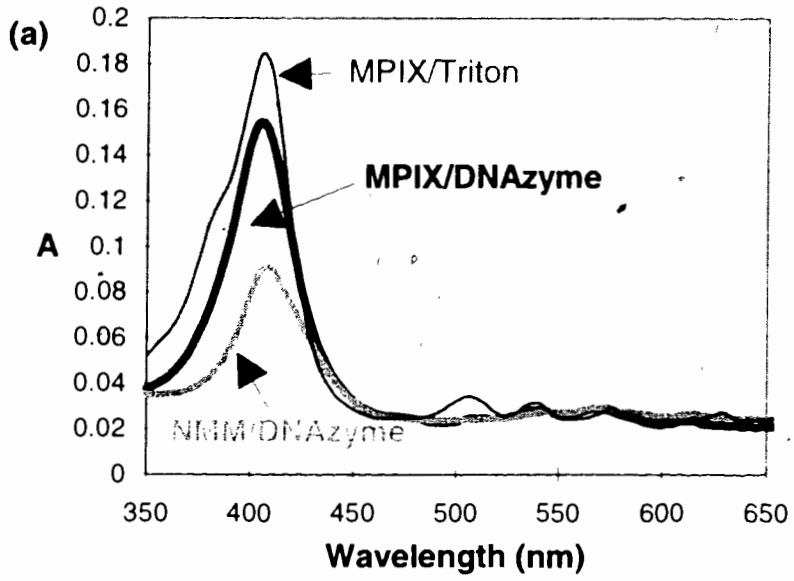

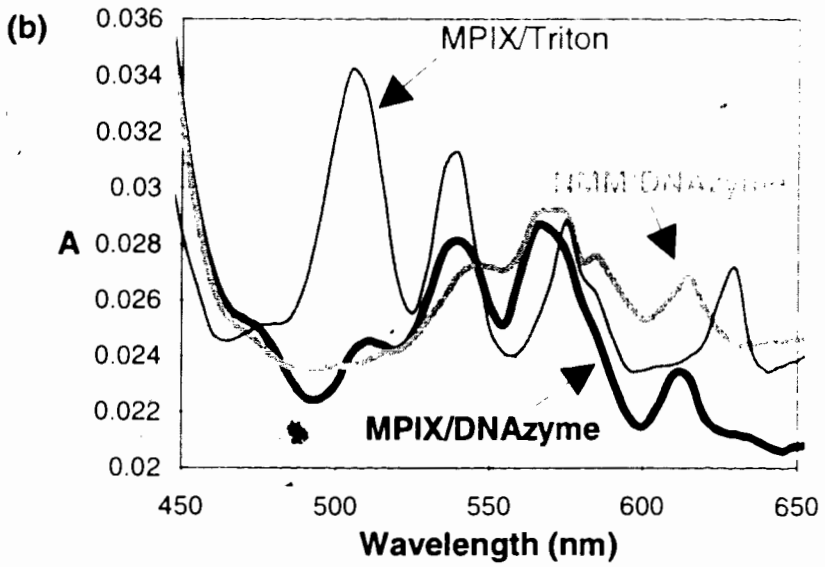

Fig. 6-6. Similarities between absorption spectra of DNAzyme-MPIX and DNAzyme-NMM. (a) The absorption spectra of PS5.ST1-MPIX, PS5.ST1-NMM, and MPIX-Triton, all taken in 40KBn buffer. (b) The region from 450 to 650 nm. NMM and MPIX were both at 1 μM, PS5.ST1 at 10 μM, Triton at 0.025%.

similar to NMM that the DNAzyme-MPIX complex has an absorption spectrum similar to that of NMM.

The above experimental observation is significant in two respects: Not only does the data confirm that NMM is indeed a good transition state analog for the metallation of MPIX, but most importantly, a direct evidence is observed of an enzyme acting on a ground-state substrate and forcing the substrate to change towards the transition state of a reaction. These notions are consistent with Pauling's conception that an enzyme catalyzes a chemical reaction by interacting more strongly with the transition state than with the ground state substrates so that the transition state is stabilized by an enzyme (Pauling, 1946).

One consequence of this proposed bending of MPIX by the DNAzyme is that the basicity of the deformed MPIX should increase significantly, a phenomenon paralleling that observed in the cases of N-alkylated porphyrins (with permanently bent porphinato cores) as opposed to their unsubstituted analogs (with planar porphinato cores) (Lavellee, 1987).

From the examination of the literature, we realized that the spectra of NMM, NMM-PS5.ST1 and MPIX-PS5.ST1 had the exact peak patterns of porphyrin compounds protonated at one of the two imine-type nitrogen atoms (the so-called monoprotonated porphyrin species, see below), while MPIX in the Triton solution had the precise peak pattern expected for non-protonated porphyrins. This pointed to the possibility that the DNAzyme may help increase the pKa value for the monoprotonated of MPIX (this pKa

value is termed pKm in this thesis). Therefore, we decided to study the pH dependences of the different spectral patterns.

3.4. pH effects on the absorption of NMM, MPIX, and MPIX-PS5.M complex

3.4.1. Porphyrin protonations and their pKa measurements

A free base porphyrin (PH_2) may accept two protons to its imine-type nitrogen atoms to form monocations (PH_3^+) and dications (PH_4^{2+}); they could also lose two pyrrole-type protons to produce the monoanion (PH^-) and dianions (P^{2-}), as indicated by the following scheme:

$$PH_4^{2+} \overset{pK_{a4}}{\rightleftharpoons} PH_3^+ \overset{pK_{a3}}{\rightleftharpoons} PH_2 \overset{pK_{a2}}{\rightleftharpoons} PH^- \overset{pK_{a1}}{\rightleftharpoons} P^{2-}$$

$$pK_m = pK_{a3} \qquad (pK_m : \text{pKa for monoprotonation})$$

Neutral porphyrins are very weak acids, being reflected by the fact that only very strong bases such as sodium alkoxides are able to remove the two pyrrole protons. Both the pKa_1 and pKa_2 were estimated to be at ~16 for etioporphyrin (Smith, 1975). Porphyrins are weak bases, relatively easy to dissolve in dilute inorganic acids. However, measuring the basicity of hydrophobic porphyrins (such as MPIX) in purely aqueous solution is not achievable because of the poor solubility of the hydrophobic porphyrins

and their tendency to aggregate. Instead, pH measurements were made in aqueous detergent solutions.

Spectroscopic titration was the main method used for the pKa measurements of porphyrin compounds. The absorption spectra of a typical porphyrin has been shown to have generalized peak patterns for its neutral (PH_2), monoprotonated (PH_3^+) and diprotonated (PH_4^{2+}) forms. As shown in Fig. 6-7, the PH_2 form has a I-II-III-IV (four peaks) pattern, the PH_3^+ form has an A-B-C (three peaks) pattern, while and PH_4^{2+} has an X-Y (two peaks) pattern. The existence of these distinct patterns of peaks for different protonated forms of porphyrins makes the pKa measurement by pH titration not only possible, but also accurate.

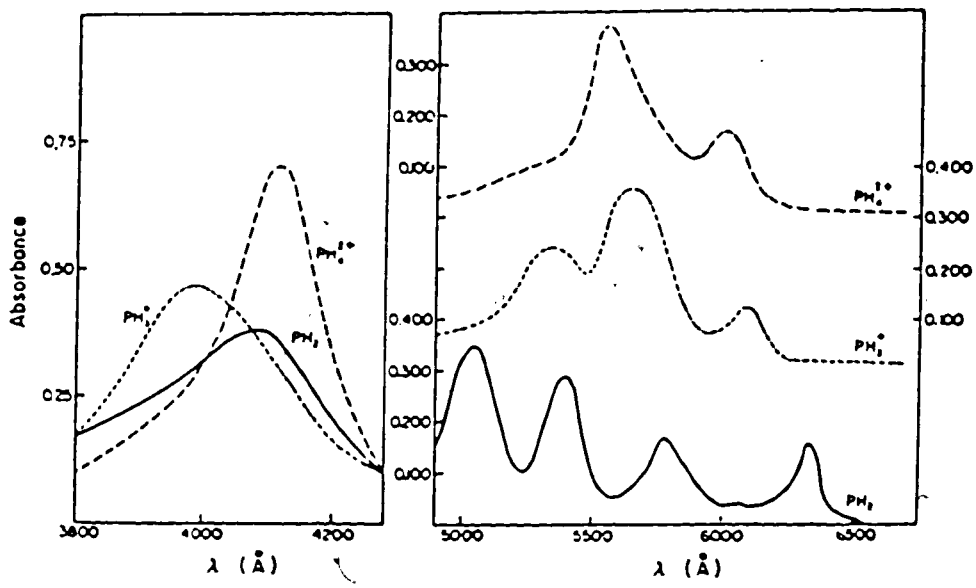

Fig. 6-7. Generalized absorption peak patterns for non-protonated, monoprotonated, and diprotonated forms of porphyrin compounds. (Reproduced from Dempsy et al., 1961)

For a hydrophobic porphyrin like MPIX, it has been reported that in nonionic and cationic detergents, only the neutral and the diprotonated species can be observed when the pH was changed (Dempsy et al., 1961). For instance, only one apparent pKa value of ~2 ($pKa_3 + pKa_4$) was observed for MPIX dimethyl ester. The failure to observe the monoprotonted porphyrin species, and the fact of one apparent pKa ($pKa_3 + pKa_4$) in cationic and nonionic detergents, were attributed to the inability of the micelles in stabilizing the positively charged monoprotonated porphyrin forms (Dempsy et al., 1961).

However, by using an anionic detergent such as SDS, all three species PH_4^{2+}, PH_3^+, PH_2 can be observed (Dempsy et al., 1961; Falk, 1964; Caughey et al., 1966). Thus, a pKa_3 of 5.8 and a pKa_4 of 2.1 were obtained for MPIX dimethyl ester (cited from Smith, 1978). The observation of a monoprotonated species in anionic detergent solution was attributed to the stabilization of monoprotonated porphyrin forms by the negatively charged micelles (Dempsy et al., 1961).

As discussed in Chapter 1, for N-alkylated porphyrins, the alkyl substitution distorts the porphyrin pyrrole ring permanently. The distortion of N-alkyl porphyrins exposes the lone-pair electrons on the tilting pyrrole ring to either metal ions (for porphyrin metallation) or protons (for protonation, Lavallee, 1987). Due to the distortion, the basicity of N-alkylated porphyrins increased significantly. The pKa values for monoprotonated forms of the distorted porphyrins ($pKm = pKa_2$ in the following scheme) were about several units (typically 3-5, depends on the structures) higher than that of their corresponding planar porphyrins, though the pKa values for diprotonated forms (pKa_3 in the following scheme) were not significantly affected (Lavallee, 1987).

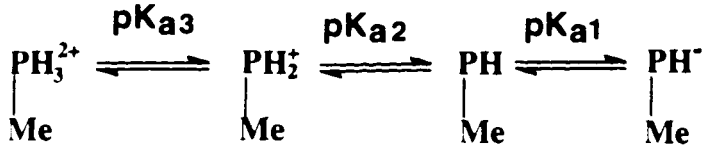

$$pK_m = pK_{a2}$$

3.4.2. pKm values of NMM and MPIX under our experimental conditions

We carried out pH titration experiments to determine the pKm values of both NMM and MPIX since no reported values have been found in literature.

In order to assay the effect of PS5.M on the pKm of MPIX, we need to obtain comparable sets of pKm values of MPIX in the absence and presence of PS5.M. However, experimentally we faced the following dilemma: without the detergents such as Triton, the pKm of MPIX could not be measured, owing to the solubility and dimerization of MPIX; whereas in the presence of detergent, the formation of the DNAzyme-MPIX complex was severely affected (see Section 3.2.2.). Given that the pKm for the MPIX/DNAzyme complex has to be measured in the absence of detergents, we had to find an indirect way to derive the pKm value for MPIX in the absence of any detergent.

Experimentally, we could determine the pKm values for the solutions of NMM itself (containing no detergents), NMM/SDS, NMM/Triton, MPIX/SDS, and MPIX/Triton (all at the same buffer conditions). From the complete set of pKm data of NMM, the effects of SDS or Triton on NMM's pKm could be determined. With the assumption that SDS and Triton have the similar effects on the pKm values of both NMM

and MPIX, we then can estimated the pKm value of MPIX in the non-detergent solution. Fig. 6-8 (p188) shows several of the normalized titration curves from our experiments, and Table 6-1 summarizes the measured pKm values of NMM and MPIX under various solution conditions.

Table 6-1. pKm values for MPIX and NMM in various solutions

Porphyrin	In 0.1% Triton	No detergent	In 1% SDS	PS5.M
MPIX	1.8[1]	N/A[2]	5.8	6.9
NMM	8.8	10.9	12.4	>10

1) for pKa_3 and pKa_4; 2) estimated at 3.9-4.3 using the set of NMM data as reference.

Both SDS and Triton affected the pKm value of NMM. In 0.1% Triton solution, the pKm was lowered by ~2 units, while 1% SDS solution shifted the value upward by at least 1.5 unit (NMM absorption in the SDS solution had not reached a complete saturation at pH 13). The pKm changes in detergent solutions may be due to the different abilities of these detergents in solvating and stabilizing the protonated NMM. SDS gave the highest pKm value since SDS micelles can provide a negatively charged shield to stabilize the positive charge on protonated NMM. Triton micelles, on the other hand, are not capable of providing this charge-charge stabilization. In addition, Triton molecules might affect the ability of water molecules in solvating the positively charged NMM. In other words, in Triton solutions, protonation equilibrium was driven towards the side of the nonprotonated NMM, and substantial protonation could only occur when the pH of

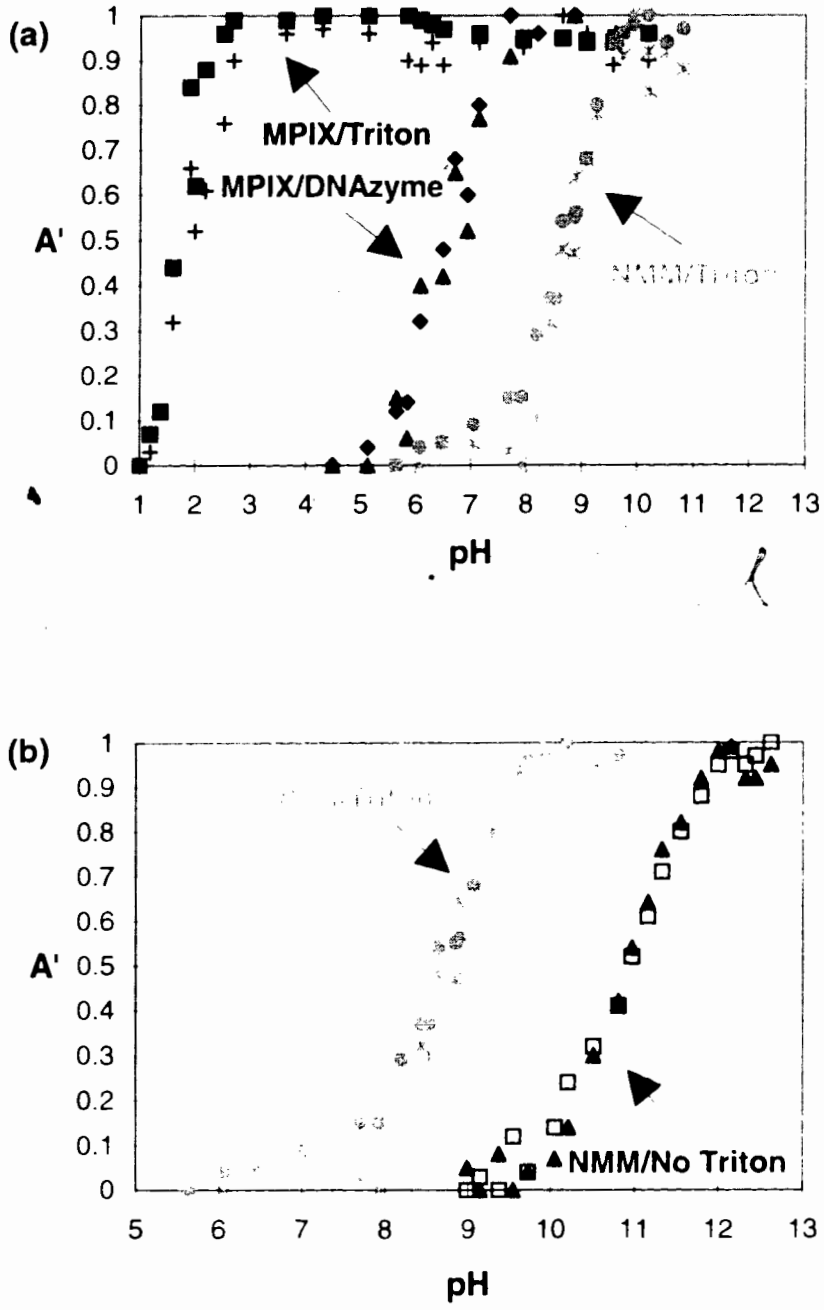

Fig. 6-8. The normalized pH titration curves for MPIX/Triton, MPIX/PS5.M, NMM/Triton, NMM/No Triton. A': normalized absorption readings, with 1 as the saturated absorption readings at the higher pH end and 0 as the saturated absorption readings at the lower pH end: MPIX in Triton at 500 (+) and 397nm (■); MPIX-DNAzyme at 500 (◆) and 604nm (▲); NMM in Triton at 397 ( ) and 560nm ( ); NMM without detergent at 397 (□) and 560nm (▲). MPIX was at 1 μM, NMM at 3 μM, Triton X-100 at 0.1%, PS5.M at 20 μM (where appliable). Other conditions are given in Material and methods.

the solution was decreased. Therefore, the pKm of NMM was smaller in the presence of Triton.

Based on the observation that the pKm of NMM, in the absence of detergents, was located between that of NMM/Triton and NMM/SDS, we think that it is reasonable that the pKm of MPIX in the absence of detergents might also lie between those of the pKm values of MPIX in the two detergent solutions. In support of this assumption was our finding that for NMM, there were 3.6 pH units separating the pKm value of the Triton solution from that of the SDS solution, whereas for MPIX this separation was an almost equal 4 units. Given this, we deduce that the true pKm value of MPIX (e.g. in aqueous solutions in the absence of detergents) lies between 3.9-4.3.

3.4.3. PS5.M increases the basicity of MPIX by 2 to 3 units

The DNAzyme-NMM complex had a pKm of 6.9 (Table 6-1). With the above assumption for the estimation of the true pKm value of MPIX (between 3.9-4.3), the porphyrin-metallating DNA enzyme seemed to increase the basicity of MPIX 2.6 to 3 units. This basicity increase is consistent with our earlier suggestion that the DNAzyme bends the structure of the planar MPIX. It is not a surprise to us that the DNA enzyme uses this bending strategy to catalyze the porphyrin metallation. First of all, we showed that the selection strategy applied by us succeeded in deriving DNA sequences which could recognize the subtle structural differences between the bent NMM and the planar MPIX (Chapter 2). Secondly, the guanine-quadruplex model proposed by us also pointed to the possibility that unique guanine quartets, containing buckled guanines in the

structure, could deform MPIX to allow a maximal π-π interaction between MPIX and guanine bases.

Nevertheless, we do not have direct evidence to allow us to either confirm or rule out simple charge-charge contributions for the observed increase of the pKm of MPIX by the DNAzyme. This will be an interesting point for future investigation.

One interesting point raised by the pH titration studies is that the pKm of MPIX bound to DNAzyme is still a few units lower than that of NMM. This may suggest that PS5.M is still not the best possible catalyst for this reaction. It would be interesting to explore whether a better DNA catalyst could be derived, that could increase the basicity of MPIX further towards that of NMM, and therefore show much larger rate enhancements for porphyrin metallation.

3.5. Catalytic DNAs showed much stronger binding to NMM than MPIX

We sought to measure dissociation constants (K_d's) of the DNAzyme-NMM and DNAzyme-MPIX complexes by spectroscopic titration methods. Fig. 6-9 (p191) shows the changes of absorbance ($A-A_0$) of both NMM (Fig. 6-9a) and MPIX (Fig. 6-9b) as functions of the concentration of the appropriate DNA sequences, at selected wavelengths.

For the catalytic DNA sequences PS5.M and TM.M2, $A-A_0$ vs [DNA] gave a plot characteristic of very tight binding mode (van Holde, 1985). The data showed that there were two contrasting states of NMM's absorbance change with increasing concentrations of the DNAzymes (at a fixed NMM concentration of 1 μM). The first was a pre-

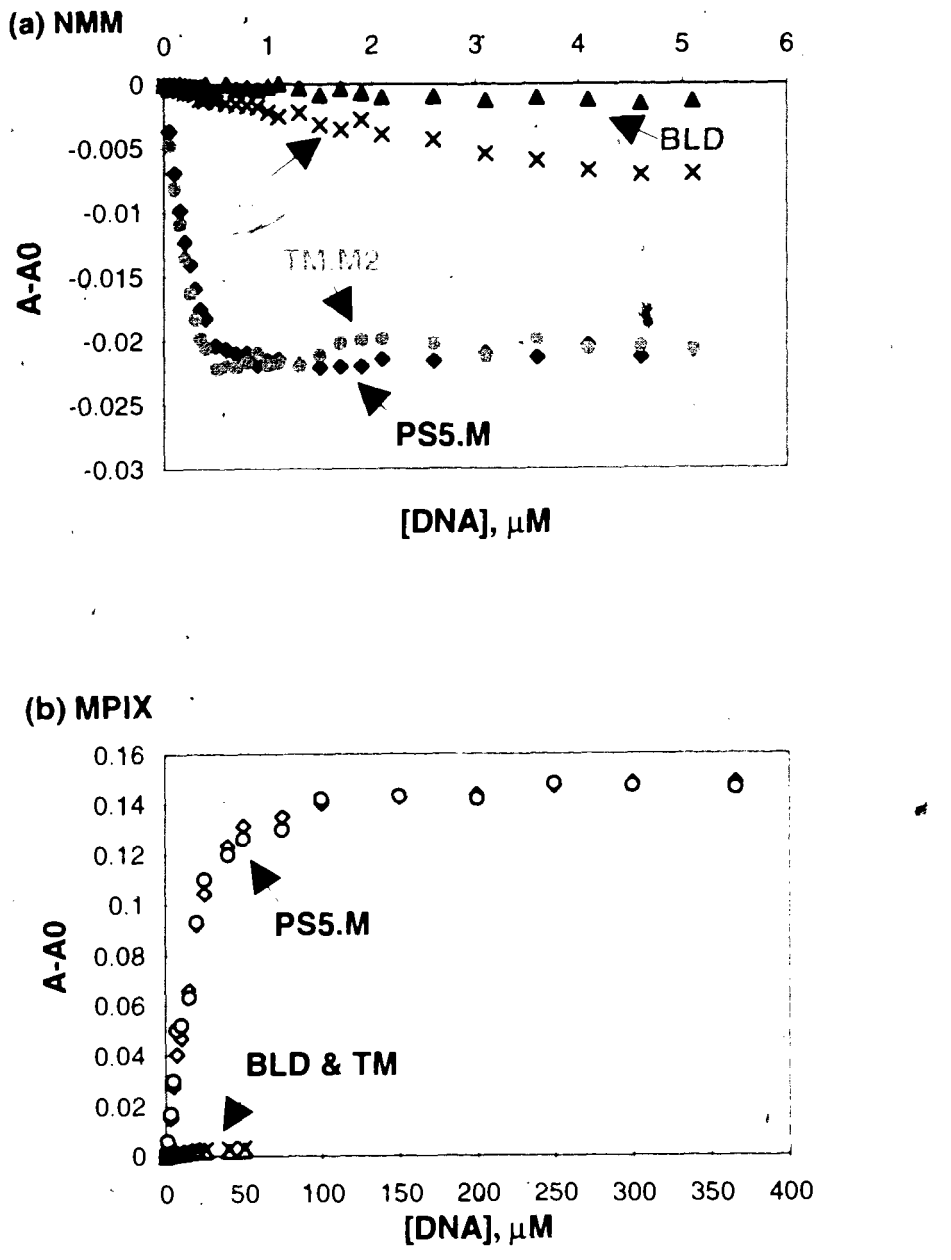

Fig. 6-9. Absorbance change ($A-A_0$) of NMM and MPIX versus the concentration of various DNA oligomers. (a) $A-A_0$ (at 380 nm) of NMM (at 1 μM) vs the concentration of PS5.M (◆), TM.M2 (●), BLD (▲), TM (×). (b) $A-A_0$ (at 399 nm) of MPIX (at 1 μM) vs. the concentration of PS5.M (○ & □), BLD (×) and TM (Δ).

saturation state, where $A-A_0$ varied linearly with the concentration of either DNAzyme (PS5.M or TM.M2); and, the second, a state of saturation, in which the increase of the DNAzyme concentration had no further effect on the absorbance of NMM. In contrast, noncatalytic DNA sequences such as TM (thrombin aptamer) and BLD (a purine-rich sequence, see Table 4-1, p103) either showed no binding to NMM (in the case of BLD) or weak binding (in the case of TM).

Interestingly, $A-A_0$ vs [DNAzyme] reached the saturation at [NMM]/[DNAzyme] = 2:1. A similar conclusion could be drawn from a fluorescence study of the NMM-PS5.M complex (data not shown). These results tentatively indicated that there might be two porphyrin molecules bound per DNAzyme. It would not be a big surprise to us if this is indeed the case. The guanine quadruplex structure we proposed could certainly have the ability to bind two porphyrin substrates via an intercalation mode, because the structure has three layers of guanine quartets. However, more detailed work needs to be carried out to confirm this 2:1 mode of binding. First of all, the quantitation of the concentration of the DNA oligomers needs to be assessed meticulously (we used a standard of 1 OD = 40 μg of single-stranded DNA for the DNA concentration calculation for every DNA oligomer). The actual amount of μg DNA per OD most likely varies between 30 and 40. This means that the actual molar DNA concentration used would be higher than that calculated. Secondly, it is not likely that every molecule of PS5.M or TM.M2 will fold to form the active structure for NMM-binding. This could lead to significant decreases of the actual DNA concentrations available for porphyrin binding.

Therefore, we need to precisely quantitate the actual DNA concentration for NMM-binding.

The plot of ($A-A_0$) of MPIX versus DNA concentration is shown in Fig. 6-9b (p191). The control oligomers BLD and TM showed no binding to MPIX, while PS5.M showed its affinity for MPIX. However, the shape of the binding curve was very different from that of PS5.M to NMM. The data indicated that MPIX bound to PS5.M much more weakly than to NMM. To have some idea on the affinity difference of PS5.M for NMM and MPIX, we fit the data to the following equation developed by Wang et al (1997):

$$[DNA]_0 = K_d(A - A_0) / (A_\infty - A) + [P]_0(A - A_0) / (A_\infty - A_0)$$

where $[DNA]_0$ and $[P]_0$ are the initial concentrations of PS5.M and porphyrins (NMM or MPIX), and A, A_∞, A_0 are the absorbance readings of the sample, totally bound NMM (or MPIX), and totally free NMM (or MPIX). From the curve-fitting, we obtained a K_d of 5.2 nM ± 2.0 nM for the NMM-PS5.M complex, and 6.9 μM ± 0.2 μM for the MPIX-PS5.M complex. These data suggested that the binding affinity of PS5.M for MPIX and NMM differed by over a thousand-fold. However, I should point out that these K_d values are more meaningful qualitatively rather than quantitatively, because the above equation is derived for the 1:1 binding mode. Nevertheless, the large difference between these two K_d's at least qualitatively suggested that PS5.M had a much higher affinity for NMM than for MPIX.

4. Summary

In this chapter, I have described that the MPIX-DNAzyme complex exhibits an absorption spectrum closely resembling that of the NMM-DNAzyme complex, while being significantly different from that of monomeric MPIX itself. We further conclude that this spectral similarity is the result of a pKm increase of MPIX by the DNAzyme, by a factor of 2 to 3 units. These data are certainly supportive of our proposal that the DNAzyme works by bending the planar MPIX towards its transition state for metallation, in which MPIX has a deformed porphinato core similar to that of NMM. Also, the absorption titration data for NMM and MPIX by PS5.M showed that PS5.M bound to NMM much more strongly than to MPIX, with a tentative 2:1 binding mode (two porphyrin mececules per DNAzyme).

References:

Abelson, J. (1990). Directed evolution of nucleic acids by independent replication and selection. *Science* **249**, 448-449.

Bai, K. S., & Martell, A. E. (1969). The interaction of 2-amino-2-(hydroxymethyl)-1,3-propanediol with copper(II) and nickel(II) ions. *J. Inorg. nucl. Chem.* **31**, 1697-1707.

Bain-Ackerman, M. J., & Lavallee, D. K. (1979). Kinetics of metal-ion complexation with N-methyltetraphenylporphyrin. Evidence concerning a general mechanism of porphyrin metallation. *Inorg. Chem.* **18**, 3358-3364.

Balikugeri, A. (1989). Acid-base properties of 2-morpholinoethanesulfonic acid (MES), complexation reaction of Cu(II)-MES, and interaction of hydrous manganese oxide surface with Cu(II) in MES buffer. *Chimia* **43**, 13-17.

Bartel, D. P., & Szostak, J. W. (1993). Isolation of new ribozymes from a large pool of random sequences. *Science* **261**, 1411-1418.

Beaudry, A. A., & Joyce, G. F. (1992). Directed evolution of an RNA enzyme. *Science* **257**, 635-641.

Benner, S. A., Ellington, A. D., & Traver, A. (1989). Modern metabolism as a palimpest of the RNA world. *Proc. Natl. Acad. Sci. USA* **86**, 7054-7058.

Blackwell, T. K., Kretzner, L., Blackwood, E. M., Eisenman, R. N., & Weintraub (1990). Sequence-specific DNA binding by the c-Mye protein. *Science* **250**, 1149-1151.

Blackwell, T. K., & Weintraub, H. (1990). Differences and similarities in DNA-binding preferences of MyoD and E2A protein complexes revealed by binding site selection. *Science* **250**, 1104-1110.

Bock, L. C., Griffin, L. C., Latham, J. A., Vermass, E. H., & Toole, J. J. (1992). Selection of single-stranded DNA molecules that bind and inhibit human thrombin. *Nature* **355**, 564-566.

Breaker, R. R. (1996). Are engineered proteins getting competition from RNA? *Curr. Opin. Biotech.* **7**, 442-448.

Breaker, R.R. (1997). *In vitro* selection of catalytic polynucleotides. *Chem. Rev.* **97**, 371-390.

Breaker, R. R., & Joyce, G. F. (1994). A DNA enzyme that cleaves RNA. *Chem. Biol.* **1**, 223-229.

Breaker, R. R., & Joyce, G. F. (1995). A DNA enzyme with Mg^{2+}-dependent RNA phosphoesterase activity. *Chem. Biol.* **2**, 655-660.

Brown, S. B., & Hatzikonstantinou, H. (1978). The dimerization of ferrihaems. *Biochim. Biophys. Acta.* **539**, 338-363.

Brown, S. B., Hatzikonstatinou, H., & Herries, D. (1980). The structure of porphyrins and haems in aqueous solution. *Int. J. Biochem.* **12**, 701-707.

Brown, S. B., & Shillcock, M. (1976). Equilibrium and kinetic studies of the aggregation of porphyrins in aqueous solution. *Biochem. J.* **153**, 279-285.

Burgess, J. Metal Ions in Solution (Ellis Horwood Ltd.: Chichester, 1978), p259-289.

Cadwell, R. G., & Joyce, G. F. (1992). Randomization of genes by PCR mutagenesis. *PCR methods appl.* **2**, 28-33.

Carmi, N., Schultz, L. A., & Breaker, R. R. (1996). *In vitro* selection of self-cleaving DNAs. *Chem. Biol.* **3**, 1039-1046.

Carvlin, F. J., & Fiel, R. J. (1983). Intercalative and nonintercalative binding of large cationic porphyrin ligands to calf thymus DNA. *Nucleic Acids Res.* **11**, 6121-6139.

Carvlin, F. J., Mark, R. J., Fiel, R. J., & Howard, J. C. (1983). Intercalative and nonintercalative binding of large cationic porphyrin ligands to polynucleotides. *Nucleic Acids Res.* **11**, 6141-6154.

Cate, J. H., Gooding, A. R., Podell, E., Zhou, K., Golden, B. L., Kundrot, C. E., Cech, T. R., & Doudna, J. A. (1996). Crystal structure of a group I ribozyme domain: principles of RNA packing. *Science* **273**, 1678-1685.

Caughey, W. S., Fujimoto, W. Y., & Johnson, B. P. (1966). Substituted deuteroporphyrins. II. Substituent effects on electronic spectra, nitrogen basicities, and ligand affinity. *Biochemistry*, **5**, 3830-3843.

Chaires, J. B. (1990). Biophysical chemistry of the daunomycin-DNA interaction. *Biophys. Chem.* **35**, 191-202.

Chapman, K., & Szostak, J. W. (1995). Isolation of a ribozyme with 5'-5' ligase activity. *Chem. Biol.* **2**, 325-333.

Cochran, A. G., & Schultz, P. G. (1990). Antibody-catalysed porphyrin metallation. *Science* **249**, 781-783.

Conn, M. M., Prudent, J. R., & Schultz, P. G. (1996). Porphyrin metalation catalyzed by a small RNA molecule. *J. Am. Chem. Soc.* **118**, 7012-7013.

Connell, G. J., Illangsekare, M., & Yarus, M. (1993). Three small ribooligonucleotides with specific arginine sites. *Biochemistry* **32**, 5497-5502.

Crick, F. H. C. (1968). The origin of the genetic code. *J. Molec. Biol.* **38**, 367-379.

Cuenoud, B., & Szostak, J. W. (1995). A DNA metalloenzyme with ligase activity. *Nature* **375**, 611-614.

Dailey, A. D. (1988). Conversion of coproporphyrinogen to protoheme in higher eukaryotes and bacteria: terminal three three enzymes. In Biosynthesis of Heme and Chlorophylls (Dailey, A.D., ed., McGraw-Hill: New York, 1988).

Dailey, A. D., & Fleming, J. E. (1983). Bovine ferrochelatase. *J. Biol. Chem.* **258**, 11453-11459.

Dailey, H. A.; & Smith, A. (1984). Differential interaction of porphyrins used in photoradiation therapy with ferrochelatase. *Biochem. J.* **223**, 441-445.

De Matteis, F., Gibbs, A. H., & Tephly, T. R. (1980). Inhibition of protohaem ferro-lyase in experimental porphyria. *Biochem. J.* **188**, 145-152.

Dempsey, B., Lowe, M. B., & Phillips, J. N. (1961). The physico-chemical behaviour of porphyrins solubilized in aqueous detergent solutions. In Haematin Enzymes (Falk., J. E., Lemberg, R., & Morton, R. K., Eds., Pergamon, London, 1961).

Dinello, R. K., & Chang, C. K. (1978). Isolation and modification of natural porphyrins. in The Porphyrins, Vol. I. (Dolphin, D., ed., Academic Press: New York, pp293, 1978).

Eichhorn, G. L., & Shin, Y. A. (1968). Interaction of metal ions with polynucleotides and related compounds. XII. The relative effects of various metal ions on DNA helicity. *J. Am. Chem. Soc.* **90**, 7323-7328.

Ekland, E. H., & Bartel, D. P. (1996). RNA-catalysed RNA polymerization using nucleoside triphosphates. *Nature* **382**, 373-376.

Ekland, E. H., Szostak, J. W., & Bartel, D. P. (1995). Structurally complex and highly active RNA ligases derived from random RNA sequences. *Science* **269**, 364-370.

Ellington, A. D., & Szostak, J. W. (1990). *In vitro* selection of RNA molecules that bind specific ligands. *Nature* **346**, 818-822.

Ellington, A. D., & Szostak, J. W. (1992). Selection *in vitro* of single-stranded DNA molecules that fold into specific ligand-binding structures. *Nature* **355**, 850-852.

Falk, J. E. (1964). Porphyrins and metalloporphyrins. (Elsevier Publ. Co.: New York, 1964).

Famulok, M., & Szostak, J. W. (1992). Stereospecific recognition of tryptophan agrose by *in vitro* selected RNA. *J. Am. Chem. Soc.* **114**, 3990-3991.

Faulhammer, D., & Famulok, M. (1996). The Ca^{2+} ion as a cofactor for a novel RNA-cleaving deoxyribozyme. *Angew. Chem. Int. Ed. Engl.* **35**, 2837-2841.

Fiel, R. J. (1989). Porphyrin-nucleic acid interactions: a review. *J. Biomol. Struc. & Dyn.* **6**, 1259-1283.

Fleischer, E. B. (1970). The structure of porphyrins and metalloporphyrins. *Acc. Chem. Res.* 3, 105-112.

Funahashi, S., Yamaguchi, Y., & Tanaka, M. (1984). Kinetics and mechanism of copper(II), zinc(II), and cadmium(II) incorporation into 5,10,15,20-tetraphenylporphine and N-methyl-5,10,15,20-tetraphenylporphine in N,N-dimethylformamide. *Bull. Chem. Soc. Jpn.* **57**, 204-208.

Geiger, A., Burgstaller, P., von der Eltz, H., Roeder, A., & Famulok, M. (1996). RNA aptamers that bind L-arginine with sub-micromolar dissociation constants and high enantioselectivity. *Nucleic Acids Res.* **24**, 1029-1036.

Geyer, C. R., & Sen, D. (1997a). Evidence for the metal cofactor-independence of a RNA phosphodiester cleaving DNAzyme. *Chem. Biol.* (submitted).

Geyer, C. R., & Sen, D. (1997b). In preparation.

Gibbs, E. J., Maurer, M. C., Zhang, J. H., Reiff, W. M., Hill, D. T., Maliska-Blaskiewicz, M., McKinnie, R. E., Liu, H. Q., & Pasternack, R.F. (1988). Interactions of porphyrins with purified DNA and more highly organized structures. *J. Inorg. Biochem.* **32**, 39-65.

Gilbert, W. (1986). The RNA world. *Nature* **319**, 618.

Gold, L., Polisky, B., Uhlenbeck, O., & Yarus, M. (1995). Diversity of oligonucleotide functions. *Annu. Rev. Biochem.* **64**, 763-797.

Goldberg, D. E., & Thomas, K. M. (1976). Crystal and molecular structure of an N-substituted porphyrin, chloro (2,3,7,8,12,13,17,18-octaethyl-N-ethylacetatoporphine) cobalt (II). *J. Am. Chem. Soc.* **98**, 913-919.

Goldin, B. R., & Little, H. N. (1969). Metalloporphyrin chelatase from barley. *Biochim. Biophys. Acta* **171**, 321-332.

Green, R., Ellington, A. D., & Szostak, J. W. (1990). *In vitro* genetic analysis of the tetrahymena self-splicing intron. *Nature* **347**, 406-408.

Guerrier-Takada, C., Gardiner, K., Marsh, T., Pace, N., & Altman, S. (1983). The RNA moiety of ribonuclease P is the catalytic subunit of the enzyme. *Cell* **35**, 849-857.

Gunter, E. W., Turner, W. E., & Huff, D. L. (1989). Investigation of protoporphyrin IX standard materials used in acid-extraction methods, and a proposed correction for the millimolar absorptivity of protoporphyrin IX. *Clinical Chem.* **35**, 1601-1608.

Guo, Q., Lu, M., Marky, L. A., & Kallenbach, N. R. (1992). Interaction of the dye ethidium bromide with DNA containing guanine repeats. *Biochemistry* **31**, 2451-2455.

Hall, J. L., Simmons, R. B., Morita, E., Joseph, E., & Gavas, J. F. (1971). Polarographic study of complexes of copper(II) ion with mono-, di-, and triisopropanolamine, with three amines formed by hydroxy substitution of 2-methyl-2-aminopropane, and with ethanolpropanolamine. *Analytic Chemistry*, **43(6)**, 634-6.

Hambright, P., & Chock, P. B. (1974). Metal-porphyrin interactions. III. A dissociative-interchange mechanism for metal ion incorporation into porphyrin molecules. *J. Am. Chem. Soc.* **96**, 3123-3131.

Harada, K., & Frankel, A. D. (1995). Identification of two novel arginine binding DNAs. *EMBO* **14**, 5798-5811.

Henderson, E. R., Hardin, C. C., Wolk, S. K., Tinoco, I., Jr., & Blackburn, E. H. (1987). Telomeric DNA oligonucleotides form novel intramolecular structures containing guanine-guanine base pairs. *Cell* **51**, 899-908.

Horton, R. M., Hunt, H. D., Ho, S. N., Pullen, J. K., & Pease, L. R. (1989). Engineering hybrid genes without the use of restriction enzymes: gene splicing by overlap extension. *Gene* **77**, 61-68.

Huizenga, D. E., & Szostak, J. W. (1995). A DNA aptamer that binds adenosine and ATP. *Biochemistry* **34**, 656-665.

Illangasekare, M., Sanchez, G., Nickles, T., & Yarus, M. (1995). Aminoacyl-RNA synthesis catalyzed by an RNA. *Science* **267**, 643-647.

Jelinek, D., Lynnot, C. K., Rifkin, D. B., & Janjic, C. (1993). High-affinity RNA ligands to basic filbroblast growth factor inhibit receptor binding. *Proc. Natl. Acad. Sci. USA* **90**, 11227-11231.

Jelinek, D., Green, L. S., Bell, C., & Janjic, C. (1994). Inhibition of receptor binding by high-affinity RNA ligands to vascular endothelial growth factor. *Biochemistry* **33**, 10450-10456.

Jencks, W.P. in Current Aspects of Biochemical Energetics, Kaplan, N. O., & Kennedy E. P., eds, Academic Press, New York, 1966.

Jenison, R. D., Gill, S. C., Pardi, A., & Polisky, B. (1994). High-resolution molecular discrimination by RNA. *Science* **263**, 1425-1479.

Joyce, G. F. (1989). RNA evolution and the origins of life. *Nature* **338**, 217-224.

Joyce, G. F. (1994). *In vitro* evolution of nucleic acids. *Current Opin. in Struc. Biol.* **4**, 331-336.

Joyce, G. F. (1996). Bulding the RNA world. *Current Biology* **6**, 965-967.

Kang, C. H., Zhang, X., Ratliff, R., Moyzis, R., & Rich, A. (1992). Crystal structure of four-stranded *Oxytricha* telomeric DNA. *Nature* **356**, 126-131.

Karns, G. A., Gallagher, W. A., & Elloit, W. B. (1979). Dimerization constants of water-soluble porphyrins in aqueous alkali. *Bioorganic Chem.* **8**, 69-81.

Kassner, R. J., & Walchak, H. (1973). Heme formation from Fe(II) and porphyrin in the absence of ferrochelatase activity. *Biochim. Biophyys. Acta* **304**, 294-303.

Kim, S. H., Quigley, G. J., Suddath, F. L., McPherson, A., Kim, J. J., Weinzierl, J., & Rich, A. (1973). Three-dimensional structure of yeast phenylalanine transfer RNA: folding of the polynucleotide chain. *Science* **179**, 285-288.

Kinzler, K. W., & Vogelstein, B. (1990). The *GLI* gene encodes a nuclear protein which binds specific sequences in the human genome. *Mol. Cell. Biol.* **10**, 634-642.

Kraut, J. (1988). How do enzymes work? *Science* **242**, 533-540.

Krueger, R. C., Melnick, J., & Klein, J. R. (1956). Formation of heme by broken-cell preparations of duck erythrocytes. *Arch. Biochem. Biophys.* **64**, 302-310.

Kruger, K., Grabowski, P. J., Zaug, A. J., Sands, J., Gottschling, D. E., & Cech, T. R. (1982). Self-splicing RNA: autoexcision and autocyclization of the ribosomal RNA intervening sequence of tetrahymena. *Cell* **31**, 147-157.

Labbe, R. F., & Hubbard, N. (1960). Preparation and properties of the iron-protoporphyrin chelating enzyme. *Biochim. Biophys. Acta* **41**, 185-191.

Lauhon, C. T., & Szostak, J. W. (1995). RNA aptamers that bind flavin and nicotinamide redox cofactors. *J. Am. Chem. Soc.* **117**, 1246-1257.

Lavallee, D. K. (1982). Crystal and molecular structure of a free-base N-methylporphyrin: N-methyl-5,10,15,20-tetrakis(p-bromophenyl)porphyrin. *J. Am. Chem. Soc.* **104**, 4707-4708.

Lavallee, D. K. (1985). Kinetics and mechanisms of metalloporphyrin reactions. *Coord. Chem. Rev.* **61**, 55-96.

Lavallee, D. K. The Chemistry and Biochemistry of N-Substituted Porphyrins. (VCH Publ., New York, 1987).

Lavallee, D. K. (1988). Porphyrin metalation reactions in biochemistry. *Mol. Struct. Energ.* **9**, 279-314.

Lavallee, D. K., & Onady, G. M. (1981). Origin of the hydrogen-deuterium kinetic isotope effect for porphyrin metalation. *Inorga. Chem.* **20**, 907-909.

Lewin, R. (1986). RNA catalysis gives fresh perspective on the origin of life. *Science* **231**, 545-546.

Li, Y., Geyer, C. R., & Sen, D. (1996). Recognition of anionic porphyrins by DNA aptamers. *Biochemistry* **35**, 6911-6922.

Li, Y., & Sen, D. (1996). A catalytic DNA for porphyrin metallation. *Nature Struct. Biol.* **3**, 743-747.

Li, Y., & Sen, D. (1997). Towards an efficient DNAzyme. *Biochemistry*. **36**, 5589-5599.

Li, F., Lim, C. K., & Peters, T. J. (1987). An HPLC assay for rat liver ferrochelatase. *Biomedical Chromatography* **2**, 164-168.

Lienhard, G. E. (1973). Enzymatic catalysis and transition-state theory. *Science* **180**, 149-154.

Lohse, P. A., & Szostak, J. W. (1996). Ribozyme-catalysed amino-acid transfer reactions. *Nature* **381**, 442-444.

Lorsch, J. R., & Szostak, J.W. (1994a). *In vitro* selection of new ribozymes with polynucleotide kinase activity. *Nature* **371**, 31-36.

Lorsch, J.R., & Szostak, J. W. (1994b). *In vitro* selection of RNA aptamers specific for cyanocobalamin. *Biochemistry* **33**, 973-982.

Lorsch, J. R., & Szostak, J. W. (1996). Chances and necessity in the selection of nucleic acid catalysts. *Acc. Chem. Res.* **29**, 103-110.

Macaya, R. F., Schultze, P., Smith, F. W., Roe, J. A., & Feigon, J. (1993). Thrombin-binding aptamer forms a unimolecular quadruplex structure in solution. *Proc. Natl. Acad. Sci. U. S. A.* **90**, 3745-3749.

Margalit, R., & Rotenberg, M. (1984). Thermodynamics of porphyrin dimerization in aqueous solutions. *Biochem. J.* **219**, 445-450.

Marzilli, L. G. (1990). Medical aspects of DNA-porphyrin interactions. *New J. Chem.* **14**, 409-420.

Matsushima, Y., & Sugata, S. (1979). Kinetics of incorporation of manganese(II), cobalt(II), and nickel(II) into tetraphenylporphine in dimethylformamide. Effects of the acetate anion. *Chem. Pharm. Bull.* **27**, 3049-3053.

Mazumdar, S., & Mitra, S. (1990). Aggregation in five-coordinate high-spin natural hemins: determination of solution structure by ^{1}H NMR. *J. Phys. Chem.* **94**, 561-566.

McLaughlin, G. (1974). Crystal and molecular structure of a non-metallo, N-substituted porphyrin, 21-ethoxycarbonylmethyl-2,3,7,8,12,13,17,18-octaethylporphyrin. *J. Chem. Soc. Perkin Trans.* **2**, 136-140.

Moras, D., Comarmond, M. B., Fischer, J., Weiss, R., Thierry, J. C, Ebel, J. P., & Giege, R. (1980). Crystal structure of yeast $tRNA^{Asp}$. *Nature* **288**, 669.

Morris, K. N., Tarasow, T. M., Julin, C. M., Simons, S.L., Hilvert, D., & Gold, L. (1994). Enrichment for RNA molecules that bind a Diels-Alder transition state analog. *Proc. Natl. Acad. Sci. USA.* **91**, 13028-13032.

Okuda, M., Kohno, H., Furukawa, T., Tokunaga, R., & Taketani, S. (1994). Overexpression in *Escherichia coli*, and one-step purification of the human recombinant ferrochelatase. *Biochim. Biophys. Acta* **1200**, 123-128.

Orgel, L. E. (1968). Evolution of the genetic apparatus. *J. Molec. Biol.* **38**, 381-393.

Ortiz de Montellano, P. R., Berlan, H. S., & Kunze, K. L. (1981). N-methylprotopporphyrin IX: chemical synthesis and identification as the green pigment produced by 3,5-diethoxycarbonyl-1,4-dihydrocollidine treatment. *Proc. Natl. Acad. Sci. USA.* **78**, 1490-1494.

Osborne, S. E., & Ellington, A. D. (1997). Nucleic acid selection and the challenge of combinatorial chemistry. *Chem. Rev.* **97**, 349-370

Padmanabhan, K., Padmanabhan, K. P., Ferrara, J. D., Sadler, J. E., & Tulinsky, A. (1993). The structure of α-thrombin inhibited by a 15-mer single-stranded DNA aptamer. *J. Biol. Chem.* **268**, 17651-17654.

Pan, T., & Uhlenbeck, O. C. (1992). *In vitro* selection of RNAs that undergo autolytic cleavage with Pb^{2+}. *Biochemistry* **31**, 3887-3895.

Pasternack, R. F., Gibbs, E. J., & Villafranca, J. J. (1983). Interactions of porphyrins with nucleic acids. *Biochemistry* **22**, 2406-2414.

Pasternack, R. F., Sutin, N., & Turner, D. J. (1976). Some very rapid reactions of porphyrins in aqueous solution. *J. Am. Chem. Soc.* **98**, 1908-1913.

Pauling, L. (1946). Molecular architecture and biological reactions. *Chem. Eng. News.* **24**, 1375-1377.

Pley, H. W., Flaherty, K. M., & McKay, D. B. (1994). Three-dimensional structure of a hammerhead ribozyme. *Nature* **372**, 68-74.

Pollock, R., & Treisman, R. (1990). A sensitive method for the determination of protein-DNA binding specificities. *Nucleic Acids Res.* **18**, 6197-6204.

Pollack, S. J., Jacobs, J. W., & Schultz, P. G. (1986). Selective chemical catalysis by an antibody. *Science* **234**, 1570-1573.

Porra, R. J., & Jones, O. T. G. (1963). Studies on ferrochelatase. *Biochem. J.* **87**, 181-185.

Prudent, J. R., Uno, T., & Schultz, P. G. (1994). Expanding the scope of RNA catalysis. *Science* **264**, 1924-1927.

Quastler, H. The Emergence of Biological Organization. (Yale University Press: New Haven, 1964).

Raillard, S. A., & Joyce, G. F. (1996). Targeting sites within HIV-1 cDNA with a DNA-cleaving ribozymes. *Biochemistry* **35**, 11693-11701.

Roberts, R. G. (1987). HPLC determination of ferrochelatase activity in human liver. *Biomedical Chromatography* **2**, 71-75.

Robertson, D. L., & Joyce, G. F. (1990). Selection *in vitro* of an RNA enzyme that specifically cleaves single-stranded DNA. *Nature* **344**, 467-468.

Robertus, J. D., Ladner, J. E., Finch, J. T., Rhodes, D., Brown, R. S., Clark, B. F. C. & Klug, A. (1974). Structure of yeast phenylalnine tRNA at 3 Å resolution. *Nature* **250**, 546-551.

Rossi, E., Costin, K. A., & Garcia-Webb, P. (1988). Ferrochelatase activity in human lymphocytes, as quantified by a new high-performance liquid-chromatographic method. *Clinical Chemistry* **34**, 2481-2485.

Santoro, S. W., & Joyce, G. F. (1997). A general-purpose RNA-cleaving DNA enzyme. *Proc. Natl. Acad. Sci. USA.* **94**, 4262-4266.

Sassanfar, M., & Szostak, J. W. (1993). An RNA motif that binds ATP. *Nature* **364**, 550-552.

Scaria, P.V., Shire, S. J., & Shafer, R. H. (1992). Quadruplex structure of $d(G_3T_4G_3)$ stabilized by K^+ or Na^+ is an asymmetric hairpin dimer. *Proc. Natl. Acad. Sci. U.S.A.* **89**, 10336-10340.

Schevitz, R. W., Podjarny, A. D., Krishnamachari, N., Hughes, J. J., & Sigler, P. B. (1979). Crystal structure of a eukaryotic initiator tRNA. *Nature* **278**, 188-190.

Schultz, P. G., & Lerner, R. A. (1995). From molecular diversity to catalysis: lessons from the immune system. *Science* **269**, 1835-1842.

Schultze, P., Macaya, R. F., & Feigon, J. (1994). Three-dimensional solution structure of the thrombin-binding DNA aptamer d(GGTTGGTGTGGTTGG). *J. Mol. Biol.* **235**, 1532-1547.

Scott, W. G., Finch, J. T., & Klug, A. (1995). The crystal structure of an all-RNA hammerhead ribozyme: A proposed mechanism for RNA catalytic cleavage. *Cell* **81**, 991-1002.

Scott, W. G., Murry, J. B., Arnold, J. R. P., Stoddard, B. L., & Klug, A. (1996). Capturing the structure of a catalytic RNA intermediate: the hammerhead ribozyme. *Science* **274**, 2065-2069.

Sen, D., & Gilbert, W. (1988). Formation of parallel four-stranded complexes by guanine-rich motifs in DNA and its implications for meiosis. *Nature* **334**, 364-366.

Sen, D., & Gilbert, W. (1990). A sodium-potassium switch in the formation of four-stranded G4-DNA. *Nature* **344**, 410-414.

Shah, B., Shears, B., & Hambright, P. (1971) Kinetic differences between the incorporation of zinc(II) and cadmium(II) into porphyrins and n-methylporphyrins. *Inorg. Chem.* **10**, 1828-1830.

Sharp, P. A. (1985). On the origin of RNA splicing and introns. *Cell* **42**, 397-400.

Smith, K. M. Porphyrins and Metalloporphyrins. (Elsevier Scientific Publishing Co.: Amsterdam,1975).

Sundquist, W. I., & Klug, A. (1989). Telomeric DNA dimerizes by formation of guanine tetrads between hairpin loops. *Nature* **342**, 825-829.

Szathmary, E. (1990). Toward the evolution of ribozymes. *Nature* **344**, 115.

Szostak, J. W. (1993). *In vitro* genetics. *Trends Biochem. Sci.* **17**, 89-93.

Taketani, S., & Tokunaga, R. (1981). Rat liver ferrochelatase. *J. Biol. Chem.* **256**, 12748-12753.

Taketani, S., & Tokunaga, R. (1982). Purification and substrate specificity of bovine liver-ferrochelatase. *Euro. J. Biochem.* **127**, 443-447.

Taketani, S., & Tokunaga, R. (1984). Non-enzymatic heme formation in the presence of fatty acids and thiol reductants. *Biochim. Biophys. Acta* **798**, 226-230.

Tephly, T. R., Gibbs, A. H. & De Matteis, F. (1979). Studies on the mechanism of experimental porphyria produced by 3,5-diethoxycarbonyl-1,4-dihydrocollidine. *Biochem. J.* **180**, 241-244.

Thiesen, H-J., & Bach, C. (1990). Target detection assay (TDA): A versatile procedure to determine DNA binding sites as demonstrated on SP1 protein. *Nucleic Acids Res.* **18**, 3203-3209.

Tramontano, A., Janda, K. D., & Lerner, R. A. (1986). Catalytic antibodies. *Science* **234**, 1566-1570.

Tsang, J., & Joyce, G. F. (1994). Evolutionary optimization of the catalytic properties of a DNA-cleaving ribozyme. *Biochemistry* **33**, 5966-5973.

Tuerk, C., & Gold, L. (1990). Systematic evolution of ligands by exponential enrichment: RNA ligands to bacteriophage T4 DNA polymerase. *Science* **249**, 505-510.

Tuerk, C. , MacDougal, S., & Gold, L. (1992). RNA pseudoknots that inhibit human immunodeficiecy virus type I reverse transcriptase. *Proc. Natl. Acad. Sci. USA.* **89**, 6988-6992.

van Holde, K. E. "Physical Biochemistry" (2nd ed.). (Prentice-Hall Inc.: Englewood Cliffs, New Jesey, 1985).

Venczel, E. A., & Sen, D. (1993). Parallel and antiparallel structures from a complex telomeric sequence. *Biochemistry* **32**, 6220-6228.

Wang, A. H., Ughetto, G., Quigley, G. J., & Rich A. (1987). Interactions between an anthracycline antibiotic and DNA: molecular structure of daunomycin complexes to d($C_pG_pT_pA_pC_pG$) at 1.2Å resolution. *Biochemistry* **26**, 1152-1163.

Wang, K. Y., Krawczyk, S. H., Bischofberger, N., Swaminathan, S., & Bolton, P. H. (1993a). The tertiary structure of a DNA aptamer which binds to and inhibits thrombin determines activity. *Biochemistry* **32**, 11285-11292.

Wang, K. Y., McCurdy, S., Shea, R. G., Swanminathan, S., & Bolton, P. H. (1993b) A DNA aptamer which binds to and inhibits thrombin exhibits a new structural motif for DNA. *Biochemistry* **32**, 1899-1904.

Wang, Y., Hamasaki, K., & Rando, R. R. (1997) Specificity of aminoglycoside binding to RNA constructs derived from the 16S rRNA decoding region and the HIV-RRE activator region. *Biochemistry* **36**, 768-779.

Ward, B., Skorobogaty, A., & Dobrowiak, J. C. (1986). DNA cleavage specificity of a group of cationic metalloporphyrins. *Biochemistry* **25**, 6875-6883.

White, H. B. III (1976). Coenzymes as fossils of an earlier metabolic state. *J. Mol. Evol.* **7**, 101-104.

Williams, K. P., Ciafre, S., & Tocchini-Valentini, G. P. (1995). Selection of novel Mg^{2+}-dependent self-cleaving ribozymes. *EMBO J.* **14**, 4551-4557.

Williamson, J. R. (1993). Guanine quartets. *Curr. Opin. Struc. Biol.* **3**, 357-362.

Williamson, J. R. (1994). G-quartet structures in telomeric DNA. *Annu. Rev. Biophys. Biomol. Struc.* **23**, 703-730.

Williamson, J. R., Raghuraman, M. K., Cech, T. R. (1989). Monovalent cation-induced structure of telomeric DNA: the G-quartet model. *Cell* **59**, 871-880.

Wilson, C., Szostak, J. W. (1995). *In vitro* evolution of a self-alkylating ribozyme. *Nature* **374**, 777-782.

Woese, C. The Genetic Code. (Harper & Row, New York, 1967).

Wolfenden, R. (1972) Analog approaches to the structure of the transition state in enzyme reactions. *Acc. Chem. Res.* **5**, 10-18.

Woo, N. H., Roe, B. A., & Rich, A. (1980). Three-dimensional structure of Escherichia coli initiator $tRNA_f^{Met}$. *Nature* **286**, 346-351.

Yarus, M. (1993). How many catalytic RNAs ? Ions and Cheshire cat conjecture. *FASEB J.* **7**, 31-39.